

**Program to Reduce the Earthquake Hazards of  
Steel Moment-Frame Structures**

**State of the Art Report on  
Connection Performance**

## DISCLAIMER

This document provides practicing engineers and building officials with a resource document for understanding the behavior of steel moment-frame buildings in earthquakes. It is one of the set of six State of the Art Reports containing detailed derivations and explanations of the basis for the design and evaluation recommendations prepared by the SAC Joint Venture. The recommendations and state of the art reports, developed by practicing engineers and researchers, are based on professional judgment and experience and supported by a large program of laboratory, field, and analytical research. **No warranty is offered with regard to the recommendations contained herein, by the Federal Emergency Management Agency, the SAC Joint Venture, the individual joint venture partners, or the partner's directors, members or employees. These organizations and their employees do not assume any legal liability or responsibility for the accuracy, completeness, or usefulness of any of the information, products or processes included in this publication. The reader is cautioned to review carefully the material presented herein and exercise independent judgment as to its suitability for application to specific engineering projects.** This publication has been prepared by the SAC Joint Venture with funding provided by the Federal Emergency Management Agency, under contract number EMW-95-C-4770.

---

**Cover Art.** The beam-column connection assembly shown on the cover depicts the standard detailing used in welded steel moment-frame construction prior to the 1994 Northridge earthquake. This connection detail was routinely specified by designers in the period 1970-1994 and was prescribed by the *Uniform Building Code* for seismic applications during the period 1985-1994. It is no longer considered to be an acceptable design for seismic applications. Following the Northridge earthquake, it was discovered that many of these beam-column connections had experienced brittle fractures at the joints between the beam flanges and column flanges.

# State of the Art Report on Connection Performance

## SAC Joint Venture

A partnership of  
**Structural Engineers Association of California (SEAOC)**  
**Applied Technology Council (ATC)**  
**California Universities for Research in Earthquake Engineering (CUREe)**

**Prepared for the SAC Joint Venture Partnership by  
Charles Roeder**

Department of Civil Engineering  
University of Washington

### Project Oversight Committee

William J. Hall, Chair

Shirin Ader  
John M. Barsom  
Roger Ferch  
Theodore V. Galambos  
John Gross

James R. Harris  
Richard Holguin  
Nestor Iwankiw  
Roy G. Johnston  
Len Joseph

Duane K. Miller  
John Theiss  
John H. Wiggins

### SAC Project Management Committee

SEAOC: William T. Holmes  
ATC: Christopher Rojahn  
CUREe: Robin Shepherd

Program Manager: Stephen A. Mahin  
Project Director for Topical Investigations:  
James O. Malley  
Project Director for Product Development:  
Ronald O. Hamburger

### Topical Investigation Team

Jim Anderson  
Hassan Astaneh-Asl  
John M. Barsom  
Vitelmo Bertero

Gregory Deierlein  
Michael Engelhardt  
Gary Fry  
Subash Goel

Matt Johnson  
Sashi Kunnath  
Roberto Leon  
Thomas Murray

James Ricles  
Stephen Schneider  
Bozidar Stojadinovic  
Chia-Ming Uang  
Andrew Whittaker

### Technical Advisory Panel

Charlie Carter  
Robert H. Dodds

Roger Ferch  
John D. Hooper

Egor Popov  
Steve Powell

Stanley T. Rolfe  
Rick Wilkinson

### SAC Joint Venture

SEAOC: [www.seaoc.org](http://www.seaoc.org)  
ATC: [www.atcouncil.org](http://www.atcouncil.org)  
CUREe: [www.curee.org](http://www.curee.org)

September 2000

## THE SAC JOINT VENTURE

SAC is a joint venture of the Structural Engineers Association of California (SEAOC), the Applied Technology Council (ATC), and California Universities for Research in Earthquake Engineering (CUREe), formed specifically to address both immediate and long-term needs related to solving performance problems with welded, steel moment-frame connections discovered following the 1994 Northridge earthquake. SEAOC is a professional organization composed of more than 3,000 practicing structural engineers in California. The volunteer efforts of SEAOC's members on various technical committees have been instrumental in the development of the earthquake design provisions contained in the *Uniform Building Code* and the 1997 *National Earthquake Hazards Reduction Program (NEHRP) Recommended Provisions for Seismic Regulations for New Buildings and other Structures*. ATC is a nonprofit corporation founded to develop structural engineering resources and applications to mitigate the effects of natural and other hazards on the built environment. Since its inception in the early 1970s, ATC has developed the technical basis for the current model national seismic design codes for buildings; the *de facto* national standard for postearthquake safety evaluation of buildings; nationally applicable guidelines and procedures for the identification, evaluation, and rehabilitation of seismically hazardous buildings; and other widely used procedures and data to improve structural engineering practice. CUREe is a nonprofit organization formed to promote and conduct research and educational activities related to earthquake hazard mitigation. CUREe's eight institutional members are the California Institute of Technology, Stanford University, the University of California at Berkeley, the University of California at Davis, the University of California at Irvine, the University of California at Los Angeles, the University of California at San Diego, and the University of Southern California. These laboratory, library, computer and faculty resources are among the most extensive in the United States. The SAC Joint Venture allows these three organizations to combine their extensive and unique resources, augmented by subcontractor universities and organizations from across the nation, into an integrated team of practitioners and researchers, uniquely qualified to solve problems related to the seismic performance of steel moment-frame buildings.

## ACKNOWLEDGEMENTS

Funding for Phases I and II of the SAC Steel Program to Reduce the Earthquake Hazards of Steel Moment-Frame Structures was principally provided by the Federal Emergency Management Agency, with ten percent of the Phase I program funded by the State of California, Office of Emergency Services. Substantial additional support, in the form of donated materials, services, and data has been provided by a number of individual consulting engineers, inspectors, researchers, fabricators, materials suppliers and industry groups. Special efforts have been made to maintain a liaison with the engineering profession, researchers, the steel industry, fabricators, code-writing organizations and model code groups, building officials, insurance and risk-management groups, and federal and state agencies active in earthquake hazard mitigation efforts. SAC wishes to acknowledge the support and participation of each of the above groups, organizations and individuals. In particular, we wish to acknowledge the contributions provided by the American Institute of Steel Construction, the Lincoln Electric Company, the National Institute of Standards and Technology, the National Science Foundation, and the Structural Shape Producers Council. SAC also takes this opportunity to acknowledge the efforts of the project participants – the managers, investigators, writers, and editorial and production staff – whose work has contributed to the development of these documents. Finally, SAC extends special acknowledgement to Mr. Michael Mahoney, FEMA Project Officer, and Dr. Robert Hanson, FEMA Technical Advisor, for their continued support and contribution to the success of this effort.

In Memory of Egor Popov, Professor Emeritus, University of California at Berkeley

## TABLE OF CONTENTS

LIST OF FIGURES .....	vii
LIST OF TABLES .....	xi
<b>1. INTRODUCTION .....</b>	<b>1-1</b>
1.1 Purpose.....	1-1
1.2 Background.....	1-3
1.3 Historic Connections.....	1-10
1.4 Development of Pre-Northridge Connection .....	1-14
1.5 Organization of Report .....	1-17
<b>2. PRE-NORTHRIDGE CONNECTIONS AND FACTORS AFFECTING THEIR PERFORMANCE.....</b>	<b>2-1</b>
2.1 Welded-Flange-Bolted-Web Connection.....	2-1
2.1.1 Evolution of the Research.....	2-1
2.1.2 Evolution of Professional Practice in Steel Frame Construction.....	2-4
2.1.3 Issues of Concern.....	2-7
2.2 Modes of Failure .....	2-8
2.2.1 Effect of Member Size and Geometry .....	2-10
2.2.2 Effect of Panel Zone Yielding .....	2-12
2.2.3 Effect of Bolts and Bolt Type .....	2-19
2.2.4 Material Properties of Steel .....	2-19
2.2.5 Weld Type and Procedures .....	2-22
2.2.6 Weld Preparation and Weld Access Hole Geometry .....	2-23
2.2.7 Slenderness and Local Buckling Considerations.....	2-24
2.2.8 Continuity Plate Requirements .....	2-26
2.2.9 Effect of Load and Deformation History .....	2-26
2.3 Methods of Predicting Strength, Stiffness and Hysteretic Behavior .....	2-29
2.3.1 Rotational Capacity.....	2-31
<b>3. POST-NORTHRIDGE WELDED FLANGE CONNECTIONS.....</b>	<b>3-1</b>
3.1 Introduction.....	3-1
3.2 Post-Northridge Connections.....	3-1
3.3 Unreinforced Connections .....	3-3
3.3.1 Welded-Flange-Bolted-Web Connections with Improved Welding.....	3-3
3.3.2 Welded-Flange-Bolted-Web Connections with Improved Weld Access Hole Details .....	3-11
3.3.3 Welded-Flange-Welded-Web Connections with Improved Weld Access Hole Details .....	3-16
3.3.4 Free-Flange Connection.....	3-22
3.4 Reinforced Connections.....	3-30
3.4.1 Haunched Connections .....	3-30
3.4.2 Coverplate Connections.....	3-40

---

3.5	Reduced-Beam-Section (RBS) Connections .....	3-56
3.6	Welded-Flange-Plate Connections .....	3-73
4.	OTHER ISSUES FOR POST-NORTHRIDGE WELDED FLANGE CONNECTIONS .....	4-1
4.1	General Introduction .....	4-1
4.2	Continuity Plates .....	4-2
4.3	Shear Yielding of Panel Zone .....	4-6
4.4	Strong-Column-Weak-Beam Connection Requirements .....	4-9
4.5	Weak-Axis-Column-Bending Connections .....	4-10
4.6	Lateral Torsional and Local Buckling .....	4-14
4.7	Deep Columns .....	4-17
4.8	Box Columns .....	4-20
4.9	Composite Slabs .....	4-27
4.10	Temperature Effects .....	4-30
4.11	Dynamic Loading .....	4-33
5.	FIELD-BOLTED CONNECTIONS FOR STEEL MOMENT FRAMES .....	5-1
5.1	Introduction .....	5-1
5.2	PR Connections .....	5-1
5.2.1	Modes of Failure, Yield Mechanisms, and Rotational Capacity of PR Connections .....	5-4
5.3	Stiff PR Connections .....	5-7
5.3.1	Extended-End-Plate Connections .....	5-7
5.3.2	Bolted-Flange-Plate Connections .....	5-23
5.4	PR Connections with Intermediate Stiffness .....	5-34
5.4.1	T-Stub Connection .....	5-35
5.5	Flexible PR Connections .....	5-48
5.5.1	Double-Flange-Angle Connections .....	5-48
5.5.2	Web-Angle Connections, Shear Tab Connections, and Other Web-Only Connections .....	5-53
6.	SUPPLEMENTAL AND OTHER CONNECTIONS .....	6-1
6.1	General Discussion of Concept .....	6-1
6.2	Supplemental Connections – Composite PR Connections .....	6-1
6.2.1	Composite-Shear-Tab Connections .....	6-1
6.2.2	Other Composite PR Connections .....	6-8
6.3	Supplemental Connections – Weld Overlay Connections .....	6-13
6.4	Supplemental Connections – Connections with Friction and Damping .....	6-19
6.5	Other Connections .....	6-20
7.	SUMMARY, CONCLUSIONS, AND UNRESOLVED ISSUES .....	7-1
7.1	Summary .....	7-1
7.2	Conclusions .....	7-2
7.3	Unresolved Issues .....	7-5

---

REFERENCES, FEMA REPORTS, SAC REPORTS, NOTATION, AND ACRONYMS.....R-1

SAC PHASE II PROJECT PARTICIPANTS .....S-1

## LIST OF FIGURES

Figure 1-1	Typical Welded Moment-Resisting Connection Prior to 1994 .....	1-5
Figure 1-2	Common Zone of Fracture Initiation in Beam-Column Connection .....	1-5
Figure 1-3	Fractures of Beam to Column Joints.....	1-6
Figure 1-4	Column Fractures.....	1-6
Figure 1-5	Vertical Fracture through Beam Shear Plate Connection.....	1-7
Figure 1-6	Built-Up Members Used in Early 1900s.....	1-11
Figure 1-7	Typical Riveted T-Stub Connection .....	1-11
Figure 1-8	Typical Riveted Double-Flange-Angle Connection .....	1-12
Figure 1-9	Typical T-Stub Connection with High-Strength Bolts .....	1-13
Figure 1-10	Moment-Rotation of Riveted Connection with Large Rotational Capacity .....	1-14
Figure 1-11	Moment-Rotation of Riveted Connection with Small Rotational Capacity .....	1-15
Figure 1-12	Fully Restrained Welded-Flange-Bolted-Web Connection.....	1-15
Figure 1-13	Moment-Rotation Behavior Observed in an Early FR Connection Test.....	1-16
Figure 2-1	T-Shaped Test Assemblage.....	2-2
Figure 2-2	Cruciform Test Subassemblage .....	2-2
Figure 2-3	Load vs. Plastic Rotation for 1988 Study .....	2-3
Figure 2-4	Total Plastic Rotation vs. Beam Depth for Pre-Northridge Connection.....	2-5
Figure 2-5	Deformed Finite Element Mesh of Connection with Panel Zone Yield.....	2-5
Figure 2-6	Moment-Rotation Curve Illustrating Resistance After Initial Failure .....	2-9
Figure 2-7	Typical Yield Mechanisms for Welded-Flange-Bolted-Web Connections.....	2-9
Figure 2-8	Typical Failure Modes for Welded-Flange-Bolted-Web Connections.....	2-10
Figure 2-9	Elastic and Plastic Strain Distribution in Beams of Different Depth .....	2-11
Figure 2-10	Schematic Illustrating Span Length Effect .....	2-12
Figure 2-11	Geometry and Equilibrium for Determining Panel Zone Shear Force, $V_{pz}$ .....	2-15
Figure 2-12	Plastic Rotation as a Function of Normalized Shear Force .....	2-16
Figure 2-13	Plastic Rotation as a Function of Relative Beam Flexure and Panel Zone Yielding .....	2-17
Figure 2-14	Normalized Panel Zone Shear Capacity as a Function of Panel Zone Yield Potential .....	2-18
Figure 2-15	Rotational Capacity of Pre-Northridge Connections Performed Since the Northridge Earthquake.....	2-20
Figure 2-16	Variation in the Measured Yield and Tensile Stress in Structural Steel (Coons, 1999).....	2-20
Figure 2-17	Rotational Capacity of Welded-Flange-Bolted-Web Connections Welded to Achieve Reduced Flaws with Notch Tough Electrodes .....	2-22
Figure 2-18	Moment-Rotation Curve for a Specimen with Notch Tough Weld Details and Recommended Improvements to the Weld Access Hole Details.....	2-24
Figure 2-19	Plastic Rotation as a Function of Beam Flange Slenderness .....	2-25
Figure 2-20	Effect of Continuity Plates on Plastic Rotation .....	2-27
Figure 2-21	Definition of Plastic Rotation Used in this Report .....	2-28
Figure 2-22	Test Programs Used in the SAC Phase 2 Research .....	2-29

Figure 3-1	Schematic of Welded-Flange-Bolted-Web Connection with Improved Welds .....	3-4
Figure 3-2	Comparison of the Rotational Capacity .....	3-5
Figure 3-3	Typical Pull Type Test Specimen .....	3-7
Figure 3-4	Japanese Welded Flange Connection Details .....	3-7
Figure 3-5	Panel Zone Shear Force in Unreinforced Post-Northridge Connections .....	3-9
Figure 3-6	Recommended Improved Weld Access Hole Detail From the Lehigh Research Program .....	3-15
Figure 3-7	Web Welding Details Evaluated in SAC Phase 2 Research .....	3-17
Figure 3-8	Moment-Rotation Curve for Lehigh Specimen LU-T1 .....	3-18
Figure 3-9	Proposed Free-Flange Connection .....	3-23
Figure 3-10	Schematic of the Forces for Design of the Free-Flange Web Plate and Welds .....	3-27
Figure 3-11	Plastic Rotation for Free-Flange and Welded Web Connections .....	3-29
Figure 3-12	Haunched Connection .....	3-31
Figure 3-13	Possible Yield Mechanisms and Failure Modes for the Haunch Connection .....	3-34
Figure 3-14	Plastic Rotation from Haunch Connection Tests .....	3-34
Figure 3-15	Geometry for Balancing Yield Mechanisms and Failure Modes for Haunched Connections .....	3-36
Figure 3-16	Coverplated Connection .....	3-41
Figure 3-17	Yield Mechanisms and Failure Modes for Coverplated Connections .....	3-48
Figure 3-18	Plastic Rotation Obtained During Past Coverplate Connection Tests .....	3-49
Figure 3-19	Plastic Rotation of Coverplate Connections as a Function of the $t_{cp}/t_{bf}$ Ratio .....	3-50
Figure 3-20	Weld Configurations for Coverplate Connection .....	3-51
Figure 3-21	Effect of Weld Configuration on Plastic Rotation of Coverplate Connections .....	3-51
Figure 3-22	Geometry for Balancing Shear and Flexural Yielding of Coverplate Connection .....	3-54
Figure 3-23	Reduced-Beam-Section Connection, a) Straight Cut RBS, b) Tapered Cut RBS, and c) Radius Cut RBS .....	3-57
Figure 3-24	Yield Mechanisms and Failure Modes for RBS Connections .....	3-62
Figure 3-25	Total Plastic Rotations from Past RBS Connection Tests .....	3-62
Figure 3-26	Comparison of Moment-Rotation Curves for DBWW and DBBW Radius Cut RBS Specimens .....	3-65
Figure 3-27	Geometry for Balancing Shear and Flexural Yielding of RBS Connection .....	3-71
Figure 3-28	Welded-Flange-Plate Connection .....	3-73
Figure 3-29	Yield Mechanisms and Failure Modes of Welded-Flange-Plate Connection .....	3-74
Figure 3-30	Geometry for Panel Zone Yielding of Welded-Flange-Plate Connection .....	3-78
Figure 4-1	Moment-Rotation Behavior of Specimen With Thick Column Flange and No Continuity Plate (LU-C1) .....	4-3

Figure 4-2	Moment-Rotation Behavior of Specimen With Thick Column Flange but With Continuity Plate (LU-C2) .....	4-4
Figure 4-3	Moment-Rotation Behavior of Specimen With Deep Column With Thin Column Flanges Without a Continuity Plate (LU-C3).....	4-4
Figure 4-4	Moment-Rotation Behavior of Specimen With Deep Column With Thin Column Flanges But With a Continuity Plate (LU-C4).....	4-5
Figure 4-5	Schematic of Various Weak-Axis-Column-Bending Connections.....	4-12
Figure 4-6	Local Longitudinal Stress Distribution in Beam Flanges .....	4-13
Figure 4-7	Distribution of Plastic Strain in a Ductile Connection .....	4-30
Figure 5-1	Relative Strength and Stiffness of PR Connections.....	5-2
Figure 5-2	Consequence of Connection Flexibility on Frame Behavior.....	5-3
Figure 5-3	Simplified Deflection Analysis for FR and PR Connections .....	5-4
Figure 5-4	Comparison of the Plastic Rotations, $\theta_p$ and $\theta_g$ .....	5-5
Figure 5-5	Effect of Beam Depth on End-Plate Connection Rotational Capacity .....	5-6
Figure 5-6	Typical Extended End-Plate Connection.....	5-8
Figure 5-7	Moment-Rotation Behavior for Extended-End-Plate Connection With Bolt Fracture .....	5-9
Figure 5-8	Moment-Rotation Behavior for Extended-End-Plate Connection With Plastic Deformation in the End-Plate.....	5-9
Figure 5-9	Moment-Rotation Behavior for Stiffened Extended-End-Plate Connection With Plastic Deformation in the Beam.....	5-10
Figure 5-10	Primary Yield Mechanisms and Common Failure Modes for Bolted Extended-End-Plate Connections .....	5-11
Figure 5-11	Typical Extended-End-Plate Configurations .....	5-14
Figure 5-12	Moment-Rotation Curve for an Unstiffened 4-Bolt Extended-End-Plate Connection .....	5-15
Figure 5-13	Schematic of Bending Moment Flange Force Distribution for Extended-End-Plate Connection.....	5-16
Figure 5-14	Geometry Needed to Define End-Plate Resistance Models .....	5-17
Figure 5-15	Typical Bolted-Flange-Plate Connection.....	5-23
Figure 5-16	Moment-Rotation of Bolted-Flange-Plate Connection With Limited Rotation Capacity .....	5-25
Figure 5-17	Moment-Rotation of Bolted-Flange-Plate Connection With Large Rotation Capacity .....	5-25
Figure 5-18	Primary Yield Mechanisms and Common Failure Modes for Bolted-Flange-Plate Connections .....	5-26
Figure 5-19	Moment-Rotation Behavior of a Bolted-Flange-Plate Connection .....	5-27
Figure 5-20	Definition of Geometry of the Bolted-Flange-Plate Equations .....	5-30
Figure 5-21	Possible Block Shear and Bolt Pull-Through Mechanisms for Bolted-Flange-Plate Connection.....	5-33
Figure 5-22	Typical T-Stub Connection.....	5-36
Figure 5-23	Moment-Rotation Behavior of T-Stub Connection with Shear Yield of Shear Connectors Between the Stem of T-Section and the Beam Flange .....	5-36

Figure 5-24	Moment-Rotation Behavior of T-Stub Connection with Flexural Yield of Flanges of T-Section.....	5-37
Figure 5-25	Primary Yield Mechanisms and Common Failure Modes for Bolted T-Stub Connections .....	5-38
Figure 5-26	Typical Pull Test Configuration .....	5-39
Figure 5-27	Typical Moment-Rotation Curve for Bolted T-Stub Connection.....	5-42
Figure 5-28	Geometry for Prying Forces and Bending of T-Section Flanges.....	5-42
Figure 5-29	Geometry for Other T-Stub Failure Modes .....	5-43
Figure 5-30	Detailed Stiffness Model for T-Stub Connection .....	5-46
Figure 5-31	Typical Double-Flange-Angle Connection.....	5-49
Figure 5-32	Primary Yield Mechanisms and Common Failure Modes for the Bolted Double-Flange-Angle Connection .....	5-50
Figure 5-33	Geometry for Failure Mode Evaluation of Double-Flange-Angle Connections .....	5-53
Figure 5-34	Typical Bolted Web-Angle Connection .....	5-54
Figure 5-35	Typical Bolted Shear Tab Connection.....	5-55
Figure 5-36	Bolted Web-T Connection .....	5-55
Figure 5-37	Moment-Rotation Behavior for Bolted Web-Angle Connection.....	5-56
Figure 5-38	Moment-Rotation Curve for the Bolted Shear Tab Connection .....	5-57
Figure 5-39	Deformation and Binding of Shear Tab Connection .....	5-58
Figure 5-40	Rotational Capacity of Shear Tab and Web-Angle Connections .....	5-62
Figure 5-41	Stiffness of Shear Tab and Web-Angle Connection .....	5-63
Figure 5-42	Evaluation of Moment Capacity of Shear Tab Bolt Group Connection.....	5-64
Figure 5-43	Equilibrium Conditions for Evaluating Shear Tab Plate and Weld.....	5-64
Figure 6-1	Typical Composite-Shear-Tab Connection .....	6-2
Figure 6-2	Moment-Rotation Curve for the Composite-Shear-Tab Connection.....	6-4
Figure 6-3	Rotational Capacity of Composite-Shear-Tab Connections .....	6-4
Figure 6-4	Comparison of Stiffness of Composite and Bare Steel Shear Tab Connection .....	6-6
Figure 6-5	Evaluation of Moment Capacity of Connection .....	6-7
Figure 6-6	Forces Applied to the Shear Tab Plate and Weld .....	6-7
Figure 6-7	Typical Composite-Seated-Beam Connection.....	6-8
Figure 6-8	Typical Composite-Double-Flange-Angle Connection .....	6-9
Figure 6-9	Typical Moment Rotation Curve for Composite PR Connection.....	6-10
Figure 6-10	Typical Composite Moment Rotation Curve.....	6-11
Figure 6-11	Schematic of Weld Overlay Method.....	6-13
Figure 6-12	Typical Moment-Rotation Curve for Weld Overlay Connection .....	6-16
Figure 6-13	Schematic of Simplified Overlay Design Method.....	6-17
Figure 6-14	Schematic of the Overlay Weld Loading with the More Complex Proposed Design Method.....	6-18
Figure 6-15	Schematic of Proposed Friction Damper Connection.....	6-20

## LIST OF TABLES

Table 2-1	Test Summary for Welded-Flange-Bolted-Web Connections .....	2-14
Table 2-2	Yield Mechanisms of Pre-Northridge Connection .....	2-30
Table 2-3	Failure Modes for Pre-Northridge Connection .....	2-30
Table 3-1	Summary of Pull Test Results .....	3-8
Table 3-2	Yield Mechanisms of Unreinforced Post-Northridge Connection .....	3-9
Table 3-3	Failure Modes of the Post-Northridge Welded-Flange-Bolted-Web Connection .....	3-10
Table 3-4	Summary of Test Results for Evaluation of the Effect of Web Attachment on the Connection Performance .....	3-13
Table 3-5	Failure Modes of the Post-Northridge Welded-Flange-Welded-Web Connection with Improved Weld Access Hole Details .....	3-19
Table 3-6	Summary of Test Results for Free-Flange Connection .....	3-24
Table 3-7	Failure Modes of the Post-Northridge Free-Flange Connection .....	3-28
Table 3-8	Summary of Past Haunch Test Results .....	3-32
Table 3-9	Yield Mechanisms of Haunch Connection .....	3-37
Table 3-10	Failure Modes for Haunch Connection .....	3-38
Table 3-11	Summary of Past Coverplate Connection Tests .....	3-42
Table 3-12	Summary of Test Results for Coverplate Connection .....	3-52
Table 3-13	Yield Mechanisms for Coverplate Connection .....	3-53
Table 3-14	Failure Modes for Coverplate Connection .....	3-55
Table 3-15	Summary of Past RBS Test Results .....	3-58
Table 3-16	Summary of SAC Phase 2 RBS Test Results .....	3-67
Table 3-17	Yield Mechanisms for RBS Connection .....	3-71
Table 3-18	Failure Modes for RBS Connection .....	3-72
Table 3-19	Summary of Test Results for Welded-Flange-Plate Connection .....	3-75
Table 3-20	Yield Mechanisms of the Welded-Flange-Plate Connections .....	3-76
Table 3-21	Failure Modes of Welded-Flange-Plate Connection .....	3-77
Table 4-1	Summary of Panel Zone Effects on Ductile Post-Northridge Connections .....	4-8
Table 4-2	Summary of Weak-Axis-Column-Bending Connections .....	4-11
Table 4-3	Summary Table of Test Results with Deep Column Sections .....	4-17
Table 4-4	Summary Table of Test Results with Box Columns .....	4-21
Table 4-5	Summary of Composite Slab Test Results .....	4-27
Table 4-6	Summary of Test Results for Specimens Tested at Low Temperatures .....	4-31
Table 4-7	Summary of Dynamic Connection Tests .....	4-34
Table 5-1	Summary Table of Extended-End-Plate Connection Tests .....	5-12
Table 5-2	Yield Mechanisms for Both 4-Bolt Unstiffened and 8-Bolt Stiffened Extended-End-Plate Connections .....	5-18
Table 5-3	Failure Modes for 4-Bolt Unstiffened Extended-End-Plate Connections .....	5-19
Table 5-4	Failure Modes for 8-Bolt Stiffened Extended-End-Plate Connections .....	5-21
Table 5-5	Summary of Bolted-Flange-Plate Test Results .....	5-28
Table 5-6	Yield Mechanisms for Bolted-Flange-Plate Connection .....	5-31

Table 5-7	Failure Modes for Bolted-Flange-Plate Connections .....	5-32
Table 5-8	Summary of Bolted T-Stub Connection Tests .....	5-40
Table 5-9	Yield Mechanisms for Bolted T-Stub Connection .....	5-43
Table 5-10	Failure Modes for Bolted T-Stub Connections .....	5-44
Table 5-11	Failure Modes for Bolted Double-Flange-Angle Connections.....	5-52
Table 5-12	Summary of Bolted Shear Tab Connection Tests.....	5-59
Table 6-1	Summary of Weld Overlay Connection Test Results .....	6-15

## 1. INTRODUCTION

### 1.1 Purpose

This report, FEMA-355D – *State of the Art Report on Connection Performance*, presents an overview of the current state of knowledge with regard to the cyclic inelastic behavior of beam-column connections that have been employed in moment-resisting steel frame structures in the past and that have been studied for potential use in such structures in the future. This state of the art report was prepared in support of the development of a series of Recommended Design Criteria documents, prepared by the SAC Joint Venture on behalf of the Federal Emergency Management Agency (FEMA) and addressing the issue of the seismic performance of moment-resisting steel frame structures. These publications include:

- *FEMA-350 – Recommended Seismic Design Criteria for New Steel Moment-Frame Buildings*. This publication provides recommended criteria, supplemental to *FEMA 302 – 1997 NEHRP Recommended Provisions for Seismic Regulations for New Buildings and other Structures*, for the design and construction of steel moment-frame buildings and provides alternative performance-based design criteria.
- *FEMA-351 – Recommended Seismic Evaluation and Upgrade Criteria for Existing Welded Steel Moment-Frame Buildings*. This publication provides recommended methods to evaluate the probable performance of existing steel moment-frame buildings in future earthquakes and to retrofit these buildings for improved performance.
- *FEMA-352 – Recommended Postearthquake Evaluation and Repair Criteria for Welded Steel Moment-Frame Buildings*. This publication provides recommendations for performing postearthquake inspections to detect damage in steel moment-frame buildings following an earthquake, evaluating the damaged buildings to determine their safety in the postearthquake environment, and repairing damaged buildings.
- *FEMA-353 – Recommended Specifications and Quality Assurance Guidelines for Steel Moment-Frame Construction for Seismic Applications*. This publication provides recommended specifications for the fabrication and erection of steel moment frames for seismic applications. The recommended design criteria contained in the other companion documents are based on the material and workmanship standards contained in this document, which also includes discussion of the basis for the quality control and quality assurance criteria contained in the recommended specifications.

Detailed derivations and explanations of the basis for these design and evaluation recommendations may be found in a series of State of the Art Report documents prepared by the SAC Joint Venture in parallel with these design criteria. These reports include:

- *FEMA-355A – State of the Art Report on Base Metals and Fracture*. This report summarizes current knowledge of the properties of structural steels commonly employed in building construction, and the production and service factors that affect these properties.
- *FEMA-355B – State of the Art Report on Welding and Inspection*. This report summarizes current knowledge of the properties of structural welding commonly employed in building

construction, the effect of various welding parameters on these properties, and the effectiveness of various inspection methodologies in characterizing the quality of welded construction.

- *FEMA-355C – State of the Art Report on Systems Performance of Steel Moment Frames Subject to Earthquake Ground Shaking.* This report summarizes an extensive series of analytical investigations into the demands induced in steel moment-frame buildings designed to various criteria, when subjected to a range of different ground motions. The behavior of frames constructed with fully restrained, partially restrained and fracture-vulnerable connections is explored for a series of ground motions, including motion anticipated at near-fault and soft-soil sites.
- *FEMA-355D – State of the Art Report on Connection Performance.* This report summarizes the current state of knowledge of the performance of different types of moment-resisting connections under large inelastic deformation demands. It includes information on fully restrained and partially restrained moment connections in welded and bolted configurations, based upon laboratory and analytical investigations.
- *FEMA-355E – State of the Art Report on Past Performance of Steel Moment-Frame Buildings in Earthquakes.* This report summarizes investigations of the performance of steel moment-frame buildings in past earthquakes, including the 1995 Kobe, 1994 Northridge, 1992 Landers, 1992 Big Bear, 1989 Loma Prieta and 1971 San Fernando events.
- *FEMA-355F – State of the Art Report on Performance Prediction and Evaluation of Steel Moment-Frame Buildings.* This report describes the results of investigations into the ability of various analytical techniques, commonly used in design, to predict the performance of steel moment-frame buildings subjected to earthquake ground motion. Also presented is the basis for performance-based evaluation procedures contained in the design criteria documents, *FEMA-350*, *FEMA-351*, and *FEMA-352*.

In addition to the recommended design criteria and the State of the Art Reports, a companion document has been prepared for building owners, local community officials and other non-technical audiences who need to understand this issue. *A Policy Guide to Steel Moment-Frame Construction (FEMA 354)*, addresses the social, economic, and political issues related to the earthquake performance of steel moment-frame buildings. *FEMA 354* also includes discussion of the relative costs and benefits of implementing the recommended criteria.

Study of connection behavior is an important element of this project. The connection performance portion of the program focused upon the seismic capacity and behavior of connections. The work was coordinated by the Connection Performance Technical Advisory Panel (TAP). Numerous research teams participated in the connection performance effort. This report summarizes the work completed in this effort.

The connection behavior study included evaluation of connections used in the past for seismic design, the pre-Northridge connection with its welded-flange and bolted-web, and alternative connections which were developed to assure acceptable seismic performance. The evaluations comprised both experimental and analytical investigations. The completed work from these investigations is summarized here, and will be combined with the efforts of other teams within the SAC Steel Project. The other teams address a wide range of important issues

related to the seismic behavior of steel frames including analytical methods, ductility demand, material properties and behavior, inspection requirements, and welding electrodes and processes.

It is clear that while the connection performance work is an important part of the total program, it is not the only issue that must be evaluated for understanding the seismic performance of steel moment-frame buildings. This State of the Art Report has been developed as a comprehensive document. It must be comprehensive because a wide range of connections have been used and can be used for seismic design. A wide range of steel buildings can be constructed for very different seismic conditions. Except for a brief historical review, this report does not consider riveted connections or historic connection details because no damage was noted in these structures; nor are these alternatives expected to be used again in the future. Braced frame connections, column splices and foundation base connections are also beyond the scope of this study and this report. However, a wide range of bolted beam-column connections, welded-beam-column connections, welded-bolted beam-column connections, and alternatives which have evolved from the steel frame damage (and are in the public domain) are included in this study and this report. Several patented connections are discussed without details since complete information on their behavior is not publicly available. The report is also comprehensive in that it considers the range of performance levels from elastic behavior, through nonlinear behavior and inelastic deformation, and ultimately into deterioration and failure of the connection. The report and the study attempt to address all possible failure modes with each of these connections, since it is clear that many of these failure modes were not considered in past research efforts.

## 1.2 Background

For many years, the basic intent of the building code seismic provisions was to provide buildings with an ability to withstand intense ground shaking without collapse, but potentially with some significant structural damage. In order to accomplish this, one of the basic principles inherent in modern code provisions is to encourage the use of building configurations, structural systems, materials and details that are capable of ductile behavior. A structure is said to behave in a ductile manner if it is capable of withstanding large inelastic deformations without significant degradation in strength, and without the development of instability and collapse. The design forces specified by building codes for particular structural systems are related to the amount of ductility the system is deemed to possess. Generally, the building code allows structural systems with more ductility to be designed for lower forces than less ductile systems, as ductile systems are deemed capable of resisting demands that are significantly greater than their elastic strength limit. Starting in the 1960s, engineers began to regard welded steel moment-frame buildings as being among the most ductile systems contained in the building code. Many engineers believed that steel moment-frame buildings were essentially invulnerable to earthquake-induced structural damage and thought that should such damage occur, it would be limited to ductile yielding of members and connections. Earthquake-induced collapse was not believed possible. Partly as a result of this belief, many large industrial, commercial and institutional structures employing steel moment-frame systems were constructed, particularly in the western United States.

The Northridge earthquake of January 17, 1994 challenged this paradigm. Following that earthquake, a number of steel moment-frame buildings were found to have experienced brittle

fractures of beam-to-column connections. The damaged buildings had heights ranging from one story to 26 stories, and a range of ages spanning from buildings as old as 30 years to structures being erected at the time of the earthquake. The damaged buildings were spread over a large geographical area, including sites that experienced only moderate levels of ground shaking. Although relatively few buildings were located on sites that experienced the strongest ground shaking, damage to buildings on these sites was, in many cases, quite extensive. Discovery of these unanticipated brittle fractures of framing connections, often with little associated architectural damage to the buildings, was alarming to all concerned. The discovery also caused some concern that similar, but undiscovered, damage may have occurred in other buildings affected by past earthquakes. Later investigations confirmed such damage in a limited number of buildings affected by the 1992 Landers, 1992 Big Bear and 1989 Loma Prieta earthquakes.

In general, steel moment-frame buildings damaged by the 1994 Northridge earthquake met the basic intent of the building codes. That is, they experienced limited structural damage, but did not collapse. However, the structures did not behave as anticipated and significant economic losses occurred as a result of the connection damage, in some cases, in buildings that had experienced ground shaking less severe than the design level. These losses included direct costs associated with the investigation and repair of this damage as well as indirect losses relating to the temporary, and in a few cases, long-term, loss of use of space within damaged buildings.

Steel moment-frame buildings are designed to resist earthquake ground shaking based on the assumption that they are capable of extensive yielding and plastic deformation, without loss of strength. The intended plastic deformation consists of plastic rotations developing within the beams, at their connections to the columns, and is theoretically capable of resulting in benign dissipation of the earthquake energy delivered to the building. Damage is expected to consist of moderate yielding and localized buckling of the steel elements, not brittle fractures. Based on this presumed behavior, building codes permit steel moment-frame buildings to be designed with a fraction of the strength that would be required to respond to design level earthquake ground shaking in an elastic manner.

Steel moment-frame buildings are anticipated to develop their ductility through the development of yielding in beam-column assemblies at the beam-column connections. This yielding may take the form of plastic hinging in the beams (or less desirably, in the columns), plastic shear deformation in the column panel zones, or through a combination of these mechanisms. It was believed that the typical connection employed in steel moment-frame construction, shown in Figure 1-1, was capable of developing large plastic rotations, on the order of 0.015 to 0.02 radians, without significant strength degradation.

Observation of damage sustained by buildings in the 1994 Northridge earthquake indicated that contrary to the intended behavior, in many cases brittle fractures initiated within the connections at very low levels of plastic demand, and in some cases, while the structures remained essentially elastic. Typically, but not always, fractures initiated at the complete joint penetration (CJP) weld between the beam bottom flange and column flange (Figure 1-2). Once initiated, these fractures progressed along a number of different paths, depending on the individual joint conditions.

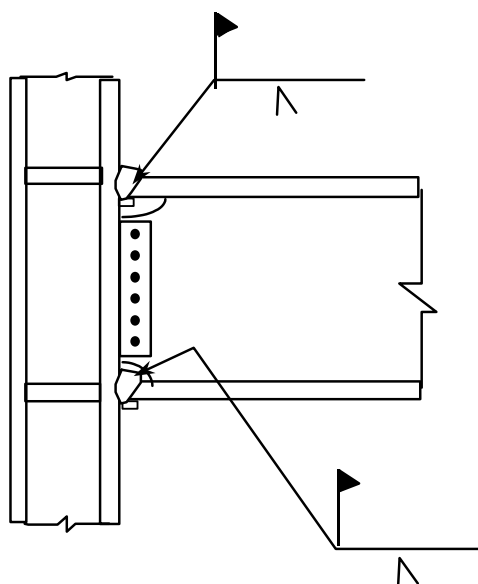


**Figure 1-1 Typical Welded Moment-Resisting Connection Prior to 1994**

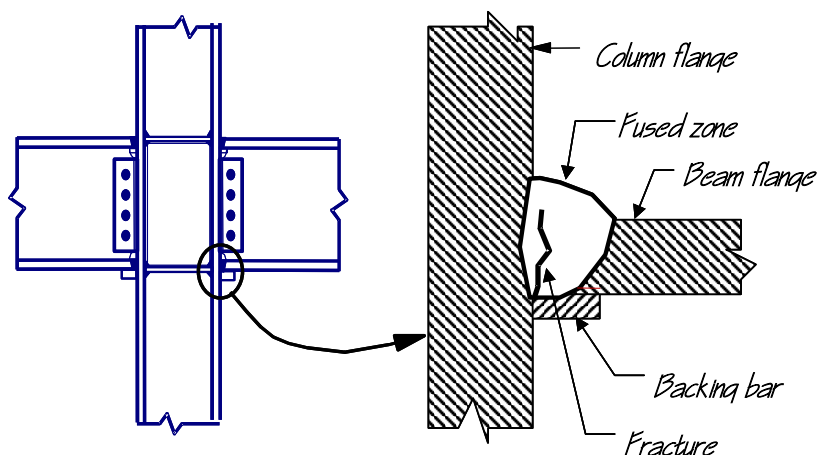


**Figure 1-2 Common Zone of Fracture Initiation in Beam-Column Connection**

In some cases, the fractures progressed completely through the thickness of the weld, and when fire protective finishes were removed, the fractures were evident as a crack through exposed faces of the weld, or the metal just behind the weld (Figure 1-3a). Other fracture patterns also developed. In some cases, the fracture developed into a crack of the column flange material behind the CJP weld (Figure 1-3b). In these cases, a portion of the column flange remained bonded to the beam flange, but pulled free from the remainder of the column. This fracture pattern has sometimes been termed a “divot” or “nugget” failure.

A number of fractures progressed completely through the column flange, along a near-horizontal plane that aligns approximately with the beam lower flange (Figure 1-4a). In some cases, these fractures extended into the column web and progressed across the panel zone (Figure 1-4b). Investigators have reported some instances where columns fractured entirely across the section.



a. Fracture at Fused Zone



b. Column Flange "Divot" Fracture

**Figure 1-3 Fractures of Beam-to-Column Joints**



a. Fractures through Column Flange



b. Fracture Progresses into Column Web

**Figure 1-4 Column Fractures**

Once such fractures have occurred, the beam-column connection has experienced a significant loss of flexural rigidity and strength to resist those loads that tend to open the crack. Residual flexural strength and rigidity must be developed through a couple consisting of forces transmitted through the remaining top flange connection and the web bolts. However, in providing this residual strength and stiffness, the bolted web connections can themselves be subject to failures. These include fracturing of the welds of the shear plate to the column, fracturing of supplemental welds to the beam web, or fracturing through the weak section of shear plate aligning with the bolt holes (Figure 1-5).

Despite the obvious local strength impairment resulting from these fractures, many damaged buildings did not display overt signs of structural damage, such as permanent drifts or damage to architectural elements, making reliable postearthquake damage evaluations difficult. In order to determine reliably if a building has sustained connection damage it is necessary to remove architectural finishes and fireproofing, and perform detailed inspections of the connections. Even if no damage is found, this is a costly process. Repair of damaged connections is even more costly. At least one steel moment-frame building sustained so much damage that it was deemed more practical to demolish the building than to repair it.



**Figure 1-5 Vertical Fracture through Beam Shear Plate Connection**

Initially, the steel construction industry took the lead in investigating the causes of this unanticipated damage and in developing design recommendations. The American Institute of Steel Construction (AISC) convened a special task committee in March, 1994 to collect and disseminate available information on the extent of the problem (AISC, 1994a). In addition, together with a private party engaged in the construction of a major steel building at the time of the earthquake, AISC participated in sponsoring a limited series of tests of alternative connection details at the University of Texas at Austin (AISC, 1994b). The American Welding Society (AWS) also convened a special task group to investigate the extent to which the damage was related to welding practice, and to determine if changes to the welding code were appropriate (AWS, 1995).

In September 1994, the SAC Joint Venture, AISC, the American Iron and Steel Institute and National Institute of Standards and Technology jointly convened an international workshop (SAC, 1994) in Los Angeles to coordinate the efforts of the various participants and to lay the foundation for systematic investigation and resolution of the problem. Following this workshop, FEMA entered into a cooperative agreement with the SAC Joint Venture to perform problem-focused studies of the seismic performance of steel moment-frame buildings and to develop recommendations for professional practice (Phase I of SAC Steel Project). Specifically, these recommendations were intended to address the following: the inspection of earthquake-affected buildings to determine if they had sustained significant damage; the repair of damaged buildings; the upgrade of existing buildings to improve their probable future performance; and the design of new structures to provide reliable seismic performance.

During the first half of 1995, an intensive program of research was conducted to explore more definitively the pertinent issues. This research included literature surveys, data collection on affected structures, statistical evaluation of the collected data, analytical studies of damaged and undamaged buildings, and laboratory testing of a series of full-scale beam-column assemblies representing typical pre-Northridge design and construction practice as well as various repair, upgrade, and alternative design details. The findings of these tasks formed the basis for the development of *FEMA-267 – Interim Guidelines: Evaluation, Repair, Modification, and Design of Welded Steel Moment Frame Structures*, which was published in August, 1995. *FEMA-267* provided the first definitive, albeit interim, recommendations for practice, following the discovery of connection damage in the 1994 Northridge earthquake.

In September 1995, the SAC Joint Venture entered into a contractual agreement with FEMA to conduct Phase II of the SAC Steel Project. Under Phase II, SAC continued its extensive problem-focused study of the performance of moment-resisting steel frames and connections of various configurations, with the ultimate goal of developing reliable seismic design criteria for steel construction. This work has included: extensive analyses of buildings; detailed finite element and fracture mechanics investigations of various connections to identify the effects of connection configuration, material strength, and toughness and weld joint quality on connection behavior; as well as more than 120 full-scale tests of connection assemblies. As a result of these studies, and independent research conducted by others, it is now known that the typical moment-resisting connection detail employed in steel moment-frame construction prior to the 1994 Northridge earthquake, and depicted in Figure 1-1, had a number of features that rendered it inherently susceptible to brittle fracture. These included the following:

- The most severe stresses in the connection assembly occurred where the beam joins to the column. Unfortunately, this is also the weakest location in the assembly. At this location, bending moments and shear forces in the beam must be transferred to the column through the combined action of the welded joints between the beam flanges and column flanges and the shear tab. The combined section properties of these elements, for example the cross sectional area and section modulus, were typically less than those of the connected beam. As a result, stresses were locally intensified at this location.
- The joint between the bottom beam flange and the column flange was typically made as a downhand field weld, often by a welder sitting on top of the beam top flange, in a so-called “wildcat” position. To make the weld from this position, each pass was interrupted at the beam web, with either a start or stop of the weld at this location. Further, the welder often completed all passes on one side of the beam web rather than alternating from one side to the other as required. This welding technique often resulted in poor quality welding at this critical location, with slag inclusions, lack of fusion, and other defects. These defects can serve as crack initiators, when the connection is subjected to severe stress and strain demands.
- The basic configuration of the connection made it difficult to detect hidden defects at the root of the welded beam-flange-to-column-flange joints. The backing bar, which was typically left in place following weld completion, restricts visual observation of the weld root. Therefore, the primary method of detecting defects in these joints was through the use of ultrasonic testing (UT). However, the geometry of the connection also made it very difficult for UT to detect flaws reliably at the bottom beam flange weld root, particularly at the center of the joint, at the beam web. As a result, many of these welded joints had undetected significant defects that can serve as crack initiators.
- Although typical design models for this connection assume that nearly all beam flexural stresses are transmitted by the flanges and all beam shear forces by the web, in reality, due to boundary conditions imposed by column deformations, the beam flanges at the connection carry a significant amount of the beam shear. This results in significant flexural stresses on the beam flange at the face of the column, and also induces large secondary stresses in the welded joint. Some of the earliest investigations of these stress concentration effects in the welded joint were conducted by Richard, et al. (1995). The stress concentrations resulting from this effect resulted in severe strength demands at the root of the complete joint

penetration welds between the beam flanges and column flanges, a region that often includes significant discontinuities and slag inclusions, which are ready crack initiators.

- Weld access holes were needed to complete both the top and bottom flange welds. Depending on their geometry, severe strain concentrations can occur in the beam flange at the toe of these weld access holes. These strain concentrations can result in low-cycle fatigue and the initiation of ductile tearing of the beam flanges after only a few cycles of moderate plastic deformation. Under large plastic flexural demands, these ductile tears can quickly become unstable and propagate across the beam flange.
- The center of the beam-flange-to-column-flange joint is restrained from movement, particularly in connections of heavy sections with thick beam flanges. This condition of restraint inhibits the development of yielding at this location, resulting in locally high stresses on the welded joint, which exacerbates the tendency to initiate fractures at defects in the welded joints.
- Design practice in the period from 1985 to 1994 encouraged connections with relatively weak panel zones. In connections with excessively weak panel zones, inelastic behavior of the assembly is dominated by shear deformation of the panel zone. This panel zone shear deformation results in a local kinking of the column flanges adjacent to the beam-flange-to-column-flange joint, and further increases the stress and strain demands in this sensitive region.

In addition to the above, additional conditions contributed significantly to the vulnerability of connections constructed prior to 1994.

- In the mid-1960s, the construction industry moved to the use of the semi-automatic, self-shielded, flux-cored arc welding process (FCAW-SS) for making the joints of these connections. The specific welding consumables that building erectors most commonly used under this process inherently produced welds with very low notch toughness. The weld quality and notch toughness of this material could be further compromised by excessive deposition rates, which unfortunately were commonly employed by welders. As a result, brittle fractures could initiate in welds with large defects, at stresses approximating the yield strength of the beam steel, precluding the development of ductile behavior.
- Early steel moment frames tended to be highly redundant and nearly every beam-column joint was constructed to behave as part of the lateral-force-resisting system. As a result, member sizes in these early frames were small and much of the early acceptance testing of this typical detail were conducted with specimens constructed of small framing members. As the cost of construction labor increased, the industry found that it was more economical to construct steel moment-frame buildings by moment-connecting a relatively small percentage of the beams and columns and by using larger members for these few moment-connected elements. The amount of strain demand placed on the connection elements of a steel moment frame is related to the span-to-depth ratio of the member. Therefore, as member sizes increased, strain demands on the welded connections also increased, making the connections more susceptible to brittle behavior.
- In the 1980s, many steel mills adopted modern production processes, including the use of scrap-based production. Steels produced by these more modern processes tended to include

micro-alloying elements that increased the yield strength of the materials so that despite the common specification of A36 material for beams, many beams actually had yield strengths that approximated or exceeded that required for grade 50 material. As a result of this increase in base metal yield strength, the weld metal in the beam-flange-to-column-flange joints became under-matched, potentially contributing to its vulnerability.

At this time, it is clear that in order to obtain reliable ductile behavior of steel moment-frame construction, a number of changes to past practices in design, materials, fabrication, erection and quality assurance are necessary. The recommendations contained in this document, and the companion publications, are based on an extensive program of research into materials, welding technology, inspection methods, frame system behavior, and laboratory and analytical investigations of different connection details.

### **1.3 Historic Connections**

While the historic connection details with riveted connections are not a part of this report or the SAC Steel Project Connection Performance study, a brief historical review is necessary to fully understand the present state of steel frame seismic connection design.

Steel moment frames have been used since very early in the 20th Century, since steel effectively replaced cast iron and wrought iron as a construction material in the last decade of the 19th Century. Prior to the 1920s, steel frames commonly were constructed as complex built-up members with gusset plates and built-up connections as illustrated in Figure 1-6. The built-up members were employed because labor costs were low, and the built-up design allowed savings in material and versatility in construction, since a wide range of members could be constructed with a small number of shapes and sizes. This permitted shipping of large quantities of a few steel sizes, and avoided shipping delays when changes were required at the job site. This was important because there was no standardization of shapes across different steel producers and rolling mills. The members and connections were riveted, and the entire steel frame was normally encased in concrete for fire protection. Few, if any, of these steel structures were designed for seismic loading, since only wind load was considered prior to about 1930. In some older buildings, even wind load received minimal consideration. These buildings invariably included many stiff, strong unreinforced masonry walls and partitions. Structural engineers relied upon these walls and partitions to help resist lateral loads, but they performed no calculations of the stiffness and resistance provided by these walls. Further, design of the connections for lateral load was completed without extensive calculations. Instead, engineers employed observations of past building performance in the design of new buildings.

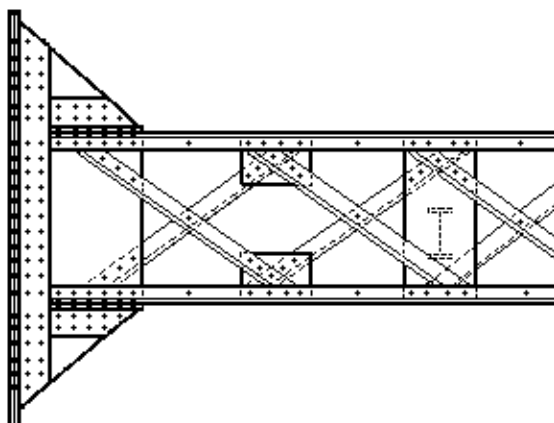


**Figure 1-6 Built-Up Members Used in Early 1900s**

Changes in steel frames began to evolve around 1920. Labor costs for the built-up elements were increasing at this time, and standard hot rolled shapes for beams and columns became the normal practice. The AISC Specification and Manual (AISC, 1928) was first developed in this period. These rolled shapes commonly were connected with riveted angles and T-sections as illustrated in Figures 1-7 and 1-8, and members and the connections were still encased in concrete for fire protection. These connections became standard and were designed with relatively simple calculations for the next 20 to 30 years. Unreinforced masonry curtain walls and partitions were still used, and the combined effect of the added strength and stiffness provided by these walls and the composite action due to the encasement supplied a major portion of the structural stiffness and resistance to lateral loads. Seismic design forces were considered in these structures, but the seismic design forces were simplified and often much smaller than those used today. These early structures were highly redundant in that every beam-column connection was a moment-resistant connection, and a large but uncalculated stiffness and resistance was provided by nonstructural elements such as architectural masonry walls and the concrete encasement for fire protection.

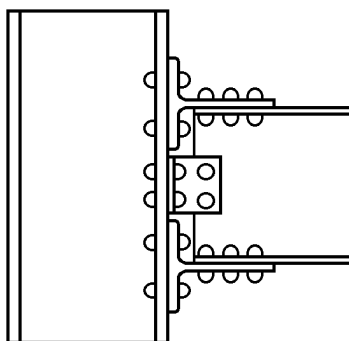


**Figure 1-7 Typical Riveted T-Stub Connection**

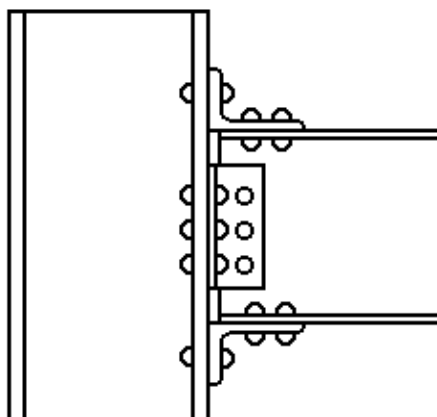


**Figure 1-8 Typical Riveted Double-Flange-Angle Connection**

The connections and construction described above and illustrated in Figures 1-7 and 1-8 were used until the mid-1950s or early 1960s. Riveted T-Stub connections such as that shown in Figure 1-7 were used in the lower floors of taller buildings, and riveted double-flange-angle connections such as illustrated in Figure 1-8 were used in the top stories of tall buildings or in smaller buildings. The seismic behavior of these older riveted connections is quite complex (Roeder et al., 1996), but the connection design used in these older buildings remained quite basic, because of redundancy in the system, conservatism in the design, and the reliance upon satisfactory past performance of these connections. After about 1960, high strength bolts began to replace the rivets in the T-stub and double-flange-angle connection as illustrated in Figure 1-9, but the connection details and geometry remained essentially the same as those used for riveted construction. Concrete encasement was also discontinued in favor of lighter fire protection materials. By this time, the seismic design procedures had evolved into methods similar to those used in modern seismic design. It was recognized that earthquake forces can be extremely large, although buildings could be designed for much smaller seismic design forces if proper care was taken toward the inelastic performance of the building and its connections. This led to increased interest in the inelastic hysteretic behavior of structures. The reduced seismic forces depended upon the mass and period of the building, and therefore engineers began to reduce the mass of the structure, since this reduced the seismic design forces. These changes generally resulted in less secondary stiffness due to fire protection, cladding and partitions than in buildings of the earlier eras. However, buildings of the 1950s and 1960s still had a substantial uncalculated strength and stiffness due to cladding and partitions, and they were very redundant, since the moment-resisting connections were used at every beam-to-column joint. This construction continued into the early 1970s.

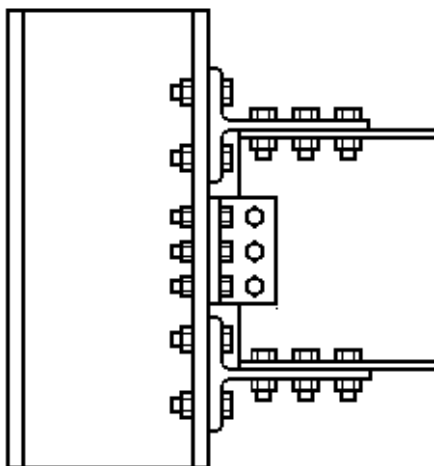


**Figure 1-9 Typical T-Stub Connection with High-Strength Bolts**

Engineers commonly and correctly note that during past U.S. earthquakes no lives have been lost in these early steel structures, and no buildings of these types have collapsed. As a consequence, it is often assumed that the inelastic performance of these early structures must be very good. In fact, this is often not the case (Roeder, et al., 1994). The inelastic behavior produced by these early connections invariably has pinched and deteriorating hysteretic curves. Very little energy is dissipated, although these connections sustain large changes in stiffness with increasing deformation. The inelastic rotation capacity for these older connections was often large as illustrated in the moment-rotation hysteresis curve in Figure 1-10. However, this rotational capacity was highly dependent upon failure mode and could be extremely small, with less desirable failure modes as shown in Figure 1-11.

The inelastic rotational capacity of these older connections is very dependent on the failure mode, and sometimes undesirable failure modes are possible. Engineers did not thoroughly calculate the strength and failure modes of these early connections. They relied upon standard practice and experience, and so the failure mode that should occur under seismic load is dependent on chance. Thus, the good performance of these older buildings is not provided solely by superior steel frames, but by the redundancy created from using these connections throughout the building, and the supplemental stiffness and resistance contributed by nonstructural components. The supplemental strength and stiffness supplied by nonstructural elements prevents the connections from reaching the deformations that would result in failure. The large number of moment-resisting connections provided redundancy, which meant that distress exhibited by a few isolated connections during a major earthquake did not have a detrimental impact on the overall structural performance.

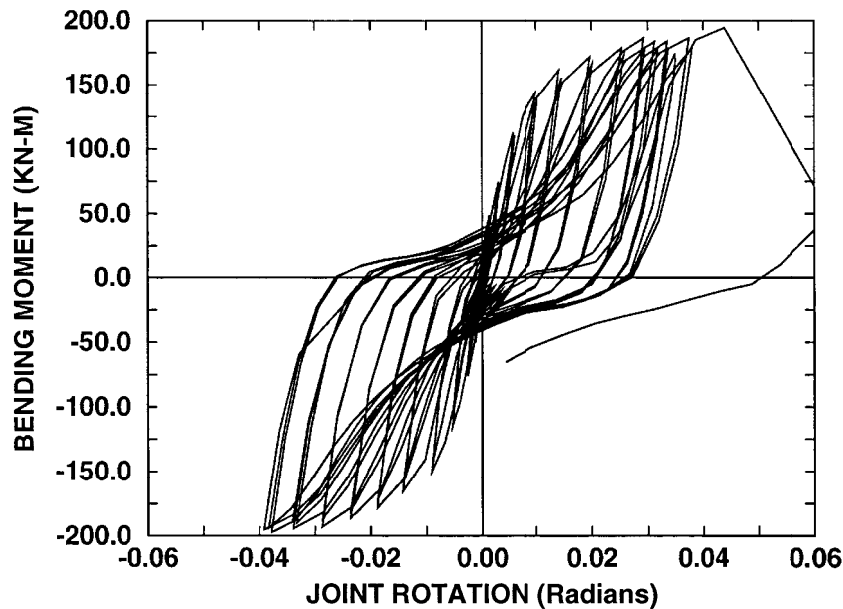


**Figure 1-10 Moment-Rotation of Riveted Connection with Large Rotational Capacity**

Welding became increasingly economical and practical during the 1960s. Welding engineers gained a better understanding of the chemistry and physics of the welding process, and they were better able to control the quality of welds with both field and shop welding. Increased economy was achieved with development of the wire feed, self shielded, flux cored arc welding (FCAW-SS) process. As a result, welded connections became increasingly practical during this decade.

#### **1.4 Development of Pre-Northridge Connection**

In the late 1960s and early 1970s, the seismic design practice for steel moment frames evolved to include increased use of welding. A few buildings were constructed with welded-flange-welded-web connections. However, the practice quickly evolved to the welded-flange-bolted-web moment resisting connection illustrated in Figure 1-12. This connection was chosen because of extensive research (Popov and Pinkney, 1969, Popov and Stephen, 1970, Krawinkler et al., 1971, and Bertero et al., 1973), and because of the greater economy of this connection over the welded web connection. The research focused on the inelastic performance of the connection, because large inelastic deformations are expected during major earthquakes due to the reduced forces used in seismic design. As illustrated in Figure 1-13, these tests showed that better inelastic cyclic behavior was achieved with the fully welded-flanges and bolted-webs than with bolted connections such as used in earlier structures. The hysteresis curves were full, and the strength and stiffness remained stable through large inelastic deformations. Furthermore, this connection developed the full plastic capacity of the beam, avoiding a potentially brittle failure in the connection or net section. It must be noted that the experiments used to justify this FR connection were on beams with a depth and weight no greater than 24 inches and 76 lbs/ft, respectively. These sizes were not serious limitations since even very tall steel frames of the

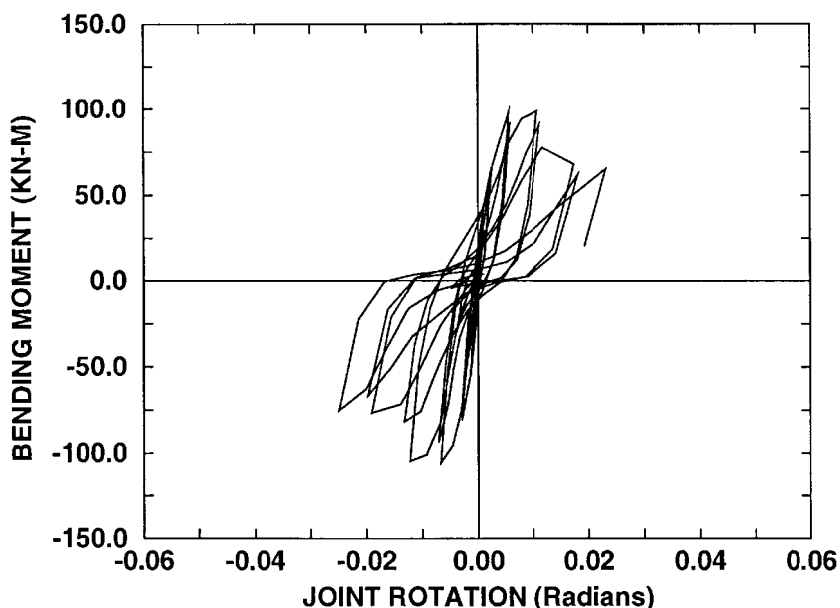


**Figure 1-11 Moment-Rotation of Riveted Connection with Small Rotational Capacity**

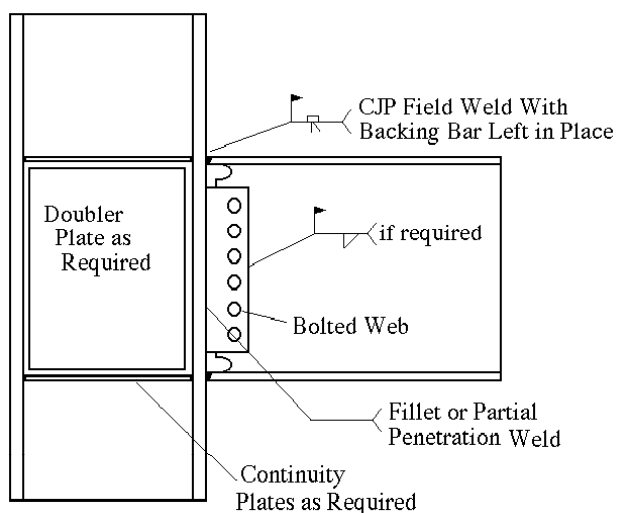


**Figure 1-12 Fully Restrained Welded-Flange-Bolted-Web Connection**

early 1970s seldom had beams greater than this depth. Therefore, welded-flange-bolted-web connections such as those schematically illustrated in Figure 1-12 became the normal connection for seismic design. These connections have a complete joint penetration (CJP) weld connecting the beam flange to the column, and an erection plate bolted to the web for transfer of shear force. Continuity plates are often required to prevent local damage to the column flange and web and to help assure uniform stress in the beam flange. Panel zone doubler plates may be required to control panel zone yield and deformation, although a few buildings used diagonal stiffeners in the panel zone rather than doubler plates.

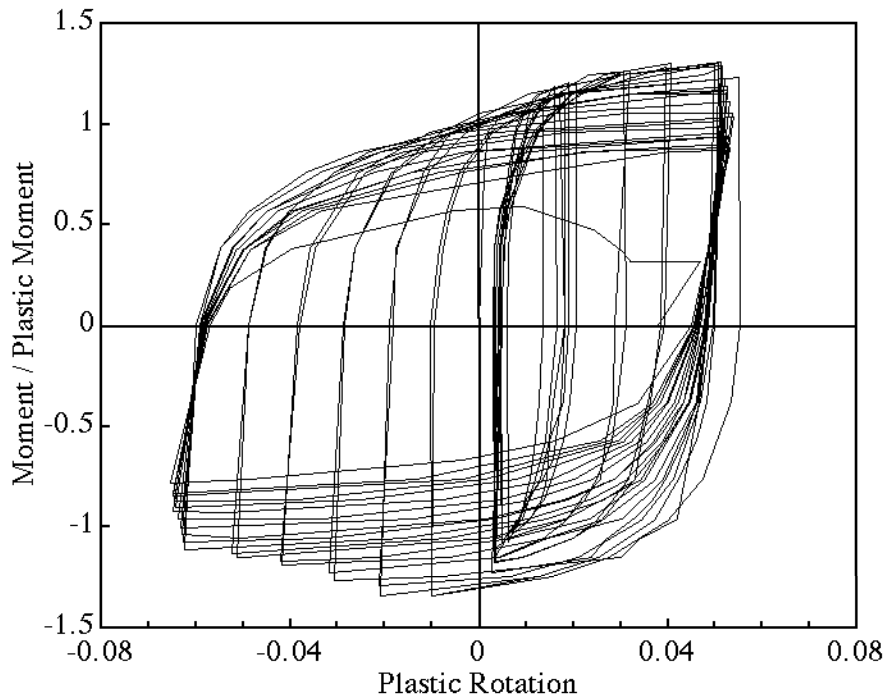


**Figure 1-13 Moment-Rotation Behavior Observed in an Early FR Connection Test**

This early research established the general directions of seismic design, and the design rules for welded-flange-bolted-web connections remained fairly stable until the mid 1980s. However, a number of changes in the design specifications and professional practice occurred during the years that followed. In 1988, the Uniform Building Code (UBC) (ICBO, 1988) increased the predicted shear strength of panel zones. This increase was based on observations of the good ductility provided by panel zone yielding in tests (Bertero, 1973, Krawinkler, 1971, Popov, 1986). These tests showed that panel zone yielding results in reliable energy dissipation with considerable strain hardening. Building codes increased the rated shear strength of the panel zone in recognition of this added strain hardening resistance. The increased panel zone strength rating meant that steel frames built since approximately 1988 will sustain larger inelastic deformation in the panel zone during an earthquake, since the panel zone will initially yield at a smaller seismic event before beam yielding occurs. Another change to the UBC (ICBO, 1988) required supplemental welding of the beam web to the shear plate for beams where more than 30% of the plastic moment capacity of the beam is developed by the web. Other changes occurred during the period after 1970 and before the Northridge earthquake. Engineers built increasingly lighter and far less redundant structures than before. Seismic resistance was concentrated in fewer frames and even single bays within individual frames. This resulted in the use of much heavier members, and these members were much deeper and heavier than those tested in the 1960s and early 1970s. At the same time, lighter partitions, cladding and fire protection were used in newer buildings. As a result, newer steel frame buildings had little secondary strength and stiffness as compared to the steel moment frames built in the 1970s and earlier.

The Northridge earthquake occurred on January 17, 1994, and steel frames experienced cracking during the earthquake. The cracking had a number of different variations, many of which had not been observed in past experiments. The damage was unexpected and ultimately led to the SAC Steel Project and funded by FEMA. The research and study of this project provides the basis for this report.

## 1.5 Organization of Report

As noted earlier, this state of the art report will provide a complete overview of seismic performance of steel moment frame connections. The report deals with the seismic capacity and performance of the connections rather than the demand, since demand issues are covered in other state of the art reports (Krawinkler, 2000; Foutch, 2000).

- This first chapter has provided a brief historical summary and overview of the connection performance issues.
- Chapter 2 focuses on the pre-Northridge welded-flange-bolted-web connections. It attempts to show what went wrong with this connection, and it discusses the connection's potential for future seismic design. Chapter 2 provides guidance as to the expected performance of these connections in future earthquakes, so that engineers may make rational decisions regarding repair or retrofit. Many general parameters affecting connection performance are introduced in this chapter, because much of our basic understanding of these parameters is based upon pre-Northridge connection experiments. Nevertheless, these same parameters also affect most other post-Northridge connections.
- Chapter 3 discusses a wide range of post-Northridge connections. In general, these connections include both bolting and welding, but several variations including improved welding, haunches, coverplates and other modifications that are used to enhance connection performance.
- Chapter 4 provides information on other general issues of concern for a wide range of connection types. These issues include the effect of static vs. dynamic load rate, column depth and orientation, presence of composite slabs, and lateral bracing of beams. The issues are important to a wide range of connection types, but they are particularly relevant to the post-Northridge connections of Chapter 3, because of their greater resistance and ductility. Some of the issues discussed in Chapter 4 are follow up discussion of topics raised in Chapter 2, since tests on post-Northridge connections provides further insight into these behaviors.
- Chapter 5 discusses a wide range of alternative connections. In general, these alternative connections are partially restrained (PR) moment connections which place increased emphasis on the use of high strength bolts. Some of these alternatives were used for seismically resistant construction in the past, but typically the design rules used in this past practice are well below the standards that would be required for present day seismic design.
- Chapter 6 discusses supplemental connections. These supplemental connections are often relatively new and may sometimes be used to reduce the amount of repair and modification that is required to retrofit existing buildings. In other cases, they may be used to enhance the performance for connections in new buildings.

- Chapter 7 summarizes the report and emphasizes the more important general conclusion from the work. This report includes many equations, which are used to estimate connection performance, and the section summarizing the notation used for these equations is included after Chapter 7.
- Finally, an extensive bibliography is included in this report so that the reader can further study specific issues. The report will attempt to provide a comprehensive understanding of connection performance under seismic loading.

## 2. PRE-NORTHRIDGE CONNECTIONS AND FACTORS AFFECTING THEIR PERFORMANCE

### 2.1 Welded-Flange-Bolted-Web Connection

Welded-flange-bolted-web connections were the mainstay of west coast steel moment-frame design for many years. These connections have CJP groove welds connecting the beam flanges to the column, and an erection plate (or shear tab) is shop welded to the column with fillet or groove welds and bolted to the beam web for transfer of shear force as illustrated in Figure 1-7. Continuity plates were often used to stiffen the column flange or web to resist the large forces transmitted by the beam flange. This connection was considered as almost ideal for inelastic seismic performance. It was prequalified (ICBO, 1988) for use in seismic design with minimal design calculations.

#### 2.1.1 Evolution of the Research

There was considerable evidence that this welded-flange-bolted-web connection was suitable for seismic design. The excellent hysteretic behavior illustrated in Figure 1-8 is one example of this strong support. However, there was also evidence that there were problems with this connection. More than 100 experiments on these connections were performed before the Northridge earthquake. Popov and Pinkney (1969) tested 24 steel beam-to-column connections with W8 beam sections. The experiments examined the consequences of directly welding the beam flange to the column flange as well as bolted or welded-flange-plate connections. Most of these earlier specimens were welded with the shielded metal arc welding (SMAW) process. Several connection variations with weak axis column bending were also examined. Popov and Stephen (1971) tested eight welded-flange connections with W18 and W24 beams. Both monotonic and cyclic tests were performed. Two of the eight specimens had welded-webs, and they both attained significantly larger plastic rotations than comparable bolted-web connections. One of the eight specimens had no web connection, and its performance was inferior to the other specimens. Figure 1-13 shows the moment-rotation hysteresis behavior achieved with the welded-flange-bolted-web connection in one of these early tests. The hysteresis curves are full with little of the pinching or deterioration that was noted with many other connection types. Deterioration of these hysteresis curves was usually caused by local buckling of the beam (flange buckling, web buckling, or lateral torsional buckling). Fracture of the flange weld was often noted, but in these early experiments fracture occurred only after plastic rotations larger (sometimes significantly) than 0.02 radians. The 0.02 plastic rotation capacity was considered adequate for seismic design at that time.

The initial connection studies used a cantilevered beam test arrangement as illustrated in Figure 2-1. Later studies (Krawinkler, et al., 1971, Bertero, et al., 1973) examined the behavior of subassemblages that simulated overall frame behavior rather than simply considering connection behavior as depicted in Figure 2-2. These tests all employed welded-flange-bolted-web connections, but unlike the earlier tests, they included the effect of gravity loading on the beams and columns. These later subassemblage tests showed the importance of panel zone yielding. They verified that panel zone yield can provide a major contribution to frame deformation, story drift, and energy dissipation. Panel zone yielding often produces excellent

inelastic performance with desirable energy dissipation characteristics. However, panel zone yielding causes much larger apparent strain hardening than does flexural yielding, because the flanges participate in shear transfer after the initial yielding of the web. The inelastic deflections of the panel zone are not easily predicted, and as a result, the inelastic response of the frame is less easily defined if panel zone yielding is employed. Further, the inelastic strain in the panel zone causes strain concentrations at critical locations near the welded flanges.

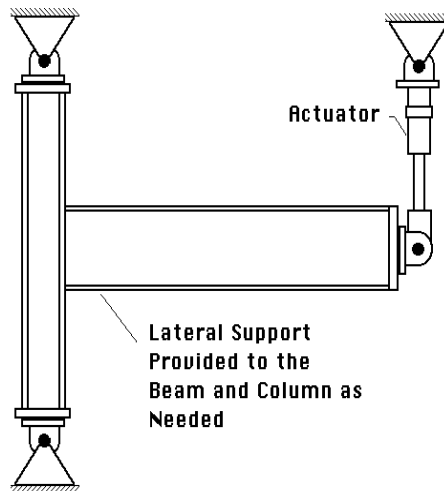


**Figure 2-1 T-Shaped Test Assemblage**

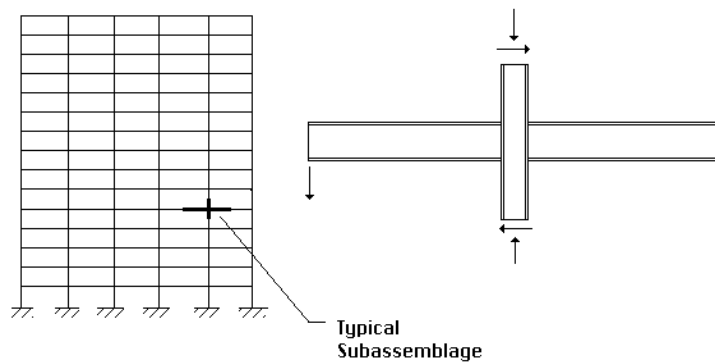


**Figure 2-2 Cruciform Test Subassemblage**

Yielding in the columns (Popov, et al., 1975) as opposed to yielding in the beams and panel zones was also examined. Flexural yielding of columns resulted in more rapid deterioration of the resistance and energy dissipation for columns with large axial load. The culmination of the early studies on welded-flange-bolted-web connections (Krawinkler, et al., 1971, Bertero, et al., 1973, Popov, et al., 1975) was used to establish design requirements including flange and web slenderness, lateral support requirements, the strong-column-weak-beam design philosophy, and continuity plate and doubler plate requirements for seismic design. This early research established the seismic design procedures that were used for the years that followed, and the welded-flange-bolted-web connection was prequalified based on this early work.

Later studies began to show the potential problems with welded-flange-bolted-web connections. In 1986, Popov and others (Popov, Amin, Louie, and Stephen, 1986) reported on connection tests with somewhat heavier flanges. These beams were W18, W21, and built-up sections, but the weight per foot was somewhat larger than comparable depths in earlier tests. Further, the beam lengths were quite short. These tests showed small flexural ductility. However, panel zone yielding occurred in many of these tests, and the consequent ductility resulted in a relatively favorable interpretation of the tests despite the lack of flexural ductility noted. Several years later, Tsai and Popov (1988) performed an experimental study on 18 connections with W18 and W21 beams. These tests were among the first to focus on the welding process used to fabricate the test specimens. The tests considered both SMAW and FCAW-SS as well as bolted-end-plate connections and connections with supplemental web welds. Again, many of these tests showed a limited specimen ductility. Figure 2-3 is one load vs. plastic rotation curve from this test program, and it shows ductility, which was clearly inadequate by seismic design criteria. Although this lack of ductility was noted by the engineering profession, it resulted in relatively minor changes in the design specifications. Supplemental welding of the web was required for connections where more than 30% of the plastic moment capacity of the beam was developed by the web.

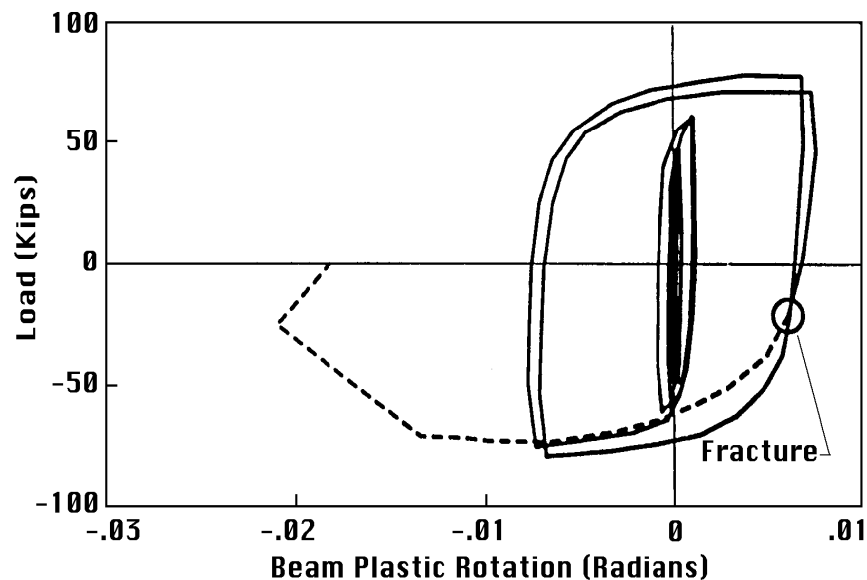


**Figure 2-3 Load vs. Plastic Rotation for 1988 Study**

Further concerns regarding moment resisting connections were raised in later studies. Schneider, et al. (1993) reported on an experimental study that addressed weak-column-strong-beam behavior. This study was initiated in response to a relaxation of the restrictions against weak-column behavior in the 1988 UBC. The study examined the experimental behavior and ductility capacity of the connections, as well as the ductility demand required with present day structural designs and earthquake acceleration records. This work clearly showed that modern structural concepts result in much larger ductility demand than the more redundant systems used earlier. The experimental results showed that weak-column steel moment frames would likely be unable to achieve adequate ductility to provide satisfactory behavior in these structures for

many of these newer systems. Also in 1993, Englehardt and Hussain (1993) reported on a series of experiments on connections with relatively deep W30 beams. These specimens had very little ductility, since the plastic rotations achieved in most of these tests were even smaller than those noted in Figure 2-3. However, the Northridge earthquake occurred approximately one month after this paper was published, and there clearly was insufficient time for the design specifications and professional practice to respond to this research prior to the earthquake.

### **2.1.2 Evolution of Professional Practice in Steel Frame Construction**

This discussion of past research shows that there was strong evidence from the earlier studies to suggest that the welded-flange-bolted-web connection would provide acceptable seismic behavior. At first, these connections were used at nearly all beam column connections in the structural system. This results in a good distribution of the lateral stiffness and resistance, and as a result, member sizes and connections were relatively small. Many 20- and 30-story steel moment-frame buildings were constructed in the 1960s and early 1970s with beams in the W21, W24, and W27 size categories. These member sizes were not inappropriate when compared to the connection tests that had been completed by that time. For increased efficiency, engineers later provided seismic resistance only in perimeter frames of the structure. Perimeter frames reduced the number of moment-frame connections and increased the member and connection size. Further reductions in the number of connections later occurred because of concentration of the seismic resistance into individual isolated frames or bays of frames, and this also resulted in a further increase in member size. This concentration of the seismic resistance into small parts of the structure meant that even 2- and 3-story buildings would require beams in the W36 and W40 size category. This practice should have been questioned, because no tests were completed on connections with members approaching these sizes until shortly before the Northridge earthquake. A more recent examination (Roeder and Foutch, 1996) of all the data summarized earlier, suggested that the pre-Northridge connection detail illustrated in Figure 1-12 might be affected by factors not usually considered in design. Figure 2-4 illustrates the measured ductility of all tests performed in the US on pre-Northridge welded-flange-bolted-web connections with strong axis bending of the column and no supplemental reinforcement of the connection. This comparison suggested that deeper beams would result in significant reductions in the plastic rotational capacity of the connection. Similar comparisons suggested that panel zone yielding and weak axis column orientation might also reduce connection ductility. Past research (Schneider, et al., 1993) has shown that the demands upon connections with the less redundant frame configurations as used in recent years can be significantly greater than that required with more redundant configurations.

Changes in the steel and welding processes and electrodes also require consideration in evaluating the seismic behavior of these connections. The average yield stress of mild structural steel steadily increased from the 1950s and later. In addition, design has historically been based upon the nominal yield stress, which is selected by statistical evaluation of the measured yield stresses to be significantly lower than the mean yield values. The actual performance of buildings, however, depends on the actual properties of the steel used in the structure. Lower yield strength and lower yield-to-tensile-strength ratios permit earlier yielding and the development of plastic deformation in the beams without developing high stresses in the welded joint. In the early 1970s, some welded-flange connections were still welded with the SMAW process. During the 1970s, the wire feed FCAW process became the dominant weld process. As

time progressed, the large diameter E70T-4 electrodes became the electrode of choice for field welding flange joints. These changes raise issues that must be considered in this state of the art report.

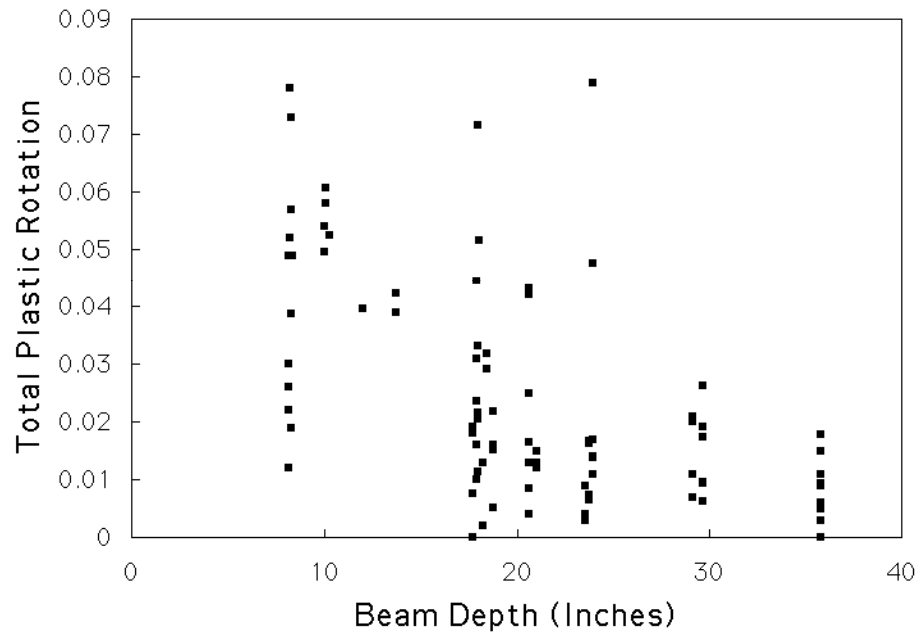


**Figure 2-4 Total Plastic Rotation vs. Beam Depth for Pre-Northridge Connection**

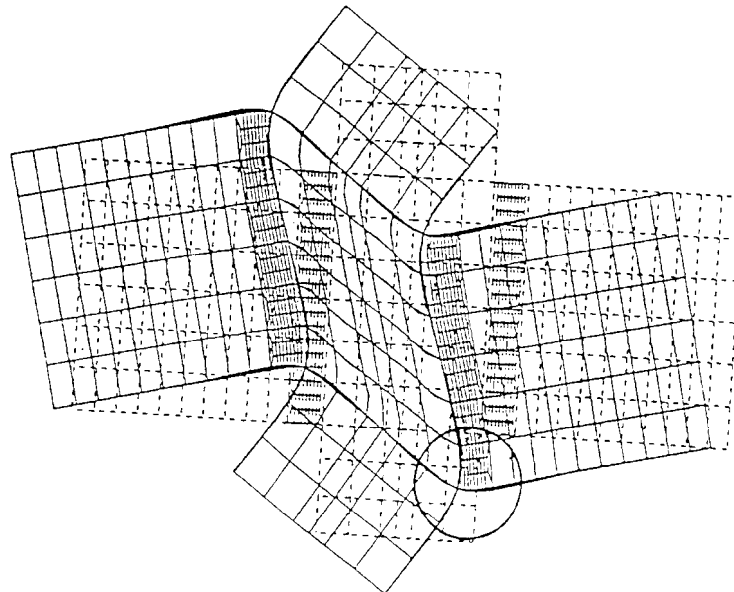


**Figure 2-5 Deformed Finite Element Mesh of Connection with Panel Zone Yield**

Design provisions for the welded-flange-bolted-web connection remained relatively unchanged throughout the 1970s and early 1980s. Building codes (ICBO, 1988) changed in

1988 to increase the rated shear strength of panel zones. This increase was based on observations of the excellent ductility and large apparent strain hardening provided by panel zone yielding. However, the increased panel zone strength rating meant that steel frames built since 1988 are more likely to sustain larger inelastic deformation in the panel zone during an earthquake. The large shear deformation in the panel zone causes large local stress and strain concentrations near the flange welds. This is illustrated by the severe local distortion noted within the circled area of the deformed finite element mesh in Figure 2-5. This local distortion causes large stresses at the weld, where it is known that ductility is least likely to occur. Further, panel zone yield invariably produces large apparent strain hardening so that significant increases in the beam moments and stresses in the flange welds must be expected. Therefore, the effect that panel zone yielding had on behavior of these connections during the Northridge earthquake is of considerable concern.

In 1988, the UBC (ICBO, 1988) required supplemental welding between the beam web and the shear tab in addition to the bolted-web connection illustrated in Figure 1-12. This supplemental welding was introduced for connections which developed more than 30% of the plastic capacity in the beam web. This supplemental welding clearly changes the stiffness and deformability of the connection, and it is not clear whether it helped or hindered the connection performance.

On January 17, 1994 the Northridge earthquake occurred. Early reports suggested that steel moment-frame buildings experienced little damage, but several weeks later reports of significant cracking and connection damage were noted. A building damage survey (Youssef, et al., 1995) and database (Bonowitz and Youssef, 1995) were accumulated in the months after the earthquake, and they provide useful information regarding the extent and type of cracking. Many of the weld cracks were visible cracks, but some were detectable only by nondestructive evaluation methods. There is evidence that the cracks detected only by ultrasonic inspection were frequently introduced during initial construction because of inadequate inspection and quality control. As a result, only cracks that were detected by visual inspection are included in the statistics discussed here. Approximately 32% of the frames inspected had cracking in the weld, beam, or column, and 15.7% of the inspected frames had cracking in the beam or column. The crack usually initiated at the flange weld, and a small number progressed through the column flange into the panel zone of the beam column connection. Most of the cracks started at the bottom flange weld, but some were noted at the top flange weld. Cracking in the beams outside the welded region was noted in a relatively few damaged frames.

The database indicates that cracking was more common in newer buildings. Approximately 50% of the inspected frames designed after 1990 had cracking in the welds, beams, or columns, and 27.7% of these newer frames had cracking in the beams or columns. This crack frequency is approximately 80% larger than the average frequency for all specimens, and the comparison suggests that buildings designed since 1990 were much more susceptible to cracking damage than the average. The database shows that buildings designed before 1980 had cracking in beams, columns, and welds in approximately 24.5% of the frames inspected, and approximately 12.5% had cracking in beams and columns. This is about 30% smaller than the average frequency, and the comparison indicates that older structures had less tendency toward cracking than average. In fact, the inference may be stronger than suggested by this statistic, since most of the cracking observed in buildings designed prior to 1975 is concentrated in a single building.

If this building is not included in the data, buildings designed before 1975 had cracking in the welds in approximately 3% of the frames inspected, and none of the frames had cracking in the beams and columns. Statistics of this type must be used with care; however, the data suggests that recent changes in the code requirements and engineering practice contribute to the problem.

The database also shows that the cracking damage was more significant in steel frames with deep beams and thick beam flanges. As noted earlier, 15.7% of the frames inspected as part of the survey had cracking in the beams or columns. However, none of the frames with beam depths less than W21 had cracking of this type, and approximately 18.5% of the floor frames with beams W30 or deeper had these visible damage types. This statistic is quite important because frames with cracking in the beams and columns usually were more severely damaged than those with weld cracking only. Weld cracking exhibits similar statistical comparisons. Deep beam sections have significantly larger frequencies of weld cracking than shallow (W21 or less) or intermediate beam depths. Further, the intermediate beam depths with visible weld cracking had greater frequency of cracking in heavier sections with thick flanges. Other factors such as span length, flange thickness, panel zone yielding, and column orientation also contribute to this observed distribution of damage. However, the concentration of damage in deeper and heavier beams must be a matter of some concern, since deeper beams are a natural consequence of the reduced redundancy and reduced number of welded-flange-bolted-web moment connections used in recent years.

### 2.1.3 Issues of Concern

This brief discussion has provided an overview of the past research into the welded-flange-bolted-web connection and the evolution of the connection design practice. The research has shown that the pre-Northridge connection will provide extremely good inelastic performance under some conditions. However, the pre-Northridge connection will provide poor performance under other conditions. It is important to be able to separate these performance levels, since they have great impact on the evaluation and retrofit of existing buildings as well as construction of new facilities. Several unanswered questions must be addressed, and numerous issues must be examined to determine their effect on the seismic behavior of the connection. These issues include:

- Effect of different types and grades of beam and column steel on connection performance.
- Role of panel zone yielding in the connection behavior.
- Geometric parameters of the connection including beam depth, flange size, and weld size.
- Effect of weld electrode and process on connection performance.
- Strain rate and dynamic effects.
- Effect of supplemental web welding on connection behavior.
- Load and deformation history.

Ductility demand is not the issue of concern in this report, but some consideration of its effect on connection performance is appropriate, since the demand may affect some connection capacity issues. The effect of redundancy and weak column behavior are two demand issues that

also affect capacity and connection behavior. In addition, degradation of resistance and stiffness are capacity issues that may also have a significant effect (Krawinkler, 2000) on the seismic demands. As a result, some of these interrelated issues are discussed in this report.

## 2.2 Modes of Failure

Capacity issues including resistance, stiffness, and ductility of connections are the parameters of primary interest of this State of the Art Report. The stiffness of welded-flange-bolted-web connections is normally large enough that the elastic flexibility of the connections does not require special consideration in the global frame analysis. Therefore, the focus of study for this connection type is on the resistance and ductility of the connection. Yield mechanisms and failure modes are the factors that control both the resistance and ductility or rotational capacity of the connection. This is illustrated by comparing the moment-rotation behavior shown in Figure 1-13 to that of Figure 2-3. Figure 1-13 shows the moment-rotation behavior of a connection with a W18 beam with significant flexural yielding of the beam and ultimate failure due to local buckling and deterioration caused by the large inelastic deformation. Figure 2-3 was a similar size specimen with weld fracture, and it provides significantly less ductility, energy dissipation, and plastic rotational capacity. Thus, the change in yield mechanism and failure mode had great impact on the relative performance of these two connections.

Failure modes and yield mechanisms are related, but are inherently different. Failure modes cause fracture, loss of deformation capacity, or significant loss of resistance. A single failure mode will cause reduced ductility and loss of resistance, but it does not necessarily result in the loss of all resistance as can be illustrated in the moment-rotation curve of Figure 2-6. This figure shows the moment-rotation curve of a connection which had an initial flange weld fracture on the first cycle to 0.02 radians plastic rotation, and a second flange fracture on the reversal of the initial cycle. It can be seen that both after the initial fracture and the second fracture, the connection retained 25% to 40% of its moment capacity at rotations significantly larger than the rotation causing fracture. This shows that, while an initial failure mode is a matter of considerable concern, it does not necessarily mean that a connection loses all ability to support load and sustain inelastic rotation when initial failure occurs.

Yield mechanisms induce inelastic deformation and result in dissipation of energy and changes in stiffness without inducing fracture or excessive loss of resistance. Some yield mechanism and failure mode combinations produce ductile behavior, others result in brittle failure, and still others produce intermediate results. Significant plastic rotational capacity can be achieved when the resistance associated with one or more ductile yield mechanisms is well below the resistance associated with all failure modes. Limited plastic rotational capacity must be expected when the resistance associated with a brittle failure mode is smaller than that associated with ductile yield mechanisms. These yield mechanisms, failure modes, and the resistance associated with them must be understood if each connection type is to be rationally used in seismic design.

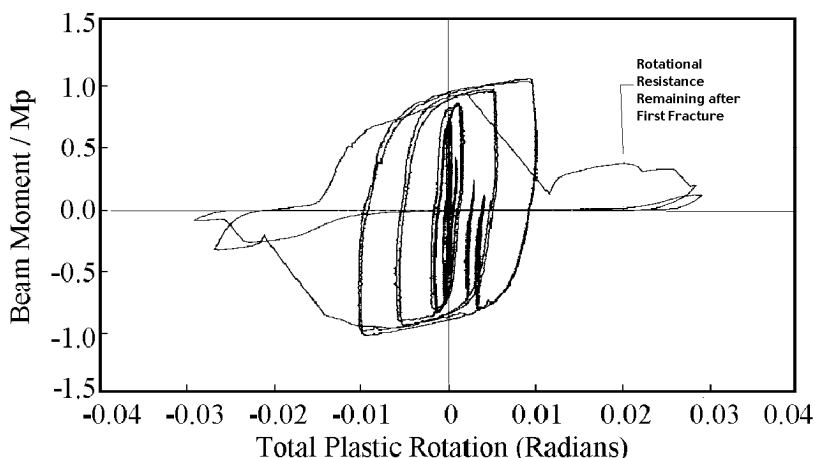


**Figure 2-6 Moment-Rotation Curve Illustrating Resistance After Initial Failure**

Figure 2-7 illustrates the common yield mechanisms for welded-flange-bolted-web connections. Yielding of the columns is normally discouraged or prohibited for the reason that frame systems built with weak-column behavior are known to have significantly larger inelastic story drifts and local ductility demands (Schneider et al., 1993) than comparable frames with yielding of the beams. As a result, flexural yielding of the beam and panel zone yielding are the yield mechanisms of common interest for framing systems that utilize this connection. Other local forms of yielding such as local yielding of the web and flange of the column may occur, and may induce some inelastic deformation, but these cannot cause large enough inelastic deformations to achieve significant plastic rotation.

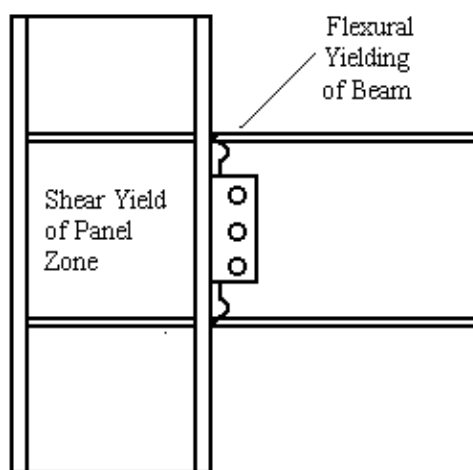


**Figure 2-7 Typical Yield Mechanisms for Welded-Flange-Bolted-Web Connections**

Figure 2-8 shows the typical failure modes that may be noted with the welded-flange-bolted-web connection. These failure modes are quite diverse. Fractures may occur in the weld or at the beam weld access hole, or fracture may initiate at the weld and progress into the column. Failure due to tearing, fracture, or excessive deformation may occur in the column web or flange

due to inadequate continuity plates. Panel zone yielding and beam flexure are clearly yield mechanisms, but they may also be failure modes, since failure also may occur due to tearing of the steel due to excessive plastic deformation. However, the resistance associated with these failure modes will be larger than the resistance associated with initial yielding, since they require consideration of the large amount of strain hardening that occurs in ductile connections. Lateral torsional buckling of the beam and local buckling of the beams and webs may also be failure modes for the connection, since they may lead to reduced resistance at larger deformations and ultimate tearing of the steel. Finally, fracture or tearing of the shear tab may occur, but past experiments have shown that this failure mode normally occurs only after another failure mode has initiated.

This section of the report will examine and explore the yield mechanisms and failure modes that are possible for welded-flange-bolted-web connections. The influence of different parameters on connection behavior will be noted. The focus will be on the pre-Northridge connection, since it is important to understand the causes of damage in this connection. However, most of the work described here will lead to improved performance of the welded-flange connections, and these improved connections will be discussed further in later chapters.

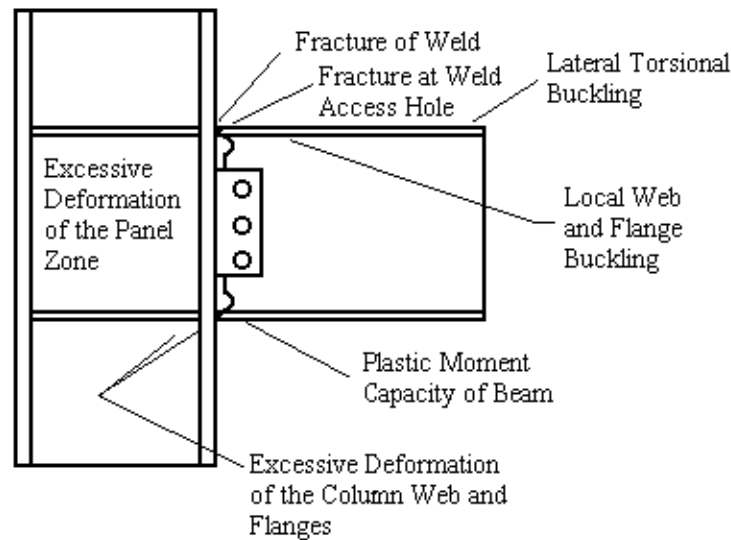


**Figure 2-8 Typical Failure Modes for Welded-Flange-Bolted-Web Connections**

### 2.2.1 Effect of Member Size and Geometry

Figure 2-4 has already shown that, on average, less ductility can be expected from deep beams than from shallow beams. This can be noted for all connection types, and the reasons for this are apparent from elementary mechanics as illustrated in Figure 2-9. This figure illustrates the elastic and plastic strain distribution in two beams which are identical except for beam depth. The plastic curvature is the difference between the plastic strains at the two extreme fibers divided by the beam depth. The plastic strain that can be tolerated by a deep beam is also a property of the material and flange geometry and is clearly not increased by increasing beam depth. Therefore, the maximum plastic curvature for a deep beam must be smaller than that

obtained for a shallow beam of the same material and flange geometry. The plastic curvature is integrated over the yield length to obtain the plastic rotation, and so smaller plastic rotations must be expected for deeper beams if the beam length is essentially constant. In general, if the beam depth is doubled, the maximum plastic rotation achievable with this connection must be, on average, reduced by half. This is observed in Figure 2-4, and it can apply to all connection types.

Short-span beams will have less inelastic rotational capacity than longer span beams. Elementary mechanics also provides a basis for understanding this phenomenon as illustrated in Figure 2-10. The moment diagram of a moment frame beam under seismic loading is in double curvature as illustrated in Figure 2-10. Welded-flange-bolted-web connections are designed so that plastic hinges form near or at the face of the column. The plastic hinge (and the corresponding plastic rotation) of the beam develops entirely over the short length of the beam where the moment is larger than the yield moment,  $M_y$ . This length is limited by the plastic moment,  $M_p$ , the strain hardening of the steel, and the length of the beam. Regardless of the length or depth of the beam,  $M_y$  will occur when the yield strain is reached at the extreme fiber, and  $M_p$  is achieved at plastic strains which are 3 to 6 times larger. The length of the beam does not change the maximum strain level capacity or the maximum curvature achievable with a given beam section. The plastic curvature is largest at the maximum moment, and it decreases to zero at the yield moment. The plastic rotation is the integration of the plastic curvature over the yield length. Therefore, the plastic rotation of the beam depends upon the length of the beam if the beam depth is constant, because the plastic curvature is accumulated over a proportionally shorter length. If the beam length is cut in half, the plastic rotation achievable by that beam is also cut in half. Variations in the strain hardening and yield to tensile ratio cloud this observation in individual experiments. Connections that do not develop their plastic hinge over a length of the beam do not exhibit this behavior.

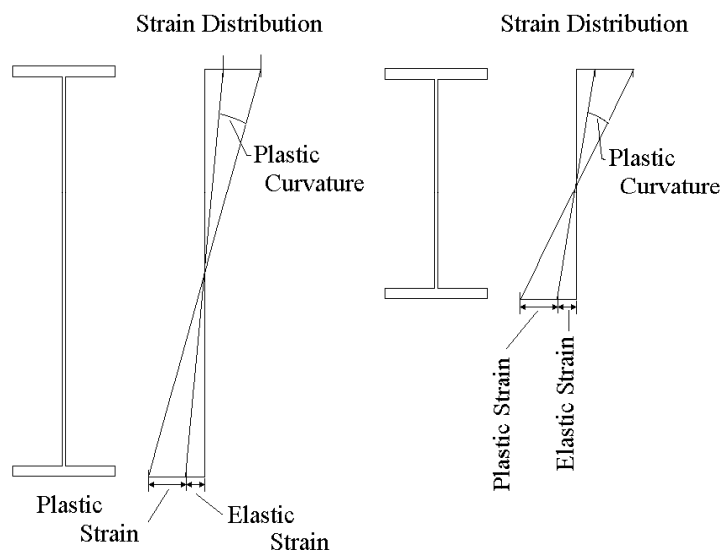


**Figure 2-9 Elastic and Plastic Strain Distribution in Beams of Different Depth**

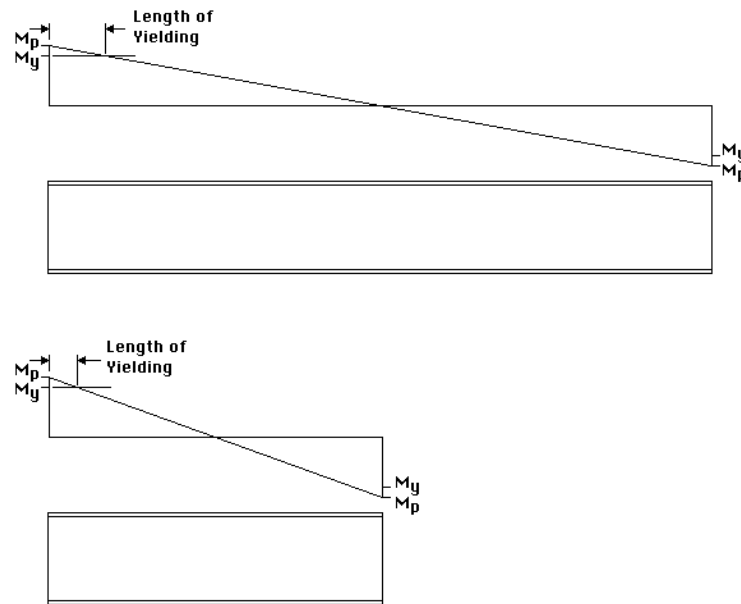


**Figure 2-10 Schematic Illustrating Span Length Effect**

These aspects of connection behavior are important to structural engineers, since they have considerable impact upon the performance that may be expected for a given structural design. As a result, span length and beam depth limits will be established for many connections throughout this report.

### 2.2.2 Effect of Panel Zone Yielding

The effect of panel zone yielding on connection performance is also an issue of concern. Panel zone yielding has been shown (Krawinkler, 1978) to provide considerable ductility in inelastic cyclic deformation, and recent building codes have placed increased emphasis upon utilizing this ductility in seismic design and reducing the number of doubler plates required in seismic design. This practice raises the logical question (Englekirk, 1999) as to whether weaker panel zones contributed to the Northridge damage and as to what level of panel zone shear yield deformation should be tolerated in seismic design. As a result, some research addressed this issue.

One study (Chi et al., 1997) performed elastic and inelastic fracture analyses of pre-Northridge and modified connections. The analyses showed that high shear stress in the panel zone and high stresses in the column flanges may direct cracks that initiate at the welded joint into the column. Column cracking is clearly one of the least acceptable modes of failure in moment-frame connections. Further, analysis showed that the CTOD (crack tip opening displacement) ductility demand was larger in connections with a larger panel zone yielding, and this implies that greater CVN toughness is required of the steel and weld metal if extensive panel zone yielding occurs. Another study (El Tawil and Kunnath, 1998) performed a wide range of 3-dimensional nonlinear analyses with the ABAQUS computer program. In these analyses, the potential for plastic yielding and fracture were evaluated at critical locations by examination of the Von Mises stress state parameter and the hydrostatic stress state parameter. These analyses

verified that extensive deformation of the panel zone must be achieved before the panel zone develops the shear capacity predicted by the AISC design provisions. These large panel zone deformations cause large local deformations such as noted earlier and depicted in Figure 2-5. The analyses showed that these large local deformations increase the hydrostatic and principle stresses at critical areas of the connection and increase the potential for connection fracture.

Part of one experimental investigation (Lee et al., 2000) was initiated to evaluate the pre-Northridge connection and connections with the same geometry but with notch-tough weld filler metals. The goal of this investigation was to address several issues including the effects of panel zone yielding, notch-tough filler metals, material properties of the steel, and the size and geometry of the specimens. The results of these tests were to be compared to the results of SAC Phase I testing (Roeder, 1996) to establish a complete picture of these issues. Table 2-1 summarizes the results of these tests. Some specimens were designed to have very strong panel zones while others had intermediate or very weak panel zones. The results of these tests did not provide a clear picture of the effect of panel zone yielding, because all specimens provided minimal ductility even when notch-tough filler metals were used. In some specimens, panel zone yielding appeared to provide a slight increase in ductility over that achieved with no panel zone yielding, but the increase was so small that the results are not conclusive. Consequently, this test program shed relatively little light on the issue.

As a result, the large body of test data, including the project tests and the older tests illustrated in Figure 2-4, were analyzed to consider the effects of panel zone behavior. Experiments clearly show that panel zone yielding occurs when the shear in panel zone,  $V_{pz}$ , reaches approximately

$$V_y = 0.55 F_{yc} d_c t_{wc} \quad (2-1)$$

Figure 2-11 shows the equilibrium conditions for computing  $V_{pz}$  for a typical cruciform test subassembly. Common practice has resulted in rounding this equation in the AISC LRFD provisions to

$$V_{yAISC} = 0.6 F_{yc} d_c t_{wc} \quad (2-2)$$

Krawinkler (1978) derived another equation which estimated the ultimate capacity of the panel zone connection. The panel zone was assumed to have an average shear strain that was four times the yield shear strain, when  $V_p$  was developed. The initial equation proposed by Krawinkler was

$$V_p = 0.55 F_{yc} d_c t_{wc} \left\{ 1 + \frac{3.45 b_c t_{cf}^3}{d_b d_c t_{wc}} \right\} \quad (2-3a)$$

This equation evolved into Equation 2-3b shortly after the initial derivation.

**Table 2-1 Test Summary for Welded-Flange-Bolted-Web Connections**

<b>ID</b>	<b>Notes</b>	<b>Beam and (Column) Size</b>	<b>Maximum Rotation at Fracture</b>	<b>Estimated Maximum Rotation for Gravity</b>	<b>Failure Mode</b>
1.1	W24 beam with E70-T4 electrode.	W24x68 (W14x120)	0.0 (0.029)	0.029	Bottom flange weld divot
1.2	W24 beam with E70-T4 electrode.	W24x68 (W14x120)	0.0 (0.04)	0.03	Bottom flange weld divot
2.1	Originally intended to evaluate				Test not completed
2.2	Older Steel				Test not completed
3.1	W24 beam with notch tough (E70TGK2) electrode.	W24x68 (W14x120)	0.016 (0.027)	0.035	Top flange tear
3.2	W24 beam with notch tough (E70TGK2) electrode.	W24x68 (W14x120)	0.017	0.04	Bottom flange tear
4.1	W30 beam with notch tough electrode and weak panel zone. Note continuity plate was not properly welded.	W30x99 (W14x145)	0.018 (0.04)	0.04	Fracture in column K-zone
4.2	W30 beam with notch tough electrode and weak panel zone.	W30x99 (W14x145)	0.008	0.03	Bottom flange fracture
5.1	W30 beam with notch tough electrode and intermediate panel zone.	W30x99 (W14x176)	0.008 (0.014)	0.03	Bottom flange fracture
5.2	W30 beam with notch tough electrode and intermediate panel zone.	W30x99 (W14x176)	0.0095 (0.03)	0.03	Top flange fracture
6.1	W30 beam with notch tough electrode and strong panel zone.	W30x99 (W14x257)	0.01 (0.04)	0.03	Top flange tearing
6.2	W30 beam with notch tough electrode and strong panel zone.	W30x99 (W14x257)	0.006 (0.02)	0.03	Top flange fracture
7.1	W36 beam with notch tough electrode.	W36x150 (W14x257)	.009	0.026	Bottom flange fracture
7.2	W36 beam with notch tough electrode.	W36x150 (W14x257)	0.017	0.035	Bottom flange fracture and ultimately in beam k-line

Note: See Lee et al. (2000)

$$V_p = 0.55 F_{yc} d_c t_{wc} \left\{ 1 + \frac{3 b_c t_{cf}^3}{d_b d_c t_{wc}} \right\} \quad (2-3b)$$

Whenever the plastic panel zone shear capacity,  $V_p$ , is discussed in this report, the shear capacity given by Equation 2-3b will be the capacity under consideration.

It should be noted that the present AISC equation for  $V_{pAISC}$  is different from that developed in the original derivation. That is,

$$V_{pAISC} = 0.6 F_{yc} d_c t_{wc} \left\{ 1 + \frac{3 b_c t_{cf}^3}{d_b d_c t_{wc}} \right\}. \quad (2-4)$$

Equation 2-4 has been given approximately a 9% increase over Equation 2-3b by this round-off operation in the *AISC Specification*.

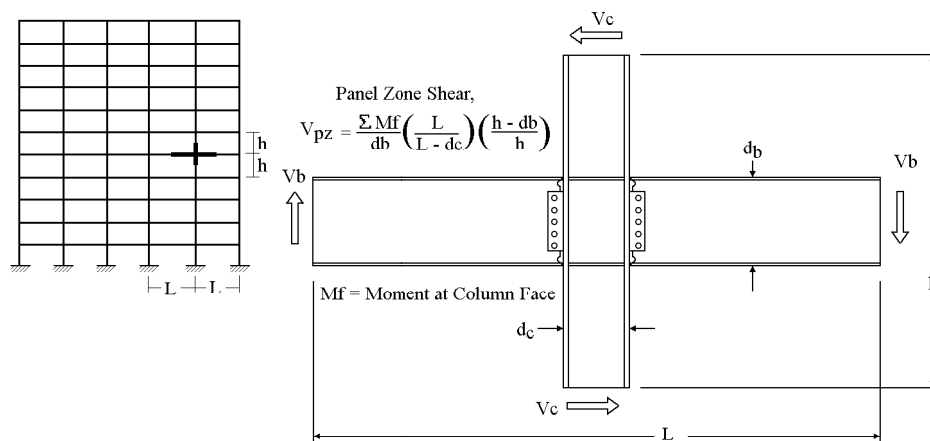


**Figure 2-11 Geometry and Equilibrium for Determining Panel Zone Shear Force,  $V_{pz}$**

Past research studies have often noted large ductility and large plastic rotations for connections with significant panel zone yielding; however, this ductility has never been consistently documented. More than a hundred welded-flange connections were examined and the plastic rotation,  $\theta_p$ , achieved with these tests was documented. These connections include some of this project's tests, but also many other pre-Northridge tests. The criteria for using the test data was that complete information on material properties, geometry, and observed behavior were available in published reports and papers. Figure 2-12 shows the plastic rotation achieved in past tests as a function of the maximum shear force in the panel zone,  $V_{pz}$ , normalized by  $V_p$  from Equation 2-3b. There is a large amount of scatter in this data, because the tests include many different beam depths and failure modes. However, specimens with large  $\frac{V_{pz}}{V_p}$  ratios are those specimens that have large amounts of panel zone shear yielding and strain hardening, and it can be seen that these specimens do not, on average, develop any more plastic deformation

than specimens with less panel zone yielding. Specimens with  $\frac{V_{pz}}{V_p}$  ratios less than 1.1 do not develop the AISC rated panel zone shear capacity as defined in Equation 2-4. It can be seen that a higher proportion of the specimens, which do not develop the AISC panel zone shear capacity, develop large plastic rotations (rotations greater than 0.03 radians) than do the specimens, which develop this target resistance.

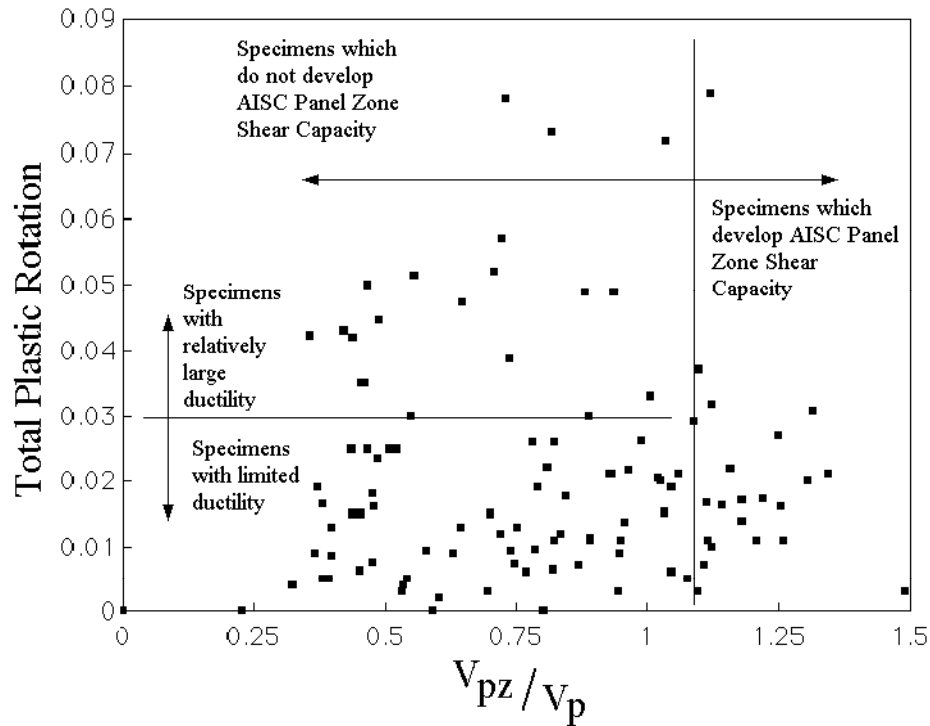


**Figure 2-12 Plastic Rotation as a Function of Normalized Shear Force**

The above comparison is important, but it does not provide a complete picture of the issue, because some specimens could not achieve  $V_p$  because flexural yielding of the beam occurred before the panel zone shear was developed. Further, panel zone yielding is clearly a yield mechanism rather than a failure mode. Panel zone yielding may lead to very much larger inelastic deformations, which may result in early failure, but panel zone yielding is a yield mechanism, and should be compared to flexural yielding in determining whether large panel zone deformations should be expected before flexural yielding of the beam occurs. Therefore, another comparison was made to illustrate the effects of the relative beam bending and panel zone resistance. The resistance associated with the panel zone yield mechanism is provided in Equation 2-1, and the resistance associated with the onset of the flexural yield mechanism,  $M_y$ , is

$$M_y = S F_y \quad (2-5)$$

where  $S$  is the elastic section modulus of the beam.

Figure 2-13 provides a comparison between initiation of the yield mechanism level for beam flexure and panel zone yielding. This figure includes the same data as Figure 2-12, but the data is expressed differently. Figure 2-13 plots the plastic rotation,  $\theta_p$ , as a function of the panel zone shear force associated in initiation of flexural yielding,  $V_{pz}M_y$ , divided by the panel zone shear yield force,  $V_y$ . Specimens with a  $\frac{V_{pz}M_y}{V_y}$  ratio less than 1.0 develop flexural yielding of the beam before panel zone yielding occurs. Specimens with ratios greater than 1.0 experience panel zone shear yielding before flexural yielding occurs. Again the test data shows that specimens yielding in flexure first, on average, have greater ductility and larger plastic rotational capacity than do specimens yielding first in panel zone shear. The largest rotational capacities are achieved with specimens which have balanced design. Balanced design implies that flexural yielding occurs first, but panel zone yielding occurs shortly thereafter. That is, the greatest ductility is achieved with specimens with ratios which are less than 1.0 but not dramatically less than this limit.

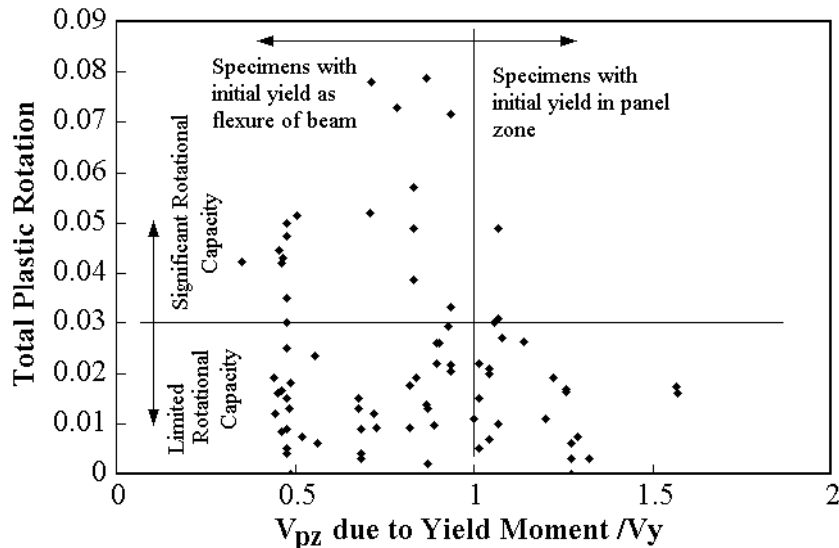


**Figure 2-13 Plastic Rotation as a Function of Relative Beam Flexure and Panel Zone Yielding**

Given that specimens with  $\frac{V_{pz}M_y}{V_y}$  ratios greater than 1.0 will experience panel zone yielding before flexural yielding, it is logical to ask whether these specimens develop the panel zone resistance predicted by present design equations. Figure 2-14 shows the normalized panel shear force as a function of the  $\frac{V_{pz}M_y}{V_y}$  ratio. Specimens with a  $\frac{V_{pz}M_y}{V_y}$  ratio less than 0.7 will have limited panel zone yielding due to flexural strain hardening. Specimens with ratios greater than about 1.1 will be dominated by panel zone yield deformation, and those between 0.7 and 1.1 will have some flexural plastic deformation and some shear panel zone yielding. If  $\frac{V_{pz}M_y}{V_y}$  is less than 0.7, the specimen generally did not reach the panel zone shear capacity predicted by  $V_p$

(Equation 2-3b) or by AISC (Equation 2-4), because yielding is dominated by flexural yielding. If  $\frac{V_{pz}M_y}{V_y}$  is greater than 1.1,  $V_p$  should clearly be achieved, because the connection is dominated by panel zone yielding. But Figure 2-14 shows that many specimens do not achieve the panel zone shear capacity of  $V_p$  (Equation 2-3b) much less the AISC panel zone resistance (Equation 2-4). Examination of the figure shows that specimens with balance conditions where  $\frac{V_{pz}M_y}{V_y}$  is greater than 0.7 but less than 1.1 have the largest number of specimens with large panel zone resistance which exceeds that predicted by Equation 2-3b.

This discussion shows that panel zone yielding can be relied upon to provide plastic rotational capacity for seismic resistant design, but total reliance on this ductility is generally inappropriate. Analyses suggest that excessive local stress and strain demands are placed upon the welded connection when large panel strains occur. Experiments suggest that specimens designed to have weak panel zones may have less plastic rotational capacity than those specimens designed for a more balanced condition. Further, experiments indicate that many specimens with weak panel zones do develop the shear resistance predicted by the design equation. At the same time, Figures 2-12 and 2-13 show that reduced ductility may be expected if the panel zone is so strong that no panel zone yielding occurs. This indicates that the best performance will be achieved in a balanced design where shear yielding of the panel zone and flexural yielding of the beam occur at nearly the same load. Panel zone yield is a yield mechanism; it is not a failure mode. Throughout all of the pre-Northridge tests, there is not a single specimen that had a web failure because of the panel zone shear force. Some specimens deformed excessively due to plastic deformation, but no failure occurred. Therefore, ductile performance is more likely if the yield capacity of the panel zone is balanced with the yield resistance of the beam in flexure. As a result, this balanced yield check is used throughout this report. A check of the ultimate shear strength of the panel zone is not recommended, for this resistance is sometimes not achieved, and the goal is to achieve balanced yield behavior rather than to prevent panel zone failure.

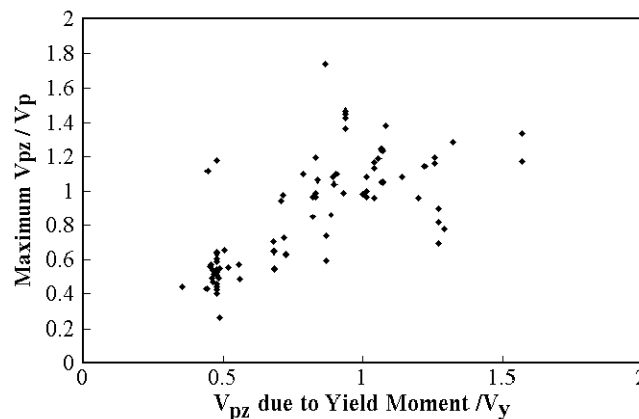


**Figure 2-14 Normalized Panel Zone Shear Capacity as a Function of Panel Zone Yield Potential**

This reasoning leads to a recommendation that balancing of the beam flexural yield mechanism with the panel zone yield equation will provide the greatest potential for connection ductility. For a connection where the flexural yielding develops at the face of the column, this balance condition means that

$$V_{pz} = \frac{\Sigma M_{\text{yield-beam}}}{d_b} \left( \frac{L}{L-d_c} \right) \left( \frac{h-d_b}{h} \right) \approx 0.9 V_y = (0.9) 0.55 F_{yc} d_c t_{wc} \quad (2-6)$$

This equation encourages panel zone yielding, because ductile connections also result in significant strain hardening. During this project's research, a number of connections showed significant ductility with large plastic rotations and had various degrees of panel zone yield deformation. These specimens are discussed further in Chapter 4.

### 2.2.3 Effect of Bolts and Bolt Type

The web connection clearly plays a critical role in the ductility and seismic performance of pre-Northridge connections. Unfortunately, the pre-Northridge test data do not contain adequate information to evaluate this effect. This issue will be discussed in detail in Chapter 3.

### 2.2.4 Material Properties of Steel

The ductility obtained with all pre-Northridge connections is illustrated in Figure 2-4. However, recent tests as included in the SAC Phase I research program and in the Phase 2 research (Lee et al., 2000) in Table 2-1 show significantly less rotational capacity than suggested by Figure 2-4. Figure 2-15 shows the rotational capacity obtained in pre-Northridge connections that have been completed since 1994. Comparison of this figure to Figure 2-4 clearly shows significantly less ductility in the more recent connection tests. The differences in ductility can be traced to differences in failure modes. The specimens illustrated in Figure 2-15 all failed through a brittle fracture initiating at the flange weld. A large number of the specimens in Figure 2-4 failed because of large cyclic strains and the local buckling associated with these large strain levels. One primary difference between the earlier tests and the more recent tests is that yield stress of the steel in the earlier tests was significantly lower than the yield stress reported in the more recent tests. This can be verified by the data illustrated in Figure 2-16. The tests used to develop the basis of the seismic design provisions for steel moment frames were completed in the late 1960s and early 1970s, and Figure 2-16 suggests that the average yield stress was in the range of 40 ksi during that period. Comparison with the average values for the early 1990s suggests that the average yield stress increased approximately 20% during that period.

The properties of structural steel have changed significantly over the years. Prior to about 1940, mild steel was sold as A9 steel with a specified minimum yield stress of 30 ksi. A9 steel effectively merged into A7 steel during the 1930s, and between about 1940 and 1960, mild structural steel was sold as A7 steel with a specified minimum yield stress of 33 ksi. After this period, until about the Northridge earthquake, mild structural steel was sold as A36 steel with a specified minimum yield stress of 36 ksi. While three different grades of steel were sold during that period and are included in Figure 2-16, there is no evidence that fundamental changes in

alloying elements or metallurgy were used to achieve the increased yield stress. The ASTM standards used to define these steels were nearly identical except for slight increases in specified minimum yield stress and slight decreases in minimum required elongation. It must be emphasized that the specified minimum yield stress is a statistical requirement, since the actual expected yield stress of the vast majority of specimens and the mean yield stress must be significantly larger than the minimum value. The seismic performance of an actual structure or connection, however, depends on the actual yield stress of the steel used in the structure.

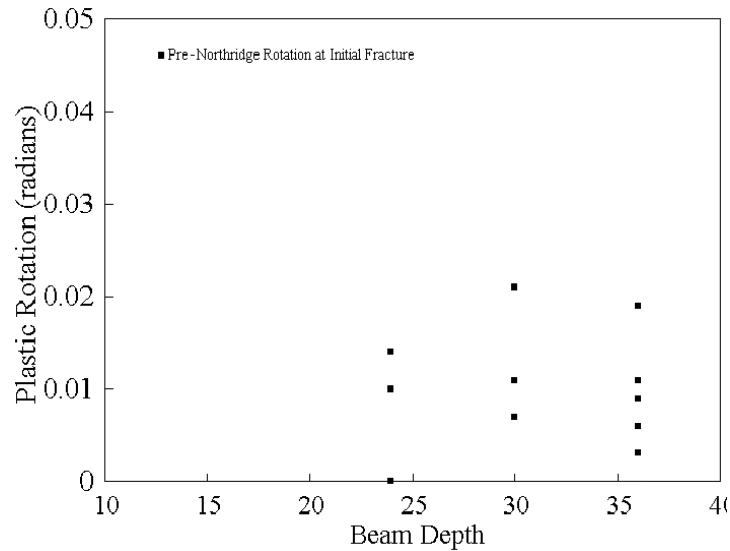


**Figure 2-15 Rotational Capacity of Pre-Northridge Connections Performed Since the Northridge Earthquake**

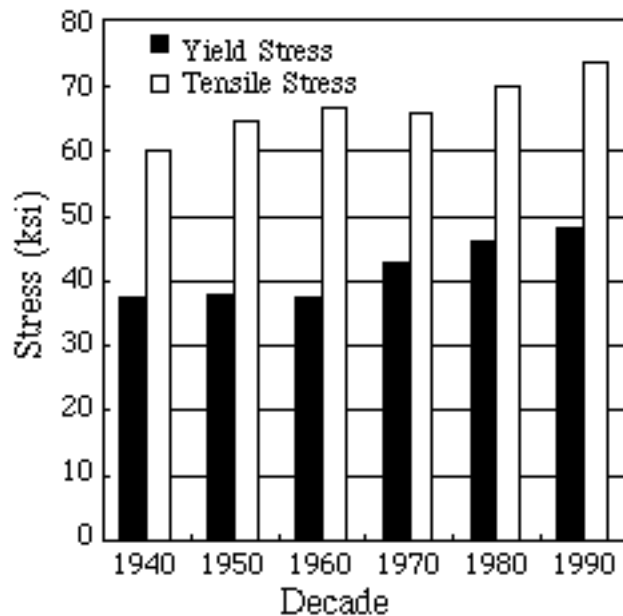


**Figure 2-16 Variation in the Measured Yield and Tensile Stress in Structural Steel (Coons, 1999)**

Analysis (Chi et al., 1997) of the fracture of pre-Northridge connections showed that reduced yield stress of the beam resulted in larger plastic strains and larger plastic rotations before the CTOD demand reached critical levels for a given initial flaw size. This indicates that there is a greater likelihood of achieving ductile behavior if the yield stress of the steel is low. Additional verification (El Tawil and Kunnath, 1998) of this was provided by ABAQUS computer analysis. These later analyses showed that early yielding in the beam, which was caused by reduced yield stress, delayed the development of high hydrostatic and principle stresses, which would otherwise tend to facilitate brittle fracture of the connection.

Attempts were made to verify this observation by experiment. However, researchers were unable to obtain beam steel with yield stresses that were sufficiently low to warrant testing. Today, wide flange shapes are all produced from recycled scrap steel using electric furnace technology rather than steel from the integrated mill process of mining, processing, and rolling. The yield stress is significantly higher, as can be seen from Figure 2-16. This figure shows the average compilation (Coons, 1999) of the measured yield and tensile stresses reported from research studies on mild steel members during the past 50 years. The steady increase in the average yield stress is quite apparent.

Comparison of the plastic rotations and failure modes obtained in the SAC Phase 1 testing (Roeder, 1996) provide verification of these analytical results. University of California at Berkeley (Popov et al., 1996) specimens PN1, PN2, and PN3, were identical specimens, except that PN3 had a yield stress of approximately 40 ksi and PN1 and PN2 had a yield stress of approximately 60 ksi. PN3 developed a plastic rotation of 0.011 radians while PN1 and PN2 averaged .006 radians. The plastic rotation achieved by PN3 is nearly twice as large as that achieved with PN1 and PN2, but the actual increase is quite small because of the low ductility resulting from the very low weld CVN toughness, pre-Northridge detailing, and the beam depth. Nevertheless, it provides confirmation of the theoretical predictions, and there should be reasonable confidence that beams with lower yield stress will, on average, provide greater ductility than beams with higher yield stress given the same post yield material behavior. The significance of this factor can be seen from Figure 2-16. The initial research for steel moment frames was completed in the late 1960s and early 1970s, and the yield stress of the steel used in those tests was typically less than 40 ksi. These early specimens clearly performed very well. By the mid 1980s, tests were showing problems with this connection, and Figure 2-16 shows that the average yield stress for mild steel was 46 to 47 ksi at that time. By the time of the Northridge earthquake, the expected yield stress was commonly larger than 50 ksi, and serious problems were noted in nearly every connection test. These observations provide evidence that the yield stress of the steel is also one of several contributors to the reduced ductility of the pre-Northridge connection, and that better performance would be expected for pre-Northridge connections built during the earlier years.

Because of the importance of the actual yield stress in evaluated yield mechanisms and failure modes, all evaluations and equations included in this report are based upon expected or median yield stress rather than specified minimum yield stress values unless otherwise noted.

## 2.2.5 Weld Type and Procedures

The flanges of the pre-Northridge connection were welded with E70T-4 FCAW-SS filler metal for a number of years prior to the Northridge earthquake. This filler metal did not have a minimum required Charpy V-Notch (CVN) toughness, and it has been shown to have very low notch toughness as defined by a CVN test. This low CVN toughness is one (Xue et al., 1996) of several contributing causes of connection fracture. The backing bar was left in place for all of these pre-Northridge welds. The backing bar hides weld flaws resulting from the weld root pass, and it provides an initial crack depth. The flaws and backing bar leave the pre-Northridge welds susceptible to crack growth, and analytical studies (Chi et al., 1997) have clearly shown that unstable crack growth must be expected at stresses slightly below the yield stress or at most at very low plastic strains. Analyses show that welds with fewer flaws and greater CVN toughness will have a greater resistance to fracture and increase the probability of achieving a ductile failure mode. Therefore, in hindsight it is clear that the E70T-4 FCAW-SS filler metal was not a good choice for this seismic application. It is logical to ask whether improved welding alone would result in satisfactory performance of welded-flange-bolted-web moment frame connections. A series of tests (Lee et al., 1999) in the SAC Phase 2 program were designed to address this issue, and the results of these tests are shown in Table 2-1 and Figure 2-17.

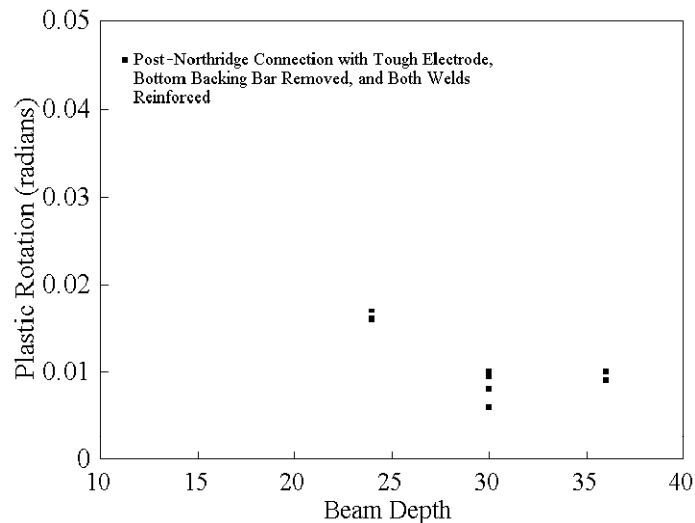


**Figure 2-17 Rotational Capacity of Welded-Flange-Bolted-Web Connections Welded to Achieve Reduced Flaws with Notch Tough Electrodes**

The tests with improved welding used the E70TG-K2 FCAW-SS electrode, which is capable of achieving 20 ft-lbs Charpy V-Notch toughness at -20oF. The backing bar was removed for the bottom flange weld, and the root pass was backgouged and reinforced with E71T-8 FCAW-SS electrodes. The backing bar was left in place for the top flange because analysis shows that this backing bar is in a less critical location for unstable crack growth. The underside of the backing bar was reinforced with a notch tough fillet weld to make any flaws to be internal. Analysis also showed that internal flaws or cracks must be significantly larger than surface flaws before they become unstable. The use of these improved weld electrodes and procedures resulted in a significant improvement in the connection performance, but it did not result in a

significant increase in the plastic rotation capacity. The performance was improved in that there were no fractures in the flange welds of these specimens. Fracture usually initiated in the beam flange outside the heat affected zone near the weld access hole. It should be noted that welded-flange-bolted-web connections with CVN notch tough filler metal may be capable of better performance than suggested by Figure 2-17. The weld access holes used in these test specimens were examined (Barsom, 1999) after the testing was complete. They were found to be outside the norm for finish and geometry, although they were permissible with pre-Northridge practice.

The next section will show that these weld access holes also contribute to reduced ductility and rotational capacity. Nevertheless, the rotations achieved with these tests are well below those required for most seismic design. This comparison clearly shows that the use of notch tough welding alone is not enough to assure adequate seismic performance of the connections. Other cracks occur at other critical locations at deformations slightly larger than those needed to crack the weld filler metal with less CVN toughness. However, at the same time, this research shows that notch tough weld metal has a higher resistance to weld cracking, and may move the critical location to another point. It is therefore important to consider all of these critical points to ensure ductile behavior of the connection.

### **2.2.6 Weld Preparation and Weld Access Hole Geometry**

The initiation of cracking at the weld access hole raises further questions about the access hole geometry. Weld access hole geometry for pre-Northridge connections was defined in the AISC Manual (AISC, 1994) based on requirements of AWS D1.1 (AWS, 1994). These requirements provide a general shape and clearance requirements of the weld access hole, but they permit latitude in the finish and geometry of the surfaces of the access hole. As noted in the last section, the finish and geometry of the weld access hole may affect the fracture potential of the beam flange. As a result, further study (Ricles and Lu, 1999) was completed in the SAC Project to determine if improvements in the access hole geometry would improve connection performance. Nonlinear computer analyses with the ABAQUS computer program were performed to evaluate the stress flow and the potential for brittle fracture of the connection. Through this analysis recommendations for improved geometry and finish of the weld access hole were developed, and these recommendations will be discussed in greater detail in Chapter 3. Experiments were performed on specimens that used these recommended weld access hole details. Figures 2-6 and 2-18 show the moment-rotation behavior of two identical specimens except that Figure 2-6 (Lee et al., 1999) employed the access hole details as commonly used in pre-Northridge conditions, while Figure 2-18 (Ricles et al., 2000) employed the improved access hole detail recommendations and a somewhat heavier column.

Comparison of the two figures shows that the specimen with improved weld access hole geometry had significantly larger ductility before initial failure occurred. Further, the failure was a more ductile tearing failure which initiated away from the weld and weld access hole area. The specimens both had W36x150 beams with W14x257 columns, and the size of these specimens suggests even better performance with lighter sections. The steel properties and web attachment were the same for both specimens. The improved weld access hole detail resulted in larger plastic rotations, but the rotations are still smaller than required for many seismic applications. In addition, it should be noted that the improved weld access hole detail resulted in significantly larger energy dissipation and plastic rotation before the initiation of fracture or

tearing. However, the consequences of the tearing for the specimen with improved details were more immediate, since the shear tab began to fail at almost the same deformation as the initial flange tear. This does not imply that the improved weld access hole caused fracture of the web connection, but it does indicate that greater interaction between the web and flange connections are required at large plastic rotations. The specimen with ordinary weld access hole details retained its web connections until it achieved a rotation similar to that noted for the improved detail.

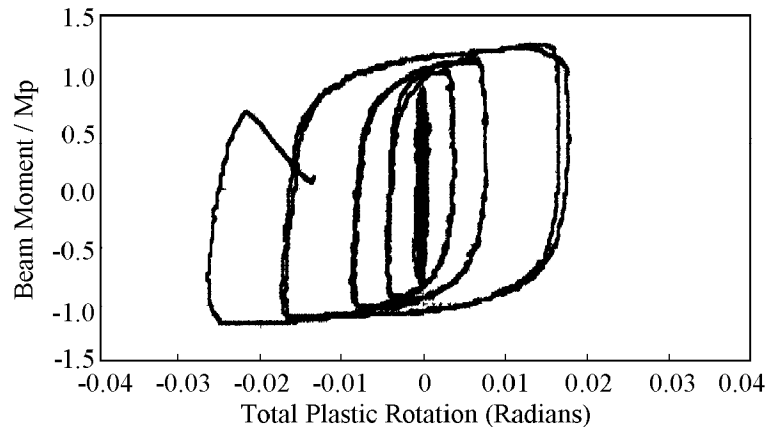


**Figure 2-18** Moment-Rotation Curve for a Specimen with Notch Tough Weld Details and Recommended Improvements to the Weld Access Hole Details

### 2.2.7 Slenderness and Local Buckling Considerations

Historically, there has been considerable interest in web buckling, flange buckling, and lateral torsional buckling when evaluating the seismic performance of steel moment-frame connections. Early pre-Northridge connection tests suggested that buckling resulted in deterioration of the resistance and loss of ductility, because of the concentrated strain that developed in the buckled region. The concerns about local buckling have been changed somewhat by the brittle fractures noted during the Northridge earthquake and by tests performed since the earthquake. However, the previous sections have shown that improved performance can be achieved if connections are welded with notch-tough electrodes, if backing bars are removed and weld is backgouged and reinforced, if there is a good balance of shear and flexural yielding, if lower yield stress steel is employed in the beams, and if the beam depth and span length are kept to appropriate proportions. Extrapolation of the previous sections would suggest that, if weld access hole details and web attachments are improved, further increases in connection ductility are possible. None of these factors acting alone was adequate to ensure satisfactory performance of the pre-Northridge connection, but each factor resulted in some improvement. With these improvements, however, it is possible to achieve the more ductile failures that make up much of the data in Figure 2-4, and local buckling issues again become increasingly important to the specimen performance. The older pre-Northridge connection tests commonly provided good connection ductility, and this data is a good starting point for evaluating the slenderness issue.

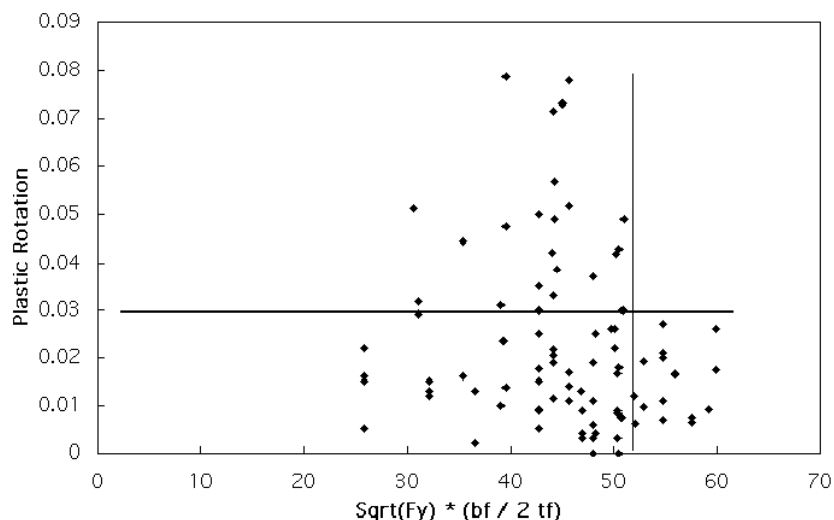


**Figure 2-19 Plastic Rotation as a Function of Beam Flange Slenderness**

Figure 2-19 shows the plastic rotation achieved from a large number of tests with different flange slenderness ratios. It should be noted that ductility requirements for special steel moment frames have historically required that

$$\frac{b_f}{2t_f} \leq \frac{52}{\sqrt{F_y}} \quad (2-7)$$

and so the rotation was plotted as a function of the beam flange slenderness. The data is widely scattered, because there are many different tests of different depths, failure modes, and test conditions. There are a number of existing tests for pre-Northridge moment-frame connections, but there are not nearly enough tests to separate the many variables and provide a one to one comparison of each test parameter. However, it should be noted that 0.015 to 0.02 radians was a benchmark rotation that was sometimes used to establish satisfactory performance of the seismic rotational capacity of moment-resisting connections for special moment frames, since the

Northridge earthquake. Figure 2-19 shows that no specimens with  $\frac{b_f}{2t_f}$  larger than  $\frac{52}{\sqrt{F_y}}$

attained a 0.03 radian rotation level, while a large portion of those specimens with stockier flanges achieved this rotation level. A larger number of specimens achieve the 0.015 to 0.02 radian limit. This provides evidence that the existing limit is appropriate for achieving ductile behavior. While Figure 2-19 shows that the present flange thickness requirement may be about right, it also indicates that it is better to avoid being far below this limit, since specimens with very stocky beam flanges do not attain particularly good plastic rotation capacity, either.

Similar evaluations were made for web buckling and lateral torsional buckling. It is not possible to make a direct comparison such as that shown in Figure 2-18 for these other buckling forms, because the design equations are somewhat more complex. As a result, analysis on these issues is deferred to Chapter 4.

## 2.2.8 Continuity Plate Requirements

Continuity plate requirements are another consideration which may be important as greater ductility is achieved from moment frame connections. Prior to the Northridge earthquake, AISC Seismic design requirements required that continuity plates be used if

$$t_{cf} \leq 0.4 \sqrt{\frac{P_{bf}}{F_{yc}}} \quad (2-8)$$

where

$$P_{bf} = 1.8 t_{fb} b_{fb} F_{yb}. \quad (2-9)$$

Past experimental data were examined to determine the effect of continuity plates and continuity plate size on connection ductility. To do this,  $P_{bf}$  was determined based upon beam flange size, and the force was then reduced by the yield capacity of the continuity plate. The required column flange thickness was then determined from this reduced force, and this required thickness was divided by the actual column thickness and plotted as a function of the plastic rotation obtained in the test. This is inverse to the application of continuity plate design practice, but it provides a measure of the validity of the design equations. The figure shows that 11 specimens have ratios greater than one, and 36% of these still have plastic rotations greater than 0.03 radians. The consensus of this evaluation must be that Equation 2-8 is a rather approximate indicator of the continuity plate requirements.

Experiments (Ricles et al., 2000) were performed to evaluate the continuity plate requirements. Further research (Dexter et al., 1999) on this issue has been funded by AISC, and is also in progress. These experiments and further evaluation of the continuity plate issue are discussed in Chapter 4, and final recommendations regarding this issue are made.

## 2.2.9 Effect of Load and Deformation History

Load and deformation history may have significant impact on the performance of moment resisting connections. This variation is yet another factor that complicates comparison of past test results. It is generally believed that monotonic tests provide an envelope to the moment-rotation hysteresis curves developed in cyclic load tests. Past test programs have been extremely variable. Some past tests were conducted as monotonic tests, and the effects of cyclic behavior were not fully reflected in those tests. Deterioration resulting from local buckling appears to be most significant on reversed and repeated inelastic cycles after initial buckling has been noted. It appears (Castiglioni et al., 1999) that these deterioration issues are related to the number of cycles of the loading and the severity of the load and deformation for those cycles. At the same time, many issues of connection behavior are related to the absolute strain, stress, or deformation levels, and deterioration models appear to be less effective in evaluating these issues. For example, inelastic fracture issues appear to be more strongly influenced by strain and deformation levels than by the number of times the strain has been repeated. As a result, there are no clear methods for consistently evaluating and comparing test results with different failure modes and different load and deformation patterns. In light of these circumstances and the fact

that connection fracture was the motivating cause of the SAC Steel Project, this report will focus on plastic rotational capacity of the connections and the maximum plastic rotational capacity that can be achieved for different limit state conditions. Figure 2-21 illustrates the difference between plastic rotation and total rotation for a given connection test.

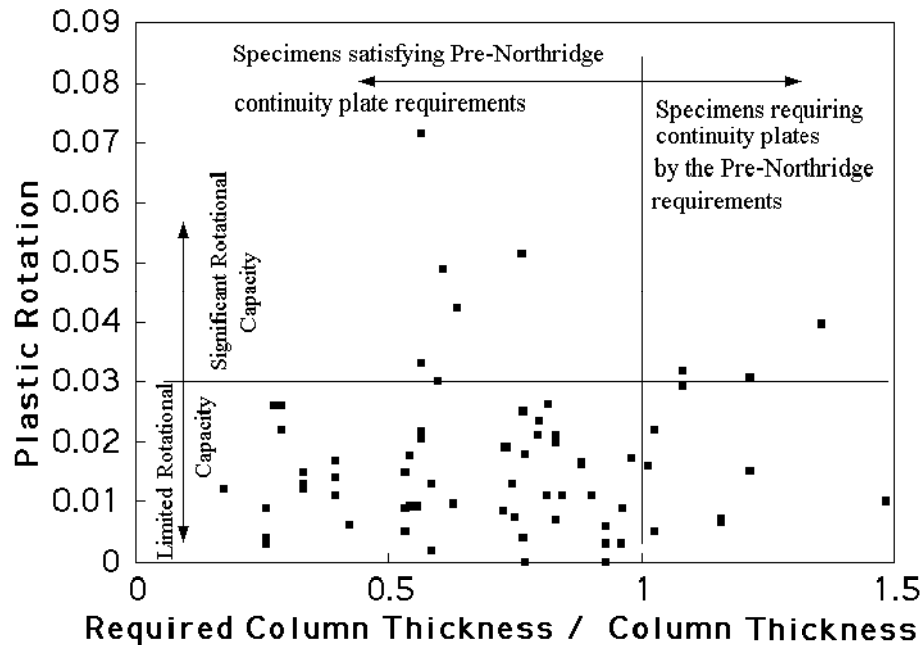


**Figure 2-20 Effect of Continuity Plates on Plastic Rotation**

At the same time, it is important that the test results truly reflect all aspects of the seismic behavior of the connection. It is important that the deformation load history reflect the magnitude of the deformations and the number of cycles expected during major earthquakes. This is important so that the connection is exposed to deformations which are appropriate for earthquake loading, and that the repetitions of these deformations be of the appropriate number so that any deterioration that can occur will be observed in the test programs. As a result, the deformation history used in all SAC Phase 2 test programs was carefully designed (Krawinkler et al., 2000; Clark et al., 1997) to ensure that

- the testing is realistic to fully evaluate the seismic performance of the connection, from elastic behavior, through plastic deformation, to fracture or failure of the connection;
- the test is severe but not unrealistic in its demands upon the connections or components;
- all possible failure modes have the appropriate opportunity to occur and no failure modes are prevented or excluded by virtue of the test program; and
- the rated capacity of individual connections are comparable across connection types and across connection yield mechanisms and failure modes.

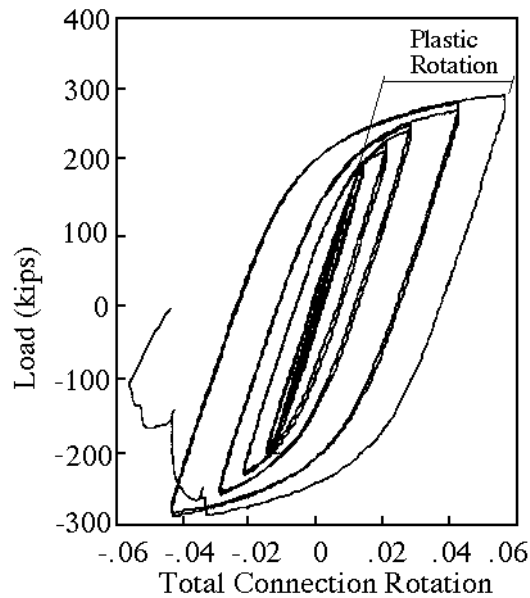


**Figure 2-21 Definition of Plastic Rotation Used in this Report**

Two different deformation load patterns were used for all tests in the SAC program and they are schematically illustrated in Figure 2-22. The first test pattern was used for the majority of the test specimens and it was based upon the ATC-24 test recommendations. The number of cycles and the deformation levels for each cycle were modified slightly from ATC-24 recommendations. The number of cycles at each deformation was selected to reflect accurately the maximum earthquake demands (at all levels of deformation) caused by a wide range of past earthquake acceleration records. Most tests used this deformation pattern, and modifications were only employed because of limitations of test equipment or because of special attributes and concerns of the individual connection type.

It is well known that near-fault acceleration records sometimes place larger seismic demands on structures and components, and the second deformation pattern was selected to simulate the maximum demands of near-fault events. As with the more general deformation pattern, the deformation levels and number of cycles for each deformation level were selected by evaluation of the inelastic dynamic response of many near fault earthquake excitations.

Finally, the interpretation of the test results and determination of the capacity of individual connections must also be rationally and consistently obtained by methods that are consistent within the test program. These methods (Krawinkler et al., 2000; Clark et al., 1997) were established and used for all projects described in this report, and further discussed later in this chapter. As nearly as possible, these same definitions were used in the evaluation of previous test results described in this report, although comparison with past tests are imperfect because of the many variations used in past test programs.

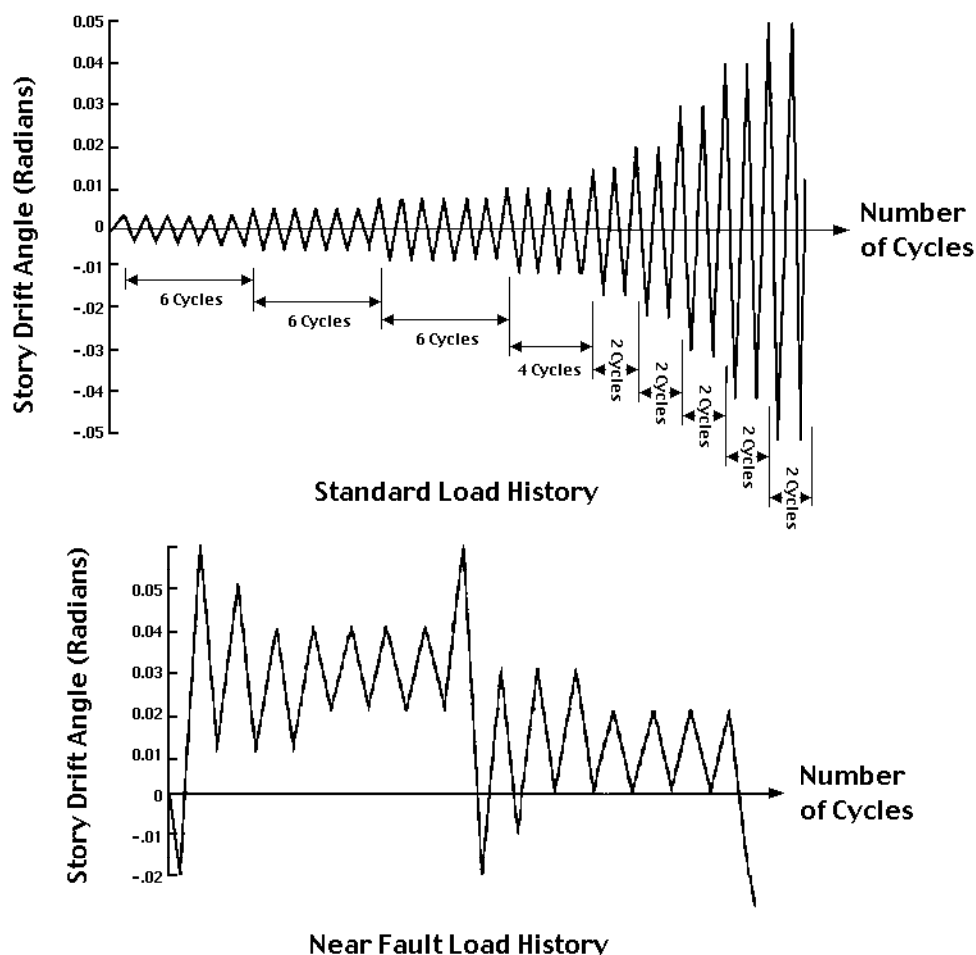


Figure 2-22 Test Programs Used in the SAC Phase 2 Research

### 2.3 Methods of Predicting Strength, Stiffness and Hysteretic Behavior

This chapter has provided an overview of the pre-Northridge welded-flange-bolted-web connection with discussion of potential causes of connection damage and possible improvements to the connection. The yield mechanisms of the pre-Northridge connection are quite simple and are illustrated in Figure 2-7. Equations for predicting these yield resistances are given in Table 2-2. Flexural yielding of the beam and panel zone yielding of the column are the only two mechanisms which are capable of sustaining significant ductility. Prior to the Northridge earthquake, engineers commonly believed that the failure modes were equally simple, since the connection was believed to provide ductile failure in all cases. This chapter clearly shows that this is not the case. Failure modes are much more complex, and Table 2-3 and Figure 2-8 provide a review of these failure modes and the equations for predicting them or methods for delaying them until adequate ductility is achieved.

**Table 2-2 Yield Mechanisms of Pre-Northridge Connection**

Yield Mechanism	Equation to Define Yield Mechanism Moment Resistance at the Face of the Column
Flexural Yielding of Beam	$M_{yield} = S F_{yb} m$
Panel Zone Yielding	Yield occurs when $V_{pz}$ equals $V_{yield} = 0.55 F_{yc} d_c t_{wc}$
Recommended Balance Condition for Maximum Plastic Rotational Capacity	$\frac{\sum M_{yield-beam}}{d_b} \left( \frac{L}{L-d_c} \right) \left( \frac{h-d_b}{h} \right) \leq (0.9) 0.55 F_{yc} d_c t_{wc}$ <p>but preferably</p> $\frac{\sum M_{yield-beam}}{d_b} \left( \frac{L}{L-d_c} \right) \left( \frac{h-d_b}{h} \right) \geq (0.6) 0.55 F_{yc} d_c t_{wc}$

Note: All material properties provided in this table are expected values rather than minimum values.

**Table 2-3 Failure Modes for Pre-Northridge Connection**

Failure Mode	Equation to Define Failure Mode Moment Resistance at the Face of the Column	Conditions Which May Reduce the Problem
Fracture of Beam Flange Weld	Not predictable but avoidable with removal of backing bars, backgouging and weld reinforcement with notch tough electrode	Older steels with lower yield stress (and yield to tensile stress ratios) may result in adequate ductility prior to weld fracture (see Section 2.2.4).
Fracture at Weld Access Hole	Not predictable but avoidable with improved finish and detailing of weld access hole.	Older steels with lower yield stress (and yield to tensile stress ratios) may result in adequate ductility prior to weld fracture (see Section 2.2.4).
Plastic Hinging of Beam	$M_p = Z F_{yb}$ is lower bound estimate and $M_{pfail} = Z \frac{F_{yb} + F_{tb}}{2}$ provides the best estimate if full bending is achieved	
Flange Buckling	controlled if $\frac{b_f}{2 t_f} \leq \frac{52}{\sqrt{F_y}}$	
Web Buckling	controlled if $\frac{d_b}{t_w} \leq \frac{418}{\sqrt{F_y}}$	See discussion in Chapter 4.
Lateral Torsional Buckling	$L_b < \frac{2500 r_y}{F_y}$	$L_b$ is the unsupported length from existing AISC LRFD Seismic Provisions.
Excessive Deformation of Column	Continuity plates required if $t_{fc} \geq 0.4 \sqrt{\frac{P_{bf}}{F_{yc}}}$ where $P_{bf} = 1.8 t_{fb} b_{fb} F_{yb}$	This equation is somewhat approximate, but it is the best estimate available at this time.

Note: All material properties provided in this table are expected values rather than minimum values.

### 2.3.1 Rotational Capacity

Prediction of resistance is important, but the rotation capacity of moment frame connections is even more important to seismic design. The rotation capacity of pre-Northridge connections is difficult to evaluate because the failure modes and yield mechanisms were not properly understood or controlled when they were designed. Past tests have indicated that ductile behavior is quite possible with modest sized members and older, lower yield stress steels as shown in Figure 2-4. However, more recent pre-Northridge construction with deeper beams with thicker flanges, and with steels with higher yield stress and higher yield to tensile stress ratios are expected to have limited rotational capacity. Methods for system performance prediction developed in other parts of the research program utilize two rotational capacities. One rotational limit deals with the rotation, which results in initial failure or significant loss of resistance in the connection. This rotation is defined as  $\theta_p$  in this state of the art report. These are the rotations summarized in Figures 2-4 and 2-17. There are many limitations in the understanding of this rotational capacity, because some tests were stopped without any clear failure or some employed test protocol which increased or decreased the rotation capacity. Nevertheless, the understanding is much better than that associated with the second rotational capacity (Foutch, 2000) used in the proposed performance prediction.

The plastic rotation at initial failure,  $\theta_p$ , is illustrated in Figure 2-21. This rotation is the maximum plastic rotation at which initial fracture occurred or where the resistance dropped below 80% of the plastic moment capacity based upon the measured yield stress of the steel. In addition,  $\theta_p$  is counted only if at least one complete cycle of the target deformation was completed before fracture occurred. The rotation,  $\theta_p$ , was estimated by a least squares fit to experimental data such as that shown in Figures 2-4 and 2-17. This process results in an unbiased estimate of the expected rotation and a standard deviation of this estimate, and these are both valuable tools in the evaluation of the connection. Standard deviations,  $\sigma_p$ , of this rotation data were also computed, because they provide a measure of the variation in the test results.

This least squares evaluation of the rotational capacity are performed on two data sets. For pre-Northridge connections with older E70T-4 welds and steels with lower yield to tensile stress ratios,

$$\theta_{p\text{mean}} = 0.051 - 0.0013 d_b, \quad (2-10a)$$

and the standard deviation

$$\sigma_p = 0.0044 + 0.0002d_b \quad (2-10b)$$

where  $\theta_{p\text{mean}}$  and  $\sigma_p$  are in radians and  $d_b$  is in inches.

For more recent pre-Northridge connections that were welded with E70T-4 electrode and with steels with larger yield to tensile stress ratios, a least squares fit was applied to this partial data set. An evaluation of rotation as a function of depth was also completed, but the effect of depth was small because of the relatively small variation in beam depths for the connections

tested since the Northridge earthquake. Thus, a one dimensional statistical evaluation was completed. This one dimensional evaluation should be valid for beam sizes up to W36 sections. Under these conditions,

$$\theta_{p\text{mean}} = 0.011 \text{ radians,} \quad (2-11a)$$

and the standard deviation

$$\sigma_p = 0.007 \text{ radians.} \quad (2-11b)$$

Comparison of the equations and Figures 2-4 and 2-17 shows that the distinction between the two categories is clearly important. This difference is largely attributable to the changes in yield stress that have occurred over the years. The difference is also consistent with the variations in frequency of damage noted with different building ages and member sizes after the Northridge earthquake. However, the distinction is fuzzy and uncertain, because the yield stress changes evolved over time rather than occurring abruptly. At the same time, the distinction is a very rational and logical distinction, because it is based upon past, valid connection tests. The benefit for using Equation 2-8 as opposed to 2-9 is useful only for steel frames with lighter framing, since most tests with heavier framing are more recent tests with larger yield stress. Therefore, it is proposed that the data for older pre-Northridge connections be used only for steel frames with W24 or lighter beam framing, where randomly selected tension samples have been taken from the beam flange, and the average yield stress to tensile stress ratio from these tension tests is less than 0.6.

The second rotational capacity that is of interest to the SAC Phase 2 Project is the rotation  $\theta_g$  at which the connection will no longer be able to support its gravity load.  $\theta_g$  is not nearly so well defined. There are several reasons for this:

- Virtually all connection tests were completed without gravity loads in place, because it is relatively difficult to apply gravity loads to beams with steel frame connection tests. Further, modern steel frames have very low gravity loads on the beams of lateral load frames, and gravity loads have historically been regarded as a secondary concern to the seismic performance of steel frame connections.
- Gravity loads on beams are highly variable depending upon the age of construction, building occupancy, and the framing system employed for the building. As a consequence, a very large sample testing program would be needed to estimate accurately this rotational capacity for all ages of construction.
- The rotation at which the connection is no longer able to support gravity loads is often so large that testing equipment is not capable of delivering the deformation.
- At these large deformations, the specimen is flexible and unstable, and researchers are unwilling to risk severe damage to their testing equipment at these large deformations.

As a result,  $\theta_g$  must be estimated with far less precise data than is  $\theta_p$ , since estimation of  $\theta_g$  requires approximation and judgment in addition to observation of experimental results. During

the SAC Phase 1 connection testing program, all tests were stopped while they had limited damage so that specimens could be repaired for the evaluation of repair methods. Prior to the Northridge earthquake, all tests focused only on the initiation of initial fracture, and even  $\theta_p$  was variably estimated because of variations in the cyclic deformation history. Tests completed during the SAC Phase 2 program made a deliberate effort to examine connection behavior beyond initial fracture or failure. However, there were limits in the accuracy of the evaluation of  $\theta_g$ , because of the problems noted earlier. As a result, two methods of estimating of  $\theta_g$  were employed, and both methods are thought to be conservative. First, if significant fracture of the shear tab or shear tab weld was noted in the test, this rotation was used as the rotational limit,  $\theta_g$ , for that test. If the specimen was not deformed to a level where shear tab tearing or fracture was observed, the moment resistance after initial fractures was used as the factor defining this rotational limit. Figure 2-6 shows a typical moment-rotation curve for a pre-Northridge connection, and it can be seen that the specimen has significant rotational capacity well after initial flange weld fracture and even after the second flange weld fracture. If this moment capacity remained larger than 15% to 20% of the plastic capacity of the beam, it could be shown that the shear capacity was normally large enough to support the gravity load carried by a beam in the lateral load frame of modern steel frame buildings. Thus, the second measure for the rotation at which gravity load could no longer be supported was the rotation at which the moment capacity in both directions drops below 15% to 20% of the plastic capacity of the beam. For the specimen of Figure 2-6, this suggested a  $\theta_g$  of approximately 0.03 radians. The two methods are thought to be conservative, because they neglect the beneficial effects of the floor slab, and they neglect the fact that adjacent connections are unlikely to lose gravity load support after the initial connection loses this capacity. A third method was used for some connections other than pre-Northridge connections, and is described in Chapter 3.

Given this two-level evaluation procedure, a number of connections with post-Northridge details or welded-flange-bolted-webs with improved welding procedures provided estimates of  $\theta_g$ . However, only two specimens with pre-Northridge details provided this rotation estimate. Comparison of these rotations, however, showed that the characteristics of this rotation limit did not vary greatly for significant changes in the connection details. That is,  $\theta_g$  obtained for a pre-Northridge connection is not dramatically different from that obtained from welded-flange-bolted-web connections, which were welded with notch tough electrodes, nor is the rotation dramatically different from strengthened connections which develop their plastic hinge at the face of the column. Therefore, the two data points for pre-Northridge connections were used to establish the mean value estimate, but the data available on post-Northridge connections welded with notch tough electrodes but without the strengthened web connection or improved weld access hole details were used to establish the standard deviation and specimen geometric effect. The resulting estimates were:

$$\theta_{g\text{mean}} = 0.043 - 0.0006 d_b, \quad (2-12a)$$

and the standard deviation

$$\sigma_g = 0.011 + .0004 d_b. \quad (2-12b)$$

Data shown in Equations 2-8 and 2-10 are not directly comparable, because they measure two different things. However,  $\theta_g$  must realistically always be larger than  $\theta_p$ , regardless of the connection details or geometry. Comparison of Equations 2-8 and 2-10 show that these equations do not satisfy this condition for smaller member sizes. The reason for this comparison is that no beams smaller than W24 were included in the data used to establish Equation 2-10, but many beams in this smaller size range affect the data of Equation 2-8. This obviously indicates that Equation 2-10 underestimates  $\theta_g$  of light framing members. However, this underestimate is not believed to be overly large, because data provided in Chapter 3 will show that connections with larger values of  $\theta_p$  commonly have smaller separations between  $\theta_p$  and  $\theta_g$ . This appears to occur because initiation of fracture or tearing of the beam flanges more rapidly progresses to the tearing or fracture of the beam web in these connections with larger inelastic strains.

## 3. POST-NORTHRIDGE WELDED FLANGE CONNECTIONS

### 3.1 Introduction

Chapter 2 discussed the seismic performance of pre-Northridge connections, and showed that pre-Northridge connections do not provide enough plastic rotational capacity for most seismic applications. The work showed, however, a number of factors may either improve or adversely affect the seismic performance of the connection. These factors included weld procedures and filler metals, geometric effects, panel zone yielding, and material properties. It was shown that no single change to the pre-Northridge connection was adequate to assure ductile performance of the welded-flange-bolted-web connection. This chapter will build upon the discussion of Chapter 2 to examine improvements to the seismic performance of these welded flange connections. All connections in this chapter are intended to develop the full plastic capacity of the beam and to be stiff enough to assure that no consideration of the connection stiffness is needed for frame analysis. Combinations of the effects noted in Chapter 2 may provide improved seismic performance and will be examined in this chapter. In addition, other connections including strengthened connections, which force plastic deformations to other locations, and other connection strategies to increase the ductility are evaluated. Several general issues that relate to all connections, but are particularly relevant to these post-Northridge connections, are deferred to Chapter 4.

### 3.2 Post-Northridge Connections

Capacity issues including resistance, stiffness, and ductility of the connection are the parameters of primary interest for connection performance in seismic design. However, the stiffness of welded-flange-bolted-web connections is normally large enough that the elastic flexibility of the connection does not require special consideration in the global frame analysis. This trend will be maintained for all connections discussed in this chapter. Therefore, Chapter 3 emphasizes resistance and ductility. Yield mechanisms and failure modes are the factors that control resistance and ductility, and there are frequent commonalities between the modes and mechanisms expected for the connections described in this chapter and those described in Chapter 2. As a result, this chapter will make frequent references to issues discussed in Chapter 2. At the same time, the connections described in this chapter are directed toward increased ductility and reduced potential for brittle fracture, and so there are also fundamental differences noted from the discussions of the pre-Northridge connection.

As noted earlier, yield mechanisms and failure modes are related, but are inherently different. Failure modes cause fracture, loss of deformational capacity, or significant loss of resistance. Yield mechanisms induce inelastic deformation and result in dissipation of energy and changes in stiffness without inducing fracture or excessive loss of resistance. Some yield mechanism and failure mode combinations produce ductile behavior, others result in brittle failure, and still others produce intermediate results. Good ductility is achieved when the resistance associated with one or more ductile yield mechanisms is significantly smaller than the resistance associated with all brittle failure modes. Poor ductility with limited plastic rotational capacity must be expected when the resistance associated with a brittle failure mode is smaller than the resistance associated with all ductile yield mechanisms. Therefore, the prediction of the resistances, yield

mechanisms, and failure modes for each connection type are a fundamental requirement for achieving good seismic performance of the connection.

As with the pre-Northridge connection, flexural yielding of the columns is discouraged or prohibited for all connection types described in this chapter, because frame systems that are built with weak column behavior are known to have significantly larger inelastic story drift and local ductility demand (Schneider et al., 1993) than comparable frames with beam yielding. This is primarily an issue of system performance (Krawinkler, 2000), and that is not the focus of this report. However, the maximum moment resistance that the connection can develop is very relevant to the column yield issue and is within the scope of this report. As a result, proposed limits for preventing flexural yielding of the column will be noted in this chapter. In addition, many forms of local yielding and buckling are not fundamentally different from those issues discussed in Chapter 2, and so there will again be references to this earlier discussion. Material properties of the steel were discussed in the pre-Northridge connection, because changes in these material properties have had an impact on the connection performance. However, the connections discussed in this chapter are all based on the material properties of steels that are produced today. Finally, several general issues such as the dynamic load rate, the depth and orientation of the column, and bracing and slenderness requirements are relevant to the connections described in this chapter, but discussion of these issues is deferred to Chapter 4.

This chapter will discuss a range of post-Northridge welded flange connections. All connections achieve the full moment capacity of the beam at the critical yield location if they develop their proper ductility. The connections are divided into four groups. The groups are:

- Unreinforced Connections
- Strengthened or Reinforced Connections
- Reduced-Beam-Section Connections
- Welded-Flange-Plate Connections

Each connection group will be discussed separately. Seven different connections are considered within the four groups. There are general overlapping characteristics within each group, and there are also unique features for each connection type. Each connection will be discussed separately, but the common features within each group will be noted. The yield mechanisms and failure modes for each connection type and each connection group will be discussed, and their impact on connection ductility and performance will be described. Simplified design models are proposed for each connection type. These models are developed based on basic concepts of engineering mechanics, and the development was coupled with evaluation of experiments performed on each connection. Wherever possible, attributes that are common to several types of connection are considered jointly for all connections. Rotational limits are proposed for each connection type based upon the rotations achieved in the experimental studies for connections that exhibit these yield mechanisms. These limits are often restricted to connections designed to achieve specific yield mechanisms and failure modes. The rotational limits are average values based upon the available experimental data. The plastic rotation,  $\theta_p$ , is directly based upon experimental results, and where adequate data is available, average values and standard deviations are computed. The plastic rotation at which loss of

gravity load resistance is expected,  $\theta_g$ , is more often based upon judgment and extrapolation of experimental results, since very few experiments have been conducted to deformations needed for loss of gravity load capacity.

### 3.3 Unreinforced Connections

Four variations of post-Northridge connections fall in the category of unreinforced connections. These include:

- Welded-flange-bolted-web connections with improved welds
- Welded-flange-bolted-web connections with improved welds and weld access hole details
- Welded-flange-welded-web connections with improved welds and weld access hole details
- Free-flange welded-flange-welded-web connections

These connections all have similar attributes in that plastic deformation is expected to occur as shear yielding of the panel zone and as flexural yielding of the beam near the face of the column. Thus, the yield mechanisms illustrated in Figure 2-7 are appropriate for these connections. Failure modes, which are shown in Figure 2.8 for the pre-Northridge connection, also apply to these unreinforced post-Northridge connections. However, it will be shown that there are significant differences in their design, which result in even larger differences in their seismic performance and the predominant failure modes observed with the unreinforced post-Northridge connections. The same failure modes may be possible with these post-Northridge connections, but changes in the design of the post-Northridge connections mean that the predominant failure modes are usually quite different from those commonly noted in pre-Northridge connections.

#### 3.3.1 Welded-Flange-Bolted-Web Connections with Improved Welding

The E70T-4 FCAW-SS electrode, which did not have any specific notch toughness rating, was used in all pre-Northridge connections (Johnson, 2000). At the same time, pre-Northridge welds clearly had substantial flaws, and analysis (Chi et al., 1997) showed that these flaws placed great local ductility demands on the welds. As a consequence, this condition, combined with other issues described in Chapter 2, resulted in fracture at relatively low stress levels on many pre-Northridge connections. This observation logically suggests that welds with greater CVN toughness and fewer flaws provide improved seismic performance over pre-Northridge connections. As noted in Chapter 2, one experimental study (Lee et al., 2000) investigated this possibility. In this study, connections as schematically illustrated in Figure 3-1 were tested for a range of moderate to large beam sizes. The connections used in this study had bolted webs which were designed for the shear force associated with plastic bending moment at each end of the beam and were identical to the web connections used for pre-Northridge connections. The flanges were welded with E70TG-K2 FCAW-SS electrodes, and the welds were ultrasonically inspected to assure a minimum level of quality control. The backing bar was removed for the bottom flange weld, the root of the weld was backgouged to remove all initial flaws, and the root was rewelded and reinforced with a fillet weld with the E71T-8 FCAW-SS electrode. The top backing bar is in a less critical location, since analysis (Chi et al., 1997; El Tawil and Kunnath, 1998) shows that the local stress and strain demand at the root of this weld is significantly less

severe than the demand at the root of the bottom flange weld. Therefore, this top backing bar was left in place but was reinforced with a E71T-8 fillet weld to assure that any flaw or defect at the root of this top flange weld was transformed into an internal flaw. Analysis (Chi et al., 1997) also shows that internal cracks must be much larger or in less notch tough material before they have unstable crack growth.

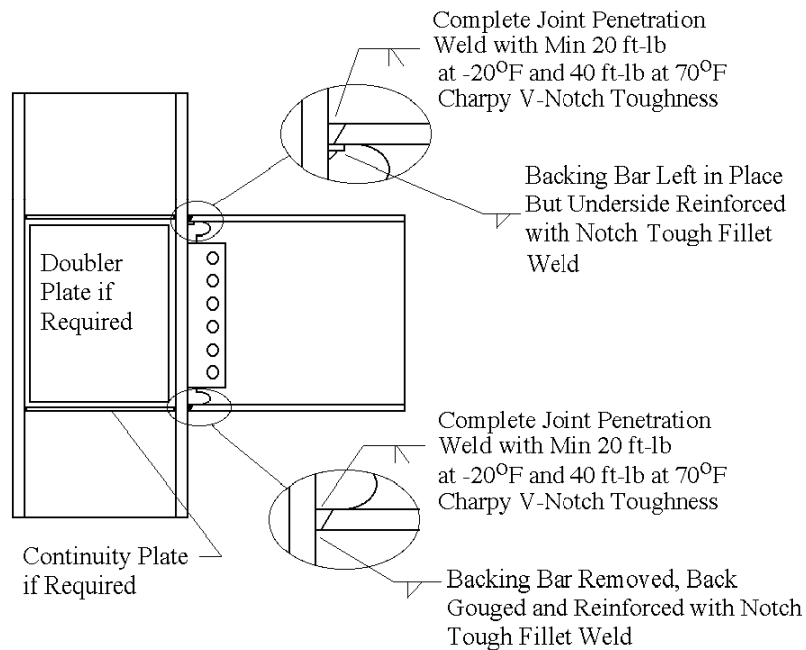


**Figure 3-1 Schematic of Welded-Flange-Bolted-Web Connection with Improved Welds**

These tests (Lee et al., 2000) were performed to provide comparison to the basic pre-Northridge connection with E70T-4 electrodes and to determine if this minimum change would provide adequate improvement to the seismic performance of welded-flange-bolted-web connections. A brief overview of these tests was provided in Chapter 2, but a more in-depth discussion is given here. Figure 3-2 compares the rotations ( $\theta_p$  and  $\theta_g$ ) achieved through the weld improvements as compared to recent pre-Northridge connections. The tests described in this figure were all fabricated since the Northridge earthquake with materials used in current practice. The diamonds represent pre-Northridge connections, and the squares represent connections with improved welding as indicated in Figure 3-1. The solid diamonds and squares show the rotation at initial fracture,  $\theta_p$ , while the hollow symbols represent the estimated rotation at loss of gravity load capacity,  $\theta_g$ . The improved welding alone did not result in larger rotational capacity for  $\theta_p$ , in that the data presented in Figure 3-2 for  $\theta_p$  overlap. The gravity load rotational capacity,  $\theta_g$ , is improved but the difference is not large. It is clear that the rotation achieved with the improved welding is still significantly lower than that required for seismic design of most special moment resisting frames. This indicates that welding with notch tough electrodes and backing bar improvements as noted in Figure 3-2 is not adequate to assure ductile behavior of welded-flange-bolted-web connections.

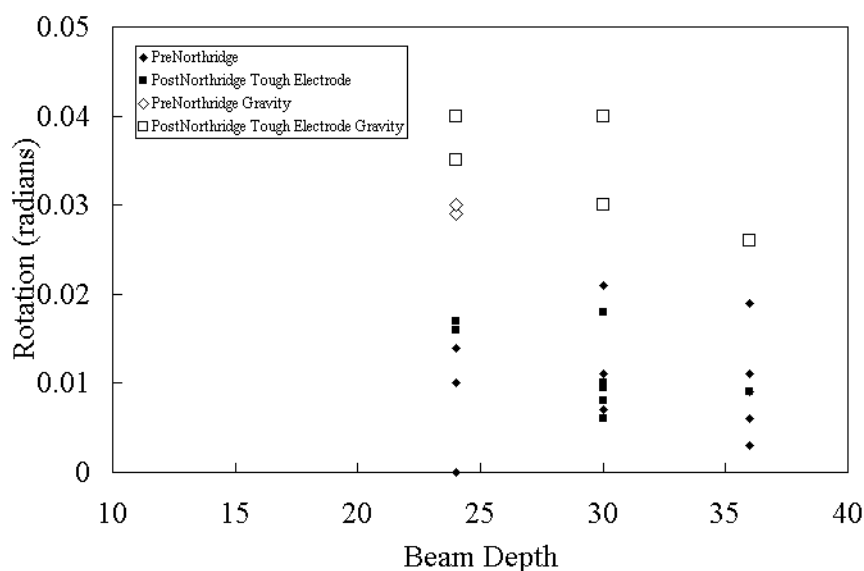


**Figure 3-2 Comparison of the Rotational Capacity**

With pre-Northridge connections and present day steel beams in the depth range of W24 to W36, fractures invariably occurred in or near the flange weld and the heat affected zone (HAZ). Connections with improved welding as depicted in Figure 3-1 avoid weld fracture for these same practical member sizes, but brittle fractures at the weld access hole were noted at deformations which were only slightly larger than the rotations achieved in pre-Northridge connections. Principles of elementary mechanics summarized in Chapter 2 show that the rotational capacity must be a function of the beam depth and beam span length. Post-Northridge welded-flange-bolted-web connections with improved welding must also expect this length and depth effect, and this behavior can on average be observed in Figure 3-2. However, the trends noted in Figure 3-2 are much less sharp than those noted for the pre-Northridge connection in Figure 2-4, because the test results are confined to a smaller range of member sizes in the post-Northridge connection tests. The trends mean that, on average, a reduction in the beam depth increases the rotational capacity of the connection, and, on average, an increase in the beam length also increases rotational capacity. These trends may have useful consequences, since they suggest that light steel frames with shallow beams in the W12 to W18 range may be able to develop adequate rotational capacity with notch tough welds and welded-flange-bolted-web details as shown in Figure 3-1. The fractures and weld access hole fabrication were examined (Barsom, 1999) after completion of these tests, and the finish and geometry of the weld access holes of many of these specimens had a rougher finish and transition with the beam flange than normally expected. This condition may contribute to the limited rotational capacity noted with these connections.

Removal of the bottom backing bar, backgouging the root of the bottom flange weld, and reinforcing the root of this weld is a relatively expensive process. In addition, weld procedures necessary to achieve the weld CVN toughness required in these post-Northridge connections are more costly than the pre-Northridge welds. As a result, studies (Ricles, et al., 2000) were made to determine if there were ways of reducing the cost of the welds while retaining the benefits of the detail shown in Figure 3-1. Fifteen pull tests were completed to examine several methods of

improving the connection economy. The pull test is a tension test under quasi-static or dynamic load with a specimen with the geometry shown in Figure 3-3. The pull tests are follow-up tests, and are comparable to the earlier pull tests completed in SAC Phase 1 testing (Kaufmann and Fisher, 1995). The pull tests do not precisely replicate the stress state (Deierlein and Chi, 1999) for the welded beam flange, but these tests provide a relative comparison of ductility achieved with different weld conditions. Six of these tests examined the effect of an enhanced weld throat with notch tough or other electrodes. These tests were performed because removal of the backing bar is very expensive, and Japanese research (AIJ, 1996) has suggested that enhanced weld throats may diminish the adverse effects of flaws at the root of the weld. It should be noted that the Japanese details leave the backing bar at a less critical location as illustrated in Figure 3-4. Further, the Japanese weld is a shop weld with the potential for avoiding all misalignment. There are other fundamental differences between the US and Japanese connection. Nevertheless, experiments (AIJ, 1997) have reported good ductility with the Japanese detail. Japanese research has also shown that grooved backing bars as depicted in Figure 3-4d provide an enhanced weld throat and good ductility. Consequently, the enhanced throat with backing bar left in place was viewed as a possible way to reduce the costs of post-Northridge flange welding. As illustrated in the lower right-hand corner of Figure 3-3, the enhanced throat was achieved by using a beveled backing bar to place the weld root below the bottom surface of the beam flange and outside of region of normal stress flow. Six of the pull tests include evaluation of misplacement of the notched backing bar relative to the weld preparation, since Specimens 4c-1 and 4c-2 had initial misalignment due to an undersize root opening in the flange weld preparation. Three specimens were designed to examine the effects of weld sequence, peening and post-treatment. Three others were designed to examine the effect of reinforcing pre-Northridge (E70T-4) welds with the backing bar left in place with a notch tough fillet weld on the bottom of the backing bar. This was considered as a possible modification to economically improve the performance of pre-Northridge connections. The last three tests examined the effect of the combination of backing bars and continuity plates on the weld performance. The general results of these 15 tests are summarized in Table 3-1.

All specimens in Table 3-1 were tested dynamically. The results show that the notched backing bar provided good ductility if electrodes with minimum CVN toughness were used and the backing bar preparation and the weld preparation were perfectly aligned. The performance of these specimens was as good as that achieved with backing bars removed, backgouged, and reinforced. However, notched backing bars did not provide good performance with low weld notch toughness and with notch tough electrodes with misalignment of the notch and weld preparation. These tests suggest that, while notched backing bars offer significant economic attraction, the potential problems outweigh the benefits, and as a result no full size connections were tested with this scheme. Reinforcement of backing bars on E70T-4 welds (Specimens 2-1, 2-2, and 2-3) did not result in an observable increase in ductility over previous tests without this reinforcement. The tests combining backing bars and continuity plates provided mixed results.

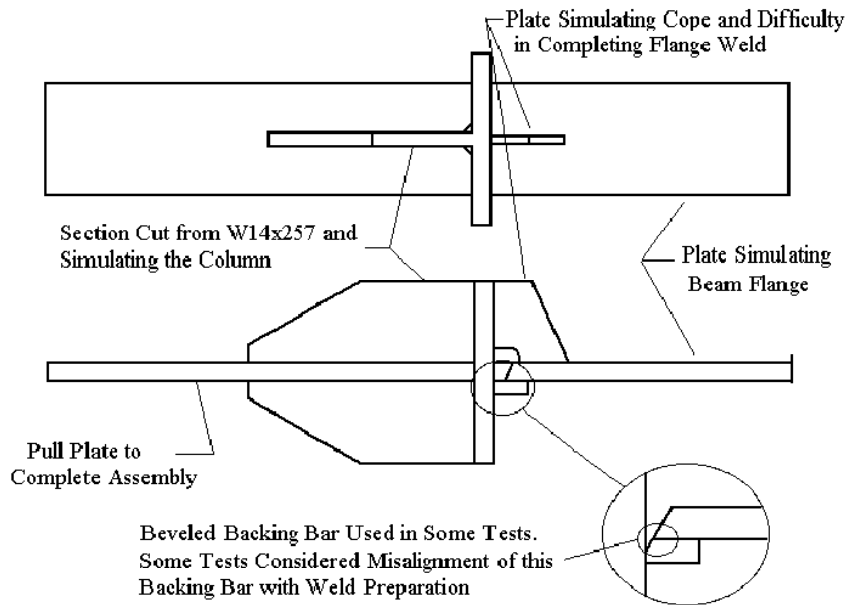


**Figure 3-3 Typical Pull Type Test Specimen**

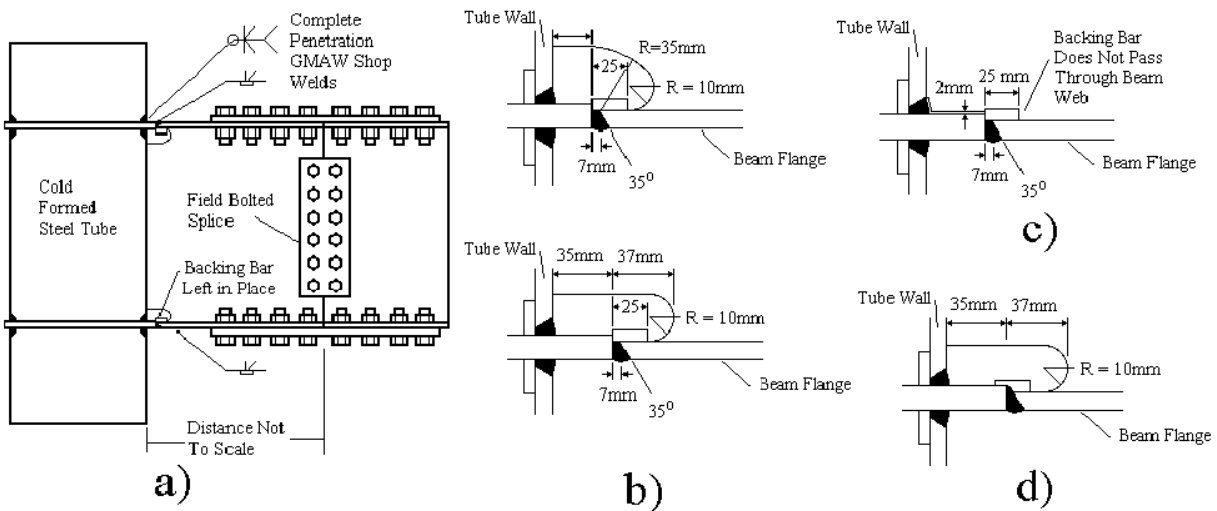


**Figure 3-4 Japanese Welded Flange Connection Details**  
**a) Standard Internal Diaphragm Connection, b) Typical Weld Access Hole Details,**  
**c) Typical Details with Weld Access Hole Eliminated, and d) Grooved Backing Bar Detail**

**Table 3-1 Summary of Pull Test Results**

Test Specimen	Weld and Objective	Displacement at Fracture	Fracture Type and Location
2-1	E70T-4 weld w/ run off tab removed but with backing bar left in place and reinforced with E7018	0.18"	Brittle Fracture in Weld Metal
2-2	Same	0.14"	Brittle Fracture in Weld Metal
2-3	Same	0.16"	Brittle Fracture in Weld Metal
4a-1	E70TG-K2 weld with backing bar and run off tab removed and underside reinforced with E71T-8	3.4"	Ductile Tearing in Base Metal
4a-2	Same	3.3"	Ductile Tearing in Base Metal
4a-3	Same	3.4"	Ductile Tearing in Base Metal
4c-1	E70TG-K2 with beveled backing bar left in place. Backing bar was misaligned with undersized weld root.	0.85"	Tearing of Beam Base Metal very near weld
4c-2	Same	1.3"	Tearing of Beam Base Metal very near weld
4c-3	E70TG-K2 with beveled backing bar left in place. Backing bar was perfectly aligned with proper sized weld root.	3.6"	Tearing of Column Base Metal
4c-4	Same	3.6"	Tearing of Column Base Metal
4c-5	E70T-4 with beveled backing bar left in place. Backing bar was perfectly aligned with proper sized weld root.	0.14"	Fracture in Weld Metal
4c-6	Same	0.14"	Fracture in Weld Metal
6-1	E70TG-K2 with run off tab removed but backing bar left in place without reinforcement fillet	3.2"	Ductile Tearing of Beam Flange
6-2	E70TG-K2 with run off tab removed but backing bar left in place without reinforcement fillet and continuity plate cut to release	3.3"	Ductile Tearing of Beam Flange
6-3	Same	1.35"	Fracture of Weld Metal

Note: See Ricles, et al. (2000).

The yield mechanisms of the unreinforced post-Northridge connection are simple, and are the same as those noted for the pre-Northridge connection. Appropriate equations for these yield mechanisms are provided in Table 3-2. Shear yield of the panel zone and flexural yield of the beam are the two mechanisms that are capable of achieving significant plastic rotation,  $\theta_p$ . The evidence presented in Chapter 2 shows that the maximum plastic rotation is likely to be achieved

when yielding in the beam and the panel zone is balanced to occur at approximately the same load or deformation. The last equation of Table 3-2 is a proposal for accomplishing this balanced condition based upon the panel zone yield equation. Figure 3-5 shows the geometry employed to develop the balance equation used in the table. As with other connection types, the balance equation assures that beam flexural yielding and panel zone yielding occur. Since this is a yield mechanism check, resistance factors are inappropriate in the balance equations. The balance equation shown in Table 3-2 will provide a slight apparent preference for flexural yielding, but discussion in Chapter 4 shows that most of the plastic rotation will still occur in the panel zone at this balance condition. The benefits of having balanced shear and flexural yield are based upon comparisons made in Chapter 2, but the observations are strengthened by discussion of post-Northridge test results in Chapter 4.

**Table 3-2 Yield Mechanisms of Unreinforced Post-Northridge Connection**

Yield Mechanism	Equation to Define Yield Mechanism Moment Resistance at the Face of the Column
Flexural Yielding of Beam	$M_{yield} = S F_{yb}$
Panel Zone Yielding	Yield occurs when $V_{pz}$ equals $V_{yield} = 0.55 F_{yc} d_c t_{wc}$
Recommended Balance Condition for Maximum Plastic Rotational Capacity	$\frac{\Sigma M_{yield-beam}}{d_b} \left( \frac{L}{L-d_c} \right) \left( \frac{h-d_b}{h} \right) \leq (0.9) 0.55 F_{yc} d_c t_{wc}$ but preferably $\frac{\Sigma M_{yield-beam}}{d_b} \left( \frac{L}{L-d_c} \right) \left( \frac{h-d_b}{h} \right) \geq (0.6) 0.55 F_{yc} d_c t_{wc}$

Note: All material properties provided in this table are expected values rather than minimum values.

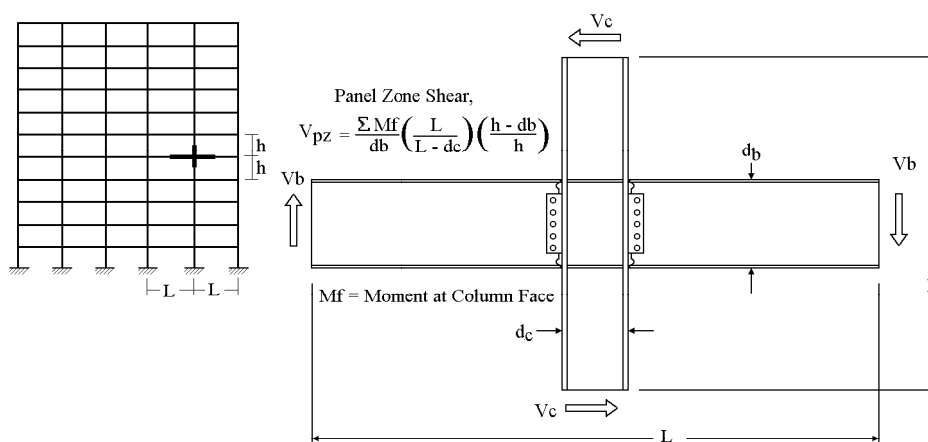


**Figure 3-5 Panel Zone Shear Force in Unreinforced Post-Northridge Connections**

The failure modes for unreinforced post-Northridge connections are also quite similar to those noted with the pre-Northridge connection in Figure 2-8. These failure modes are more

complex than the yield mechanisms, and equations for predicting them are summarized in Table 3-3. However, welded-flange-bolted-web connections with notch tough electrodes and backing bar details illustrated in Figure 3-1 increase the plastic rotational capacity slightly over that achieved with the pre-Northridge connection and the changes shift the common failure mode from brittle fracture of the weld to a somewhat less brittle fracture at the beam weld access hole. Analysis (El Tawil and Kunnath, 1998) showed that large local stress demands develop around the transition region of the weld access hole with beam flange. Shear transfer by the short beam flange segment causes local bending, which adds to the local concentrations. Finally, roughness and surface irregularities provide a source for crack development. The combination of these effects (Barsom, 2000) provides a ready source for low cycle fatigue cracking when cyclic inelastic deformations are applied. These observations, combined with the results of past Japanese research, suggest that possible improvements in connection performance can be made if the shape and transition of the weld access hole are improved. The desire to avoid these combined effects provides a basis for the connections with improved weld access hole details in the next section.

**Table 3-3 Failure Modes of the Post-Northridge Welded-Flange-Bolted-Web Connection**

Failure Mode	Equation to Define Failure Mode Moment Resistance at the Face of the Column	Related Issues
Fracture of Beam Flange Weld	Experiments indicate that this mode of failure is avoided for post-Northridge connections with notch tough electrodes and backing bar details as shown in Figure 3-1	
Fracture at Weld Access Hole	Experiments indicate that this mode of failure must be expected at moments of approximately $M_{pfail} = Z F_{yb}$ with ordinary weld access hole details such as illustrated in Figure 3.1	Problem is avoidable with improved weld access hole detailing and finish.
Plastic Bending of Beam	$M_{pfail} = Z \frac{F_{yb} + F_{tb}}{2}$ This failure mode is unlikely to be achieved with these connections except for very shallow beam depths.	Estimated lower bound on moment capacity if full bending moment achieved.
Flange Buckling	for flange - $\frac{b_f}{2 t_f} \leq \frac{52}{\sqrt{F_y}}$	
Web Buckling	controlled if $\frac{d_b}{t_w} \leq \frac{418}{\sqrt{F_y}}$	See discussion in Chapter 4.
Lateral Torsional Buckling	$L_b < \frac{2500 r_y}{F_y}$	$L_b$ is the unsupported length and equation is from existing AISC LRFD Seismic Provisions.
Continuity Plates	Continuity Plates required if $t_{cf} \geq 0.4 \sqrt{\frac{P_{bf}}{F_{yc}}}$ where $P_{bf} = 1.8 t_{fb} b_{fb} F_{yb}$	This equation is somewhat approximate, but it is the best estimate available at this time.
Weak Column Bending	$1.1 < \frac{\sum Z_c (F_{yc} - \frac{P_{uc}}{A_g})}{\sum Z_b F_{yb}}$	Limited strain hardening occurs with this connection, and so this is the existing design limit.

Note: All material properties provided in this table are expected values rather than minimum values.

The ductility achieved by the post-Northridge welded-flange-bolted-web connection is increased over that noted for the pre-Northridge connection. A regression analysis of results from tests completed since the Northridge earthquake on newer steels with notch tough electrodes and backing bar details such as shown in Figure 3-1 show that

$$\theta_{p\text{mean}} = 0.021 - 0.0003 d_b, \quad (3-1a)$$

and the standard deviation,  $\sigma_p$ , is

$$\sigma_p = 0.012 - 0.0004 d_b \quad (3-1b)$$

where  $\theta_{p\text{mean}}$  and  $\sigma_p$  are in radians, and  $d_b$  is in inches.

The maximum rotation for supporting gravity loads,  $\theta_g$ , were estimated based upon the two methods described in Chapter 2, Section 2.3. A regression analysis was completed for these estimated rotations and

$$\theta_{g\text{mean}} = 0.050 - 0.0006 d_b, \quad (3-2a)$$

and the standard deviation,  $\sigma_g$ , is

$$\sigma_g = 0.011 + .0004 d_b. \quad (3-2b)$$

### 3.3.2 Welded-Flange-Bolted-Web Connections with Improved Weld Access Hole Details

The previous section showed that notch tough welds with improved backing bar details were not enough to assure satisfactory performance of welded-flange-bolted-web connections. Both analyses (Chi et al., 1997; El Tawil and Kunnath, 1998) and experiments (Lee et al., 2000) showed that, as the notch toughness of the weld metal was increased, the conditions necessary for fracture were then shifted to the toe of the weld access hole region. Weld access hole details are defined in the AWS D1.1 (AWS, 1994) and AISC LRFD Specifications (AISC, 1994), but there is considerable latitude in the geometry and finish permitted for this detail. Another experimental study (Ricles et al., 2000) was undertaken to examine further improvements to the weld access hole region with the goal of further improving the seismic performance of the connection. This study was partially motivated by recent Japanese research (AIJ, 1997; Nakashima et al., 1999), which emphasized improvements in the weld access hole and welding details. Recent Japanese research (AIJ, 1996; AIJ, 1997) has investigated weld access holes, weld preparations, and variations in the weld process for the cold form tubular column connection as depicted in Figure 3-4a. Figure 3-4b shows the details of a recommended weld access hole geometry of this welded flange connection (AIJ, 1996). Based on the observation that fracture is often initiated from the toe of the weld access hole (in which stress/strain concentration is significant), Japanese research has examined the elimination of the weld access hole, which is possible with today's building standards as depicted in Figure 3-4c. All Japanese weld access holes and weld preparations are machined to a relatively smooth finish, while US weld access holes are often flame cut or drilled and flame cut. Grinding to finish is required for

weld access holes in heavy sections in the US, but the present standards for this finish are vague or ambiguous. While the Japanese research results are valuable, Japanese steel frame connections are fundamentally different from those used in the US. Japanese columns are usually cold formed steel tubes, and the weld is a shop weld which is placed a short distance away from the face of the column. The field splice is bolted as shown in Figure 3-4a. The critical location (or hot spot) of the Japanese welded connection occurs at the tip of the flanges rather than at the center of the flange as noted in US connections. These differences limit our ability to directly use Japanese research results. Nevertheless, Japanese research suggests that weld access hole details are an important area requiring research consideration.

Inelastic computer analyses (Ricles et al., 2000) were performed with the ABAQUS computer program to examine how different weld access hole details affect the state of stress and strain in the critical region around the weld access hole and flange weld. Modifications to these details were then examined. First, analyses were performed to evaluate the stress and strain state and potential for fracture and connection yielding, with different weld access hole geometries. The geometries focused on the transition angle between the weld access hole and the beam flange. Several different access hole geometries with different weld access hole lengths and different transitions from the weld access hole to the beam flange were considered. The analysis showed that the largest effective plastic strain (PEEQ), which is a measure of the local plastic strain demand, occurred at the toe of the weld access hole if the transition angle was relatively sharp. This location of the maximum PEEQ moved up into the web along the weld access hole as the transition angle became smaller. At the same time, the local hydrostatic stresses and maximum stress levels were reduced as the weld access hole was lengthened and the transition angle was reduced. Second, analyses showed that welded webs reduced the demands on the critical weld access hole region, and this observation provides the basis of another connection modification described in the next section of this chapter. These observations led to the proposed weld access hole geometry shown in Figure 3-6, since the changes in the hydrostatic stress and PEEQ suggested significant reductions in the fracture potential at both the weld and the toe of the weld access hole with this configuration. The surface of the weld access hole must have a 250 rms surface finish or better, since the high inelastic strains in the region combine with overly rough weld access hole surfaces to form crack initiation sites. The surface finish was evaluated by empirically examining the surface finish of several weld access holes and the surface cracking that developed during testing of the connections, which are summarized in Table 3-4. It should be noted that this weld access hole geometry and finish is combined with the weld requirements of Figure 3-1 to establish the full connection requirements.

Experimental studies were performed at Lehigh University (Ricles et al., 2000) to verify the effect of the weld access hole modifications. Table 3-4 summarizes the test results. Specimen LU-T4 evaluates the effect of the improved weld access hole detail on the performance of post-Northridge welded-flange-bolted-web connections, and this specimen is directly comparable to Specimens 7.1 and 7.2 of the Michigan study (Lee et al., 2000). All three specimens had W36x150 beams with bolted webs, the flanges were welded with E70TG-K2 electrodes, and the backing bars were treated as shown in Figure 3-1. In all three cases, the web connection employed 1" diameter A325 bolts in bearing type connections with shear tabs of similar

**Table 3-4 Summary of Test Results for Evaluation of the Effect of Web Attachment on the Connection Performance**

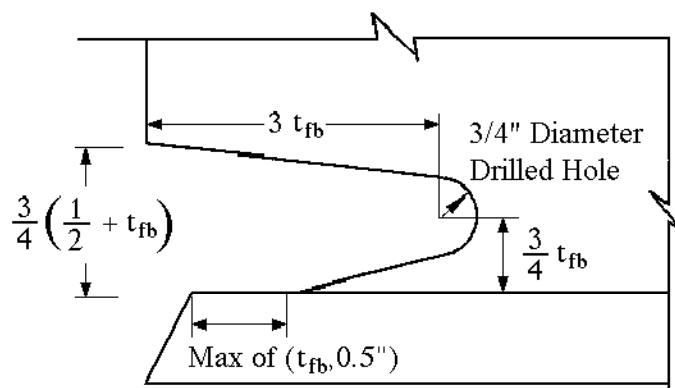
Test Specimen	General Description and Information	Beam and (Column) Sizes	Plastic Rotation at Initial Failure	Plastic Rotation Due to Panel Zone Yielding	Max. Moment (Moment at End of Test) Divided by $M_p$	Plastic Rotation at End of Test	Max. Moment Divided by $\frac{F_y + F_t}{2} Z$
LU-T1	Web attached w/1/2" groove weld to column flange and 3/8" fillet weld to 5/8" erection plate. Fracture of bottom flange in HAZ and erection plate weld @ 0.035.	W36x150 (W14x311)	0.035	.023	1.36 (0.45)	0.035	1.17
LU-T2	Web attached w/1/2" groove weld to column flange. Fracture of top flange @ 0.025 and web weld @ 0.35.	W36x150 (W14x311)	0.025	0.018	1.34 (0.6)	0.035	1.15
LU-T3	Web attached w/3/8" fillet weld to 5/8" erection plate. Fracture at bottom flange base metal and erection plate @ 0.019	W36x150 (W14x311)	0.019	0.005	1.06 (0)	0.019	0.91
LU-T4	Web attached w/Ten 1" A325X bolts to 5/8" erection plate. Fracture in top flange base metal)	W36x150 (W14x311)	0.018 (0.026 @ incomplete cycle)	0.008	1.12 (0)	0.026	0.96
LU-C1	Cruciform Specimen with same connection as LU-T1 except for no continuity plate	W36x150 (W14x398 and 3/4" doubler both sides)	0.025 for west beam & 0.038 for east beam after release	0.007	1.29 (east) 1.30 (west) (0.55)	0.04	1.13 (east) 1.14 (west)
LU-C2	Cruciform Specimen same as LU-C1 except that continuity plate included	W36x150 (W14x398 and 3/4" doubler both sides)	0.05 Fracture of flanges	0.007	1.31 (east) 1.26 (west) (0.35)	0.05	1.15 (east) 1.10 (west)

**Table 3-4 Summary of Test Results for Evaluation of the Effect of Web Attachment on the Connection Performance (continued)**

Test Specimen	General Description and Information	Beam and (Column) Sizes	Plastic Rotation at Initial Failure	Plastic Rotation Due to Panel Zone Yielding	Max. Moment (Moment at End of Test) Divided by $M_p$	Plastic Rotation at End of Test	Max. Moment Divided by $\frac{F_y + F_t}{2} Z$
LU-C3	Cruciform Specimen with same connection as LU-C1 except for no continuity plate and a column with lighter flanges to evaluate continuity plate effects	W36X150 (W27X258 and 5/8" doubler both sides)	0.038 0.038 partial flange fracture of west beam	0.001	1.42 (east) 1.34 (west) (0.25)	0.05	1.24 (east) 1.18 (west)
LU-C4	Cruciform Specimen same as LU-C3 except that continuity plate included	W36X150 (W27X258 and 5/8" doubler both sides)	0.052 0.052 west beam flange fracture	0.001	1.39 (east) 1.41 (west) (0)	0.052	1.22 (east) 1.23 (west)
LU-C5	Cruciform Specimen with same connection as LU-C1 except that 3.5" composite slab over 3" metal deck was employed. 4.75" long 3/4" shear connectors spaced at 12" on center. East beam fractured at shear stud weld location approximately 9" from column face.	W36X150 (W27X398 and 3/4" doubler both sides)	0.025 east beam fracture 0.046 at west beam fracture after east beam released	0.011	Composite behavior increases moment capacity somewhat and this comparison is not relevant.	0.046	Composite behavior increases moment capacity and this comparison is not relevant.

Notes:

1. Plastic rotations are rotations prior to significant loss of resistance or initial fracture of the connection.
2. All flange welds are E70TG-K2 CJP welds. Bottom flange backing bar removed, backgouged, and reinforced with 1/4" fillet of E71-T8.
3. Plastic moment capacity of LU-C1, LU-C2, LU-C3, and LU-C4 are based on mill certification results.
4. See Ricles, et al. (2000).



#### Typical Detail Requirements

1. Hole to be drilled.
2. Grind all flame cut surfaces of the weld access hole to a 250 microinch or better finish.
3. Similar finish requirements at the final weld transitions

**Figure 3-6 Recommended Improved Weld Access Hole Detail From the Lehigh Research Program**

geometry. A comparison of the results of Specimen LU-T4 with the results of University of Michigan tests (Table 2-1, and Lee, et al., 2000) show that the improved weld access hole detail significantly increased the ductility of the connection. Specimen LU-T4 obtained a plastic rotation that was approximately 100% larger than that achieved with Specimen 7.1. The plastic rotational capacity of Specimens LU-T4 and 7.2 appear to be similar, but LU-T4 is significantly better, because Specimen 7.2 fractured shortly after completing a single cycle of 0.017 radians while Specimen LU-T4 completed both cycles at 0.018 radians and was sustaining a single excursion to 0.027 radians before fracture occurred. Japanese researchers (AIJ, 1996; AIJ, 1997) have observed the importance of the weld access hole geometry and finish. Therefore, the combined observations from these two sources show that weld access hole geometry and finish are important criteria for the welded-flange-bolted-web connections. The weld access hole finish is important, because the largest plastic demands occur at or near the face of the column, and irregularity or roughness provides a potential source of flange fracture. Specimen LU-T4 fractured in the beam flange base metal in the heat affected zone, but cracking was noted in the weld access hole region after relatively large inelastic deformations. Thus, the improved weld access hole detail was successful at moving the fracture location away from the weld access hole transition. While the surface finish and weld access hole geometry are important, the comparison also shows that changes to the weld access hole alone are not enough to assure adequate seismic performance. There are insufficient test data to document a reliable  $\theta_p$  for this connection, and so detailed design information for this connection option are not provided. Nevertheless, the performance of specimen LU-T4 suggests that post-Northridge welded-flange-bolted-web connections with the improved weld access hole details may achieve rotations in the order of twice those indicated for Equation 3-1. The depth and span length reasoning presented in Chapter 2 and verified in Figure 2-4 also applies to these post-Northridge connections. The

improvements illustrated by Specimen LU-T4 indicate that there is a high probability that welded-flange-bolted-web connections with weld details, as illustrated in Figure 3-1, and weld access hole geometry and finish as illustrated in Figure 3-6, will develop the ductility required for even the most demanding seismic applications with lighter framing and beam depths in the range of W21, W24 or less.

### 3.3.3 Welded-Flange-Welded-Web Connections with Improved Weld Access Hole Details

The combined benefit of improved welding, improved backing bars, and improved weld access hole details is not adequate without other improvements to assure ductile behavior for the large members used in new steel frame construction. Further, nonlinear analysis (Ricles et al., 2000) showed that stiffer and stronger web attachments reduced the inelastic demands on the critical areas of the connection. As a result, the effect of the web connection was examined as a means of providing further improvement in the connection performance.

Inelastic analysis of connection behavior (El Tawil and Kunnath, 1998; Ricles et al., 2000) shows that web attachments often provide very little shear force transfer until large inelastic strains develop. This shear force transfer depends upon the size of the members and the stiffness and resistance of the web connection. When the web connection does not transfer its full share of the beam shear force, the analyses show that increased local stress and strain demands develop in the beam flanges between the weld access hole and the face of the column. As a result, welding of the beam web was experimentally examined (Ricles et al., 2000) as a method for further improving the seismic performance of the welded flange moment frame connection. Three levels of web welding were examined. Minimal web bolting was employed to simulate a temporary erection connection, flange welds were treated as illustrated in Figure 3-1, and weld access hole geometry and finish were treated as shown in Figure 3-6. The first and more economical level of welding considered only the fillet weld at the edge of the shear tab as illustrated in Figure 3-7. The second level of web welding consisted of a CJP groove weld illustrated in the figure. A third level of web welding consisted of both the first and second level welding. Web welding had considerable influence on the connection behavior as will be shown in later discussion.

Specimens LU-T1, LU-T2, and LU-T3 were identical to the previously discussed bolted web specimen (Specimen LU-T4) except for modifications to the web attachment. As noted earlier, LU-T4 had the same flange welds and bolted web attachments as the Michigan tests (Lee et al., 2000), but the weld access hole details and finish were improved to that illustrated in Figures 3-1 and 3-6. Specimen LU-T3 had only two bolts, which simulate the temporary connection that would be needed to hold the beam in place during erection and welding, but the web was attached with a fillet weld between the edge of the shear tab and beam web (first level welding) as depicted in Figure 3-7. As shown in Table 3-4, the plastic rotation achieved with this specimen is nearly identical to that achieved with the bolted web, but examination of the moment-rotation curves shows that the bolted web did somewhat better, since it completed both cycles at  $\theta_p$  of 0.018 radians and fractured during the initial cycle of 0.025 radians, while Specimen LU-T3 was unable to complete the second cycle at 0.019 radians. This comparison indicates that fillet welded web connections are comparable or may be slightly inferior to welded-flange-bolted-web connections.

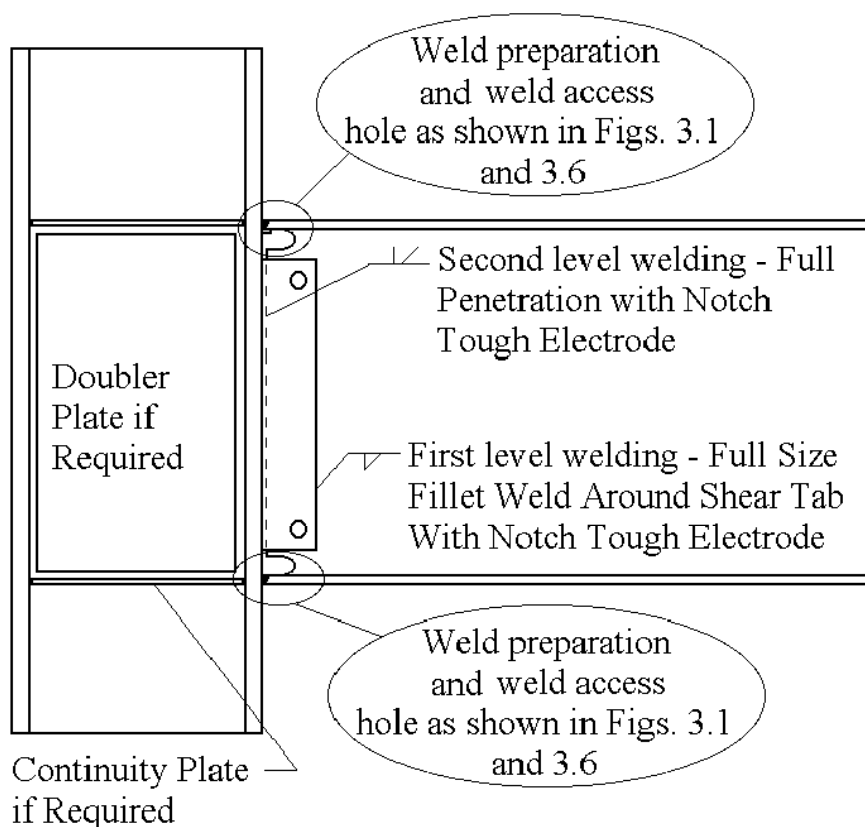


**Figure 3-7 Web Welding Details Evaluated in SAC Phase 2 Research**

It should be emphasized, however, that past research (Tsai and Popov, 1988) showed that fully bolted webs with significant supplemental fillet welds performed significantly better than bolted webs only. The web of Specimen LU-T2 was attached with a CJP groove weld between the beam web and the face of the column (second level welding), and this specimen achieved a  $\theta_p$  of 0.025 radians.

Examination of the moment-rotation curve of this specimen shows that the behavior is somewhat better than suggested by this assigned plastic rotation, because the specimen achieved both cycles of 0.025 radians, and initial fracture occurred during the second half of the 0.035 radian cycle. The comparison of LU-T2 to LU-T3 and LU-T4 shows that a CJP groove weld at the beam web results in significantly better rotational capacity than achieved with bolted webs or fillet welded webs. Finally, LU-T1 was welded with both first and second level web welding, and the specimen completed a full cycle of 0.035 radian rotation. It should be emphasized that these are deep W36 beams, and the good rotational capacity achieved with these tests shows that connections with fully welded webs, notch tough flange welds with backing bar details as illustrated in Figure 3-1, and weld access hole detail and finish as illustrated in Figure 3-6 can achieve adequate ductility for a wide range of member sizes and seismic applications. This can be seen by comparing the moment-rotation curve of specimen LU-T1 in Figure 3-8 with the LU-T4 in Figure 2-18 and Michigan specimen 7.1 in Figure 2-6. As a consequence of the good rotational capacity achieved with Specimen LU-T1, the dual level web welding was also used in

Specimens LU-C1 through LU-C4. These C-series tests were performed for the development of an adequate database for evaluating the connection and for examining the effects of continuity plates and column depth on the connection performance. These specimens also achieved good ductility with similar failure modes as can be seen in Table 3-4. These later C-series tests are discussed in greater detail later in Chapter 4.

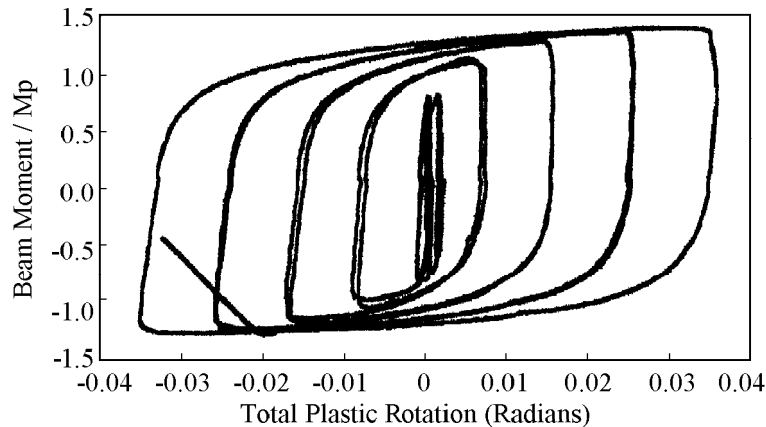


**Figure 3-8 Moment-Rotation Curve for Lehigh Specimen LU-T1**

The yield mechanism for this fully welded web connection and the balance equations for shear and flexural yielding are the same as those noted for welded-flange-bolted-web connections in Table 3-2. Failure modes are different, however, and they are summarized in Table 3-5.

Experiments show other consequences of a stiff, strong web attachment. First, Table 3-4 clearly shows that specimens with stiff, strong web attachments develop much more strain hardening in the beams. The maximum moments greatly exceed  $M_p$  for connections with strong web attachments because of this large beam strain hardening. Table 3-4 shows that the connections with these enhanced web attachments all develop maximum moments at the face of the column that were at least 26% and as much as 42% larger than the plastic moment capacity of the beam,  $M_p$ , based upon the actual yield stress of the beam steel. The beams also consistently develop moments at the face of the column that are 10% to 20% larger than

$$M_{pfail} = Z \frac{F_{yb} + F_{tb}}{2} \quad (3-3)$$

where  $F_{tb}$  is the expected tensile stress of the beam steel. Past research (Coons, 1999) also has shown that moments in excess of Equation 3-3 will be consistently achieved in ductile connections, and this can be regarded as an approximate lower bound to the maximum moment achieved in a ductile member or connection. The larger strain hardening means that larger bending moments are transferred to the column. It is customary to design steel frames as strong-column-weak-beam structural systems. The welded-flange-welded-web connection causes increased bending moments in the columns because the flexural yield moment of the beam is

**Table 3-5 Failure Modes of the Post-Northridge Welded-Flange-Welded-Web Connection with Improved Weld Access Hole Details**

Failure Mode	Equation to Define Failure Mode Moment Resistance at the Face of the Column	Related Issues
Fracture of Beam Flange Weld	Experiments indicate that this mode of failure is avoided for post-Northridge connections with notch tough electrodes and backing bar details as shown in Figure 3-1.	
Fracture at Weld access hole	Experiments indicate that this mode of failure is avoided for connections with backing bar details as shown in Figure 3-1 combined with improved weld access hole geometry as shown in Figure 3-6, and web welding as shown in Figure 3-7.	
Tearing Initiated at Welded Web Connection	This is the probable failure mode with this connection. Tearing of the welded web connection may ultimately lead to fracture of beam flanges.	This failure mode is likely to occur after large plastic deformations and after the plastic bending failure moment is attained.
Plastic Bending of Beam	$M_{pfail} = Z \frac{F_{yb} + F_{tb}}{2}$	This moment capacity is likely to be exceeded with this connection.
Flange Buckling	for flange - $\frac{b_f}{2 t_f} \leq \frac{52}{\sqrt{F_y}}$	
Web Buckling	controlled if $\frac{d_b}{t_w} \leq \frac{418}{\sqrt{F_y}}$	See discussion in Chapter 4.
Lateral Torsional Buckling	$L_b < \frac{2500 r_y}{F_y}$	$L_b$ is the unsupported length and equation is from existing AISC LRFD Seismic Provisions.
Continuity Plates	Continuity Plates required if $t_{fc} \geq 0.4 \sqrt{\frac{P_{bf}}{F_{yc}}}$ where $P_{bf} = 1.8 t_{fb} b_{fb} \frac{F_{yb} + F_{tb}}{2}$	This equation is somewhat approximate, but it is the best estimate available at this time.
Weak Column Bending	$1.1 < \frac{\sum Z_c \left( F_{yc} - \frac{P_{uc}}{A_g} \right)}{\sum Z_b \frac{F_{yb} + F_{tb}}{2}}$	Significant strain hardening occurs with this connection, and so the proposed limit for controlling plastic deformation of column reflects this fact.

Note: All material properties provided in this table are expected values rather than minimum values.

increased significantly by strain hardening. It is well known that the AISC equation for assuring strong column-weak beam behavior does not prevent column yielding (Nakashima and Sawaizumi, 1999), but rather the AISC equation limits yielding so that neither excessive inelastic deformation of the columns nor a story mechanism occurs. These equations are based upon the hypothesis that connections do not develop moments much larger than  $M_p$ . The

connections described in this section are much stronger, and the increased connection moment is passed to the column. This increased moment must be considered when evaluating strong-column-weak-beam (SCWB) behavior, and so

$$1.1 < \frac{\sum Z_c \left( F_{yc} - \frac{P_{uc}}{A_g} \right)}{\sum Z_b \frac{F_{yb} + F_{tb}}{2}} \quad (3-4)$$

This equation is of the same format as that used for the other unreinforced connections, and this recommendation is reflected in the last two lines of Table 3-5.

The large strain hardening also places greater demands upon panel zones. Specimens LU-T1 through LU-T4 had moderately strong panel zones, and they would have strong panel zones by the balance condition of Equation 2-6 for the actual measured yield stress of the steel. That is,

$$V_{pz} = \frac{\sum M_{\text{yield-beam}}}{d_b} \left( \frac{L}{L-d_c} \right) \left( \frac{h-d_b}{h} \right) \leq (0.9) 0.55 F_{yc} d_c t_{wc} \quad (3-5)$$

Despite the relatively large panel zone yield resistance, large panel zone shear strains were noted in Specimen LU-T1, because of the large flexural strain hardening observed in the experiments. Specimen LU-T4 is unlikely to have tolerated the large panel zone shear strains that would have results with a much weaker panel zone, because its ultimate failure started at the web attachment due to the large panel zone deformation. Specimen LU-T4 achieved much less strain hardening and plastic rotation because of the weaker connection, and the panel rotation demands for this connection were quite modest. However, the stronger welded web connection resulted in larger strain hardening and larger moments in the beams, and this produces dramatic increases in the deformations of the panel zone.

The failure modes observed with the welded web connections also provide insight into the connection behavior. Specimens LU-T4 and LU-T3 developed very modest plastic rotational capacity, very little strain hardening, and very little panel zone yielding. These connections developed initial cracking which generally initiated in the beam flange region. LU-T1, LU-C1, LU-C2, LU-C3, and LU-C4 developed much larger plastic rotation, much larger strain hardening, and significant panel zone yielding. The initial crack development of these specimens appears to be strongly influenced by the large panel zone deformations. The stiffer and stronger web attachment causes larger shear forces in the web attachment, but the greater stiffness makes the web attachment even more susceptible to distortion induced by panel zone yielding. Consequently, the changes in the failure mode are likely influenced by the increased panel zone yield deformation. These factors illustrate the importance of achieving the balanced yield condition shown in the last line of Table 3-2.

The issue of the rotation at which gravity loads can no longer be supported,  $\theta_g$ , also appears to be strongly influenced by stiffer, stronger web connections. Due to limitations in testing

equipment and setup, the researchers have not carried the experiments to large enough deformations to precisely determine this rotation. However, examination of the condition of the specimen at the conclusion of the tests provides considerable insight into this issue. Table 3-4 shows that some tests have relatively little rotational resistance after the initial fracture. The stiff, strong web connection appears to result in much more rigid connection behavior, so that cracking and fracture of the beam flange is closely coupled with and accompanied by cracking and fracture of the web connection. Thus, it appears that  $\theta_g$  will be only slightly larger than  $\theta_p$  for these connections.

The research has shown that the addition of a stiffer, stronger web connection enhances the connection performance. Therefore, connections with

- notch tough electrodes used for the flange welds,
- bottom backing bars removed, backgouged, and reinforced with notch tough welds as illustrated in Figure 3-1,
- top backing bars reinforced with a notch tough fillet weld as illustrated in Figure 3-1,
- weld access hole finish and geometry improved to that of Figure 3-6, and
- a CJP groove weld between the beam web and the column and a supplemental fillet weld between the beam web and the erection plate as illustrated in Figure 3-7

will result in a significant increase in connection ductility. This ductility depends upon the beam depth by reasoning described in Chapter 2. However, the test data for such connections are all completed with W36 beam sections, and so the depth behavior cannot be established from test data. A statistical analysis of the tests completed since the Northridge earthquake, where the connections met the above conditions, show that

$$\theta_{p\text{mean}} = 0.041 \quad (3-6a)$$

and the standard deviation

$$\sigma_p = 0.003. \quad (3-6b)$$

Decreased beam depth will, on average, result in increased rotation capacity, and so these limits should be usable for all connections with beam depth less than W36.

The maximum rotation for supporting gravity loads,  $\theta_g$ , could not be directly determined from most of these tests, because the tests were not carried to large enough deformations. Methods used in Chapter 2 were employed if the rotational resistance deteriorated adequately in the test. As a third method, it was noted that, in all cases,  $\theta_g$  will be larger than  $\theta_p$ . Thus, specimens which were not tested to a state that  $\theta_g$  seemed imminent, were assigned a  $\theta_g$  that was 0.01 radians larger than  $\theta_p$ , since this should be a conservative estimate for these specimens. Therefore,

$$\theta_{g\text{mean}} = 0.054, \quad (3-7a)$$

and the standard deviation

$$\sigma_g = 0.002. \quad (3-7b)$$

Again, this limit can conservatively be applied for all connections with beams less than W36 in depth.

### 3.3.4 Free-Flange Connection

The free-flange connection is illustrated in Figure 3-9 and was proposed (Goel, et al., 1997; Choi et al., 2000) in response to detailed finite element analysis of connection performance. These analyses showed that the beam web carried relatively little shear stress through the web attachment under elastic stress conditions. Large parts of the beam shear force transferred to the beam flanges near the face of the column. A truss analogy (Goel, et al., 1997) was proposed as a method for simulating this behavior, and the free-flange connection depicted in Figure 3-9 was presented as a method of achieving this truss action at the connection (Choi, et al., 2000). The cut back web section of the free-flange connection reduces the local stresses in the beam flanges and reduces the potential for beam flange fracture at the weld access hole. At the same time, the heavy tapered web plate helps to transfer the shear force from the more highly stressed regions of the beam web a short distance from the column to the face of the column. This web plate is significantly heavier and stiffer than the shear tab used in the pre-Northridge connection. The stiffer, stronger web plate of the free-flange connection results in larger shear force transfer from the beam web through the web plate to the face of the column. As a result, large fillet welds are required between the web plate and the beam web both on the perimeter of the plate and at the end of the cut back beam as shown in the figure.

The free-flange serves two purposes. First, it reduces the shear force transferred by the beam flanges to the column, and second, it provides a free gage length to allow the spread of yielding without high strain concentrations in that region. A longer free-flange length provides a longer flange length for yielding and development of plastic rotation, but the free length also must be kept moderately short to control buckling of the free-flange length. The balance point between buckling of the free-flange and yielding of the free-flange occurs at a slenderness ratio of approximately 20 or a length of approximately 5 to 6 times the flange thickness. The web connection is designed for the expected shear force, and a portion of the flange force associated with the bending moment of the connection. A portion of the web plate near the mid height need not be welded to the beam or the column or included in the strength calculations, because the design analogy postulates relatively little stress in this region. The tapered shape of the web plate is also selected to reflect the flow of stress postulated with the design model.

The free-flange connection was developed by a different line of reasoning (Goel, et al., 1997; Tide et al., 1994) than the welded-flange-welded-web connection, but the consequences are much the same. Both connections better develop the web of the beam in both bending and shear, and they both reduce the demands on the weld and weld access hole region. Both connections provide smoother transition in the weld access hole region, and this reduces the sources of crack development. The consequence is increased plastic rotational capacity and greater strain hardening of the connection.

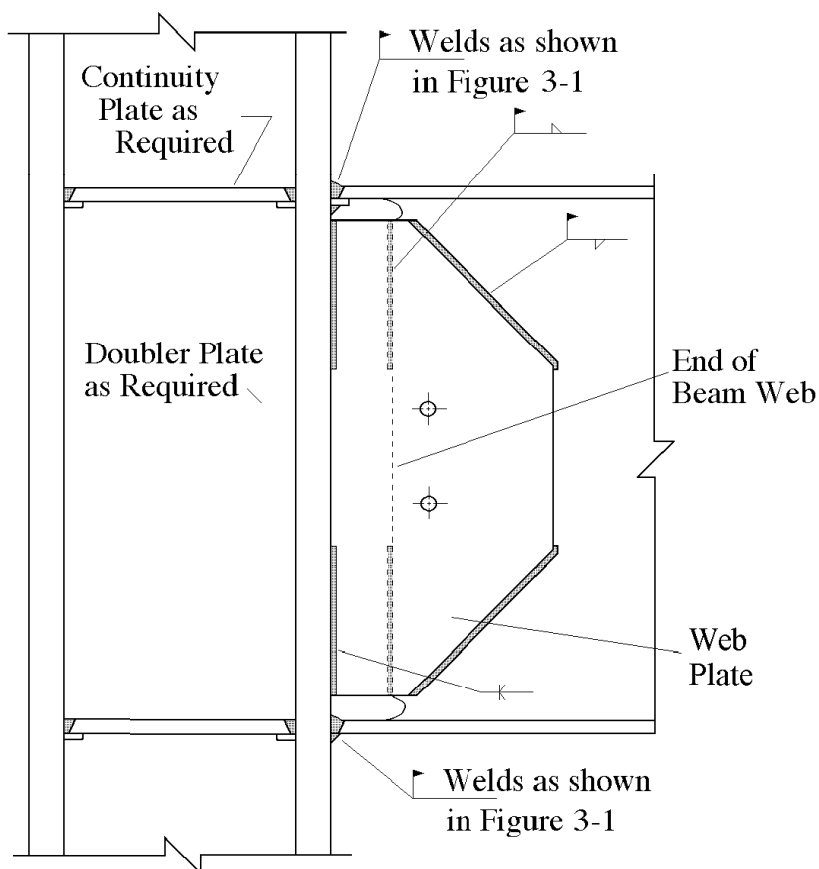


**Figure 3-9 Proposed Free-Flange Connection**

A series of experiments were completed on the free-flange connection and are summarized in Table 3-6. The stiffer, stronger nature of the web joints for free-flange connections can be illustrated by comparing the web plate of free-flange specimen 8.2 with the otherwise identical specimens 3.1 and 3.2 for the welded-flange-bolted-web connection tests in Table 2-1. It can be seen that the thickness of the web plate for the free-flange connection is approximately twice the thickness of the shear tabs used in comparable welded-flange-bolted-web connections, and the depth of the free-flange web plate is also greater than the comparable bolted web shear tabs. The eccentricity of the connection is also increased, but the stiffness of the web plate is clearly playing a greater role in transmitting moment and shear to the column with the free-flange connection. In addition, cutting back the web section permits more room for flange welding and provides reduced local stresses in the critical beam flange region. Table 3-6 shows that the free-flange connections provide a significant increase in  $\theta_p$  over that noted with welded-flange-bolted-web connections in Table 2-1. It can be seen that the free-flange specimens all develop strain hardening with increased rotation, and the maximum moments all exceed Equation 3-3. Comparison of the data in Table 3-6 to the data in Table 3-4 shows that the free-flange and welded web connection both result in considerable strain hardening, but the hardening is slightly smaller for the free-flange connection.

**Table 3-6 Summary of Test Results for Free-Flange Connection**

Test Specimen	General Description and Information	Beam and (Column) Sizes	Plastic Rotation at Initial Failure	Plastic Rotation Due to Panel Zone Yielding	Max. Moment (Moment at End of Test) Divided by $M_p$	Plastic Rotation at End of Test	Max. Moment Divided by $\frac{F_y + F_t}{2} Z$
Michigan 8.2 (Choi, et al., 2000)	Specimen appeared to be stroke limited in that larger rotations were possible. No fracture.	W24x68 (W14x120) 3/4" web plate	0.04	0.0	1.43 (0.83)	0.04	1.21
Michigan 9.1 (Choi, et al., 2000)	Deeper W30 beam with lower yield stress $F_y=44$ ksi. Tear in top flange.	W30x99 (W14x176) 1" web plate	0.035	0.022	1.51 (0.43)	0.04	1.26
Michigan 9.2 (Choi, et al., 2000)	Deeper W30 beam with higher yield stress $F_y=57.5$ ksi. Note that cycles are one sided and 0.03 was not attained in both directions. Lateral torsional buckling.	W30x99 (W14x176) 1" web plate	0.03 Note one sided plots	0.0	1.27 (0.55)	0.03	1.13
Michigan 10.1 (Choi, et al., 2000)	Heavier W30 section with no doubler plate. Significant panel zone yielding. Small web plate crack.	W30x124 (W14x257) 1" web plate	0.025 Extra cycles at max deformation	0.017	Not Available	0.017	Not Available
Michigan 10.2 (Choi, et al., 2000)	Heavier W30 section with doubler plate. Little panel zone yielding. Small flange crack at toe of access hole.	W30x124 (W14x257) 1" web plate 1/2" doubler	0.027 One extra cycle	0.007	Not Available	0.007	Not Available

**Table 3-6 Summary of Test Results for Free-Flange Connection (continued)**

UCSD Specimen (Gilton, et al., 2000) UCSD-FF	W36 section with light doubler plate. Cracking developed at the weld of the web plate to column flange and propagated into the column. Flange cracking also noted.	W36x150 (W14x257) 1 1/4" web plate 1/4" doubler	0.018	0.018	Estimated 0.06	0.024	Estimated 1.2
UT Austin Specimen (Venti, 2000) UTA-FF	Cruciform Specimen with Composite Slab. Specimen is comparable to non-composite UCSD test. Cracking observed at the top and bottom of web plate, but bottom flange of north beam fractured during the 4 <sup>th</sup> cycle at the maximum story drift. Rotational capacity of this specimen is thus in part limited by test apparatus.	W36x150 (W14x398) 1 1/8" web plate 3/4" doubler	0.034	0.018	Composite behavior increases moment capacity somewhat and this comparison is not relevant.	0.034	Composite behavior increases moment capacity somewhat and this comparison is not relevant.

1. Plastic rotations are rotations prior to significant loss of resistance or initial fracture of the connection.
2. All flange welds are E70TG-K2 CJP groove welds. Top backing bars left in place but reinforced with 1/4" E71-T8 fillet welds but bottom backing bar removed, backgouged, and reinforced with E71T-8 fillet welds.
3. Incomplete information was available for some tests completed late in the research, and estimated values are identified and used for some parameters.
4. See Choi, et al. (2000), Gilton et al. (2000), and Englehard (2000).

The yield mechanisms of the free-flange connection are the same as those noted for other unreinforced connections and are summarized in Figure 2-7 and Table 3-2. However, flexural yielding of the beam progresses further out into the beam flange with the free-flange connection than it does for the welded web connection. The failure modes are also much the same as for the welded-flange-welded-web post-Northridge connection, but there are slight differences, and the failure modes are summarized in Table 3-7. However, both the welded-flange-welded-web connection and the free-flange connection are less prone to the more brittle modes of weld fracture and beam flange fracture at the weld access hole than are the welded-flange-bolted-web connections. They both develop significant local buckling before ultimate failure occurs. The test results suggest that the ultimate failure of the welded web initiates as cracking and tearing of the web connection. The ultimate failure of the free-flange connection may also start from the web attachment, but flange cracking due to large inelastic strains also seems to be a likely source of ultimate failure.

The design parameters of the free-flange connection share many aspects of the other unreinforced connections, and the equations provided in Table 3-5 for the welded web connection are also applicable to the free-flange connection. However, the free-flange connection requires special consideration of the amount of cut back in the beam web, the geometry and finish for the cut back, and the design requirements for the web connection. To accomplish these special requirements, three basic steps (Choi, et al., 2000) are required.

- Step 1. Determine the design shear force for the web attachment. This design shear force for the free-flange web,  $V_{ffw}$ , is determined by using 110% of the expected plastic moment of beam at each end of the beam in double curvature, so that

$$V_{ffw} = \frac{1.1 Z_b F_{yb}}{L} + V_g$$

where  $L$  is the clear span length of the beam from the face of each column, and  $V_g$  is the shear force due to gravity load. The web attachment is designed for this full shear force as illustrated in Figure 3-10.

- Step 2. Determine the free-flange length. The free-flange length,  $L_{ff}$ , is determined from a ratio,  $\alpha$ , where

$$\alpha = \frac{L_{ff}}{t_{fb}}$$

and where  $5.0 \leq \alpha \leq 6.0$ . A 0.5" radius is used where the cut back web section transitions into the beam flange. The end of the beam web is held a clear distance,  $a$ , from the face of the column as shown in Figure 3-10, and  $a$  is taken as three times the thickness of the web plate.

- Step 3. Web plate and welds are designed. The web plate and the welds are designed to resist the combined shear force,  $V_{ffw}$ , and the couple caused by the tensile force,  $T_{ffst}$ ,

and the compressive force,  $C_{ffst}$ , as illustrated in the figure. The compressive and

$$\text{tensile forces are determined as } C_{ffst} = T_{ffst} = \frac{0.25 t_w d_b^2 F_{yb}}{h_{ffst} - h_{seff}}$$

The height of the free-flange web plate,  $h_{ffst}$ , is set to achieve a minimum weld clearance,  $b$ , at the top and bottom of the beam, where  $b$  is approximately 2 inches, so that

$$h_{ffst} = d_b - 2 t_{bf} - 2b.$$

Only a portion of the web plate height,  $h_{seff}$ , is considered to be effective in resisting the tensile and shear force in the web plate as illustrated in Figure 3-10. This partial height is approximately 25% of the beam depth as shown in Figure 3-10. Therefore, the top and bottom portions of the web plate and the welds within that region are designed to develop the combined shear and tensile force as illustrated in the figure. The web plate is attached to the column with CJP, double bevel welds over the length,  $h_{seff}$ , at the top and bottom of the web plate. Fillet welds along weld lines A and B are designed to take the combined tensile and shear force with the effective height,  $h_{seff}$ . The plate geometry must be designed so that the horizontal extension of the plate to the 45° taper clears the weld access hole region as shown in the figure.

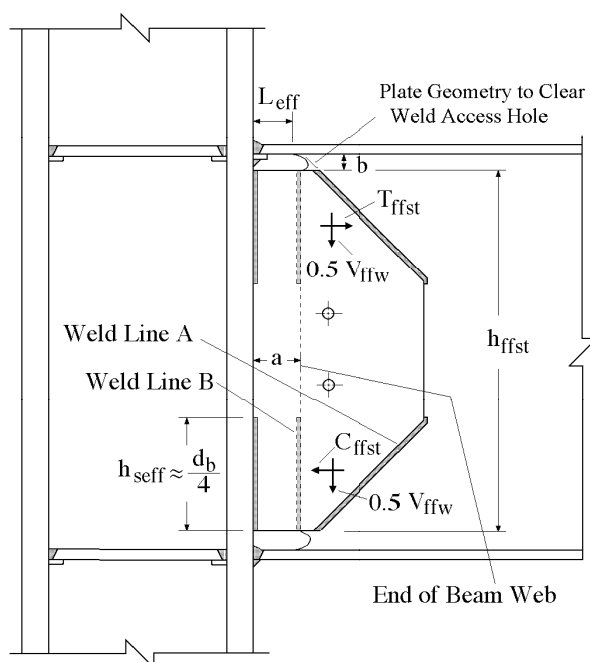


**Figure 3-10 Schematic of the Forces for Design of the Free-Flange Web Plate and Welds**

**Table 3-7 Failure Modes of the Post-Northridge Free-Flange Connection**

Failure Mode	Equation to Define Failure Mode Moment Resistance at the Face of the Column	Related Issues
Fracture of Beam Flange Weld	Experiments indicate that this mode of failure is avoided with notch tough electrodes and backing bar details as shown in Figure 3-1.	
Fracture at Weld Access Hole	The free-flange connection avoids this mode of failure with details illustrated in Figures 3-9 and 3-10.	
Tearing Initiated at Welded Web Connection	The web connection requires special design considerations as noted earlier. These require that the web connection have adequate strength and stiffness to assure good connection performance.	
Plastic Bending of Beam	$M_{pfail} = Z \frac{F_{yb} + F_{tb}}{2}$	This moment capacity is likely to be exceeded with this connection.
Flange Buckling	for flange $\frac{b_f}{2 t_f} \leq \frac{52}{\sqrt{F_y}}$	
Web Buckling	controlled if $\frac{d_b}{t_w} \leq \frac{418}{\sqrt{F_y}}$	See discussion in Chapter 4.
Lateral Torsional Buckling	$L_b < \frac{2500 r_y}{F_y}$	$L_b$ is the unsupported length and the equation is from existing AISC LRFD Seismic Provisions.
Continuity Plates for Control of Damage to Column Web and Flange	Continuity Plates required if $t_{cf} \geq 0.4 \sqrt{\frac{P_{bf}}{F_{yc}}}$ where $P_{bf} = 1.8 t_{fb} b_{fb} \frac{F_{yb} + F_{tb}}{2}$	This equation is somewhat approximate, but it is the best estimate available at this time.
Weak Column Bending	$1.1 < \frac{\sum Z_c \left( F_{yc} - \frac{P_{uc}}{A_g} \right)}{\sum Z_b \frac{F_{yb} + F_{tb}}{2}}$	Significant strain hardening occurs with this connection, and so the proposed limit for controlling plastic deformation of column reflects this fact.

Note: All material properties provided in this table are expected values rather than minimum values.

As with the welded-flange-welded-web connection with improved weld access hole details (Ricles et al., 2000), the free-flange connection (Choi, et al., 1999) results in significant improvements in rotational capacity over that achieved with the welded-flange-bolted-web connection. This can be seen by comparing the total plastic rotations at initial failure,  $\theta_p$ , for the free-flange and welded web connections in Figure 3-11 with the rotations for recent pre-Northridge connections in Figure 2-15, and post-Northridge connections with bolted webs and unimproved weld access hole details in Figure 2-17. Comparison of these figures shows significantly larger plastic rotation with both the free-flange and welded web alternatives, but the

data suggests that the welded web connection will achieve slightly larger  $\theta_p$  for the greater beam depths. Comparison of Tables 3-4 and 3-6 also supports this observation. This smaller rotational capacity occurs because Specimen UCSD-FF with W36 beams fractured into the column at a smaller rotation than commonly achieved with the tests summarized in Table 3-4. Further, Specimens 10.1 and 10.2 were stopped at rotations that limit the rated capacity. These tests were stopped because of limitations of the test apparatus, but the description of the observed behavior suggests that these specimens may not have sustained the next larger rotation cycles. There are a limited number of free-flange connection tests. The connection shows considerable promise for providing good seismic performance, and increased rotational capacity may be possible as refinements are made to the design and additional tests are completed.

On the other hand, examination of the ultimate failure of both the free-flange and welded web connections suggests that the free-flange connection may provide slightly larger maximum rotation for support of gravity loads,  $\theta_g$ . None of the tests were continued to large enough deformations to accurately determine  $\theta_g$ , but the actual mode of failure observed in the welded web connections suggest that  $\theta_g$  will not be much larger than  $\theta_p$ . The free-flange connection appears to be able to better separate web and flange deformations, and should be able to achieve larger  $\theta_g$  after initial fracture occurs.

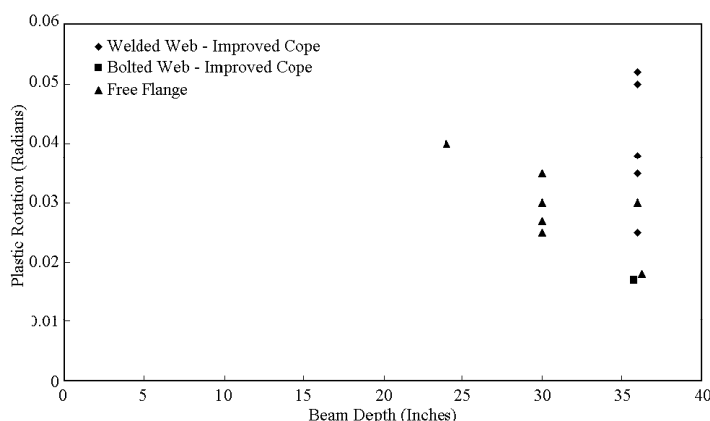


**Figure 3-11 Plastic Rotation for Free-Flange and Welded Web Connections**

The rotational capacity that can be achieved with the free-flange connection was estimated by a regression analysis of the experimental results. These results indicate that

$$\theta_{p\text{mean}} = 0.067 - 0.0012 d_b, \quad (3-8a)$$

and the standard deviation of the plastic rotation is

$$\sigma_p = 0.016 + .0005 d_b \quad (3-8b)$$

where  $\theta_{p\text{mean}}$  and  $\sigma_p$  are in radians, and the  $d_b$  is in inches. The tests on free-flange connections were typically stopped too soon to obtain a good measure of  $\theta_g$ . Further, the web

connection frequently appeared relatively stable when most tests were completed, although limited cracking was noted around some web plate welds. As a result,  $\theta_g$  was defined as 0.02 radians larger than  $\theta_p$ , since this should be a conservative estimate of the rotational capacity. Thus, this rotation estimate was used for all specimens except UCSD-FF, which fractured into the column and was unlikely to sustain this increased rotation. The resulting statistical estimates are

$$\theta_{g\text{mean}} = 0.094 - 0.0016 d_b, \quad (3-9a)$$

and the standard deviation of  $\theta_g$  is

$$\sigma_g = 0.028 + .0009 d_b. \quad (3-9b)$$

### 3.4 Reinforced Connections

The haunch and coverplated connection have similarities because they both achieve improved seismic performance by strengthening or reinforcing the connection at the column face so that they avoid fracture at the beam flange weld. This is accomplished by moving the flexural plastic deformation to the end of the strengthened segment or by a combination of panel zone yielding with flexural plastic deformation at the end of the strengthened connection. At the same time, there are numerous unique features of these connections. They are, therefore, combined in this section, but discussed individually.

#### 3.4.1 Haunched Connections

The haunched connection depicted in Figure 3-12 was studied during Phase I of this research program (SAC, 1996). This connection effectively reinforces the connection so that flexural yielding of the beam at the end of the haunch provides the required connection ductility. The connection has been used in a wide range of configurations including triangular haunches top and bottom as shown in Figure 3-12, and rectangular haunches, or haunches at the bottom flange only. This connection is quite expensive, and as a result, its future use is expected to be for repair of damaged connections, for upgrade of existing connections, and for new connections with very heavy framing. As a result of these limitations, no experimental research was performed on this connection during this phase of the research. Past research showed that the haunch connection provides good seismic performance, and design guidelines for this connection are already available (FEMA 267, 1995). Nevertheless, additional research has been performed through the National Institute for Standards and Technology (NIST, 1998; Gross, et al., 1999) funding and commercial qualification tests. These additional test results will be examined in this report to determine if modifications to these past design recommendations are needed.

Table 3-8 summarizes the results of these tests. Figure 3-13 illustrates the possible yield mechanisms and failure modes for the haunch connection. Figure 3-14 shows the total plastic rotation reported from the tests summarized in Table 3-8 as a function of beam depth. Beam depth is less relevant with the haunch connection because the dimensions of the haunch distort the span length and beam depth characteristics of the connection.

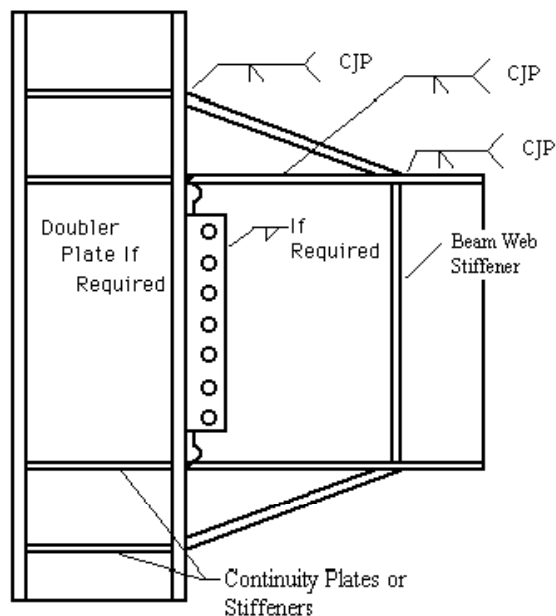


**Figure 3-12 Haunched Connection**

Nevertheless, beam depth provides a means of spreading the data in the plot. The haunch connection has a reputation of being a connection which can develop significant rotational capacity. A brief examination of Table 3-8 suggests that the ductility may be overestimated in some cases, because a number of specimens did not achieve particularly large rotations before the initial failure occurred. On the other hand, it must be recognized that some tests were stopped because of lateral torsional buckling and excess distortion. Further, the rotation achieved with a given connection was often limited by deterioration of the resistance below 80% of the plastic capacity of the ductile element. These later rotations do not represent a true failure condition. This statement is also true of other connection types.

To evaluate the ductility of the haunched connection rationally, it is necessary to recognize that the haunch could be used for both new construction and repair or retrofit. In addition, the haunch has been used for the bottom flange only or for both the top and bottom flange. If the haunch is used for the bottom flange only in existing construction, the top flange would most likely have an E70T-4 flange weld with or without a concrete floor slab. For new construction, a bottom-only haunch would, as a minimum, have a top flange weld with notch tough electrodes. With top and bottom haunches, it is less important whether the beam flange is welded with E70T-4 electrodes or another notch tough electrode, since the largest demands do not occur at the beam flange weld. The rotations shown in Figure 3-14 are divided into these three categories based upon how closely the test conditions matched the categories stated above. This breakdown brings a modest understanding to the rotational capacity of haunch connections.

**Table 3-8 Summary of Past Haunch Test Results**

Identification	Haunch Information	Beam (Column)	Haunch	Haunch Length and (Depth)	Total Plastic Rotation	Failure Mode
Popov UCBR2 (SAC, 1996)	Bottom only	W36x150 (W14x257)	cut from W18x143	18" (9.75")	0.014	Fracture of flange at end of haunch
Popov UCAN1 (SAC, 1996)	Bottom only – rectangular haunch	W36x150 (W14x257)			0.015	Fracture of top flange weld
Bertero RFSR2 (SAC, 1996)	Top and bottom	W30x99 (W14x176)	cut from W30x148	18" (14.1")	0.028 @ 0.8 Mp	Top flange fracture outside haunch
Bertero RFSR3 (SAC, 1996)	Top and bottom	W30x99 (W14x176)	cut from W30x148	18" (12.25")	0.028 @ 0.8 Mp	Top flange fracture outside haunch
Uang UCSDR1 (SAC, 1996)	Bottom flange only	W30x99 (W14x176)	cut from W21x93	18" (10.75")	0.025 @ 0.8 Mp 0.038 @ top flange buckle	Buckling and fracture of top flange
UCSDR3 (SAC, 1996)	Bottom flange only w/ E71T8 top flange weld	W30x99 (W14x176)	cut from W21x93	18" (10.75")	0.045	Beam web fracture
UCSDR4 (SAC, 1996)	Bottom flange only w/ E70T4 top flange weld reinforced	W30x99 (W14x176)	cut from W21x93	18" (10.75")	0.014	Top flange weld fracture
UCSDR5 (SAC, 1996)	Bottom flange only w/ E71T8 top flange weld	W30x99 (W14x176)	cut from W21x93	18" (10.75")	0.014	Fracture of beam flange outside haunch
UTAR1 (SAC, 1996)	Bottom flange only w/ E70T4 top flange weld backgouged and reinforced by E71T8	W36x150 (W14x257)	cut from W18x143	18" (11.1")	0.019	Top flange weld fracture

**Table 3-8 Summary of Past Haunch Test Results (continued)**

UTAR1B (SAC, 1996)	Bottom Flange only w/ E71T8 top flange weld	W36x150 (W14x257)	cut from W18x143	18" (11.1")	0.028	Stopped because of buckling deformation
UTAR3 (SAC, 1996)	Top and bottom flange	W36x150 (W14x257)	cut from W18x143	18" (11.1")	0.023	Stopped because of buckling deformation
NSF-UTA	Bottom flange only	W36x150 (W14x455)	cut from W18x143	20.125" (20.125")	0.015	Top flange weld fracture
SF Civic Center 1 (Noel and Uang, 1996)	Bottom flange only with 1" cover plate for top flange and beam flange welded with E71T8	W18x86 (W24x2790)	built-up w/1" flange & ¾' web	18" (12")	0.37	Low cycle fatigue flange fracture
NIST UCSD- 2 (NIST, 1998)	Bottom flange only, bolted web and E70T4 top flange weld	W36x150 (W14x426)	cut from W18x143	18" (10.75")	0.008 first beam and 0.024 for 2 <sup>nd</sup>	Weld fracture of top flange
NIST UCSD- 2 (NIST, 1998)	Bottom flange only, bolted web and E70T4 top flange weld - with slab	W36x150 (W14x426)	cut from W18x143	18" (10.75")	0.03	Test stopped due to buckling
NIST UT1 (NIST, 1998)	Bottom flange only, bolted web and E70T4 top flange weld – with slab	W30x99 (W12x279)	cut from W21x93	18" (10.75")	0.015 first beam and 0.027 for 2 <sup>nd</sup>	Top flange weld fracture
NIST UT2 (NIST, 1998)	Bottom flange only, bolted web and E70T4 top flange weld – with slab	W30x99 (W12x279)	cut from W21x93	18" (10.75")	0.03	Test stopped due to buckling
NIST UT3 (NIST, 1998)	Bottom flange only, bolted web and E70T4 top flange weld	W30x99 (W12x279)	cut from W21x93	18" (10.75")	0.013 first beam and 0.025 for 2 <sup>nd</sup>	Top flange fracture of both beams
NIST UT4 (NIST, 1998)	Bottom flange only, bolted web and E70T4 top flange weld – with slab	W30x99 (W12x279)	cut from W21x93	18" (10.75")	0.031	Test stopped due to buckling

Note: See Noel and Uang (1996); SAC (1996); NIST (1998); and Uang, et al. (1998).

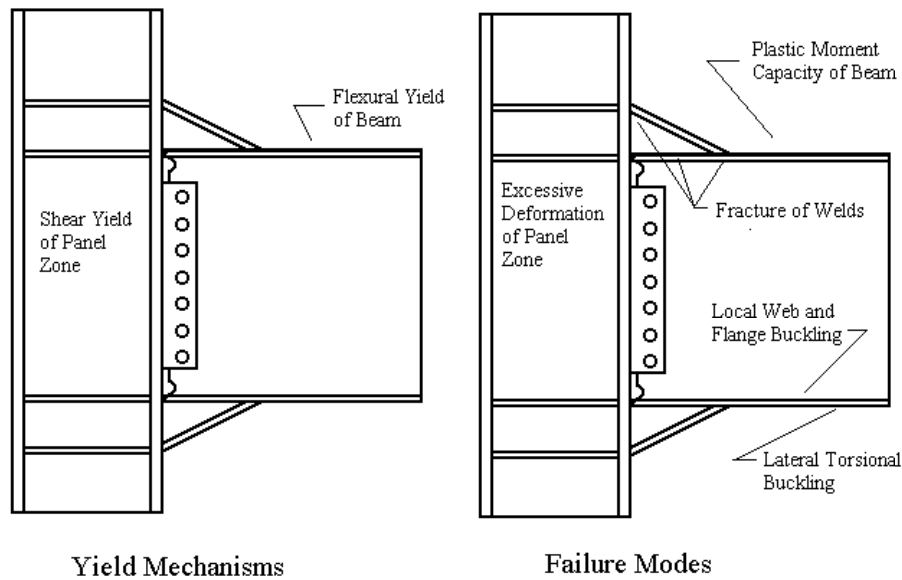


**Figure 3-13 Possible Yield Mechanisms and Failure Modes for the Haunch Connection**

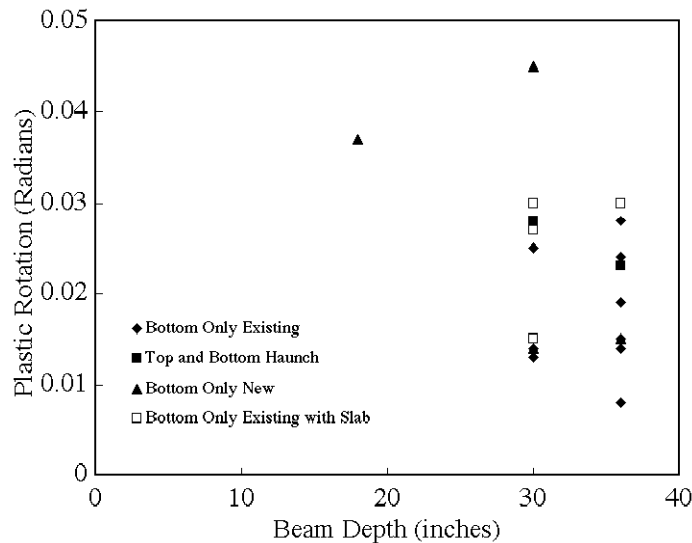


**Figure 3-14 Plastic Rotation from Haunch Connection Tests**

Examination of Figure 3-14 provides several interesting observations. First, it can be seen that haunch connections can provide large rotational capacity for new construction. Bottom only haunches with notch tough welds or coverplated connections for the top flange are identified as solid triangles in the figure, and they consistently provide good rotational capacity. Top and bottom haunches may reasonably well represent new or existing construction regardless of the beam flange welds, and these also provide good rotational capacity, since they are identified as solid squares in Figure 3-15. Nevertheless, the rotations achieved with these connections are often smaller than those achieved with other enhanced post-Northridge connections as shown by the rotations given in Figure 3-11. Bottom only connections for existing connections (with

E70T-4 electrode top flange welds) are identified by the solid diamonds in the figure. Their total plastic rotations are quite mixed, but relatively large rotations are possible. The hollow squares identify bottom only connections with E70T-4 top flange welds and composite slabs, and it can be seen that the presence of the slab is, on average, beneficial to the overall performance of the connection. It should be noted that these slab tests were funded by NIST (NIST, 1998), and they provide valuable insight into overall connection behavior, since the effect of the slab on the connection behavior has been a major question after the Northridge earthquake.

The plastic rotations shown in Figure 3-14 are total plastic rotations, and they represent the rotation at which an initial fracture occurs, where significant loss of resistance occurs due to buckling, or where the test was stopped for some other reason. Top and bottom haunch connections did not normally fracture, and so it is logical to expect that these connections had significant reserve rotational capacity when the test was concluded. None of the tests in Table 3-8 and Figure 3-14 were continued to deformations large enough to determine  $\theta_g$ , but  $\theta_g$  should be significantly larger than  $\theta_p$  for the top and bottom haunch connection. The bottom only haunch with pre-Northridge top flange welds commonly had weld fracture. There appears to be significantly less reserve rotational capacity for these haunch connections.

The haunch connection has similar yield mechanisms and failure modes as the unreinforced connections described earlier. However, the geometry of the connection becomes important in balancing these modes of behavior. Figure 3-15 illustrates the geometry used for determination of the panel zone shear force. The yield mechanisms of the pre-Northridge connection are quite simple and are similar to those noted for the post-Northridge connection. With the haunch connection, the moment capacity of the beam at the end of the haunch must be used to achieve the required balance between flexural yielding and panel zone yielding. Further, panel zone yielding is a greater uncertainty for the haunch connection than for other connections, because the panel zone shear may concentrate in individual portions of the panel zone. This concentration was noted in SAC Phase 1 tests on haunch connections (SAC, 1996), and it occurs because the distribution of panel zone shear stress is unclear (Uang and Bondad, 1998; Roeder, 1996). On the other hand, the average panel zone shear is reduced by the haunch section based upon the effective depth of the haunch,  $d_{eff}$ , shown in the figure. As a consequence, it is recommended that the plastic capacity of the beam be balanced to the panel zone shear yield force. The average panel zone shear computed by methods as illustrated in Figure 3-15 are therefore limited to no more than the yield moment, so that  $(0.9) V_{yield}$  is approximately equal to

$$\frac{\Sigma M_y}{d_{eff}} \left( \frac{L}{L - d_c - L_h} \right) \left( \frac{h - d_{eff}}{h} \right).$$

The haunch connection causes increased bending moments in the columns because the flexural yield moment of the beam is developed at the end of the haunch and the moment is increased proportionally by the geometry of the haunch as shown in Figure 3-15. In addition, the maximum moment at the end of the haunch will greatly exceed  $M_p$  because of the strain hardening of the steel. This increased moment must be considered if strong column-weak beam behavior is to be insured. SCWB behavior can be enforced by the equation

$$1.1 < \frac{\Sigma Z_c \left( F_{yc} - \frac{P_{uc}}{A_g} \right)}{\left( \frac{L - d_c}{L - d_c - 2 L_h} \right) \Sigma Z_b \frac{F_{yb} + F_{tb}}{2}} \quad (3-10)$$

This equation is of the same format as that used for the unreinforced connections.

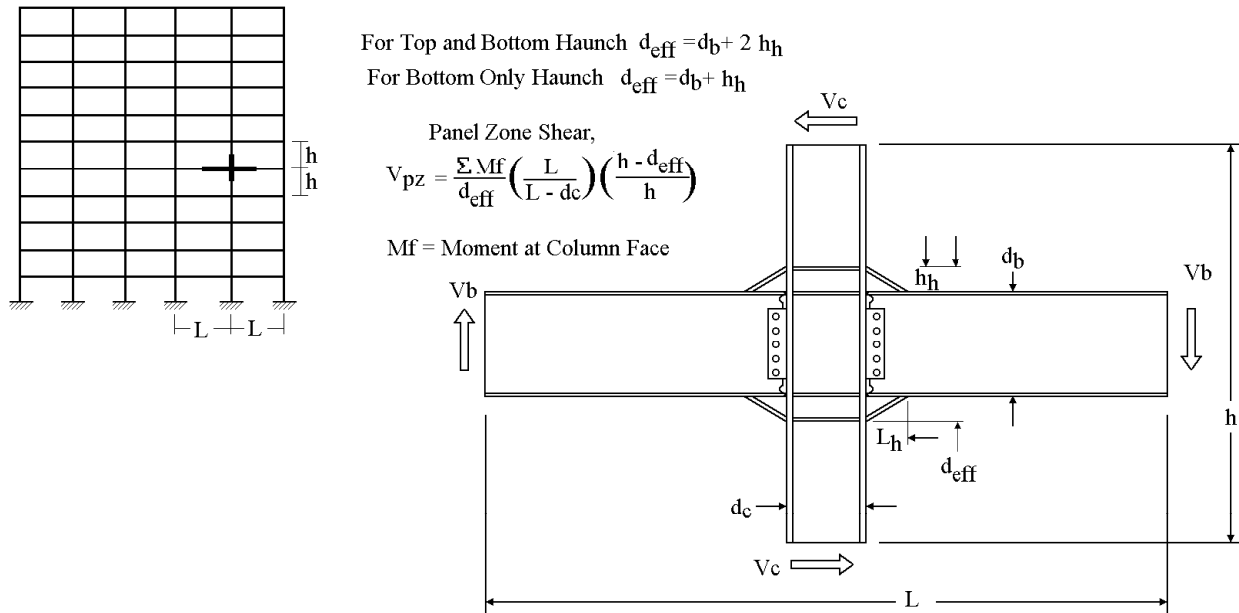


**Figure 3-15 Geometry for Balancing Yield Mechanisms and Failure Modes for Haunched Connection**

Other details of haunch connection behavior appear to be basically unchanged since Phase I of this research program was completed, and so the reader is referred to earlier publications (SAC, 1996) for design details (FEMA 267, 1995). Earlier recommendations have suggested that triangular haunches have slopes of 2 to 1 (2 horizontal and 1 vertical), and the depth of the haunch is suggested to be approximately  $\frac{d_b}{3}$ . It must be recognized that the plastic rotation occurs at the end of the haunch, and rotation at this location is larger than would be predicted by the normal story drift rotation. Equations for approximating the yield mechanisms and failure modes of the haunch connection are provided in Tables 3-9 and 3-10. The design of haunched members and connections can be difficult, because the stress distribution is not well defined in the tapered section. The normal rules of beam shear and flexural stress are not applicable to tapered sections. Guidelines have been developed for modeling the stress in the tapered haunch, and the reader is referred elsewhere (Gross, et al., 1999) for details on these design and modeling methods.

**Table 3-9 Yield Mechanisms of Haunch Connection**

Yield Mechanism	Equation to Define Yield Mechanism Moment Resistance at the Face of the Column
Flexural Yielding of Beam – Moment at the Face of the Column	$M_{yield} = S F_{ybm} \left( \frac{L}{L - d_c - 2 L_h} \right)$
Panel Zone Yielding	$V_{yield} = 0.55 d_c t_{w-c} F_{yc}$
Balancing of Panel Zone and Flexural Yield	$(0.9) 0.55 d_c t_{wc} F_{yc} \geq \frac{\sum M_y}{d_{eff}} \left( \frac{L}{L - d_c - 2 L_h} \right) \left( \frac{h - d_{eff}}{h} \right)$ <p>but preferably</p> $(0.6) 0.55 d_c t_{wc} F_{yc} \leq \frac{\sum M_y}{d_{eff}} \left( \frac{L}{L - d_c - 2 L_h} \right) \left( \frac{h - d_{eff}}{h} \right)$ <p>Note that <math>t_{wc}</math> includes the thickness of any doubler plate used in the column panel zone.</p>

Note: All material properties provided in this table are expected values rather than minimum values.

The rotational capacity that can be achieved with the haunch connection varies depending upon whether the haunch is a bottom flange or a top and bottom flange haunch, whether it is new construction or a repair, or whether the beam has a composite slab or not. The rotations should rationally depend upon beam depth, but nearly all tests were completed on W30 or W36 beams, and so the tests do not provide enough variation to characterize the depth effect. As a result, statistical evaluations were performed for four categories of haunch connection, and these estimates are conservative for those connections which satisfy the conditions and have a beam depth no greater than 36 inches.

For haunch connections with both top and bottom haunches, regardless of whether the construction is new, a repair, or a retrofit, the plastic rotational capacity is

$$\theta_{pmean} = 0.027, \quad (3-11a)$$

and the standard deviation is

$$\sigma_p = 0.0017. \quad (3-11b)$$

The tests of these connections generally did not continue for large enough deformation to establish the maximum rotation at which gravity loads could be supported. Further, the rotational capacity was often limited by the deterioration of the moment capacity of the connection below the 80% limit. As a result,  $\theta_g$  is likely to be significantly larger than  $\theta_p$ . Therefore, it is appropriate that  $\theta_g$  be at least 0.02 radians larger than  $\theta_p$ , since severe cracking would be required to cause loss of gravity load support, and so

$$\theta_{gmean} = 0.047, \quad (3-12a)$$

**Table 3-10 Failure Modes for Haunch Connection**

Failure Mode	Equation to Define Failure Mode Moment Resistance at the Face of the Column	Related Issues
Fracture of Beam Flange Weld	Is not a concern if the Haunch is welded with notch tough electrodes.	
Fracture at Weld Access Hole	Not relevant with the haunch connection	
Plastic Bending of Beam	$M_{pfail} = Z \frac{F_{yb} + F_{tb}}{2} \left( \frac{L - d_c}{L - d_c - 2 L_h} \right)$	Lower bound estimate of full bending moment achieved with these connections.
Flange Buckling	for flange $-\frac{b_f}{2 t_f} \leq \frac{52}{\sqrt{F_y}}$	
Web Buckling	controlled if $\frac{d_b}{t_w} \leq \frac{418}{\sqrt{F_y}}$	See discussion in Chapter 4.
Lateral Torsional Buckling	$L_b < \frac{2500 r_y}{F_y}$	$L_b$ is the unsupported length and equation is from existing AISC LRFD Seismic Provisions.
Continuity Plates	Continuity Plates required for these connections because the flange force of the haunch and beam flange are not known. It is further recommended that a vertical beam web stiffener be placed at the end of the haunch to deal with the unknown vertical component of force at that location.	
Control of Weak Column Behavior	$1.1 < \frac{\sum Z_c \left( F_{yc} - \frac{P_{uc}}{A_g} \right)}{\left( \frac{L - d_c}{L - d_c - 2 L_h} \right) \sum Z_b \frac{F_{yb} + F_{tb}}{2}}$	Significant strain hardening with these more ductile connections.

Note: All material properties provided in this table are expected values rather than minimum values.

and the standard deviation is

$$\sigma_g = 0.0017. \quad (3-12b)$$

For haunch connections with bottom only haunches and with new top flange details, such as the coverplated connection described later in this chapter or notch tough electrode details described earlier in this chapter, the plastic rotational capacity is

$$\theta_{pmean} = 0.028, \quad (3-13a)$$

and its standard deviation is

$$\sigma_p = 0.001. \quad (3-13b)$$

It appears somewhat unusual that this rotational capacity is similar to the limit for the top and bottom haunch detail, but it must be recalled that this detail uses notch tough electrodes for all welds. Further, while the rotational limits for the two options are similar, the test results show that there is a higher probability of a fracture failure mode with the bottom only haunch option.

The tests of these connections again did not continue for large enough deformation to establish the maximum rotation at which gravity loads could be supported, however it is appropriate that  $\theta_g$  be 0.02 radians larger than  $\theta_p$ , since severe cracking would be required to cause loss of gravity load support. Therefore,

$$\theta_{g\text{mean}} = 0.048, \quad (3-14a)$$

and the standard deviation of  $\theta_g$  is

$$\sigma_g = 0.001. \quad (3-14b)$$

The presence of a composite slab enhances the performance of bottom flange only haunch connections. For haunch connections with bottom only haunches and pre-Northridge top flange welds with E70T-4 FCAW-SS electrodes and with a composite slab, the plastic rotational capacity is

$$\theta_{p\text{mean}} = 0.026, \quad (3-15a)$$

and its standard deviation is

$$\sigma_p = 0.003. \quad (3-15b)$$

The tests of these connections again did not continue for large enough deformation to establish the maximum rotation at which gravity loads could be supported. It is appropriate that  $\theta_g$  be larger than  $\theta_p$ , but the increase is smaller than for the previous cases because of increased fracture potential of E70T-4 electrodes. Therefore,

$$\theta_{g\text{mean}} = 0.036, \quad (3-16a)$$

and the standard deviation is

$$\sigma_g = 0.003. \quad (3-16b)$$

For haunch connections with bottom only haunches and pre-Northridge top flange welds with E70T-4 FCAW-SS electrodes but without a composite slab,

$$\theta_{p\text{mean}} = 0.018, \quad (3-17a)$$

and

$$\sigma_p = 0.002. \quad (3-17b)$$

The tests of these connections again did not continue for large enough deformation to establish the maximum rotation at which gravity loads could be supported. These connections are somewhat less ductile and so it is appropriate that  $\theta_g$  be only 0.005 radians larger than  $\theta_p$ , and so

$$\theta_{g\text{mean}} = 0.023, \quad (3-18a)$$

and the standard deviation of  $\theta_g$  is

$$\sigma_g = 0.002. \quad (3-18b)$$

### 3.4.2 Coverplate Connections

The coverplate connection depicted in Figure 3-16 was also studied during Phase I of this research program (SAC, 1996). This connection effectively strengthens the connection so that flexural yielding of the beam at the end of the coverplate can provide the connection ductility. The connection has been used with either top and bottom coverplates as shown in Figure 3-16 or coverplates at the bottom flange only. Bottom flange only coverplates have been considered primarily as a modification to existing pre-Northridge connections with E70T-4 flange welds, since the bottom flange has shown a somewhat greater tendency toward fracture than has the top flange weld. Phase I research (SAC, 1996) and other tests, which were funded by AISC and NSF shortly after the Northridge earthquake (Engelhardt and Sabol, 1998), show that the coverplate connection can provide good seismic performance. More recently, tests funded by the Structural Shape Producers Council (SSPC) (Bjorhovde et al., 1999), and other commercial qualification tests also have examined coverplate connection behavior. Table 3-11 summarizes some of these past tests. This table is by no means all inclusive, since it includes only those tests with reasonable documentation of the research and the test results. Design guidelines for this connection are already available (FEMA 267, 1995). However, a few very large commercial tests that were performed since the SAC Phase 1 testing have shown that dramatic brittle fractures are possible with this connection. While the general results of these tests are known, detailed information adequate for inclusion in Table 3-11 is not available. As a result, experiments (Kim et al., 2000) were completed during this research program to address these brittle fracture issues.

Figure 3-17 summarizes the yield mechanisms and failure modes which are relevant for the coverplate connection. The yield mechanisms for the coverplate connection are quite simple, since significant plastic rotation is developed only through either flexure of the beam at the end of the coverplate or shear yielding of the panel zone. Several tests were performed during (SAC, 1996) or immediately after (Engelhardt and Sabol, 1998) the SAC Phase 1 program and these

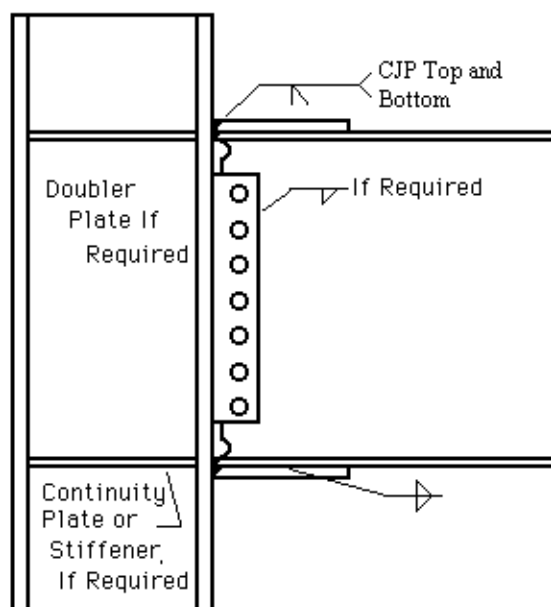


**Figure 3-16 Coverplated Connection**

specimens provided relatively good ductility. Rules were developed (FEMA, 1995) for designing these connections, based on this limited test history. These rules required that:

- all welds have a minimum notch toughness,
- the coverplate and its weld to the face of the column have adequate size and capacity to limit the stresses at the face of the column,
- the panel zone have adequate strength to balance the plastic hinge in the beam at the end of the coverplate,
- and the welds between the coverplate and the beam flange be of adequate size and strength to develop the required force in the coverplate.

Failure modes are more numerous as indicated in Figure 3-17. Local buckling, lateral torsional buckling, excessive plastic deformation of the beam or panel zone, or general loss of resistance due to a combination of these factors were noted during past tests. The coverplate connection is generally regarded as more economical than the haunch connection, and it has been frequently used since the Northridge earthquake. As a result, a number of commercial qualification tests have been performed. The majority of these commercial connection tests provided good plastic rotational capacity. However, some specimens had dramatic brittle fractures through the beam at the end of the coverplate or through the column flange at the contact surface between the coverplate and beam flange as shown in Figure 3-17. The brittle fractures were unexpected and not understood.

**Table 3-11 Summary of Past Coverplate Connection Tests**

Identification	General Information	Beam (Column)	Coverplate Length, Width and Thickness	Total Plastic Rotation	Failure Mode
AD9 (SAC DATABASE)	Bottom only cover plate, modification, bolted web	W21x68 W12x106 1/2,, Doubler 3/4,, Continuity	3/4,,x14" CJP at column face, PJP on sides and fillet at end fillet at end – E70T-4 beam flange weld and E7018 coverplate weld	0.017	Fracture
AD5 (SAC DATABASE)	Top and bottom, modification, bolted web	W21x68 W12x106 1/2,, Doubler 3/4,, Continuity	3/4,,x14" CJP at column face, PJP on sides and fillet at end – E70T-4 beam flange and E7018 coverplate	0.030	Equipment Limit
AD8 (SAC DATABASE)	Top and bottom, modification, bolted web	W21x68 W12x106 1/2,, Doubler 3/4,, Continuity	3/4,,x4"x7" rectangular CP at column face, PP on sides and fillet at end – E70T-4 beam flange and E7018 coverplate	0.045	Equipment Limit
AD7 (SAC DATABASE)	Top and bottom, modification, bolted web	W21x68 W12x106 No Doubler 3/4,, Continuity	3/4,,x14" CJP at column face, PJP on sides and fillet at end – E70T-4 beam flange and E7018 coverplate	0.040	Equipment Limit
UTNSF6 (Engelhardt and Sabol, 1998)	Top and bottom, welded web – top weld Detail 3	W30x148 W14x257	top 5/8" tapered and bottom 5/8" rectangular – E71T-8 weld	0.038	Equipment Limit
UTAISC7B (Engelhardt and Sabol, 1998)	Top and bottom, welded and bolted web – top weld Detail 1	W36x150 W14x426 No Doubler 1" Continuity	top 5/8" tapered and bottom 5/8" rectangular – E70T-7 welds	0.035	Equipment Limit
UTAISC5B (Engelhardt and Sabol, 1998)	Top and bottom, bolted and welded web – top weld Detail 1	W36x150 W14x426 No Doubler 1" Continuity	1" Tapered top and bottom – E70TG-K2 welds	0.005	Fracture

**Table 3-11 Summary of Past Coverplate Connection Tests (continued)**

UTAISC5A (Engelhardt and Sabol, 1998)	Top and bottom, bolted and welded web – top weld Detail 1	W36x150 W14x426 No Doubler	1" Tapered top and bottom – E70TG-K2 welds	0.025	Fracture
UTAISC8A (Engelhardt and Sabol, 1998)	Top and bottom, bolted and welded web – top weld Detail 1	W36x150 W14x426 No Doubler 1" Continuity	Top $\frac{3}{4}$ " tapered and bottom $\frac{5}{8}$ " rectangular – E70T-7 welds	0.035	Equipment Limit
UTAISC3B (Engelhardt and Sabol, 1998)	Top and bottom, bolted and welded web – top weld Detail 1	W36x150 W14x455 No Doubler No Continuity pl	Top $\frac{3}{4}$ " tapered and bottom $\frac{5}{8}$ " rectangular – E70T-4 welds	0.025	Fracture
UTAISC3A (Engelhardt and Sabol, 1998)	Top and bottom, bolted and welded web – top weld Detail 1	W36x150 W14x455 No Doubler No Continuity pl	Top $\frac{3}{4}$ " tapered and bottom $\frac{5}{8}$ " rectangular – E70T-4 welds	0.008	Fracture
UTNSF7 (Engelhardt and Sabol, 1998)	Top and bottom, welded web – top weld Detail 3	W36x150 W14x455 1" Continuity	Top $\frac{1}{2}$ " tapered and bottom $\frac{1}{2}$ " rectangular – E71T-8 welds	0.038	Equipment Limit
UTAISC8B (Engelhardt and Sabol, 1998)	Top and bottom, bolted and welded web – top weld Detail 1	W36x150 W14x426 No Doubler 1" Continuity	Top $\frac{3}{4}$ " tapered and bottom $\frac{5}{8}$ " rectangular – E70T-7 welds	0.035	Equipment Limit
UTNSF5 (Engelhardt and Sabol, 1998)	Top and bottom, welded web – top weld Detail 1	W36x150 W14x426	Top $\frac{1}{2}$ " tapered and bottom $\frac{1}{2}$ " rectangular – E71T-8 welds	0.033	Equipment Limit
UTAISC7A (Engelhardt and Sabol, 1998)	Top and bottom, bolted and welded web – top weld Detail 1	W36x150 W14x426 No Doubler 1" Continuity	Top $\frac{3}{4}$ " tapered and bottom $\frac{5}{8}$ " rectangular – E70T-7 welds	0.035	Equipment Limit
CB2 (Chen, 1999)	Top and bottom, bolted web	W21x62bu BX18x18x280 No Doubler 1 $\frac{7}{16}$ " continuity	Tapered top and bottom – E70T-7 welds	0.038	Complete

**Table 3-11 Summary of Past Coverplate Connection Tests (continued)**

CB1 (Chen, 1999)	Top and bottom, bolted web	W21x62bu BX18x18x280 No Doubler 1 <sup>7</sup> / <sub>16</sub> " continuity	Tapered top and bottom - E70T-7 welds	0.033	Complete
CB3 (Chen, 1999)	Top and bottom, bolted web	W21x62bu BX18x18x280 1 <sup>7</sup> / <sub>16</sub> " continuity	Top tapered and bottom rectangular - E70T-7 welds	0.029	Fracture
CB4 (Chen, 1999)	Top and bottom, bolted web	W21x62bu BX18x18x280 No Doubler 1 <sup>7</sup> / <sub>16</sub> " continuity	Top tapered and bottom rectangular - E70T-7 welds	0.025	Fracture
C1W (SAC DATABASE)	Top and bottom, bolted and welded web	W24x62 CFT 16x16x0.5 w/continuity	Top and bottom <sup>7</sup> / <sub>8</sub> " rectangular plate 3.5" long - E70T-7 welds with E71T-8 fillet	0.020	Fracture
C1E (SAC DATABASE)	Top and bottom, bolted and welded web	W24x62 CFT 16x16x0.5 w/continuity	Top and bottom <sup>7</sup> / <sub>8</sub> " rectangular plate 3.5" long - E70T-7 welds with E71T-8 fillet	0.020	Fracture
NSF1 (SAC DATABASE)	Top and bottom, with slot in column web, welded web	W36x150 W14x211 1 <sup>1</sup> / <sub>2</sub> " Doubler	1 <sup>1</sup> / <sub>2</sub> " tapered - E70T-7 welds	0.010	Fracture
A1 (Bjorhovde, et al., 1998)	Top and bottom, weld Detail 1 at top, and weld Detail 2 at bottom, bolted web w/10 1 <sup>1</sup> / <sub>8</sub> " A325 SC bolts, rotary straightened	W21X122 W14X176 No Doubler 1 <sup>1</sup> / <sub>8</sub> " continuity	1 <sup>5</sup> / <sub>8</sub> " tapered coverplate 23" long - E70TG-K2 welds	0.027	Cracking from outside of CP weld into column web along K- line
A2 (Bjorhovde, et al., 1998)	Top and bottom, Weld Detail 1 at top, and Weld Detail 2 at bottom, bolted web w/10 1 <sup>1</sup> / <sub>8</sub> " A325 SC bolts, rotary straightened	Same	1 <sup>5</sup> / <sub>8</sub> " tapered coverplate 23" long - E70TG-K2 welds	0.027	Same

**Table 3-11 Summary of Past Coverplate Connection Tests (continued)**

A3 (Bjorhovde, et al., 1998)	Top and bottom, Weld Detail 1 at top, and weld Detail 2 at bottom, bolted web w/10  1 1/8" A325 SC bolts, rotary straightened	Same	1 5/8" tapered coverplate 23" long - E70TG-K2 welds	0.017	Same
A4 (Bjorhovde, et al., 1998)	Top and bottom, weld Detail 1 at top, and Weld Detail 2 at bottom, bolted web w/10  1 1/8" A325 SC bolts, rotary straightened, dynamically tested	Same	1 5/8" tapered coverplate 23" long - E70TG-K2 welds	0.028	Cracking from outside of CP weld into column web across column depth
A5 (Bjorhovde, et al., 1998)	Top and bottom, Weld Detail 1 at top, and Weld Detail 2 at bottom, bolted web w/10  1 1/8" A325 SC bolts, rotary straightened, dynamically tested	Same	1 5/8" tapered coverplate 23" long - E70TG-K2 welds	0.017	Same
A6 (Bjorhovde, et al., 1998)	Top and bottom, Weld Detail 1 at top, and Weld Detail 2 at bottom, bolted web w/10  1 1/8" A325 SC bolts, gag straightened, dynamically tested	Same	1 5/8" tapered coverplate 23" long - E70TG-K2 welds	0.028	Crack initiated at CP weld into column web along K-line
A7 (Bjorhovde, et al., 1998)	Top and bottom, Weld Detail 1 at top, and Weld Detail 2 at bottom, bolted web w/10  1 1/8" A325 SC bolts, gag straightened, dynamically tested	Same	1 5/8" tapered coverplate 23" long - E70TG-K2 welds	0.028	Crack initiated at CP weld into column web across column depth

**Table 3-11 Summary of Past Coverplate Connection Tests (continued)**

A8 (Bjorhovde, et al., 1998)	Top and bottom, Weld Detail 1 at top, and Weld Detail 2 at bottom, bolted web w/10  1 <sup>1</sup> / <sub>8</sub> " A325 SC bolts, unstraightened	Same	1 <sup>5</sup> / <sub>8</sub> " tapered coverplate 23" long - E70TG-K2 welds	0.028	Crack at toe of coverplate CJP weld
R1-1 (Bjorhovde, et al., 1998)	Top and bottom, Weld Detail 3 at top, and Weld Detail 2 at bottom, bolted web w/10  1 <sup>1</sup> / <sub>8</sub> " A325 SC bolts, rotary straightened	Same	1" tapered coverplate 23" long - E70TG-K2 welds	0.043	Crack initiated at CP weld into column web along K-line
R1-2 (Bjorhovde, et al., 1998)	Top and bottom, Weld Detail 3 at top, and Weld Detail 2 at bottom, bolted web w/10  1 <sup>1</sup> / <sub>8</sub> " A325 SC bolts, rotary straightened	W21X122 W14X176 No Doubler 1 <sup>1</sup> / <sub>8</sub> " continuity	1" tapered coverplate 23" long - E70TG-K2 welds	0.027	Same
R1-3 (Bjorhovde, et al., 1998)	Top and bottom, Weld Detail 3 at top, and Weld Detail 2 at bottom, bolted web w/10  1 <sup>1</sup> / <sub>8</sub> " A325 SC bolts, rotary straightened	W21X122 W14X176 No Doubler 1 <sup>1</sup> / <sub>8</sub> " continuity	1" tapered coverplate 23" long - E70TG-K2 welds	0.027	Same
R1-4 (Bjorhovde, et al., 1998)	Top and bottom, Weld Detail 3 at top, and weld Detail 2 at bottom, bolted web w/10  1 <sup>1</sup> / <sub>8</sub> " A325 SC bolts, rotary straightened, dynamically tested	W21X122 W14X176 No Doubler 1 <sup>1</sup> / <sub>8</sub> " continuity	1" tapered coverplate 23" long - E70TG-K2 welds	0.03	Same
R1-5 (Bjorhovde, et al., 1998)	Top and bottom, Weld Detail 3 at top, and Weld Detail 2 at bottom, bolted web w/10  1 <sup>1</sup> / <sub>8</sub> " A325 SC bolts, rotary straightened	W21X122 W14X176 No Doubler 1 <sup>1</sup> / <sub>8</sub> " continuity	1" tapered coverplate 23" long - E70TG-K2 welds	0.03	Same

**Table 3-11 Summary of Past Coverplate Connection Tests (continued)**

R1-6 (Bjorhovde, et al., 1998)	Top and bottom, Weld Detail 3 at top, and Weld Detail 2 at bottom, bolted web w/10  1 <sup>1</sup> / <sub>8</sub> " A325 SC bolts, unstraightened	W21X122 W14X176 No Doubler 1 <sup>1</sup> / <sub>8</sub> " continuity	1" tapered coverplate 23" long - E70TG-K2 welds	0.027	Same
R2 (Bjorhovde, et al., 1998)	Top and bottom, Reinforced Weld Detail 3 at top, and Reinforced Weld Detail 2 at bottom, bolted and welded web w/10  1 <sup>1</sup> / <sub>8</sub> " A325 SC bolts and <sup>5</sup> / <sub>16</sub> " fillet, rotary straightened, dynamically tested	W21X122 W14X176 No Doubler 1 <sup>1</sup> / <sub>8</sub> " continuity	1 <sup>5</sup> / <sub>8</sub> " tapered coverplate 23" long - E70TG-K2 welds	0.038	Crack from bottom coverplate weld through the column flange and across web
R3-1 (Bjorhovde, et al., 1998)	Top and bottom, Reinforced Weld Detail 3 at top, and Reinforced Weld Detail 2 at bottom, bolted and welded web w/10  1 <sup>1</sup> / <sub>8</sub> " A325 SC bolts and <sup>5</sup> / <sub>16</sub> " fillet, rotary straightened, dynamically tested	W21X122 W14X176 No Doubler 1 <sup>1</sup> / <sub>8</sub> " continuity	1" tapered coverplate 23" long - E70TG-K2 welds	0.037	Crack into column from the interface of plate and flange (weld root)
R3-2 (Bjorhovde, et al., 1998)	Top and bottom, Reinforced Weld Detail 3 at top, and Reinforced Weld Detail 2 at bottom, bolted and welded web w/10  1 <sup>1</sup> / <sub>8</sub> " A325 SC bolts and <sup>5</sup> / <sub>16</sub> " fillet, rotary straightened, dynamically tested	W21X122 W14X176 No Doubler 1 <sup>1</sup> / <sub>8</sub> " continuity	1" tapered coverplate 23" long - E70TG-K2 welds	0.039	Similar but top flange only

Notes:

1. Weld Detail 1 means the same bevel for flange and coverplate. Weld Detail 2 means bottom flange welded from above and bottom cover plate welded from below. Weld Detail 3 is top flange and coverplate welded from above but with discontinuous CJB weld bevels. Reinforced details are details 2 or 3 with 1/2" fillet reinforcement on top of weld at the extreme fiber of beam flange.
2. See SAC (1996); Engelhardt and Sabol, (1998); Bjorhovde, et al., (1998).

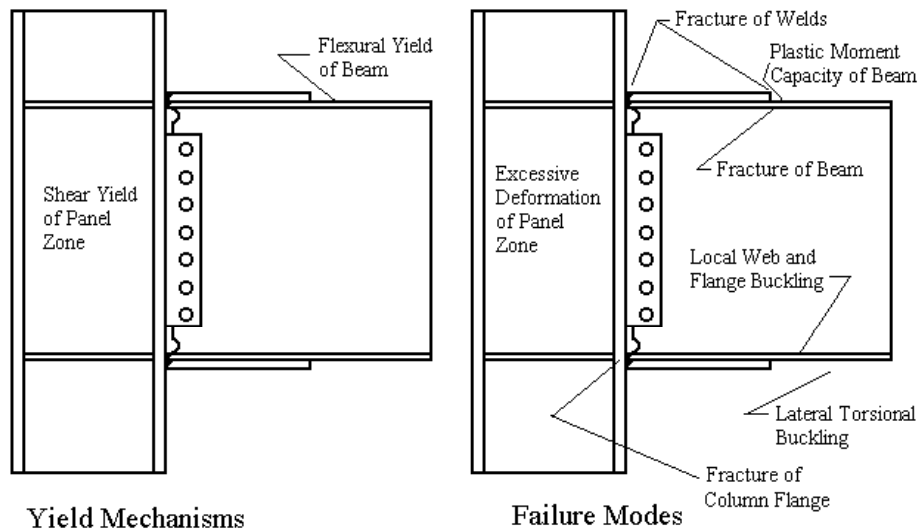


**Figure 3-17 Yield Mechanisms and Failure Modes for Coverplated Connections**

The combination of the data from these tests has raised doubts about the plastic rotational capacity of the coverplate connections. Figure 3-18 shows the plastic rotation obtained from the past tests documented in Table 3-11. Many of the specimens in this figure were tested to relatively large deformations, and some tests were stopped due to limitations of the test apparatus. This is a fairly common problem, which leads to underestimated connection ductility, and those specimens are identified as squares in the figure. The solid squares are connections for new post-Northridge construction, which had flange and coverplate welds made with notch tough electrodes, and the hollow squares simulate possible pre-Northridge modifications since the flanges were welded with E70T-4 electrodes. However, many specimens produced fractures within the connections, and those specimens are identified as diamonds on the figure. The hollow and solid diamonds again indicate pre-Northridge modifications and post-Northridge connections, respectively. It can be seen that large plastic rotations were often obtained before fracture occurred. However, some specimens fractured with only limited plastic rotational capacity,  $\theta_p$ . It can be seen that these specimens generally had smaller rotational capacity with greater beam depth. Some cracking with the coverplate connection tests started at the CJP groove weld and progressed through the column flange and into the column web. This later form of damage is a serious concern, since column cracking is viewed as one of the most serious forms of damage from the Northridge earthquake. This column cracking has been analyzed (Chi, et al., 1997; Deierlein, 1999) in crack propagation studies completed during this research. The analyses showed that this cracking is driven by the apparent notch provided by the contact surface of the coverplate and the beam flange. This interface is effective in causing further crack growth because there is significant stress in both the beam flange and the coverplate. Further, the analysis suggests that Detail 3 welds as defined in Figure 3-20 may have a greater tendency toward developing column flange cracks because the root of the coverplate weld lies at this interface. The propensity for column cracking suggests that the maximum rotation at which gravity loads can be supported,  $\theta_g$ , may not be much larger than  $\theta_p$  for the coverplate connection. At the same time, it must be remembered that many specimens obtained large rotations without any indication of fracture.

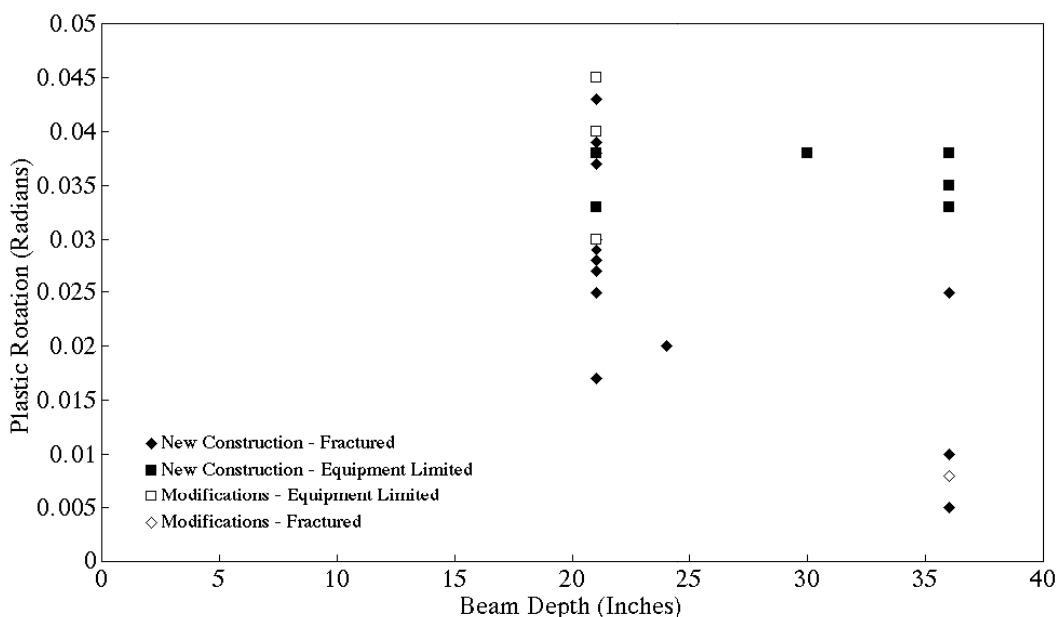


**Figure 3-18 Plastic Rotation Obtained During Past Coverplate Connection Tests**

The characteristics of the specimens that fractured were examined to determine how they are different from the specimens that did not. This examination may lead to additional design requirements. One possible source of concern is the relative size of the coverplate. The coverplate is added to reinforce the connection, to reduce the stress at the beam flange weld, and to force yielding at the end of the coverplate. Therefore, some engineers have used relatively heavy coverplates, since they result in greater reductions in the nominal flange weld stress at the column face. This could be a questionable practice (Engelhardt and Sabol, 1998), since larger welds lead to increased problems with distortion and shrinkage. The coverplates are usually of similar width to the beam flange, and so the comparison of the thickness of the coverplate to the thickness of the beam flange is an approximate comparison of the relative strengths of the beam flange and the coverplate. Steel wide flanges have shape factors of 1.12 to 1.2, and so specimens with  $\frac{t_{cp}}{t_{bf}}$  ratios in excess of 1.2 or 1.3 normally have coverplates that increase the moment capacity at the column face more than 100% over the plastic capacity of the beam. Figure 3-19 shows the plastic rotations obtained from these past tests as a function of the  $\frac{t_{cp}}{t_{bf}}$  ratio. There is considerable scatter in the data, but it can be seen that 10 specimens had a  $\frac{t_{cp}}{t_{bf}}$  ratio greater than 1.2. Only 10% of these specimens had  $\theta_p$  greater than 0.03 radians, and all of these specimens fractured. Twenty four specimens of Figure 3-19 had a ratio of less than 1.2, 70.8% of these specimens had  $\theta_p$  greater than 0.03 radians, and 45.8% did not fracture. This information suggests that the size of coverplates should be limited to no more than 120% of the area of the beam flange if good ductility is to be assured. Even smaller coverplates may be appropriate for maximum optimal connection performance.

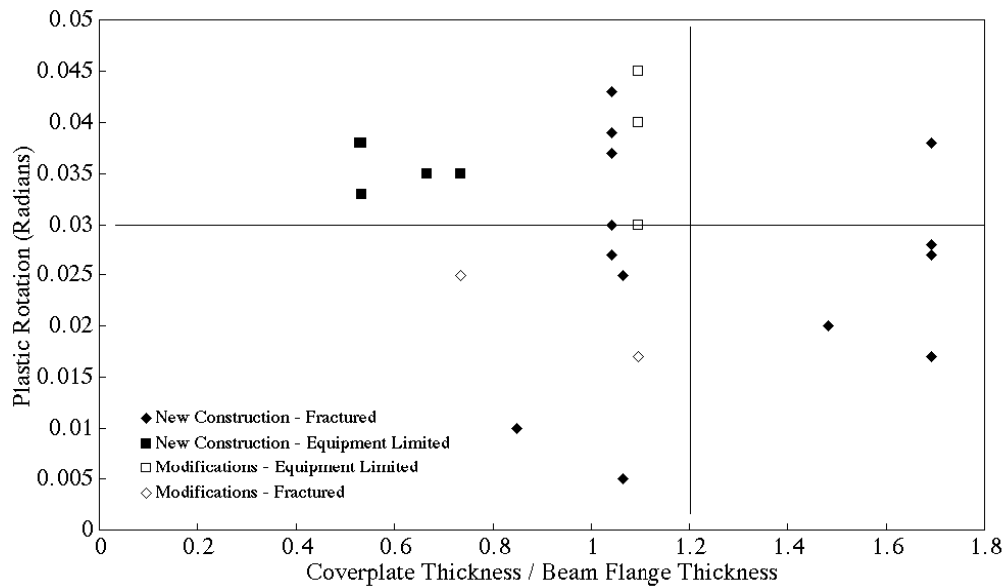


**Figure 3-19 Plastic Rotation of Coverplate Connections as a Function of the  $\frac{t_{cp}}{t_{bf}}$  Ratio**

Another factor which may affect the rotational capacity of the connection is the weld configurations for the beam flanges and coverplates. Figure 3-20 illustrates three weld configurations that have been used, and the configurations are defined as Details 1, 2, and 3. Detail 2 is commonly used for the bottom flange and coverplate as shown in the figure. Detail 2 is probably the only viable option for the bottom flange coverplate for modification of existing connections, but Details 1 and 3 are possible for the top and bottom flanges of new construction and for top flange coverplates for existing construction. However, Detail 1 requires a larger volume of weld metal than Detail 3. Detail 3 requires less welding, but the root of the coverplate weld lies in the critical region between the coverplate and beam flange. Analysis (Chi, Deierlein and Ingraffea, 1997) indicates that the combined effect of the flaws at the root pass of the weld and the deep apparent initial crack caused by the coverplate beam flange interface may be a source of cracking for the column flange. The information regarding the flange welds is incomplete for some specimens in Table 3-11, but Figure 3-21 illustrates the plastic rotation achieved for coverplate connections where the top flange weld detail was known. Specimens welded with Detail 1 are identified as squares in the figure, and Detail 3 is identified as diamonds. Examination of the failures reported for these specimens noted that some Detail 3 welds (Bjorhovde et al., 1999) produced column flange fractures. However, the specimens in Figure 3-21 show that only 3 of 11 specimens with Detail 1 welds achieved a plastic rotation of 0.03 radians, while only 5 of 17 connections with Detail 3 welds achieved 0.03 radians plastic rotation. This observation suggests that Detail 1 welds do not improve the performance of the connection.

In view of the unanswered questions regarding the coverplate connection, a limited study (Kim, et al., 2000) was started to consider these issues and finalize the design requirements for the connection. Table 3-12 summarizes the results of this test program.

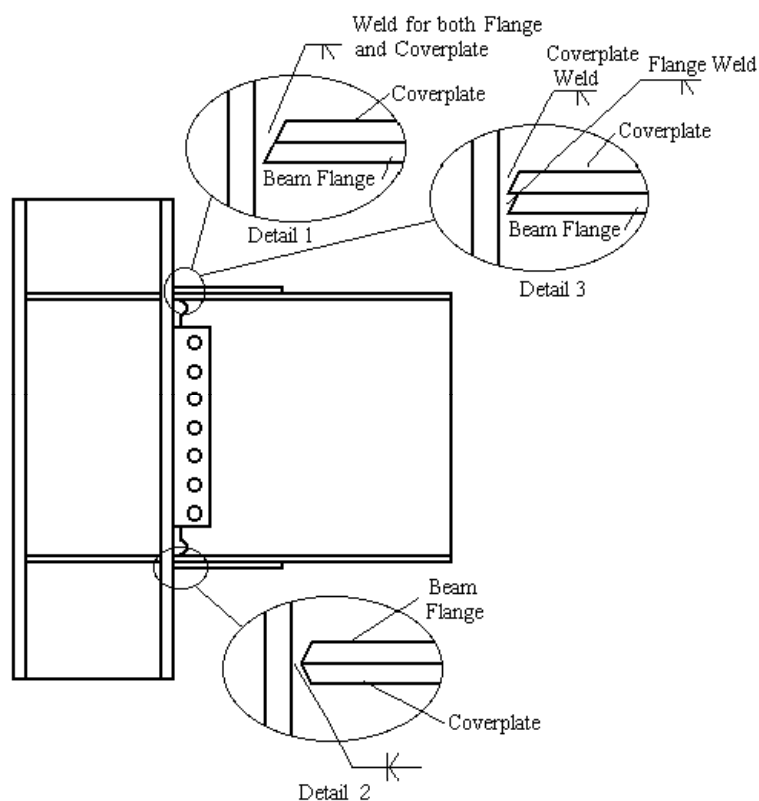


**Figure 3-20 Weld Configurations for Coverplate Connection**

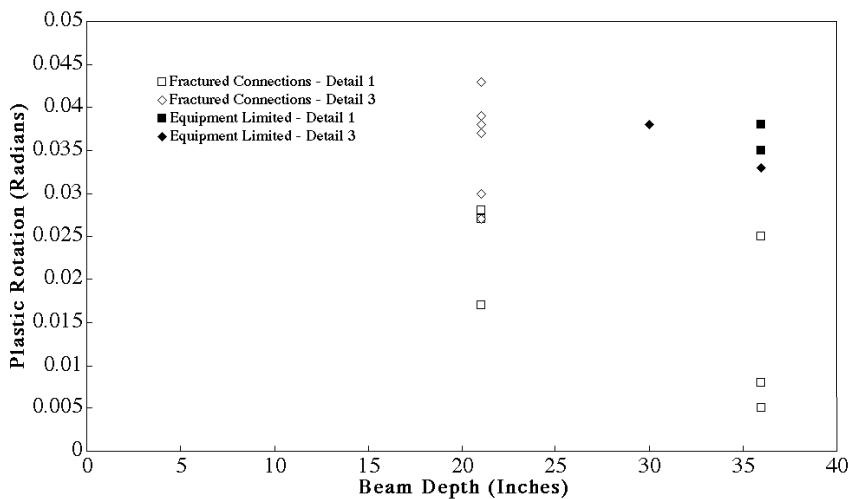


**Figure 3-21 Effect of Weld Configuration on Plastic Rotation of Coverplate Connections**

**Table 3-12 Summary of Test Results for Coverplate Connection**

Test Specimen	General Description and Information	Beam and (Column) Sizes	Plastic Rotation at Initial Failure	Plastic Rotation Due to Panel Zone Yielding	Max. Moment (Moment at End of Test) Divided by $M_p$	Plastic Rotation at End of Test	Max. Moment Divided by $\frac{F_y + F_t}{2} Z$
UCB-RC01	5/8" x 12" x 14 1/4" long coverplate Strong panel zone - Propagation of tear in flange fillet weld into the beam flanges - Flange Weld Detail 1- Backing bar removed and reinforced with fillet	W30x99 (W14x176) welded web - 3/8" doubler-	0.03 at 80% 0.041 at flange tear	Very slight by not yet defined	22000 (1.19)	0.041	1.04
UCB-RC02	5/8" x 12" x 14 1/4" long coverplate Strong panel zone - Flange Weld Detail 1- Backing bar left in place - Lateral bracing added at plastic hinge - Fracture at LTB support	W30x99 (W14x176) welded web - 3/8" doubler-	0.03 at 80% 0.043 fracture at LTB support	Very slight by not yet defined	22500 (1.22)	0.043	1.06
UCB-RC03	5/8" x 12" x 14 1/4" long coverplate Strong panel zone - Flange Weld Detail 1- Backing bar removed and reinforced with fillet - K-line tear	W30x99 (W14x176) welded web - 3/8" doubler-	0.03 at 80% 0.044 at K-line tear	Very slight by not yet defined	22500 (1.22)	0.044	1.06
UCB-RC05	11/16" thick, 10 1/2" wide, 14 1/4" long trapezoidal coverplate Strong panel zone - Flange Weld Detail 1- Backing bar removed and reinforced with fillet - flange tearing due to LTB and local buckling	W30x99 (W14x176) welded web - 3/8" doubler-	0.03 at 80% 0.052 at flange tear	Very slight by not yet defined	21800 (1.18)	0.052	1.03

Notes.

1. Plastic rotations are rotations prior to significant loss of resistance or initial fracture of the connection.
2. All flange welds are with notch-tough electrodes.
3. Plastic capacities determined from mill test reports, and adjusted for geometry since they occur at end of coverplate.
4. See Kim, et al. (2000).

The results of the combined test results shown in Tables 3-11 and 3-12 and observations from commercial testing send a mixed message. The coverplate connection is clearly capable of providing good connection ductility and large inelastic rotational capacity. At the same time, it requires a delicate balance in its design if problems are to be avoided. Analysis suggests that the use of weld details such as Detail 3 are more likely to lead to brittle fracture than are Detail 1, but this is not supported by the experimental results. Both analyses and experiments suggest that the use of overly large coverplates and large coverplate welds should be avoided. Further, as with many other connection types, the use of bigger and heavier members exacerbates the problem.

As noted earlier, the yield mechanisms for the coverplate connection are relatively simple, since all significant plastic rotation occurs as flexural yielding of the beam at the end of the coverplate, or as shear yielding of the web of the column due to panel zone deformation. The equations for balancing these yield mechanisms are provided in Table 3-13. These equations require consideration of the geometry of the coverplate and the connections, since yielding occurs at two different locations. Figure 3-22 illustrates the geometry needed to define these equations for the coverplate connection. Table 3-14 provides equations for the failure modes of the connection.

**Table 3-13 Yield Mechanisms for Coverplate Connection**

Yield Mechanism	Equation to Define Yield Mechanism  Moment Resistance at the Face of the Column
Flexural Yielding of Beam - Moment at the Face of the Column	$M_{\text{yield}} = S F_{yb} \left( \frac{L - d_c}{L - d_c - 2 L_{cp}} \right)$
Panel Zone Yielding	$V_{\text{yield}} = 0.55 d_c t_{wc}$
Balancing of Panel Zone and Flexural Yield	$(0.9) 0.55 d_c F_{yc} t_{wc} \geq \frac{\sum S F_{yb}}{d_{\text{eff}}} \left( \frac{L}{L - d_c - 2 L_{cp}} \right) \left( \frac{h - d_b}{h} \right)$ <p>but preferably</p> $(0.6) 0.55 d_c F_{yc} t_{wc} \leq \frac{\sum S F_{yb}}{d_{\text{eff}}} \left( \frac{L}{L - d_c - 2 L_{cp}} \right) \left( \frac{h - d_b}{h} \right)$ <p>Note that <math>t_{wc}</math> includes both the thickness of the column web and the doubler plate.</p>

Note: All material properties provided in this table are expected values rather than minimum values.

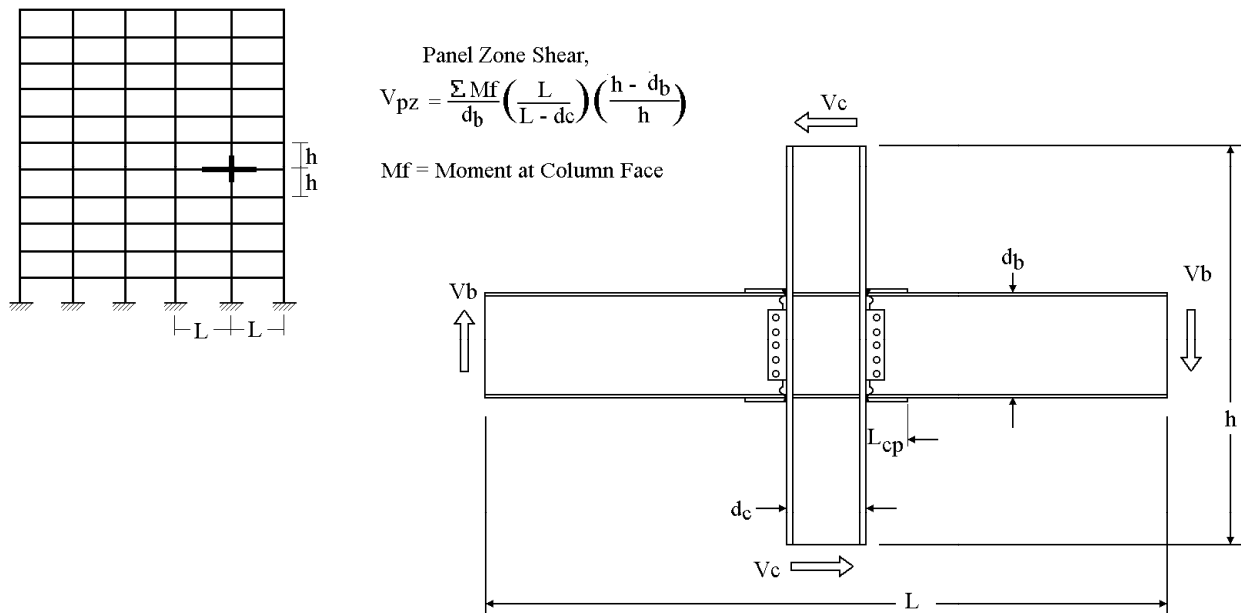


**Figure 3-22 Geometry for Balancing Shear and Flexural Yielding of Coverplate Connection**

The rotational capacity of the coverplate connection was estimated by a regression analysis of the experimental results. Recommended rotation limits are provided only for connections with both top and bottom coverplates where the area of the coverplate is less than or equal to 1.2 times the area of the beam flange. For coverplated connections that satisfy these conditions, with both the beam flange and coverplate welded with notch tough electrodes,

$$\theta_{p\text{mean}} = 0.031, \quad (3-19a)$$

and the standard deviation of  $\theta_p$  is

$$\sigma_p = 0.0015. \quad (3-19b)$$

There were a fairly large number of data points in this evaluation, but the data was concentrated in two beam sizes. As a result, there was no significant depth effect in this data, but the standard deviation was relatively small. This rotational limit is valid only for beams up to W36 sections, since this range is where the test data was concentrated. A large number of column fractures were noted with these connections, and it is recommended that  $\theta_g$  be the same as  $\theta_p$  for these coverplated connections, since column cracking is regarded as a more severe form of connection damage, which places deformation capacity beyond  $\theta_p$  in doubt.

The plastic rotation for modified pre-Northridge connections with both top and bottom coverplates where the beam flange is welded with E70T-4 electrodes and the coverplate is welded with an electrode with the minimum required notch toughness is

**Table 3-14 Failure Modes for Coverplate Connection**

	<b>Equation to Define Failure Mode Moment Resistance at the Face of the Column</b>	<b>Related Issues</b>
Fracture of Beam Flange Weld	Notch tough electrodes are required for the coverplate welds for existing construction and for both the flange welds and coverplate welds for new construction.	
Fracture of Column Flange	It is recommended that the area of the coverplate should not exceed 1.2 times the area of the flange.	
Web Connection	The web connection must be designed for the shear associated with the full plastic moment capacity of the beam at the end of the coverplate $V = \frac{2.2 F_{yb} Z_b}{L - d_c - 2 L_{cp}}$	The 1.1 factor on the moment capacity provides a reserve for strain hardening and uncertainty in the ultimate moment capacity.
Plastic Bending of Beam	$M_{pfail} = Z \frac{F_{yb} + F_{tb}}{2} \left( \frac{L - d_c}{L - d_c - 2 L_{cp}} \right)$	Lower bound estimate of full bending moment achieved.
Flange Buckling	for flange - $\frac{b_f}{2 t_f} \leq \frac{52}{\sqrt{F_y}}$	
Web Buckling	for web - $\frac{d_b}{t_w} \leq \frac{418}{\sqrt{F_y}}$	See discussion in Chapter 4.
Lateral Torsional Buckling	$L_b < \frac{2500 r_y}{F_y}$	$L_b$ is the unsupported length and equation is from existing AISC LRFD Seismic Provisions.
Continuity Plates	Continuity Plates required if $t_{fc} > 0.4 \sqrt{\frac{P_{bf}}{F_{yc}}}$ where $P_{bf} = 1.8 t_{fb} b_{fb} F_{yb} \left( \frac{L - d_c}{L - d_c - 2 L_{cp}} \right)$	Significant strain hardening occurs with this connection.
Weak Column Bending	$1.1 < \frac{S Z_c \left( F_{yc} - \frac{P_{uc}}{A_g} \right)}{S Z_b \frac{F_{yb} + F_{tb}}{2} \left( \frac{L - d_c}{L - d_c - 2 L_{cp}} \right)}$	Significant strain hardening occurs, and is reflected in SCWB limit.

Note: All material properties provided in this table are expected values rather than minimum values.

$$\theta_{pmean} = 0.056 - .0011 d_b, \quad (3-20a)$$

and the standard deviation is

$$\sigma_p = 0.019 + .0007 d_b, \quad (3-20b)$$

where  $\theta_{p\text{mean}}$  and  $\sigma_p$  are in radians and  $d_b$  is in inches. The dependency upon beam depth is quite strong with this test data, and the standard deviation is quite large because of the relatively small number of test results for this evaluation. The recommendations are valid for beam depths up to W36 sections. As with the new construction details, it is recommended that  $\theta_g$  be the same as  $\theta_p$ , since column cracking is regarded as a more severe form of connection damage.

These plastic rotation limits were based upon column spacing in the order of 25 to 30 ft. If longer column spacings are employed, larger rotations are possible, but smaller spans will result in smaller plastic rotation. As with the haunch connection, the actual flexural rotation at the end of the coverplate is larger than the normal rotation determined from story drift.

### 3.5 Reduced-Beam-Section (RBS) Connections

The reduced beam section schematically illustrated in Figure 3-23 has been developed (Chen, 1996; Iwankiw and Carter, 1996; Engelhardt, et al., 1996; Engelhardt, et. al., 1998) as an alternative connection since the Northridge earthquake. As with other connections, earlier proposals (Plumier, 1990) for RBS connections were made, but the connection did not have common usage until recent developmental work was complete. The RBS connection reduces the section of the beam at a distance from the beam-column connection so that yielding is concentrated in this reduced area at moments slightly lower than those that induce the full inelastic demand on the connection. This fuse protects the connection against early fracture. A number of reduced section geometries have been proposed including straight cut sections (shown in Figure 3-23a), tapered beam sections (shown in Figure 3-23b), and the radius cut (illustrated in Figure 3-23c). The straight cut RBS has not performed well in past tests, since it fractures after initial yielding due to stress and strain concentrations at the corner of the cut. The tapered beam section is theoretically quite rational, since it proposes to fit the tapered beam flange width to the moment diagram. Therefore, the yielding should be relatively uniform along the tapered cut length, and the length of the cut can be adjusted to the ductility demand. However, early tests of the tapered RBS provided variable performance because of fracture initiating from discontinuities at the return from the tapered section to the full beam flange width. The radius cut RBS is more empirical in its approach, since it does not adjust the reduced section to the seismic demand. The yielding is distributed over the length of the reduced section but in a variable pattern. While the tapered RBS shown in Figure 3-23 is quite rational, the radius RBS is much more commonly used in the US for reasons noted later in this discussion. The RBS connection has been commonly used for seismic design since the Northridge earthquake.

A substantial number of RBS connection tests have been completed including tests funded by AISC, NIST, tests completed for commercial projects, and other test programs. Table 3-15 summarizes some of these past tests which are reasonably well documented. Figure 3-24 shows the yield mechanisms and failure modes of this connection. Yielding primarily occurs as flexural yielding in the reduced section and shear yield of the panel zone. Limited yielding occurs in the beam outside the reduced section, but this contributes little to the plastic rotation. Examination of Table 3-15 suggests substantial scatter in the plastic rotation achieved with RBS connections, and implies relatively variable behavior from some failure modes. However, this observation is

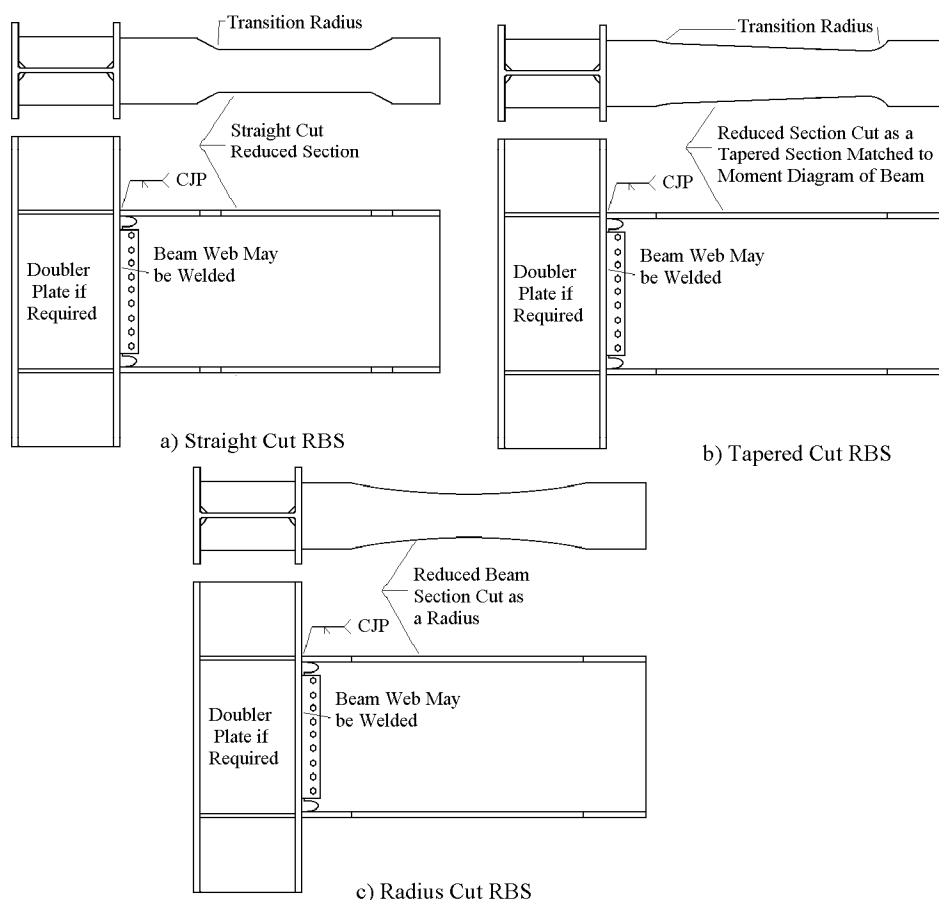


**Figure 3-23 Reduced-Beam-Section Connection, a) Straight Cut RBS, b) Tapered Cut RBS, and c) Radius Cut RBS**

somewhat misleading. Figure 3-25 plots the total plastic rotations summarized in Table 3-15, but the figure groups the connections into logical groupings. Tapered RBS specimens are identified by diamond symbols in Figure 3-25. Solid diamonds have welded web connections, and hollow diamonds have bolted web connections. Radius cut RBS specimens are identified as squares or circles in the figure. Solid squares have welded web connections and hollow squares have bolted webs. Two radius RBS specimens are identified as solid circles in the figure, and these are the only two radius cut RBS specimens which resulted in fracture of the specimen. Several observations can be made from the tapered RBS specimens. First, some specimens clearly develop large plastic rotational capacity, and  $\theta_p$  is even larger than suggested by this figure for many of the specimens because some tests were stopped due to limitations in the test apparatus. At the same time, a substantial number of the tapered RBS sections fractured in the beam flange. This shows that, while the tapered RBS is very rational, it is clearly a very sensitive connection, since the fractures commonly develop at the returns at the end of the tapered reduced section. Many of the early tests with these fractures had relatively sharp transitions at the returns from the tapered section to the full beam flange width. Recent research (Chen, et al., 2000) suggests that these problems are avoidable with radiused returns such as schematically shown in Figure 3-23b. Third, the fractured connections show a strong

dependency upon the beam depth as would be expected. Finally, and perhaps most important, the behavior exhibited by the tapered RBS sections with welded webs does not vary significantly from that exhibited by the tapered RBS sections with bolted webs. This suggests that the RBS section shields the beam-to-column connection enough that the enhanced behavior noted with welded web connection in the ordinary post-Northridge welded flange connections is not a critical factor.

**Table 3-15 Summary of Past RBS Test Results**

Specimen	Reduced Section and Failure	Web (Flange) Connection	Beam (Column)	Plastic Rotation $\theta_p$
DBT1B (SAC DATABASE)	Radius cut, test stopped equipment limitations	Welded-Bolted (E70TG-K2)	W30x99 W14x176	0.045
DBT1A (SAC DATABASE)	Radius cut, test stopped equipment limitations	Welded-Bolted (E70TG-K2)	W30x99 W14x176	0.028
TRS3 (SAC DATABASE)	Radius cut, test complete	Bolted (E71T-8)	W21x62 W14x120	0.02
TRS2A (Tremblay, 1997)	Radius cut, test stopped equipment limitations	Bolted (E71T-8)	W21x62 W14x120	0.04
TRS4 (Tremblay, 1997)	Radius cut, test complete	Bolted (E71T-8)	W21x62 W14x120	0.02
TLDB2 (SAC DATABASE)	Radius cut, fracture	Bolted (E70T-7)	W27x94 W14 (19x2x1)	0.017
TLDB1 (SAC DATABASE)	Radius cut, fracture	Welded (E70T-7)	W27x94 W14 (19x2x1)	0.013
WG4 (SAC DATABASE)	Radius cut, test stopped equipment limitations	Bolted (E70TG-K2 Fillet:E70T-8)	W36x300 W14x550	0.049

**Table 3-15 Summary of Past RBS Test Results (continued)**

WG1 (SAC DATABASE)	Radius cut, fracture	Bolted (E70TG-K2 Fillet:E70T-8)	W36x201 W14x311	0.033
WG2 (SAC DATABASE)	Radius cut, test stopped equipment limitations	Bolted (E70TG-K2 Fillet:E70T-8)	W36x201 W14x311	0.032
WG3 (SAC DATABASE)	Radius cut, test stopped equipment limitations	Bolted (E70TG-K2 Fillet:E70T-8)	W36x300 W14x550	0.035
YC-1 (Chen, 1996)	Tapered cut, fractured flange at weld access hole	Bolted (FCAW-SS E70T-7)	Built-up W24 (Built-up Box)	0.021
YC-2 (Chen, 1996)	Tapered cut, fractured flange at weld access hole	Bolted (FCAW-SS E70T-7)	Built-up W24 (Built-up Box)	0.025
PC-1 (Chen, 1996)	Tapered cut, fractured flange at weld access hole	Bolted (FCAW-SS E70T-7)	Built-up W24 (Built-up Box)	0.035
PC-2 (Chen, 1996)	Tapered cut, fractured flange at weld access hole	Bolted (FCAW-SS E70T-7)	Built-up W24 (Built-up Box)	0.041
PC-3 (Chen, 1996)	Tapered cut, fractured flange at weld access hole	Bolted (FCAW-SS E70T-7)	Built-up W24 (Built-up Box)	0.033
1A (Iwankiw, et al., 1996)	Tapered cut, no failure	Bolted (E70TG-K2)	W30X99 (W14X176)	0.027
1B (Iwankiw, et al., 1996)	Tapered cut, no failure	Bolted (E70TG-K2)	W30X99 (W14X176)	0.038
2A (Iwankiw et al., 1996)	Tapered cut, fracture near groove weld	Bolted (E70TG-K2)	W36x150 (W14x257)	0.033
2B (Iwankiw, et al., 1996)	Tapered cut, fracture flange weld	Bolted (E70TG-K2)	W36x150 (W14x257)	0.017

**Table 3-15 Summary of Past RBS Test Results (continued)**

ARUP-1 (Zekioglu, et al., 1997)	Tapered cut, fracture at minimum section	Groove Weld (E70TG-K2)	W36x150 (W14x426)	0.033
COH-1 (Zekioglu, et al., 1997)	Tapered cut, fracture at minimum section	Groove Weld (E70TG-K2)	W27x178 (W14x455)	0.033
COH-2 (Zekioglu, et al., 1997)	Tapered cut, fracture at minimum section	Groove Weld (E70TG-K2)	W27x178 (W14x455)	0.035
COH-3 (Zekioglu, et al., 1997)	Tapered cut, fracture at minimum section	Groove Weld (E70TG-K2)	W33x152 (W14x455)	0.030
COH-4 (Zekioglu, et al., 1997)	Tapered cut, fracture at minimum section	Groove Weld (E70TG-K2)	W33x152 (W14x455)	0.037
COH-5 (Zekioglu, et al., 1997)	Tapered cut, fracture at minimum section	Groove Weld (E70TG-K2)	W33x152 (W14x455)	0.017
DB1 (Engelhardt, et al., 1996)	Constant cut, flange fracture at reduced section	Groove Weld (E71T-8)	W36x160 (W14x426)	0.019
DB2 (Engelhardt, et al., 1996)	Radius cut, test stopped due to equipment limitations	Groove Weld (E71T-8)	W36x150 (W14x426)	0.028
DB3 (Engelhardt, et al., 1996)	Radius cut, test stopped due to equipment limitations	Groove Weld (E71T-8)	W36x170 (W14x426)	0.036
DB4 (Engelhardt, et al., 1996)	Radius cut, test stopped due to equipment limitations	Groove Weld (E71T-8)	W36x194 (W14x426)	0.035
DB5 (Engelhardt, et al., 1996)	Radius cut, large panel zone yielding. Test stopped due to equipment limitations	Groove Weld (E71T-8)	W30x148 (W14x426)	0.038
DB1 (Popov, et al., 1996)	Radius cut, test stopped due to equipment limitations	Groove Weld (E71T-8)	W36x135 (W14x257)	0.028

**Table 3-15 Summary of Past RBS Test Results (continued)**

DB2 (Popov, et al., 1996)	Radius cut, test stopped due to equipment limitations	"Heavily" Welded (E71-T8)	W36x245 (W14x398)	0.028
S-1 (Tremblay, et al., 1997)	Radius cut, monotonic test, no failure	Bolted (E71T-8)	W21x54 (W14x120)	0.083
S-2A (Tremblay, et al., 1997)	Radius cut, test stopped due to equipment limitations	Groove Weld (E71T-8)	W21x54 (W14x120)	0.033
SC-1 (Tremblay, et al., 1997)	Radius cut, composite slab, test stopped due to equipment limitations	Groove Weld (E71T-8)	W21x54 (W14x120)	0.031
UT-RBS-1 (NIST, 1998)	Radius cut, bottom flange only, bottom weld fracture	Bolted (E70T-4)	W30x99 (W12x279)	0.006
UT-RBS-2 (NIST, 1998)	Radius cut, bottom flange only, composite slab, K-line fracture	Bolted (Rewelded E71T-8)	W30x99 (W12x279)	0.021
UCSD RBS-1 Beam 1 (NIST, 1998)	Radius cut, bottom flange only, top weld fracture	Bolted (E70T-4)	W36x150 (W14x426)	0.0
Beam 2 (NIST, 1998)	Top weld fracture			0.012
UCSD RBS-2 (NIST, 1998)	Radius cut, bottom flange only, composite slab, top flange weld fracture	Bolted (E70T-4)	W36x150 (W14x426)	0.01
UCSD RBS-2R (NIST, 1998)	Radius cut, bottom flange only, composite slab, top flange weld fracture	Bolted (E70T-4)	W36x150 (W14x426)	0.008
UCSD RBS-3 Beam 1 (NIST, 1998)	Radius cut, bottom flange only, K-line fracture	Bolted (E70T-4)	W36x150 (W14x426)	0.029
Beam (NIST, 1998)	Test stopped			0.01
UCSD RBS-4 (NIST, 1998)	Radius cut, bottom flange only, composite slab, K-line fracture	Bolted (E70T-4)	W36x150 (14x426)	0.03

Note: See Chen (1996); Engelhardt, et al. (1996); Iwankiw, et al. (1996); Tremblay, et al. (1997); NIST, (1998); Zekioglu, et al. (1997).

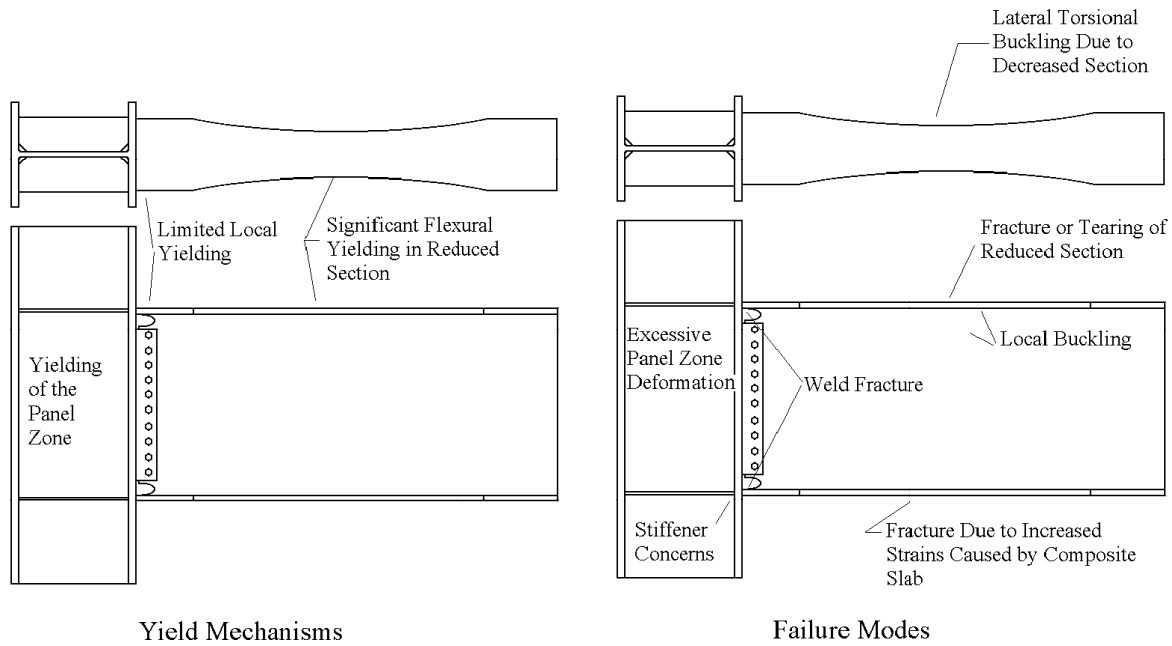


**Figure 3-24 Yield Mechanisms and Failure Modes for RBS Connections**

The radius cut RBS section is illustrated in Figure 3-23c, and it is the most common RBS configuration for US practice. Radius RBS specimens with both top and bottom flange reductions that were tested without any evidence of fracture are identified as triangles in Figure 3-25. Thus, there is more reserve rotational capacity in these connections. The two solid circles in the figure are radius RBS systems where fracture occurred. These fractures are attributed to roughness of the flame cut curved surface. Plastic rotations were relatively small for these specimens, and this clearly shows the importance of the surface finish for the reduced section.

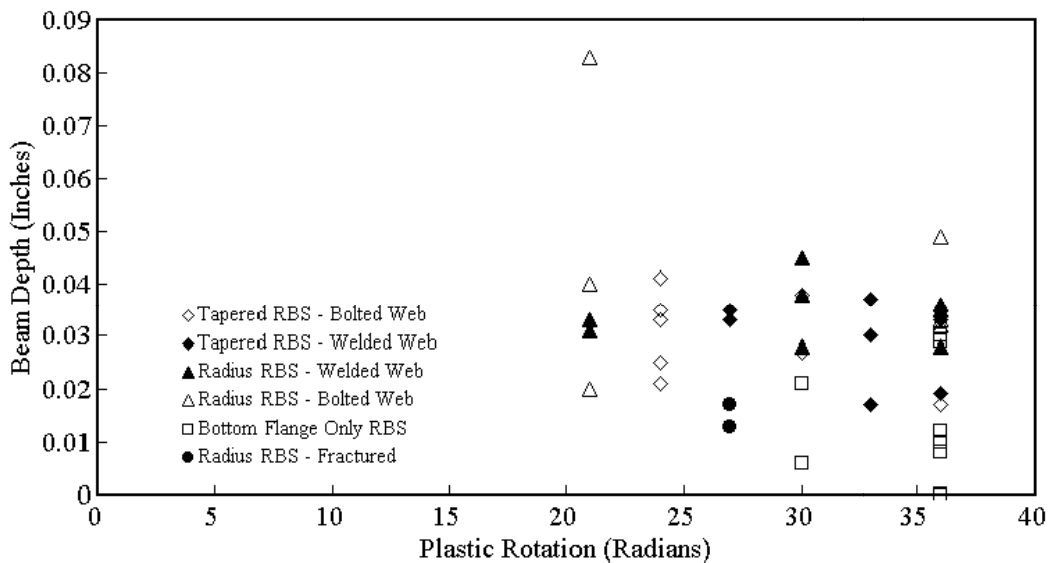


**Figure 3-25 Total Plastic Rotations from Past RBS Connection Tests**

The radius cut RBS system is a more empirical method, since there is no rational model for defining the radius and reduced section based upon the beam length and geometry. However, the radius cut RBS system clearly achieves significant plastic rotational capacity, and it is clearly less sensitive to fabrication details than is the tapered RBS section. The reduced sensitivity is noted by observing that there is no apparent dependency on depth for the specimens shown in the figure, and only two of the radius cut RBS specimens in the figure fractured the specimen. That is, the large majority of radius cut RBS specimen tests in the figure were stopped because of limitations of test apparatus, and so the  $\theta_p$  indicated for these specimens in the figure is clearly a lower bound of the real plastic rotation limit. The hollow squares shown in Figure 3-25 are also radius cut RBS systems, but these reduced sections were applied to the bottom flange only. The specimens were tested with or without composite slabs. These bottom flange RBS specimens were tested in a research program funded by AISC and NIST (NIST, 1998) as an examination of possible modification to pre-Northridge steel frame buildings. Most of these specimens failed at very small plastic rotations, and rather brittle failures were noted. These results suggest that the bottom flange only RBS is not an effective connection for achieving large plastic rotations, and for shielding a brittle beam flange weld from the demands of inelastic deformation.

While the tapered RBS has the more rational design approach, the prior discussion showed that it is very sensitive to initial flaws caused by normal fabrication. In particular, sharp corners at the returns from the tapered section to the full beam width were sources of flange fracture. Research into the required geometry of the returns could lead to a connection which has even more ductility than the radius cut RBS. On the other hand, the radius cut RBS system may be more empirical, but it is less sensitive to fabrication flaws, and past tests indicate that it has substantial rotational capacity. As a result, the radius cut RBS is the more commonly used RBS system in the US, and a design procedure (Engelhardt, 1998) for the radius cut RBS was developed based on the behavior observed in past tests. This procedure:

- limits the reduced section to a proportional range of the beam flange width,
- establishes the radius and arc length based upon empirical limits which depend on the beam geometry, and
- selects the placement of the section so that the full plastic capacity is developed in the reduced section before overly large nominal stresses develop at the welded beam flange to column connection.

The RBS system reduces the section of the beam, and this clearly must reduce the stiffness of the building. Studies (Grubbs, 1997; Iwankiw, et al., 1996; Almudhafar and Chambers, 2000) have been completed to determine the effect of the reduced section on the overall frame stiffness. It was determined that, for the normal 40% flange width reductions employed in the RBS design procedure, the reduction in frame stiffness is in the range of 4 to 5%.

A large number of radius cut RBS connections have been designed with this design procedure, and commercial verification tests have shown good behavior, with no significant problems noted. As a result, research (Engelhardt et al., 2000) completed for this report emphasized full development of the design procedure and the examination of issues which may

prevent good performance of the radius cut RBS system or which may affect the economy of the system. These issues include:

- the effect of composite slabs on the RBS system, since the slab may raise the neutral axis and increase the strain and deformation demands on the reduced section,
- the effect of lateral torsional buckling on the system behavior, since the reduced section decreases the torsional stiffness properties and AISC (1997) requires lateral support at all plastic hinge locations. The RBS system develops this plastic hinge well away from the face of the column, and there is an economic desire to minimize the bracing requirements at these locations.
- the effect of bolted vs. welded web connections, since bolted web connections are viewed as more economical than welded web connections, and the tapered RBS test results suggest that bolted webs behave about the same as the welded web connection,
- the effect of large one sided deformation demand such as caused by near fault records on the RBS behavior,
- the finish required for the curved section,
- the effect of dynamic load rates on the system ductility, and
- the effect of panel zone yielding on RBS behavior.

Nonlinear analyses with the ABAQUS computer program were performed as part of this study to examine the placement of the RBS system, to determine the strain demands at critical locations where fracture may occur, and to address other related issues. Analysis (Engelhardt et al., 2000) clearly indicates that the RBS does not eliminate all inelastic strain demands at the beam flange weld, but a significant reduction in this demand (Deierlein, et al., 1999) is noted. As a consequence, all flange welds for the RBS tests were welded with E70T-6 FCAW-SS electrodes, since the weld has somewhat smaller expected notch toughness than the E70TG-K2 electrode used for other post-Northridge connection.

Seventeen large-scale tests were performed (Engelhardt et al., 2000; Yu, et al., 2000; Gilton, et al., 2000B) to further address these issues. Table 3-16 summarizes these test results. Note that some experiments in the table used cruciform specimens, and two connection moments are provided for these specimens. The results show that composite slabs increase the strain demands for some locations of the RBS system but they do not have an overall detrimental effect on the rotational capacity of the connection. Four tests were run with bolted webs and four identical tests were completed with welded webs. The welded web tests at Texas A&M had less constraint at the supports. This resulted in more rapid deterioration in moment capacity of the connection, and reduced rotational capacities for those tests. To illustrate this, the behavior of Texas A&M specimen DBWW is compared to very similar University of Texas specimen DBBW in Figure 3-26. The full plastic moment capacity of the reduced section is achieved when the moment capacity at the face of the column is approximately 26,000 kip-in. By the FEMA/SAC test protocol (Clark, et al., 1997), the rated plastic rotation for a specimen is determined by initial fracture or the rotation at which 80% of the plastic moment capacity is not achieved. Specimen DBWW was not able to retain the moment capacity through a complete 0.03 cycle of rotation, while DBBW was able to retain larger rotation. DBWW is a welded web

specimen, and ordinarily one would expect less deterioration with that connection. The differences between other tests such as DBWP and DBSPZ are even more dramatic. Because of these differences, the Texas A&M specimens are thought to show more rapid deterioration and smaller rotational capacity than the RBS connection would ordinarily provide. As a result, some information on these connections is not included in the table, because this information could provide misleading comparisons regarding the relative merits of bolted and welded webs and the effect of panel zone yield. At the same time, the Texas A&M specimens clearly show how the slab can benefit connection performance as is discussed in Chapter 4.

Comparison of the bolted webs with other past welded web tests indicates that bolted webs provide quite satisfactory seismic performance. The curved surface was flame cut and the cut surface ground to a finish of approximately 500 micro inches RMS for all of the SAC RBS specimens, and this finish provided good seismic performance. This finish was estimated by comparison of the tested specimens with standard surface finish gages.

Weak panel zones clearly lead to larger inelastic deformations in the panel zone and smaller plastic deformations in the reduced section, but this yielding also provides additional rotation, which compensates for the loss of the yield in the reduced section. Comparison of weak panel zone specimens with strong panel zone specimens shows that connection performance is not

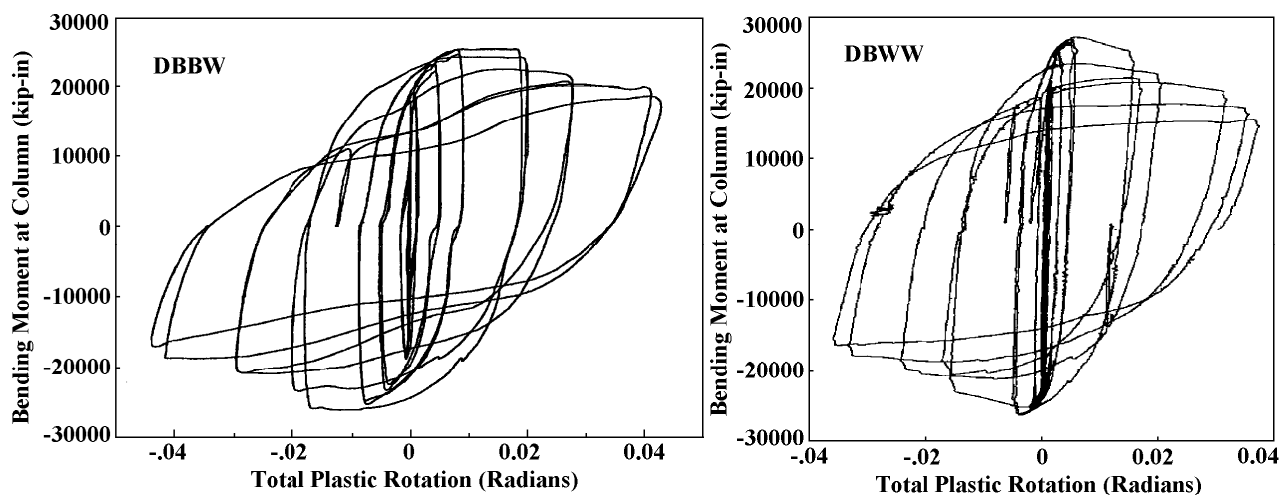


**Figure 3-26 Comparison of Moment-Rotation Curves for DBWW and DBBW Radius Cut RBS Specimens**

particularly sensitive to the amount of panel zone deformation. The strain hardening noted with the radius cut RBS connection is significant, but it is somewhat less than that noted with other post-Northridge connections. The radius cut RBS can clearly achieve large  $\theta_p$ , and it is less sensitive to adverse effects than are other connections. It is consequently viewed as one of the most attractive connection options for heavy steel framing with large seismic demands.

The RBS connection appears to be relatively robust, since it appears to be less sensitive to minor imperfections than are many other alternatives. A design procedure (Engelhardt, 1998)

has been developed and is retained for this connection. The procedure is quite empirical, and it does not consider many important factors such as the span length and ductility demand. The vast majority of the tests on radius cut RBS connections had relatively heavy beams (W30 and W36) with column spacing of approximately 25 ft. Tables 3-17 and 3-18 summarize the yield mechanisms and failure modes, respectively, for the radius cut RBS connection. Figure 3-27 illustrates the geometry used for some of these equations.

The rotational capacity of the radius cut RBS connection was estimated by a regression analysis of the experimental results. Only the bare steel experimental results from this research program were used in this evaluation, and the Texas A&M tests were excluded because the plastic rotations of these tests were more than one standard deviation smaller than the other tests. Further, the smaller plastic rotations achieved with these tests were limited by the test setup rather than a problem with the connection. The resulting recommendation is:

$$\theta_{p\text{mean}} = 0.05 - .0003 d_b, \quad (3-21a)$$

and the standard deviation of  $\theta_p$  is

$$\sigma_p = 0.02 + .0006 d_b, \quad (3-21b)$$

where  $\theta_{p\text{mean}}$  and  $\sigma_p$  are in radians and  $d_b$  is in inches. The dependency upon beam depth is not strong, because of the limited depth range of the RBS specimens tested and the ductility achieved with nearly all tests. This recommendation is valid for all beam depths up to W36.

For estimating the maximum rotations for support of gravity loads, it must be noted that only three of the radius cut RBS specimens summarized in Tables 3-15 and 3-16 experienced any fracture. Significant deterioration was noted on occasion, but the connection appeared to hold together well. As a result, it is not possible to accurately estimate  $\theta_g$ , but it appears that  $\theta_g$  is significantly larger than  $\theta_p$ . Consequently,  $\theta_g$  was set as 0.02 radians larger than  $\theta_p$ , and

$$\theta_{g\text{mean}} = 0.07 - .0003 d_b. \quad (3-22)$$

**Table 3-16 Summary of SAC Phase 2 RBS Test Results**

<b>Test Specimen</b>	<b>General Description and Information</b>	<b>Beam and (Column) Sizes Web Connection</b>	<b>Plastic Rotation at Initial Failure</b>	<b>Plastic Rotation Due to Panel Zone Yielding</b>	<b>Max. Moment in Reduced Section &amp; Divided by Reduced <math>M_p</math></b>	<b>Moment at Face of Column &amp; Divided by <math>M_p</math></b>
UTA DBBW  (Engelhardt, Fry, et al., 2000)	Cruciform specimen, strong panel zone, bolted web, without composite slab - no fracture	W36x150 (W14x398) 10-1"A490	0.04  (slightly less than 80%)	0.007	20800 (20800) 0.95	24800 (24800) 0.76
UTA DBBWC  (Engelhardt, Fry, et al., 2000)	Same as UTA DBBW with composite slab - south beam flange fractured near weld access hole at 0.038	W36x150 (W14x398) 10-1"A490	0.05 (less than 80%) and 0.038 at fracture	0.01	26050 (26300) Ratio is misleading for composite behavior	31015 (31300) Ratio is misleading for composite behavior
UTA DBWP  (Engelhardt, Fry, et al., 2000)	Cruciform specimen, weak panel zone, bolted web, without composite slab - Significant panel zone yield deformation - south beam flange fractured	W36x150 (W14x283) 10-1"A490	0.045 at approx, & 0.027 at fracture	0.045 (one direction) 0.028 (other)	22259 (19272) 0.96 (0.83)	26464 (22913) 0.80 (0.70)
UTA DBWPC  (Engelhardt, Fry, et al., 2000)	Cruciform specimen, weak panel zone, bolted web, with composite slab – Bottom flange fracture in both beams at large deformations	W36x150 (W14x283) 10-1"A490	0.05	0.04	20700 (24900) Ratio is misleading for composite behavior	24600 (29619) Ratio is misleading for composite behavior

**Table 3-16 Summary of SAC Phase 2 RBS Test Results (continued)**

TA&M DBWW  (Engelhardt, Fry, et al., 2000)	Cruciform specimen, strong panel zone, welded web, without composite slab – This specimen had limited restraint at the support and this results in rapid deterioration in resistance. Test terminated because of out of plane buckling	W36x150 (W14x398) 4-1” bolts with welded web	0.03 (less than 80%) 0.02 (by test protocol rules)	0.008	May be misleading	May be misleading
TA&M DBWW-C  (Engelhardt, Fry, et al., 2000)	Same as TA&M DBWW but with composite slab. This specimen also had limited restraint at the support, and the reduced deterioration in resistance as compared to DBWW clearly shows the beneficial effect of the slab on the restraint of the specimen. Tearing at buckle of both flanges at initial $\theta = 0.06$ cycle	W36x150 (W14x398) 4-1” bolts with welded web	East and west beam PR 0.05 (w/ significant deterioration) 0.04 (slightly below 80%)	0.013	May be misleading	May be misleading
TA&M DBWWSPZ  (Engelhardt, Fry, et al., 2000)	Cruciform specimen, very strong panel zone, welded web, without composite slab. This specimen also had limited restraint at the support, and test was terminated at a small plastic rotation because of out of plane buckling	W36x150 (W14x398) ¾” doubler both sides 4-1” bolts w/ welded web	0.015	0.00	May be misleading	May be misleading
TA&M DBWW SPZ-C  (Engelhardt, Fry, et al., 2000)	Same as TA&M DBWWSPZ but with composite slab. Significantly less rapid deterioration in resistance than DBWWSPZ because of restraint of slab. Comparison with DBWWSPZ clearly illustrates the benefits of the slab in restraining the specimen. Test terminated because of out of plane buckling	W36x150 (W14x398) ¾” doubler both sides 4-1” bolts w/ welded web	0.05	0.00	May be misleading	May be misleading

**Table 3-16 Summary of SAC Phase 2 RBS Test Results (continued)**

UCSD LS-1  (Yu, et al., 2000)	T-shaped specimen tested with standard deformation pattern	W30x99 (W14x176) 3-1" bolts w/ welded web	0.045 @ approx 45% and 0.03 at approx 80%	0.007	14306 (1.25)	16260 (0.95)
UCSD LS-2  (Yu, et al., 2000)	T-shaped specimen tested with special near fault deformation pattern	W30x99 (W14x176) 3-1" bolts w/ welded web	0.05 multiple one sided cycles	0.014	14051 (1.22)	15980 (0.94)
UCSD LS-3  (Yu, et al., 2000)	T-shaped specimen tested with special near fault deformation pattern	W30x99 (W14x176) 3-1" bolts w/ welded web	0.05 multiple one sided cycles	0.006	13060 (1.14)	14845 (0.87)
UCSD LS-4  (Yu, et al., 2000)	T-shaped specimen tested with standard deformation pattern. Additional lateral restraint than LS-1 at reduced section - no fracture - somewhat less deterioration than LS-1	W30x99 (W14x176) 3-1" bolts w/ welded web	0.04	0.008	14555 (1.27)	16540 (0.97)
UCSD DC-1  (Gilton, et al., 2000B)	T-shaped specimen - tested with standard deformation protocol to evaluate effect of deep columns. Comparable to UCSD LS-1 as a prototype. Test stopped due to twisting of column	W36x150 (W27x146) w/ 3/8" doubler 4-1" bolts w/ welded web	.044 (test stopped - column twisting) .028 (at 80%)	0.015	25200 (1.31)	31000 (1.07)
UCSD DC-2  (Gilton, et al., 2000B)	Similar to UCSD DC-1 but heavier column. Test stopped after single cycle 0.044 with large out of plane deformation, twisting of column and loss of resistance	W36x150 (W27x194) no doubler 4-1" bolts w/ welded web	0.03 (2 cycles) 0.044 (single cycle)	0.012	26020 (1.26)	32000 (1.10)

**Table 3-16 Summary of SAC Phase 2 RBS Test Results (continued)**

UCSD DC-3  (Gilton, et al., 2000B)	Similar to UCSD DC-1 but heavier column with doubler. Brittle fracture at K-line	W27x194 (W27x194) w/ 5/8" doubler 4-1" bolts w/ welded web	0.028  (brittle fracture in second cycle)	0.01	29700  (1.38)	36000  (1.14)
UCSD CW-1  (Gilton, et al., 2000B)	Weak axis bending specimen. Test stopped due to deterioration of resistance	W36x150 (W14x398)	0.042  at less than approx 40% 0.02 at 80%	not applicable	26390  (1.28)	32000  (1.10)
UCSD Cw-2  (Gilton, et al., 2000B)	Weak axis bending specimen. Test stopped due to deterioration of resistance	W24x62 (W14x176)	0.045 at approx. 55% 0.02 at 80%	not applicable	679  (1.29)	7500  (0.98)

Notes:

1. Plastic rotations are rotations prior to significant loss of resistance or initial fracture of the connection and are story drift rotations.
2. All flange welds are E70T-6 CJP welds. All bottom flange backing bars removed, backgouged, and reinforced with 1/4" fillet of E71T-8.
3. For DC-1, DC-2, Dc-3, CW-1, and CW-2 moment at face of column determined graphically, yield stress assumed to be nominal 50 ksi, and dimensions inferred from test setup for LS-2.
4. See Engelhardt, et al. (2000); Yu, et al. (2000); Gilton, et al. (2000B).

**Table 3-17 Yield Mechanisms for RBS Connection**

Yield Mechanism	Equation to Define Yield Mechanism Moment Resistance at the Face of the Column
Flexural Yielding of Beam - Moment at the Face of the Column	$M_{yield} = S_{RBS} F_{yb} \left( \frac{L - d_c}{L - d_c - 2 L_{RBS}} \right)$ <p>where <math>S_{RBS}</math> is the elastic section modulus of the Reduced-beam-section</p>
Panel Zone Yielding	$V_{yield} = 0.55 d_c t_{wc}$
Balancing of Panel Zone and Flexural Yield	$(0.9) 0.55 d_c F_{yc} t_{wc} \geq \frac{\Sigma S_{RBS} F_{ybm}}{d_b} \left( \frac{L}{L - d_c - 2 L_{RBS}} \right) \left( \frac{h - d_b}{h} \right)$ <p>but preferably</p> $(0.6) 0.55 d_c F_{yc} t_{wc} \leq \frac{\Sigma S_{RBS} F_{ybm}}{d_b} \left( \frac{L}{L - d_c - 2 L_{RBS}} \right) \left( \frac{h - d_b}{h} \right)$ <p>Note that <math>t_{wc}</math> includes both the thickness of the column web and the thickness of doubler plate.</p>

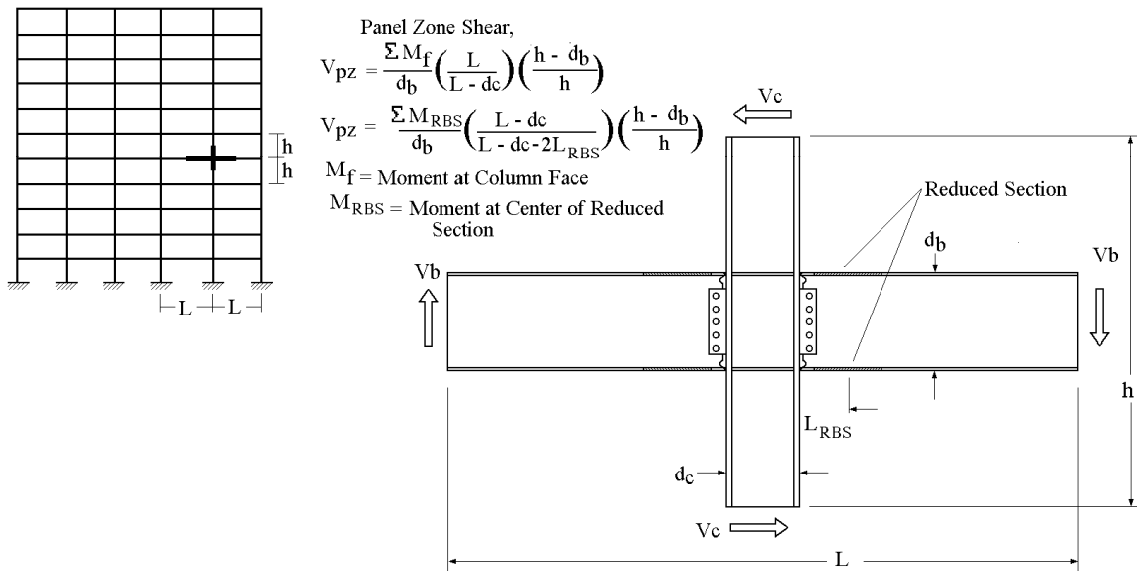


**Figure 3-27 Geometry for Balancing Shear and Flexural Yielding of RBS Connection**

**Table 3-18 Failure Modes for RBS Connection**

Failure Mode	Equation to Define Failure Mode Moment Resistance at the Face of the Column	Related Issues
Fracture of Beam Flange Weld	The beam flange weld is partially protected by the reduced-beam-section. Notch tough weld metal (E70T-6) is required at the flange weld, but this weld metal is often of slightly lower notch toughness than used for other welded flange post-Northridge connections.	
Plastic Bending of Beam	$M_{pfail} = Z_{RBS} \frac{F_{yb} + F_{tb}}{2} \left( \frac{L - d_c}{L - d_c - 2 L_{RBS}} \right)$ <p>The RBS commonly gets slightly less strain hardening than many other post-Northridge connections, and so this is not always achieved.</p>	$Z_{RBS}$ is the plastic section modulus of the reduced-beam-section.
Fracture of the Reduced Section	The radius cut RBS avoids the mode of fracture by assuring that the surface finish of the curve surface has an adequate finish of the cut surface. It is recommended that this surface be no rougher than 500 rms.	
Web Connection	The web connection must be designed for the shear associated with the full plastic moment capacity of the beam at the end of the coverplate $V = \frac{2.2 F_{yb} Z_{RBS}}{L - d_c - 2 L_{RBS}}$	The 1.1 provides a reserve for strain hardening and uncertainty in the ultimate moment capacity.
Flange Buckling	for flange - $\frac{b_f}{2 t_f} \leq \frac{52}{\sqrt{F_y}}$	
Web Buckling	for web - $\frac{d_b}{t_w} \leq \frac{418}{\sqrt{F_y}}$	See discussion in Chapter 4.
Lateral Torsional Buckling	$L_b < \frac{2500 r_y}{F_y}$ <p><math>L_b</math> is the unsupported length and equation is from existing AISC LRFD Seismic Provisions</p>	Lateral bracing not required at reduced section itself. See Chapter 4.
Continuity Plates to prevent damage to the web and flange of column.	Continuity Plates required if $t_{fc} \geq 0.4 \sqrt{\frac{P_{bf}}{F_{yc}}}$ <p>where <math>P_{bf} = 1.8 t_{fb} b_{RBS} F_{yb} \left( \frac{L - d_c}{L - d_c - 2 L_{RBS}} \right)</math></p>	$b_{RBS}$ is the flange width at the reduced section.
Weak Column Bending	$1.1 < \frac{\sum Z_c \left( F_{yc} - \frac{P_{uc}}{A_g} \right)}{\sum Z_b \frac{F_{yb} + F_{tb}}{2} \left( \frac{L - d_c}{L - d_c - 2 L_{RBS}} \right)}$	Strain hardening is significant but smaller than other post-Northridge connections

For most post-Northridge connections, an increase in span length will increase the plastic rotation, but this will not be true with the RBS connection, because the radius length and reduced section do not depend upon the span length. The vast majority of the RBS connection tests were

completed with W30 and W36 beams and a column spacing of approximately 25 ft. Significantly longer or shorter column spacing may result in reduced rotational capacity for the RBS connection because of the empirical nature of the design procedure and the fact that the geometry of the RBS is not keyed to the span length or the ductility demand. Therefore, care must be taken to avoid extrapolation of the performance of the RBS connection behavior to conditions beyond those tested.

### 3.6 Welded-Flange-Plate Connections

Welded-flange-plate connections, as illustrated in Figure 3-28, have also been used. Welded-flange-plate connections have similarities with the bolted-flange-plate connection discussed in Chapter 5, but the welded-flange-plate connection can be designed more easily to develop the full plastic capacity of the beam. The yield mechanisms and failure modes of the welded-flange-plate connection are shown in Figure 3-29. The yield mechanisms are primarily shear yielding of the panel zone and flexural yielding of the beam. Tensile yielding of the flange-plate is also possible if rectangular flange-plates of appropriate size are used, but tensile yield of the plate cannot be permitted with tapered plates such as illustrated for the top flange of Figure 3-28. Failure modes include tensile fracture of the flange-plate or CJP weld, fracture of the fillet weld between the beam and flange-plate, local and lateral torsional buckling, and excessive deformation of the beam or column. Net section failure modes are a major concern with the bolted-flange-plate connection, but they are largely avoided with the welded-flange-plate connection. As a result, it is easier to achieve large rotational capacity and full strength connections with the welded-flange-plate connection than with the bolted-flange-plate connection.

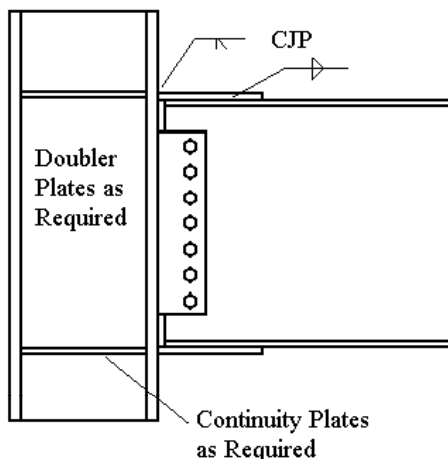


**Figure 3-28** Welded-Flange-Plate Connection

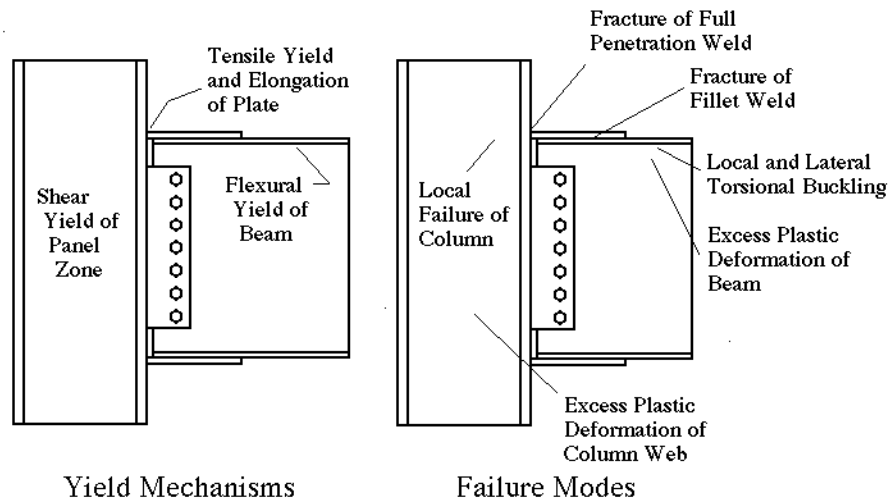


**Figure 3-29 Yield Mechanisms and Failure Modes of Welded-Flange-Plate Connection**

Relatively few tests of these connections (Popov and Pinkney, 1969; Whittaker and Gilani, 1996; Noel and Uang, 1996) were reported prior to the SAC Steel project. The tests that were completed provided mixed results, but they clearly showed that great ductility was possible, and that the connections could develop the full moment capacity of the beam. A limited test program (Kim et al., 2000) was completed during this research program, and these tests are summarized in Table 3-19. These specimens all had relatively deep beams, and none of the specimens fractured at a plastic rotation smaller than 0.04 radians. The bolted-flange-plate connection study and the welded coverplate connection both provide considerable insight into the behavior and ductility expected with the welded-flange-plate connection. The bolted-flange-plate study showed that connections which combined the panel zone shear yielding, tensile plate yielding, and flexural yielding of the beam achieved the greatest ductility and best seismic performance. The welded-flange-plate connection did not specifically study this issue, but the tests verified this observation since Specimen UCB-RC09 came closest to that ideal and provided the best performance of the specimens tested. Table 3-20 provides equations for estimating the resistance associated with each of these yield mechanisms, and it provides a basis for balancing these yield conditions. Figure 3-30 illustrates the geometry needed to evaluate the yield conditions. Table 3-21 provides equations for estimating the failure modes of the welded-flange-plate connection.

The rotational capacity of the radius welded connection was estimated by a regression analysis of the experimental results. The recommended rotation limit is:

$$\theta_{p\text{mean}} = 0.03, \quad (3-23a)$$

and the standard deviation of  $\theta_p$  is

$$\sigma_p = 0.003. \quad (3-23b)$$

where  $\theta_{p\text{mean}}$  and  $\sigma_p$  are in radians. The limit is independent of beam depth, since all tests were on W30 beam sections. It is applicable to beams up to W30. The rotation limit depends upon

**Table 3-19 Summary of Test Results for Welded-Flange-Plate Connection**

Test Specimen	General Description and Information	Beam and (Column) Sizes	Plastic Rotation at Initial Failure	Plastic Rotation Due to Panel Zone Yielding	Max. Moment at Face of Column (Divided by $M_p$ )	Plastic Rotation at End of Test	Max. Moment Divided by $\frac{F_y+F_t}{2} Z$
UCB-RC04	1 1/8" curved dove-tailed flange-plate to permit more fillet welding over the cover plate length - Strong panel zone - Ductile tearing of flange	W30x99 (W14x176) welded web - 3/8" doubler-	0.02 at 80% 0.049 at flange tear	Very little but not yet defined	21200 (1.15)	0.049	1.00
UCB-RC06	Designed to have primarily beam flexural yielding - 1" x 13 1/4" x 15" long flange-plate - Ductile tearing of beam flange.	W30x99 (W14x176) welded web - 3/8" doubler	.03 at 80% 0.042	Very little but not yet defined	22200 (1.20)	0.042	1.04
UCB-RC07	Designed to have primarily beam flexural yielding - Near fault load pattern - 1" x 13 1/4" x 15" long flange-plate - Ductile tearing of beam flange.	W30x99 (W14x176) welded web - 3/8" doubler-	check this but the plot seems wrong	Very little but not yet defined	21300 (1.15)	0.05	1.00
UCB-RC08	Designed to have some balance in coverplate and beam flexural yielding but little panel zone yielding- 7/8" x 13 1/4" x 15" long flange-plate - Ductile tearing of beam flange after initiation at K-line.	W30x99 (W14x176) welded web - 7/8" doubler-	0.03 at 80% 0.04 at seve		22500 (1.22)	0.05 (26% of maximum resistance)	1.06
UCB-RC09	Designed to have balanced yielding between the beam, panel zone and coverplate - 7/8" x 13 1/4" x 15" long flange-plate - Ductile tearing of beam flange after initiation at K-line.	W30x99 (W14x176) welded web - no doubler-	0.04 at 80% 0.055 at ductile tear	Significant but not yet defined.	21575 (1.18)	0.055	1.02

## Notes:

1. Plastic rotations are rotations prior to significant loss of resistance or initial fracture of the connection.
2. All flange welds are with notch tough electrodes.
3. Plastic capacities are determined from mill test reports, and adjusted for geometry since they occur at end of flange-plate.
4. See Kim, et al. (2000).

span length, and this rated rotation,  $\theta_p$ , decreases with decreasing beam span length, and the above rotation is valid for column spacing larger than 25 ft.

For estimating the maximum rotations for support of gravity loads,  $\theta_g$ , it should be noted that welded-flange-plate connections were tested to rotations of greater than 0.049 radians without any connection losing its ability to support gravity load. Thus,  $\theta_g$  must be somewhat larger than this rotation value. As a result,  $\theta_g$  was set as 0.01 radians larger and

$$\theta_{g\text{mean}} = 0.06 . \quad (3-24)$$

**Table 3-20 Yield Mechanisms of the Welded-Flange-Plate Connections**

Yield Mechanism	Equation to Define Yield Mechanism Moment Resistance at the Face of the Column	Remarks
Plastic Flexure of Beam	$M_{\text{yield}} = S F_{yb} \left( \frac{L - d_c}{L - d_c - 2 L_{fp}} \right)$	
Tensile Yield of Flange-Plate	$M_{\text{yield}} = F_{yp} t_p b_p (d_b + t_p t)$ This formulation assumes the top and bottom plate have the same plate thickness.	Not valid for tapered flange-plates. This should not be the primary yield mechanism.
Panel Zone Yielding	$V_{\text{yield}} = 0.55 F_{yc} d_c t_{wc}$	
Balanced Yield Condition	As the primary yield mechanism combination $(0.9) 0.55 d_c F_{yc} t_{wc} \geq \frac{\Sigma S F_{yb}}{d_{\text{eff}}} \left( \frac{L}{L - d_c - 2 L_{fp}} \right) \left( \frac{h - d_b}{h} \right)$ but preferably $(0.6) 0.55 d_c F_{yc} t_{wc} \leq \frac{\Sigma S F_{yb}}{d_{\text{eff}}} \left( \frac{L}{L - d_c - 2 L_{fp}} \right) \left( \frac{h - d_b}{h} \right)$ Note that $t_{wc}$ includes both the thickness of the column web and the doubler plate. As a secondary yield mechanism it is preferable that $M_{\text{yield-beam}} \approx M_{\text{yield-flange-plate}}$	

**Table 3-21 Failure Modes of Welded-Flange-Plate Connection**

Failure Mode	Equation to Define Failure Mode Moment Resistance at the Face of the Column	Related Issues
Fracture of Beam Flange Weld	Notch tough electrodes are required for the coverplate welds for existing construction and for both the flange welds and coverplate welds for new construction.	
Fracture of Fillet Weld	The fillet weld should be designed for a flange force, $F$ $F = 1.1 \left( \frac{Z_b}{d_b} \right) \left( \frac{F_{yb} + F_{tb}}{2} \right) \left( \frac{L - d_c}{L - d_c - 2 L_{fp}} \right)$	
Web Connection	CJP weld between the beam web and column required. Bolted connections may well work, but no tests completed during this research had bolted webs and the bolted connection has not been verified.	
Plastic Bending of Beam	$M_{fail-beam} = Z \frac{F_{yb} + F_{tb}}{2} \left( \frac{L - d_c}{L - d_c - 2 L_{fp}} \right)$	Reasonably accurate estimate of full bending capacity.
Flange Buckling	for flange - $\frac{b_f}{2 t_f} \leq \frac{52}{\sqrt{F_y}}$	
Web Buckling	for web - $\frac{d_b}{t_w} \leq \frac{450}{\sqrt{F_y}}$	See discussion in Chapter 4.
Lateral Torsional Buckling	$L_b < \frac{2500 r_y}{F_y}$	$L_b$ is the unsupported length and equation is from existing AISC LRFD Seismic Provisions.
Continuity Plates	Continuity Plates required if $t_{fc} \geq 0.4 \sqrt{\frac{P_{bf}}{F_{yc}}}$ where $P_{bf} = 1.8 t_{fb} b_{fb} F_{yb} \left( \frac{L - d_c}{L - d_c - 2 L_{cp}} \right)$	Significant strain hardening occurs with this connection.
Weak Column Bending	$1.1 < \frac{\sum Z_c (F_{yc} - \frac{P_{uc}}{A_g})}{\sum Z_b \frac{F_{yb} + F_{tb}}{2} \left( \frac{L - d_c}{L - d_c - 2 L_{fp}} \right)}$	Significant strain hardening occurs, and is reflected in SCWB limit.

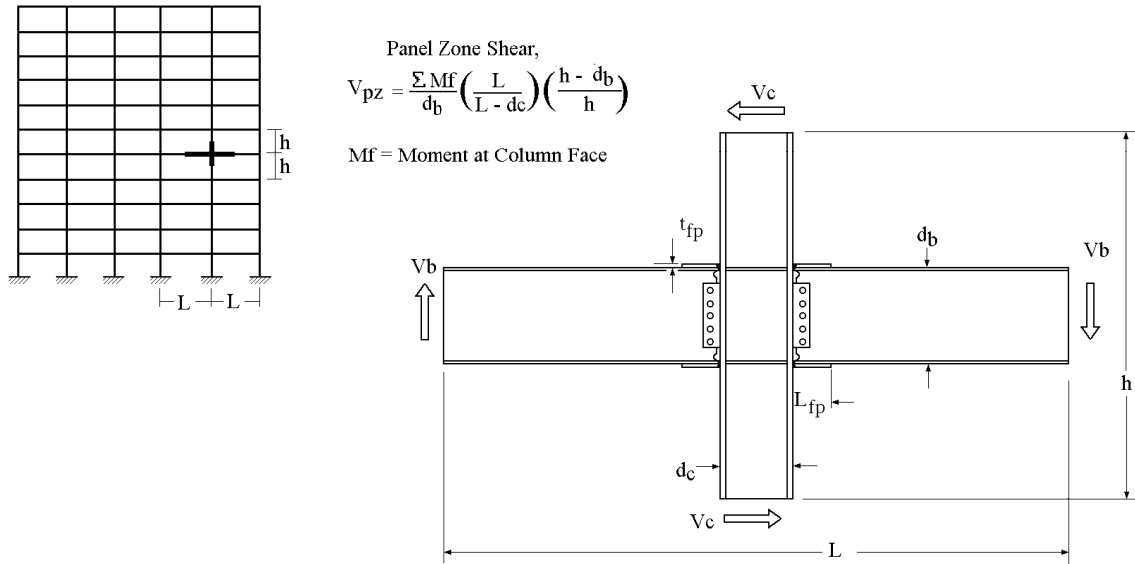


**Figure 3-30** Geometry for Panel Zone Yielding of Welded-Flange-Plate Connection

## 4. OTHER ISSUES FOR POST-NORTHRIDGE WELDED FLANGE CONNECTIONS

### 4.1 General Introduction

Pre-Northridge connection behavior and several general issues, which relate to a wide range of connection types, were discussed in Chapter 2. General issues were discussed because there was a large amount of pre-Northridge connection test data and that data aided in understanding the questions. At the same time, discussion in Chapter 2 helped to clarify the causes and contributing factors of the pre-Northridge connection damage. Chapter 3 reviewed a number of post-Northridge welded flange connections. It was shown that these connections can provide much greater ductility if certain conditions are met, and these conditions were discussed for each connection type. Chapter 4 will examine a number of general issues, related to all connection types, which are based upon post-Northridge connection test results. They were deferred to this chapter, because the discussion here combines test results from more than one connection type. This chapter will also introduce connection tests from other countries, because these tests aid in understanding some issues that were not fully evaluated in this research program.

The topics discussed in this chapter are particularly relevant to welded flange post-Northridge connections as described in Chapter 3, but many issues relate to steel moment frame connections in general and the bolted and composite connections discussed in later chapters. This chapter considers issues that may affect the ductility of connections, and evaluates some issues that are common today but were uncommon when pre-Northridge connections were developed. Post-Northridge connection test results are beneficial for both of these general goals due to their larger inelastic deformations and their more timely nature.

This chapter will examine in detail:

- Continuity plate requirements. This issue was discussed in Chapter 2, but the post-Northridge welded flange connection tests provide more insight into the question, because a portion of this testing and analysis program addressed continuity plate requirements.
- Panel zone yielding. This issue also was discussed in Chapter 2. However, the post-Northridge welded flange connection tests also provide more insight into this question, since large inelastic deformations and strain hardening are noted in these more ductile connections.
- Strong-Column-Weak-Beam (SCWB) requirements. SCWB behavior is required for seismic design because of the increased local demands caused by weak-column-strong-beam (WCSB) behavior. As noted earlier, this report does not consider seismic demand, but the large strain hardening noted with many of the more ductile moment frame connections has important consequences for SCWB design requirements. These issues are capacity issues and are discussed here.
- Weak-axis column bending. This issue was quite relevant to the pre-Northridge connection, but it was not discussed at that time because of the limited test data. Additional tests on this issue were completed during this research.

- Lateral torsional and local buckling. These issues also were discussed in Chapter 2, but the post-Northridge welded flange connection tests provide additional insight into this question. In addition, analytical studies performed as part of the SAC Phase 2 project help to define appropriate recommendations.
- Deep columns. Since deep columns were not commonly used when the pre-Northridge connection was developed, there was no pre-Northridge information on this question.
- Box columns. Since box columns were not commonly used when the pre-Northridge connection was developed, there also was no pre-Northridge information on this concern.
- Effect of composite slabs. Composite slabs are not usually considered in seismic design, but they are commonly used for beams supporting gravity loads. Further, inadvertent composite action develops because shear connectors required to transfer forces from diaphragms to lateral load frames develop it. Numerous questions have been asked as to how this composite action affects connection performance, and no experimental data on these issues was available prior to the Northridge earthquake.
- Thermal effects. It is well known that low temperatures change the performance and ductility of materials and structural systems. The Northridge earthquake occurred in mid-winter in the early morning. Some engineers have questioned whether low temperatures contributed to the Northridge steel frame damage, even though Los Angeles is not normally regarded as a cold climate. This section will help clarify whether thermal effects affected past damage or are likely to contribute to future earthquake damage in colder regions of the United States.
- Dynamic effects. Many Northridge acceleration records cause relatively high strain rates in buildings. High strain rates are also known to affect the ductility and performance of materials and structural systems. This section will review past research to show the expected effect of this dynamic load rate on connection performance.

These issues are discussed in the sections that follow. The discussion often focuses on individual connection types, but the observations made on these issues are applicable to a wide range of steel frame connections.

## 4.2 Continuity Plates

Continuity plates were discussed in Chapter 2, Section 2.2.8. It was noted that continuity plates improved the connection performance, since specimens which had substantial continuity plates had a higher probability of providing ductile connection performance than those that did not. In addition, computer analysis showed the benefits of continuity plates for some connections. However, Chapter 2 also showed that continuity plates were not always essential for good seismic performance, since some tests provided good performance without them. There was clearly a lot of scatter in the data, but in Chapter 2, it was recommended that Equations 2-8 and 2-9 be used to determine continuity plate requirements. These equations were the AISC LRFD Seismic requirements for continuity plates prior to the Northridge earthquake. It must be very clear that these equations are not precise indicators of the need for continuity plates or of connection performance. There is room for considerable improvement in the continuity plate

design requirements, but the past test data showed that Equations 2-8 and 2-9 were better than requiring continuity plates for all applications or using no continuity plates at all.

A limited portion of this research program was directed toward further examination of this issue. Specimens LU-C1, LU-C2, LU-C3, and LU-C4 of the Lehigh research study (summarized in Table 3-4) were designed to consider continuity plate requirements for post-Northridge welded-flange-welded-web connections, which develop larger connection moments due to strain hardening and large connection ductility. LU-C1 and LU-C2 were connections without continuity plates and with substantial continuity plates, respectively, and with thick column flanges which would not require continuity plates by Equations 2-8 and 2-9. The column was a W14x398 with a flange thickness of 2.845". The computed required thickness based upon Equations 2-8 and 2-9 was between 1.80" and 1.85" depending whether nominal yield stress or the yield stress reported in the mill certificates was employed. Thus, it is clear that continuity plates would not be required for either of these connections. Figures 4-1 and 4-2 show the moment-rotation behavior obtained during these two tests. It can be seen that LU-C2 (Figure 4-2) provided improved performance over LU-C1, but the performance of LU-C1 is clearly adequate for nearly all seismic applications. Specimen LU-C2 had large plastic rotations before initial beam flange fracture, and a nearly identical rate of deterioration in resistance as noted for LU-C1. While LU-C2 provided better performance, the difference cannot entirely be attributed to the continuity plates, since a modification to the web welds also was made for this specimen. LU-C2 had run off tabs added to the web welds to permit a complete joint penetration weld over the full depth of the beam web. Specimens LU-C1 and LU-T1 were welded only over the depth of the shear tab. Thus, the improvement in the performance of LU-C2 also further strengthens past observations on the importance of the web attachment. In view of this performance, it is clear that connections can provide adequate ductility without continuity plates.

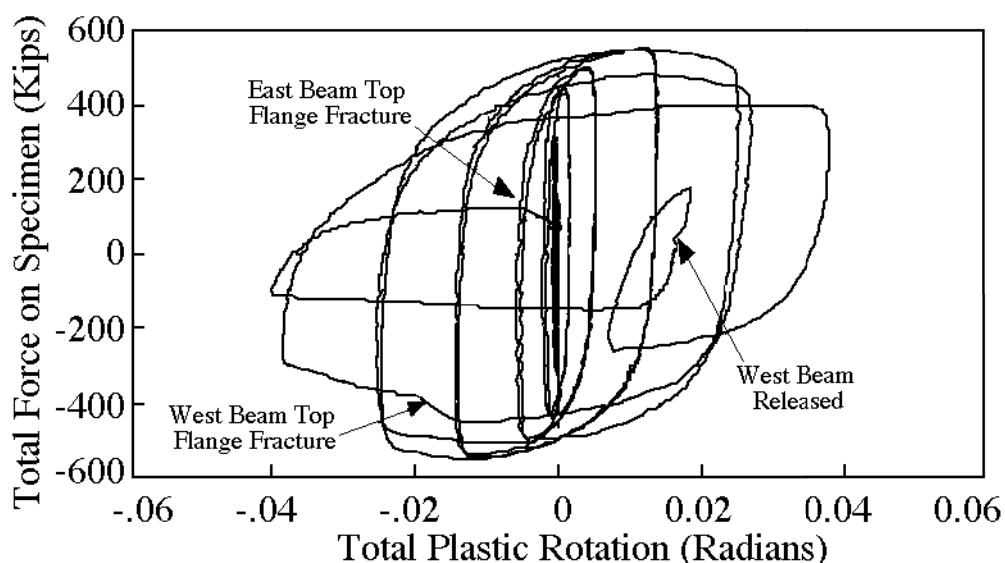


**Figure 4-1** Moment-Rotation Behavior of Specimen With Thick Column Flange and No Continuity Plate (LU-C1)

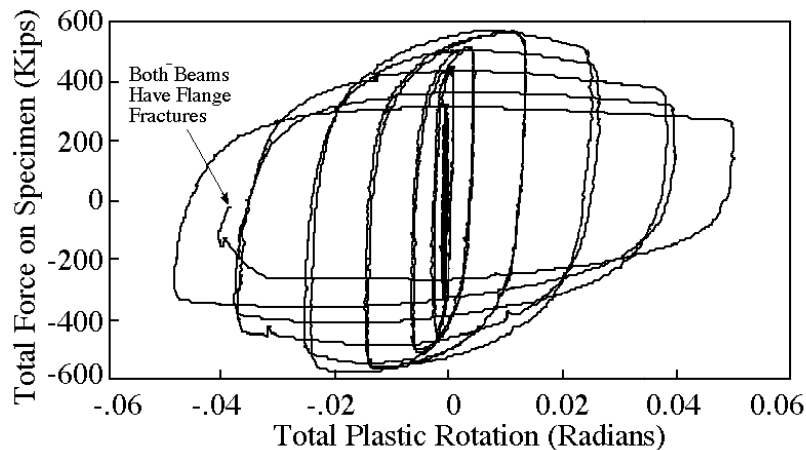


**Figure 4-2** Moment-Rotation Behavior of Specimen With Thick Column Flange but With Continuity Plate (LU-C2)

Specimens LU-C3 and LU-C4 also were without continuity plates and with substantial continuity plates, respectively, but the specimens had thinner column flanges, which would require a continuity plate by Equations 2-8 and 2-9. The column for these two specimens was a W27x258, and the column flange thickness was 1.77". This thickness is somewhat less than that required by Equations 2-8 and 2-9, and so continuity plates would be required for both of these specimens. Figures 4-3 and 4-4 provide the moment-rotation curves for these two specimens. It can be seen that the difference between 4-3 and 4-4 is greater than that noted between 4-1 and 4-2. Specimen LU-C3 (Figure 4-3) had no continuity plate. It fractured at a significantly smaller rotation, and it has slightly greater deterioration in resistance at large rotations. Nevertheless, both specimens provide adequate plastic rotation for most seismic demands. As a result, the continuity plate clearly made a greater difference with these more slender column flanges. However, both LU-C3 and LU-C4 provided satisfactory seismic performance.

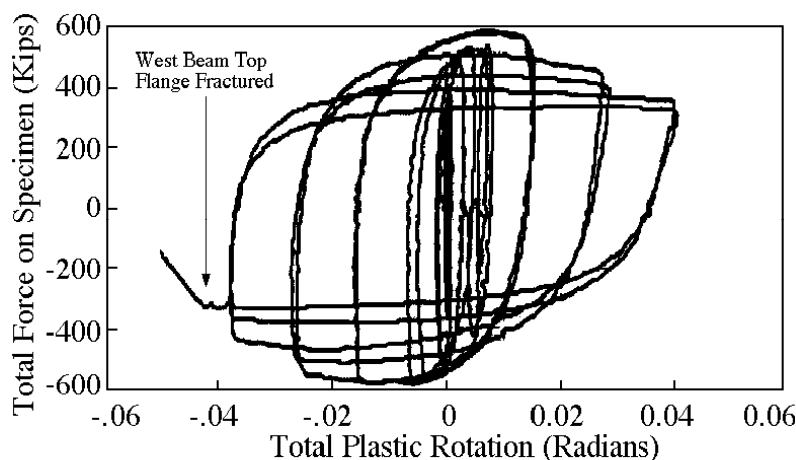


**Figure 4-3** Moment-Rotation Behavior of Specimen With Deep Column With Thin Column Flanges Without a Continuity Plate (LU-C3)

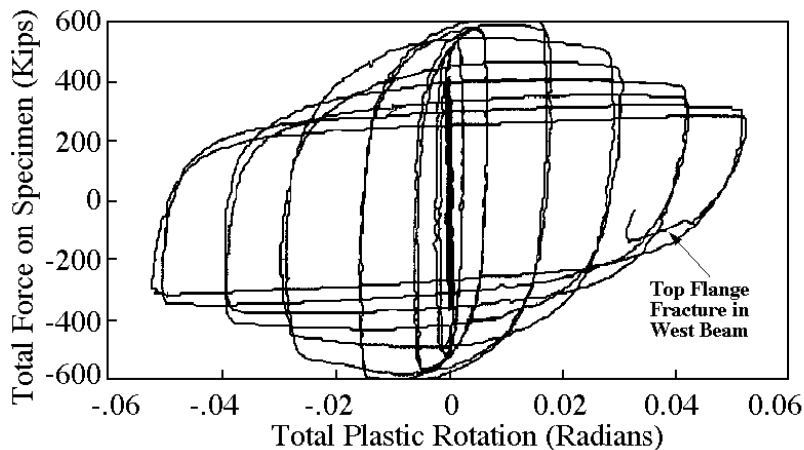


**Figure 4-4 Moment-Rotation Behavior of Specimen With Deep Column With Thin Column Flanges But With a Continuity Plate (LU-C4)**

The results of the four tests clearly show that continuity plates improve inelastic seismic performance of the connections, but the results also show that adequate performance can be achieved without continuity plates if the column flanges are sufficiently heavy. Based upon these four tests, another equation for defining continuity plate requirements has been proposed (Ricles et al., 2000). This equation proposes that no continuity plates be required if the column flange thickness,  $t_{fc}$ , satisfies

$$t_{fc} \geq \frac{b_{fb}}{5.2}, \quad (4-1a)$$

and a continuity plate with a minimum thickness of one half of  $t_{bf}$  is required if

$$\frac{b_{fb}}{5.2} \geq t_{fc} \geq \frac{b_{fb}}{7}. \quad (4-1b)$$

For column flange thickness less than  $\frac{b_{fb}}{7}$ , continuity plates with thickness equal to or greater than  $t_{bf}$  are recommended. This equation is simpler than Equations 2-8 and 2-9, and it would require continuity plates for Specimens LU-C3 and LU-C4 but not LU-C1 and LU-C2. Further, Equation 4-1 results a step function with abrupt changes in continuity plate requirements. Equations 2-8 and 2-9 have a long history of use despite the limitations of these equations. It is not rational to change a long-standing practice based upon only four tests. Particularly when the tests consider such a limited range of behavior. The four tests suggest that Equations 2-8 and 2-9 combine to provide a conservative measure of continuity plate requirements. Thus, when these observations are combined with those of Chapter 2, it is appropriate to return to these limits until more definitive design limits can be developed. Further study of the continuity plate issue is clearly needed, and work on this topic is in progress (Dexter, et al., 1999) with funding from AISC.

### 4.3 Shear Yielding of Panel Zone

Chapter 2 discussed the distribution of inelastic deformations between shear yield of the panel zone and flexural yielding of the beam. There was great scatter in the observed behavior. However, experimental results showed that connections with relatively weak panel zones had a lower probability of achieving the large plastic rotations required during large earthquakes. At the same time, these weaker panel zones frequently did not develop the panel zone shear strength predicted by the present AISC design equation (Equation 2-4 of this report). Chapter 2 also showed that very strong panel zones were equally detrimental to the connection performance, since connections with balanced yield capacity in shear and flexure had the largest proportion of connections achieving large rotational capacity. This led to the recommendation that a balancing of the beam flexural yield mechanism with the theoretical panel zone yield equation (Equation 2-1 of this report) would provide the greatest potential for connection ductility and also encourage panel zone yielding. For a connection where the flexural yielding develops at the face of the column, this balance condition means that

$$V_{pz} = \frac{\Sigma M_{\text{yield-beam}}}{d_b} \left( \frac{L}{L-d_c} \right) \left( \frac{h - d_b}{h} \right) \leq (0.9) V_y = (0.9) 0.55 F_{yc} d_c t_{wc} \quad (4-2)$$

During this research, six specimens (Lee, et al., 2000) (4.1, 4.2, 5.1, 5.2, 6.1 and 6.2) of Table 2-1 were designed to evaluate this yield balance effect. Specimens 4.1 and 4.2 were designed with very weak panel zones, and specimens 6.1 and 6.2 were designed to have strong panel zones with no shear yielding. Specimens 5.1 and 5.2 were designed for intermediate behavior. Table 2-1 shows that only one of the six specimens achieved a rotation larger than 0.01 radians, and so it was impossible to distinguish any useful trends from the test results.

However, further understanding of the issue was obtained from other ductile test specimens. The free-flange connection tests and the welded-flange-welded-web connection tests are particularly instructive because they had relatively large plastic rotations. The panel zone effects of these specimens are tabulated in Table 4-1. Note that multiple connections with identical characteristics are entered as single entries in this table. The relative strength of the panel zone is evaluated by the  $\frac{V_{pz}}{V_y}$  ratio, where  $V_{pz}$  is defined by equilibrium as illustrated for the welded-flange-bolted-web connection in Figure 2-11 and  $V_y$  is defined by Equation 2-1. This ratio is equal to 1.0 when the initiation of flexural yield and panel zone shear yield are expected to occur at the same beam moment, and the ratio equals 0.9 when the balance condition of Equation 4-2 is precisely met. The ratio is less than 0.9 when the panel zone is stronger than required by the balance condition, and more than 0.9 when the panel zone is weaker than the recommended balance condition. It can be seen that virtually all specimens in Table 4-1 had strong panel zones, and despite the strong panel zones, very large plastic rotations in the panel zone were commonly noted. All specimens with  $\frac{V_{pz}}{V_y}$  ratios greater than approximately 0.6 or 0.7 had some panel zone yielding. Specimens with  $\frac{V_{pz}}{V_y}$  ratios greater than 0.8 had large plastic deformations in the panel zone. This occurs because ductile connections develop large strain hardening which

causes increased panel zone shear forces and increased distribution of inelastic rotation into the panel zone.

In addition, Table 4-1 shows that specimens which had ratios near or larger than 0.9 demonstrated increased probability of crack development in the web connection. As noted earlier, analysis (Chi et al., 1997; El Tawil and Kunnath, 1998) has shown that large panel zone yield deformation increases the potential for connection fracture and reduces the potential for large plastic rotations. Comparisons of experimental data in Chapter 2 revealed that, on average, specimens with very weak panel zones do not achieve as large plastic rotations as do specimens with more balanced design. Chapter 2 also showed that many weak panel zone specimens do not achieve the panel zone shear resistance predicted by the present AISC panel zone design equations (Equation 2-4 of this report). The discussion in this section reinforces the recommendation for the balanced condition proposed in Chapter 2 and restated in Equation 4-2. Further, the data of Table 4-1 provides evidence as to why the balance point is selected as  $\frac{V_{pz}}{V_y} = 0.9$  rather than 1.0, because specimens with ratios larger than 0.9 had beam or column flange fracture rather than the more ductile deterioration in resistance noted with other specimens. This recommendation of balanced yield potential is made for all connections in Chapters 3 and 5. However, flexural yielding may occur at different locations for different connection types, and this variation in location is considered in the individual connection recommendations.

Table 4-1 also provides further evidence as to an appropriate lower bound on the balance condition noted in Equation 4-2. The table shows that specimens with  $\frac{V_{pz}}{V_y}$  ratios less than approximately 0.6 had virtually no panel zone yielding. The goal is to economically achieve a balance of panel zone yielding and flexural yielding, since this provides the greatest opportunity for developing large plastic rotations despite the uncertainties and variations in the yield stress of the beam and column steel. Further, all connections with  $\frac{V_{pz}}{V_y}$  ratios between 0.6 and 0.9 achieved large inelastic rotations without any early fractures. As a result, the recommendation for the design balance condition for the welded-flange-welded-web and the free-flange connection is

$$\frac{\Sigma M_{\text{yield-beam}}}{d_b} \left( \frac{L}{L-d_c} \right) \left( \frac{h-d_b}{h} \right) \leq (0.9) 0.55 F_{yc} d_c t_{wc} \quad (4-3)$$

but preferably

$$\frac{\Sigma M_{\text{yield-beam}}}{d_b} \left( \frac{L}{L-d_c} \right) \left( \frac{h-d_b}{h} \right) \geq (0.6) 0.55 F_{yc} d_c t_{wc} . \quad (4-4)$$

Comparable equations are developed for all other connection types.

**Table 4-1 Summary of Panel Zone Effects on Ductile Post-Northridge Connections**

Specimen Identification	Connection Type	$\frac{V_{pz}}{V_y}$ where $V_{pz}$ is panel zone shear due to yield moment	Maximum Plastic Rotation Achieved	Maximum Plastic Rotation in Panel Zone	Outcome of test
LU-C1 and LU-C2 (Ricles et al., 2000)	Welded-flange-welded-web connections	0.73	Min 0.025 Max 0.05 AVG 0.041	0.007	Ductile behavior with flange fracture
U. of M. Sp 8.2 (Choi, et al., 2000)	Free-flange connection	0.68	0.04	0.0	No fracture. Test stopped by equipment limitations
U. of M. Sp 9.1	Free-flange connection	1.10	0.035	0.022	Tear in top flange
U. of M. Sp 9.2 (Choi, et al., 2000)	Free-flange connection	0.48	0.03	0.0	Test stopped due to lateral torsional buckling
U. of M. Sp 10.1 (Choi, et al., 2000)	Free-flange connection	0.71 based on $F_{yb} = 50$ ksi	0.025	0.017	Test stopped. Small shear tab crack.
U. of M. Sp 10.2 (Choi, et al., 2000)	Free-flange connection	0.52	0.027	0.007	Test stopped Small flange crack at toe of access hole
UCSD-FF (Gilton, et al., 1999)	Free-flange connection	0.87 based on $F_{yb} = F_{yc} = 50$ ksi 1.22 based on $F_{yb} = 50$ ksi & $F_{yc} = 36$ ksi	0.018 on return excursion to 0.025	0.018	Fracture into column flange and panel zone
UTA-FF (Engelhardt, 2000)	Free-flange connection with composite slab	1.30 Does not consider the increased effective beam depth due to composite action. If increased depth of composite beam considered then 1.11	0.034	0.018	Beam flange fracture at large inelastic deformation

Notes.

- $V_{pz}$  is the computed panel zone shear force at the development of  $M_y$  at the critical yield location of the connection.
- Mill certification yield stress values used unless otherwise noted.

#### 4.4 Strong-Column-Weak-Beam Connection Requirements

Steel moment frames are designed by a strong-column-weak-beam (SCWB) design concept. This concept encourages plastic deformation of the beam and discourages plastic deformation of the column. It is well known (Schneider et al., 1993) that weak-column-strong-beam (WCSB) frames concentrate the inelastic deformation into individual stories of a building, and as a consequence seismic demands are much larger for these local parts of the structure. Since the major consequence of WCSB behavior is the increased demand, and demand is the focus of other portions (Krawinkler, 2000; Foutch, 2000) of the research program, WCSB behavior is outside the scope of this report.

However, SCWB behavior is directly related to the capacity of members and connections, and connection capacity is clearly within the scope of this State of the Art Report. The AISC LRFD Seismic Design provisions control WCSB behavior by balancing the plastic capacity of the beams with the plastic capacity of the columns in an equation so that

$$1.0 < \frac{\sum Z_c \left( F_{yc} - \frac{P_{uc}}{A_g} \right)}{\sum (1.1 R_y Z_b F_{yb} + M_v)} \quad (4-5)$$

where  $M_v$  is the additional moment due to shear amplification from the location of the plastic hinge. In Equation 4-5, the yield stress is a specified minimum yield stress, while expected yield stress is used in other equations of this report. It is nonetheless recognized that the AISC equation does not prevent column yielding (Nakashima and Sawaizumi, 1999). Yielding occurs in the columns due to strain hardening during inelastic deformation and because the moments in beams and columns are not balanced as ideally assumed in design calculations. Inflection points may not occur at mid span of beams and mid height of columns as hypothesized by Equation 4-4. Individual members may even be in single curvature for short periods of time. The AISC equation (Equation 4-5) is relatively simple, but it does not prevent column yielding. Instead, it limits yielding so that excessive inelastic WCSB deformation does not occur. Research has shown (Nakashima and Sawaizumi, 1999) that if the yielding in the column is limited to less than 120% of  $M_p$ , the adverse effects of concentration of plastic deformation are controlled.

Equation 4-5 is based upon the hypothesis that beams and connections do not develop moments much larger than  $M_p$ . However, the ductile connections described in this report often develop moments which are 40 to 50% larger than  $M_p$ . This can be readily seen for the welded-flange-welded web and free-flange connections in Tables 3-4 and 3-6, respectively. Comparable strain hardening can also be seen for all other ductile connections in Chapters 3 and 5. Further, the geometric corrections, which are needed to account for the plastic hinge location, vary widely with individual connections, since the moment transferred to the column depends upon the relative location as well as the magnitude of the moment at the plastic hinge. These connection moments due to strain hardening are much larger than those needed to assure that WCSB effects will not adversely affect the ductility demands of the structural system, since 20% increases are viewed (Nakashima and Sawaizumi, 1999) as the maximum that can be tolerated without experiencing excessive increases in local demand. As a result, all connections in this report are evaluated both from the perspective of the maximum strain hardening that can be

expected and the location of the plastic hinge. Limits on the beam to column moment ratio considering the maximum moment or strain hardening expected for that connection and the moment location are defined for each connection type. These limits are included in failure mode recommendations provided in tables for each connection type. The resulting equations have the form of

$$1.1 < \frac{\sum Z_c \left( F_{yc} - \frac{P_{uc}}{A_g} \right)}{\sum Z_b F_{\text{StrainHardeningStress}} C_{\text{GeometricCorrection}}} \quad (4-6)$$

The geometric correction term,  $C_{\text{GeometricCorrection}}$ , considers the location of the plastic hinge relative to the column. This is an equation based upon equilibrium of a connection subassembly. Figure 3-22 illustrates the geometry and equilibrium conditions for a coverplate connection. The strain hardening stress,  $F_{\text{StrainHardeningStress}}$ , is really based upon a ratio of the maximum moment to the plastic moment and considers the maximum bending stress that can be consistently achieved with the connection. Very ductile connections commonly achieve moments that are 40 to 50% larger than  $M_p$ , and the stress limit  $\frac{F_{yb} + F_{tb}}{2}$  is commonly used for those equations, since it more closely represents the maximum moment, and is still 15 to 20% smaller than the maximum moment achieved with these very ductile connections. This concept is used for all moment resisting connections discussed in Chapters 2, 3, and 5, and is based upon the standard AISC provisions as noted above. The coverplate connection is one connection with significant strain hardening and a sizable geometric effect, and is used here as an illustration of the methods employed in this report. The proposed equation for this connection appears as

$$1.1 < \frac{\sum Z_c \left( F_{yc} - \frac{P_{uc}}{A_g} \right)}{\sum Z_b \frac{F_{yb} + F_{tb}}{2} \left( \frac{L - d_c}{L - d_c - 2 L_{cp}} \right)} \quad (4-7)$$

#### 4.5 Weak-Axis-Column-Bending Connections

Beam-to-column connections that induce weak-axis bending of the column may be needed at some corner columns and in highly redundant structural systems where moment resisting connections are used for all or nearly all beam-to-column connections. Several pre-Northridge connection tests considered these connections, and Table 4-2 summarizes some points which are relevant to those earlier tests. Additional earlier tests were completed but are not included in the table. Early tests (ASCE Manual 41, 1971) were performed at Lehigh with the beam connected directly to the column web without benefit of a column flange and web stiffener or continuity plate. Adequate seismic performance of these direct web welded connections requires transfer of large stresses through the column web, and this is unlikely to be achieved for practical seismic design. These direct welded web connections are consequently not included in the table, and welded column web and flange stiffeners are required for weak-axis-column-bending connections with some common configurations shown in Figure 4-5. Since the beam flange is directly welded to this stiffener in all cases, the stiffener must be aligned with and thicker than the beam flange to permit complete joint penetration groove welding.

**Table 4-2 Summary of Weak-Axis-Column-Bending Connections**

<b>Specimen Identification</b>	<b>Beam (Column) Sizes</b>	<b>Information on Connection</b>	<b>Maximum Plastic Rotation Achieved</b>	<b>Outcome of test</b>
W1-C1 (Popov and Pinkney, 1969)	8WF20 (8WF48)	Flush stiffener plate, right angle juncture, bolted and welded web	0.037	Increasing amplitude cycles - 5 cycles each - Fracture at weld at initial excursion
W1-C4 (Popov and Pinkney, 1969)	8WF20 (8WF48)	Flush stiffener plate, right angle juncture, bolted and welded web	0.027	Fracture at weld at 0.013 on return cycle of first complete excursion
W1-C7 (Popov and Pinkney, 1969)	8WF20 (8WF48)	Flush stiffener plate, right angle juncture, bolted and welded web	0.018	Increasing amplitude cycles - 15 cycles each amplitude - Weld fracture during second cycle at max rotation
W1-C9 (Popov and Pinkney, 1969)	8WF20 (8WF48)	Flush stiffener plate, right angle juncture, bolted and welded web	0.017	Increasing amplitude cycles after 2 initial one sided cycles - 15 cycles each amplitude - fracture near flange weld
W2-C7 (Popov and Pinkney, 1969)	8WF20 (8WF48)	Tapered stiffener plate, right angle juncture, bolted and welded web	0.025	Increasing amplitude cycles - 15 cycles each - flange fracture on 3rd complete cycle at max rotation
W2-C10 (Popov and Pinkney, 1969)	8WF20 (8WF48)	Radiused stiffener plate, right angle juncture, bolted and welded web	0.018	Increasing amplitude cycles after 5 initial large two sided cycles- 15 cycles each
Specimen 2 (Tsai and Popov, 1988)	W18x40 (W12x133)	Flush stiffener plate, right angle juncture, bolted web	0.018	ATC-24 type loading - beam flange fracture near weld access hole
Specimen 4 (Tsai and Popov, 1988)	W18x40 (W12x133)	Flush stiffener plate, right angle juncture, bolted web with supplemental welding	0.008	ATC-24 type loading - bottom flange fracture
Specimen 2 (Tsai and Popov, 1988)	W18x40 (W12x133)	Extended stiffener plate, right angle juncture, bolted web	0.007	ATC-24 type loading - top flange weld fracture
CW-1 (Gilton, et al., 2000B)	W36x150 (W14x398)	RBS connection with and extended stiffener detail with the stiffener width approximating beam flange width	0.042 at less than approx 40% 0.02 at 80%	FEMA/SAC Protocol - Test stopped because of deterioration of loading
CW-2 (Gilton, et al., 2000B)	W24x62 (W14x176)	RBS connection with tapered stiffener detail	0.045 at approx. 55% 0.02 at 80%	FEMA/SAC Protocol - Test stopped because of deterioration of loading

Note: See Popov and Pinkney (1969); Tsai and Popov (1988); Gilton, et al. (2000B).

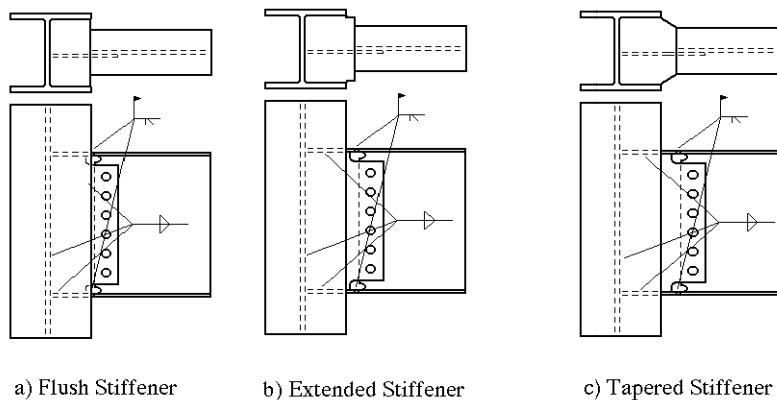


**Figure 4-5 Schematic of Various Weak-Axis-Column-Bending Connections**

Nine of the 11 tests included in Table 4-2 are pre-Northridge connections, and most of those connections are on small size specimens. Two weak-axis-column-bending connections (UCSD CW-1 and CW-2 of Table 3-16) were completed during this research program. Only three of the pre-Northridge connections are of modest size. Specimen size may be less of a concern with these connections, because they will be used only when highly redundant frames with moment-resisting connections in both directions are employed. Smaller members inherently occur under these conditions. Most of the past test specimens used the flush stiffener detail as schematically illustrated in Figure 4-5a, and others employed an extended stiffener as illustrated in Figure 4-5b. Only two of the specimens employed a tapered stiffener as illustrated in Figure 4-5c. Table 4-2 shows that the rotational capacity of the pre-Northridge connections was not particularly good, and the extensive use of the flush stiffener detail and the extended stiffener detail combined with low weld toughness contribute to this behavior. The stress distribution varies across the width of the flange of all welded flange connections, and this distribution is quite different for the strong-axis-column-bending connection than for the weak-axis-column-bending connection as illustrated in Figure 4-6. With the normal strong-axis-column-bending, the largest local flange stresses occur at approximately mid-width of the column flange, while the weak-axis-column-bending connection will have larger stresses near the outside edges. This occurs because the strong-axis-column connection has a concentration of stiffness at the juncture of the web and flange of the column, while the weak-axis-column-bending connection has greater stiffness at the outside edge because of the bending stiffness of the column flanges. The actual magnitudes of the local stresses vary widely depending upon the geometry of the connection and the specimen. This means that fractures and tears of connections with strong axis column bending normally initiate near the center of the beam flange, while fractures and tears of connections with weak axis column bending usually start near the flange tips. These differences can be observed in the description of the actual behavior noted in individual tests. Since connections with weak-axis-column-bending commonly initiate fractures from the flange tips, sharp discontinuities such as shown in Figures 4-5a and 4-5b for the flush stiffener and extended stiffener connection are not wise, because these details introduce flaws and discontinuities at the location of crack initiation. This is one reason that weak-column-connections commonly provide less apparent plastic rotation than strong-axis-column-bending connections. Tapered stiffeners such as depicted in Figure 4-5c reduce these flaws and irregularities and improve connection performance.

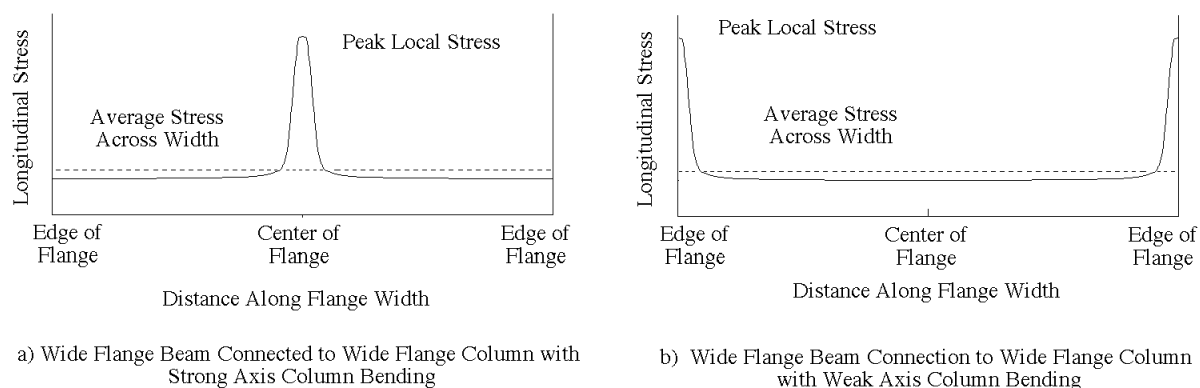


**Figure 4-6 Local Longitudinal Stress Distribution in Beam Flanges**

Comparison of Table 4-2 with other test data shows that connections with weak-axis-column-bending usually have inferior seismic performance and reduced rotational capacity as compared to similar strong-axis-column-bending connections. However, this does not suggest that weak-axis-column-bending connections are incapable of providing adequate seismic performance. Part of this inferiority is due to the discontinuity that was employed in many of these connections as noted earlier. There are three other reasons for this inferior performance. First, it has been shown that balancing the inelastic deformation between flexural yielding of the beams and panel zone yielding provides the greatest potential for large plastic rotations. Panel zone yielding is not possible with these weak-axis-column-bending connections, and so this important source of plastic deformation is not available for these connections. Second, Chapters 2 and 3 showed that stiffening and strengthening the web connection increases the rotational capacity of welded flange connections. Unfortunately, the ability to increase the strength and stiffness of the web connection is reduced with the weak axis column bending connection, since the column flanges carry nearly all of the shear and bending. The force path for transferring shear forces and bending moments from the beam web to the column flanges is less direct, and so the weak-axis-column-bending connection may be unable to activate this added stiffness and resistance. Third, the out-of-plane restraint provided by the column to the beam and connection is smaller with weak axis column bending connections than with strong axis bending connections. Theoretically, the out-of-plane restraint is provided by the major-axis bending of the column, but the actual connection has a large eccentricity, since the connection is made beyond the tip of the column flanges. Twisting or out-of-plane movement of the beam at the connection interface depends on the plate bending stiffness of the column flanges for weak axis connections. This occurs because the column is not able to utilize its large warping torsion stiffness to prevent out-of-plane bending of the beam. In addition, the beam flange is welded to a stiff column flange for strong-axis-column-bending connections, but the beam flange is welded to a more flexible stiffener for weak-axis connections. This introduces a stiff boundary restraint for flange buckling of strong-axis connections and a more flexible end restraint with weak axis connections. Local flange and web buckling of compact sections requires development of yield stress over a sufficient length and region to permit development of the buckled shape. The stiffer end condition for strong axis connections requires a longer yield length for these buckled shapes. The consequence is that weak-axis-column-bending connections usually buckle at smaller plastic rotations than do strong-axis-bending connections. Their resistance deteriorates more quickly at

smaller plastic deformations. This more rapid deterioration can be seen by comparing the moment-rotation capacity of UCSD WC-1 with UTA DBBW in Table 3-16. The weak axis connection developed comparable plastic rotation and maximum resistance to the strong axis connection, but more rapid deterioration of the moment capacity can easily be noted.

This discussion reveals that weak-axis-column-bending connections are capable of providing adequate ductility and rotational capacity, but there will typically be greater deterioration in resistance than noted for strong-axis connections. Weak-axis-column-bending connections are unable to mobilize panel zone yielding and increased strength and stiffness of the web connection as a means of increasing inelastic rotation capacity. As a result, greater care must be taken with the detailing and transitions of flange welds to assure that the maximum possible ductility is developed through flexural yielding.

#### 4.6 Lateral Torsional and Local Buckling

The AISC LRFD Seismic Design Provisions (AISC, 1997) requires that lateral support be applied at all plastic hinge locations, and that support be applied at intervals of  $L_b$  from these locations where

$$L_b \leq \frac{2500 r_y}{F_y} . \quad (4-8)$$

With most historic moment frames, the plastic hinging occurs in the beam at the face of the column, and lateral support at the hinge location is provided by the column and the beam-column connection. However, many post-Northridge connections, including the RBS, coverplate, and the haunch connections, move the plastic hinge to a location away from the face of the column. Application of the AISC LRFD requirements to these post-Northridge connections require lateral support at these hinge locations. It may be difficult to provide this support, because the lateral supports are expensive, and research has shown that attachments to yielding flanges may cause local fracture. Further, many tests have been completed without lateral support at these locations, and so some research was completed to examine these lateral bracing requirements.

One important issue in examining bracing requirements is to note the damage observed in past earthquakes. There was no evidence that lateral torsional buckling caused a reduction in the seismic performance of the structure during the Northridge earthquake. However, because of the brittle fractures noted during this earthquake, there was little evidence of inelastic deformation in steel moment frames, and the lack of lateral torsional buckling has limited value in interpreting design results. On the other hand, significant inelastic deformation and local buckling was noted in many steel frame buildings after the 1995 Kobe earthquake. Despite this inelastic deformation, damage reports (AIJ, 1995) show little evidence of buildings that sustained serious damage due to lateral torsional buckling during the Kobe earthquake. At the same time, it must be recognized that Japanese engineering practice employs much longer unbraced lengths than those employed in the US. The provisions provided by the Building Center of Japan permit

$$L_b \leq 130 r_y \quad (4-9)$$

for SN490 steels (steels with approximately 50 ksi yield stress and 70 ksi tensile strength) when the bracing is uniformly spaced over span length. This bracing length is approximately 150% longer than that permitted by the AISC Seismic Design provisions, and the lack of serious damage due to lateral torsional buckling suggests that the lateral support requirements in US seismic design practice are more conservative than needed for good seismic performance.

Two radius cut RBS specimens (UCSD LS-1 and LS-4 in Table 3-16) were tested to evaluate the bracing requirements. Specimen LS-1 had lateral support provided near the end of the beam. Specimen LS-4 had another added lateral restraint at the reduced section to determine if the increased lateral support improved the seismic performance of the connection. Comparison of the moment-rotation curves for Specimens LS-1 and LS-4 showed that LS-4 had less rapid deterioration of the moment capacity with increased plastic rotation than specimen LS-1, and the lateral bracing failed at large deformations. The lateral support was intended to be stiff and strong without restricting beam deflections and deformations. However, it is clear that the lateral support for specimen LS-4 was not nearly as effective as intended. The lateral restraint was not stiff enough to restrict the out of plane deformation, but it still improved the seismic performance of the specimen. It is quite clear that this improvement would have been greater had the lateral support been as effective as desired, but it is equally clear that specimens without lateral support provided adequate seismic performance. Thus, these experiments show that increased lateral support reduces the rate of deterioration of the resistance at increased plastic rotations, but at the same time lateral support is not necessarily required at the reduced section to assure adequate performance.

Additional analytical studies (Kwasniewski, et al., 1999; Uang and Fan, 1999) were completed to further address the lateral bracing issue. Nonlinear computer analysis with the ABACUS computer program (Kwasniewski, et al., 1999) was used to evaluate how different parameters affect the inelastic stability of moment frames. The web slenderness, flange slenderness, relative lateral support, and the axial restraint were varied for a normal welded flange connection with W30x99 beams and for several comparable RBS connections. The analysis showed that axial restraint provided a significant reduction in the post buckling deterioration of the predicted inelastic performance of these subassemblages. Concrete slabs in real buildings should provide this axial restraint, and this is viewed as a beneficial effect in reducing the adverse effects of lateral torsional buckling. The analysis suggested that the inelastic behavior was not very sensitive to flange slenderness or the unsupported length, but somewhat greater sensitivity was noted for the web slenderness. Further, the analysis suggested that RBS connections buckle at smaller rotations, but they appear to have less rapid deterioration after buckling occurs than for many other connection types.

The second study (Uang and Fan, 1999) reviewed the results of past RBS experiments, and used regression analysis to estimate trends in behavior. The results of this analysis suggested that web slenderness  $\frac{d_b}{t_{wb}}$  had a greater effect on connection ductility than flange slenderness and unsupported length. It was recommended that

$$\frac{d_b}{t_{wb}} \leq \frac{440}{\sqrt{F_y}} \quad (4-10)$$

is a more rational limit for controlling web buckling, and that this web slenderness limit is more critical to the ductility of the connection than is lateral bracing at the reduced section. This study also showed that the slab provided increased moment capacity and increased rotational capacity for RBS connections in positive bending, but the difference appeared to be less clear for negative bending. It should be noted that the observations on web slenderness are reasonably consistent with some other past research studies (Kemp, 1996), but there are also some basic inconsistencies with the observations reported here and those noted in earlier work.

The results of this work are persuasive but not fully conclusive. It appears that significant increases in the minimum unsupported length requirements are possible without adversely affecting the seismic performance of steel moment frames and their connections. Improvements in the web and flange slenderness requirements for seismic design also appear to be possible. The beneficial effect of the axial restraint provided by the slab on the reduced section and connection also appear to be important. In this report it is recommended that lateral bracing not be required for RBS connections which are connected to the slab outside the region of the reduced section, since the results of the analysis indicate that this restraint reduces the adverse effects of lateral torsional buckling. Beyond this limitation, the current AISC Seismic Design Provision recommendations for lateral support (Equation 4-8) are recommended until research can be completed to better evaluate this complex problem. In addition, the concern that web buckling has a more adverse effect on rotational capacity appears to be reasonably well supported. However, Equation 4-10 is rounded to a more even number because of the limited accuracy of the equation, and it is recommended that the limit

$$\frac{d_b}{t_{wb}} \leq \frac{418}{\sqrt{F_y}} \quad (4-11)$$

be used for all post-Northridge connections because of their greater ductility and ductility demands. Equation 4-11 is more restrictive than the limit defined in Equation 4-10. This more restrictive slenderness limit is recommended because the  $\frac{418}{\sqrt{F_y}}$  limit is already employed as a slenderness limit in the existing AISC LRFD provisions. The rationale behind Equation 4-10 is sound, but the accuracy of the recommendations are not so precise that they justify a unique slenderness limit. Nevertheless, it must be recognized that the reasons for requiring the slenderness limit of Equation 4-11 in seismic design are quite different from those requiring the existing limit in the shear design provisions of the AISC LRFD specification. The limit in Equation 4-11 appears to be significantly different from present design requirements, but the actual consequences are not that great. The slenderness limit of Equation 4-11 will have no effect on most seismic design, because the rolled wide flange beams used for seismic design usually will satisfy this requirement for the steels that are commonly used for seismic design. However, the limit is used because it should provide a significant benefit for the few buildings where built-up sections are employed in seismic design. As a result, Equation 4-11 and Equation 4-8 are included in the recommendations for each connection discussed in Chapters 3 and 5 of

this report. It is also recommended that further research be made to address the minimum unsupported length issue and the maximum slenderness issues, since these appear to be areas where further economy and improved seismic performance are possible.

#### 4.7 Deep Columns

Modern steel moment frames frequently concentrate the seismic resistance into a few frames or a few bays within some plane frames. One consequence of this practice is that columns in those isolated frames are often dominated by bending moment rather than axial load. As a result, it may be attractive to use deeper sections for columns in these lateral-load frames. Limited research has been performed on this issue, and Table 4-3 provides a tabulation of some past tests addressing this issue. It should be noted that this table includes tests performed in this program (Lehigh Specimens LU-C3 and LU-C4 of Table 3-4 and San Diego Specimens DC-1, DC-2 and DC-3 of Table 3-16), tests performed in other countries, and tests performed for confirmation testing.

**Table 4-3 Summary Table of Test Results with Deep Column Sections**

Specimen Identification	Beam (Column) Sizes	Information on Connection	Maximum Plastic Rotation Achieved	Outcome of test
LU-C3 (Ricles et al., 2000)	W36X150 (W27X258 and 5/8" doubler both sides)	Welded-flange-welded-web connection - two sided connection	0.038	Partial flange fracture of west beam
UCSD DC-1 (Gilton, et al., 2000B)	W36x150 (W27x146) w/ 3/8" doubler welded web	RBS connection - one sided specimen	0.044 (at conclusion) .028 (at 80%)	Test stopped due to twisting of column
UCSD DC-2 (Gilton, et al., 2000B)	W36x150 (W27x194) no doubler welded web	RBS connection - one sided specimen	0.03	Test stopped after single cycle 0.044 with large out of plane deformation, twisting of column and loss of resistance
UCSD DC-3 (Gilton, et al., 2000B)	W27x194 (W27x194) w/ 5/8" doubler welded web	RBS connection - one sided specimen	0.028	Brittle fracture at K-line
FUSD1 (Whittaker and Gillani, 1996)	W21x50 (W21x111)	Welded Flange Plate Connection	0.025	Beam flange fracture
FUSD2 (Whittaker and Gillani, 1996)	W24x62 (W21x111)	Welded Flange Plate Connection	0.033	Beam flange fracture

**Table 4-3 Summary Table of Test Results with Deep Column Sections (continued)**

FUSD3 (Whittaker and Gillani, 1996)	W24x76 (W21x101)	Welded Flange Plate Connection	0.036	Beam flange fracture
SESB4 (SAC DATABASE)	W36x135 (W24x229)	Straight Cut RBS	0.018	Fracture
SESB1 (SAC DATABASE)	W33x169 (W24X335)	Straight Cut RBS	0.03	Test Stopped
SESB2 (SAC DATABASE)	W36x135 (W24X229)	Straight Cut RBS	0.021	Unknown
SESB3 (SAC DATABASE)	W27x94 (W24X162)	Straight Cut RBS	0.04	Unknown
AD15 (SAC DATABASE)	W36x135 (W30x173)	Pre-Northridge Repaired Connection	0.02	Test stopped
SFCCC-2 (Noel and Uang, 1996)	W24x94 (W24X279)	Welded flange plate connection – two sided specimen – very short beam	0.030 and 0.030	Cracking of fillet weld
SFCCC-3 (Noel and Uang, 1996)	W18x86 (W24x279)	Welded flange plate connection – two sided specimen – very short beam	0.030 and 0.013	Cracking of fillet weld between beam flange and flange plate
SFCCC-4 (Noel and Uang, 1996)	W24x94 (W24X279)	Welded flange plate connection – two sided specimen – very short beam	0.034 and 0.046	Cracking of fillet weld between beam flange and flange plate
SFCCC-6 (Noel and Uang, 1996)	W18x86 (W24x279)	Top welded flange plate and bottom haunch – two sided specimen – very short beam	0.014 and 0.015	Cracking of fillet weld between beam flange and flange plate
SFCCC-8 (Noel and Uang, 1996)	W18x86 (W24x279)	Top welded flange plate and bottom haunch – two sided specimen – very short beam	0.043 and 0.045	Significant local buckling flange fracture after number of cycles at max deformation

Table 4-3 shows substantial scatter in the test results. In general, most specimens achieved a rotation well in excess of 0.03 radians, and those that did not had extenuating circumstances beyond the deep column section. Comparison of Figures 4-2 to 4-4 is a direct comparison of a connection with a deep column (Figure 4-4) to an essentially identical specimen with a normal W14 column section (Figure 4-2). Both specimens have heavy stiffeners. Examination of the moment-rotation curves of these two specimens reveals that the maximum moment, the maximum plastic rotation, and the rate of deterioration of the two specimens are nearly identical. This comparison indicates that the use of deep columns does not inherently produce poor connection performance.

The specimens of Table 4-3 cover a wide range of connection types. Two of the welded flange plate connections (SFCCC-3 and SFCCC-4) fracture at plastic rotations well below those that would be expected for ductile connections, but it must be noted that the column spacing for these two connections is relatively short (approx. 20 ft). The effective beam length is further reduced by the deep column and the long flange plate. Discussion in Chapter 2 has shown that these reduced beam lengths result in larger plastic strains for a given rotation and reduced plastic rotation capacity for the connection. Further, the flange plates for these two connections are not designed to the balanced conditions recommended in this report for the welded flange plate connection, and it is likely that these other issues contribute to the limited ductility achieved with these two connections. Two of the straight cut RBS specimens had limited ductility, but discussion in Chapter 3 noted that the straight cut RBS specimens had questionable ductility because of the sharp transitions at the ends of the straight cut.

The deep column connections in Table 4-3 with limited ductility can all be partially explained by other factors. Nevertheless, if one-to-one comparisons are made between the behavior achieved with deep column connections as compared to identical connections with normal column sections, the average behavior obtained for deep column connections will be inferior to that achieved with normal column section connections. This is not to say that the deep column sections do not provide adequate seismic performance, but there is clearly less margin for error in achieving good seismic performance in connections with deep column sections.

There are four major reasons for the inferior performance. First, the deep column section is affected differently by continuity plates than are connections with normal column sections. Deeper columns normally have thinner webs and flanges and have greater need for continuity plates. Comparison of the moment-rotation curves of Figures 4-1 with 4-3 shows the importance of this issue. Both of these specimens have no continuity plates, and continuity plates would only be marginally required by the existing design criteria as discussed earlier in this chapter. Greater deterioration and loss of resistance can be noted in the deeper column section because of the absence of a continuity plate. Second, deep columns have different panel zone yielding characteristics than do normal W12 and W14 column sections. The webs are much thinner, and if panel zone yielding occurs, this increases the likelihood of inelastic shear buckling of the web. As noted earlier in this chapter, panel zone yield deformation has both beneficial and detrimental effects. Excess panel zone deformation increases the potential for early connection failure due to the large concentration of local deformation occurring in these connections. However, connections without any panel zone deformation are less likely to achieve adequate plastic rotation, since panel zone yielding contributes significant inelastic rotation. Because of these conflicting requirements, the panel zone yield balancing conditions were proposed in Section 4-3. The five SAC Phase 2 specimens included in Table 4-3 all achieved reasonable ductility because all of these specimens had reasonable balanced yield conditions and developed significant plastic rotation due to both flexural and panel-zone yielding. Third, deep columns provide less resistance to out-of-plane moment and lateral torsional buckling than do normal W14 columns. This occurs because the St Venant torsional stiffness is significantly smaller than the warping torsional stiffness for deeper sections. The flanges of deep sections are relatively narrow, and the weak axis moment of inertia is smaller. Therefore, twisting and out-of-plane deformation at the beam-to-column connection are more likely to occur, and deterioration due to

these effects must be expected with deep column sections. This behavior is similar to that noted for the weak-axis column-bending connection, but the degree of this effect is likely to be smaller than that noted for the weak-axis connection. Further, a concrete slab, which is integral to the beam and the column, should restrain much of this deformation and reduce the deterioration effects due to twisting and out-of-plane movement. On the other hand, the deep column itself requires lateral support for its bending moments, and engineers sometimes fail to consider the consequences of lateral torsional buckling of the column. Inadequate column support increases the effective unbraced length of the beam and the connection, and exacerbates this lateral deformation issue. Finally, columns made from deep beam sections are more commonly rotary straightened (Frank, 2000) than are the heavy W12 and W14 column sections. This rotary straightening process is known to decrease the notch toughness of the steel in the k-area, and this increases the potential for k-area fractures.

In view of these four concerns, it is appropriate to require that continuity plates always be employed with deep column connections, because of this k-area concern as well as the continuity plate issue discussed earlier. Continuity plates can help to reduce the local demands on the k-area, and enhance the lateral stability of the column and the connection. At the same, welding should be minimized or avoided, if possible, in the critical region, and so the detailing and geometry of the continuity plate should be designed accordingly. In addition, lateral support should be provided to the bottom flange of the beam at the connection, because deep column flanges may not be stiff enough to assure ductile behavior.

This discussion concludes that connections with deep columns will, on average, provide less desirable seismic performance than will comparable strong axis connections with W12 and W14 column sections. Nevertheless, connections with deep columns should provide adequate seismic performance if care is taken to assure that:

- good connection details and geometry are employed,
- panel zone and flexural yielding are appropriately balanced,
- adequate lateral supports are provided to both the column and beam flanges in the region of the connection, and
- the continuity plates are designed as noted above.

If these factors are dealt with, connections with deep columns should provide adequate seismic performance. It is not possible to prequalify this connection for a wide range of applications because of the concerns noted in this section and the existing test results. However, certification tests are likely to be successful if the above issues are addressed. Additional testing of connections with deep columns is recommended, and the effect of the beam slab should be included in these tests, since the slab may benefit the connection performance.

## 4.8 Box Columns

Many connections with box columns have been tested. Most of the tests were conducted in other countries, but some took place in the US. Table 4-4 summarizes a number of these test results. This table is quite long, but examination of it shows very few specimens that did not achieve a plastic rotation of 0.03 radians. Of the specimens that did not achieve this rotation,

most were either pre-Northridge connections or an unusual connection detail which would not be similar to those prequalified during this research program. The Japanese connection tests are all based upon the internal diaphragm connection as depicted in Figure 3-4 with cold-formed tubular connections. Connection details with bolted webs and field-welded flanges are also used with built-up box columns in Japan. However, no significant damage was noted to those connections, and so there is no extensive research body since the 1995 Hyogoken-Nanbu (Kobe) earthquake. It is widely accepted within Japanese practice that the seismic performance of connections to built-up columns is better than that achieved with cold-formed tubular columns. However, internal diaphragms are always used regardless of the connection type. The Japanese connections included in Table 4-4 considered a range of backing bar details, weld access hole preparations, and run off tabs. The variations in ductility achieved with the Japanese tests are almost totally attributable to these variations. Finally, the connections in Table 4-4 are all of moderate beam size. This is appropriate, because box columns are likely to be used in US practice only when moment frame connections are employed in both directions, and this practice should result in smaller member and connection sizes.

**Table 4-4 Summary Table of Test Results with Box Columns**

Specimen Identification	Beam (Column) Sizes	Information on Connection	Maximum Plastic Rotation Achieved	Outcome of test
SFCCC-7 (Noel and Uang, 1996)	W18x86 (Bx20x20x2)	Welded flange plate connection - one sided specimen – very short beam	0.022	Cracking of fillet weld between flange plate and beam flange
CB2 (Chen, 1999)	W21x62bu (Bx18x18x280lbs)	Coverplated connection - 1 7/16" continuity	0.038	Test Stopped
CB1 (Chen, 1999)	W21x62bu (Bx18x18x280lbs)	Coverplated connection - 1 7/16" continuity	0.033	Test Stopped
CB3 (Chen, 1999)	W21x62bu (Bx18x18x 280lbs)	Coverplated connection - 1 7/16" continuity	0.029	Fracture
CB4 (Chen, 1999)	W21x62bu (Bx18x18x280lbs)	Coverplated connection - 1 7/16" continuity	0.025	Fracture
CHYC1 (Chen, 1996)	W24x104sim (Bx20x20x200lbs)	Tapered RBS connection	0.024	Fracture
CHPC2 (Chen, 1996)	W24x104sim (Bx20x20x200lbs)	Tapered RBS connection	0.048	Fracture
CHYC2 (Chen, 1996)	W24x104sim (Bx20x20x200lbs)	Tapered RBS connection	0.029	Fracture
CHPC3 (Chen, 1996)	W24x104sim (Bx20x20x200lbs)	Tapered RBS connection	0.038	Fracture

**Table 4-4 Summary Table of Test Results with Box Columns (continued)**

CHPC1 (Chen, 1996)	W24x104sim (Bx20x20x200lbs)	Tapered RBS connection	0.041	Fracture
NB2 (Chen, 1999)	W21x62bu (Bx18x18x280lbs)	Pre-Northridge connection	0.028	Fracture
NB1 (Chen, 1999)	W21x62bu (Bx18x18x280lbs)	Pre-Northridge connection	0.014	Fracture
WB1 (Chen, 1999)	W21x62bu (Bx18x18x280lbs)	Taper "wing" plates to match column flange	0.029	Fracture
TLHB2 (SAC DATABASE)	W27x94 (Bx20x20x400lbs)	Reduced beam section with drilled holes	0.025	Fracture
WB2 (Chen, 1999)	W21x62bu (Bx18x18x280lbs)	Taper "wing" plates to match column flange	0.028	Fracture
TLHB1 (SAC DATABASE)	W27x94 (Bx20x20x400lbs)	Reduced beam section with drilled holes	0.025	Fracture
SE5Z3F-Kb1 (AIJ, 1997)	Bu20x51 (Bx13.8x13.8x0.47)	Conv. Japanese detail-thin diaphragm w/flux tab	0.041	Fracture from toe of access hole
SE5Z6F-Kb1 (AIJ, 1997)	Bu20x51 (Bx13.8x13.8x0.47)	Conv. Japanese detail-inter diaphragm w/flux tab	0.04	Fracture from toe of access hole
SE5A3F-Kb1 (AIJ, 1997)	Bu20x51 (Bx13.8x13.8x0.47)	Mod. A Japanese detail- thick diaphragm w/flux tab	0.04	Deterioration of Load - Local Buckling
SE5A6F-Kb1 (AIJ, 1997)	Bu20x51 (Bx13.8x13.8x0.47)	Mod. Japanese A detail-inter diaphragm w/flux tab	0.04	Deterioration of Load - Local Buckling
SE5A3F-Kb2 (AIJ, 1997)	Bu20x51 (Bx13.8x13.8x0.47)	Mod. A Japanese detail- thick diaphragm w/flux tab	0.04	Fracture initiating from edge of weld
SE5A3F-Kb3 (AIJ, 1997)	Bu20x51 (Bx13.8x13.8x0.47)	Mod. A Japanese detail- thick diaphragm w/flux tab	0.04	Deterioration of Load - Local Buckling
SE5A3F-Kb4 (AIJ, 1997)	Bu20x51 (Bx13.8x13.8x0.47)	Mod. A Japanese detail- thick diaphragm w/steel run off tab	0.04	Fracture initiating from edge of weld
SE5A6F-KB2 (AIJ, 1997)	Bu20x51 (Bx13.8x13.8x0.47)	Mod. A Japanese detail w/flux tab	0.04	Deterioration of Load - Local Buckling
SE5A6F-Kb3 (AIJ, 1997)	Bu20x51 (Bx13.8x13.8x0.47)	Mod. A Japanese detail w/flux tab	0.04	Deterioration of Load - Local Buckling
SE5B3F-Kb1 (AIJ, 1997)	Bu20x51 (Bx13.8x13.8x0.47)	Mod. B Japanese detail w/flux tab	0.04	Deterioration of Load - Local Buckling
SEFB6F-Kb1 (AIJ, 1997)	Bu20x51 (Bx13.8x13.8x0.47)	Mod. B Japanese detail w/flux tab	0.04	Deterioration of Load - Local Buckling

**Table 4-4 Summary Table of Test Results with Box Columns (continued)**

SE5B3F-Kb2 (AIJ, 1997)	Bu20x51 (Bx13.8x13.8x0.47)	Mod. B Japanese detail w/flux tab	0.04	Fracture initiating from edge of weld
SEFB6F-Kb2 (AIJ, 1997)	Bu20x51 (Bx13.8x13.8x0.47)	Mod. B Japanese detail w/flux tab	0.04	Fracture initiating from edge of weld
SB6Z3-Kn1 (AIJ, 1997)	Bu24x73 (Bx17.7x17.7x0.74)	Conv. Japanese detail with steel tab	0.025	Fracture initiating from edge of weld
SB6Z3-Kn2 (AIJ, 1997)	Bu24x73 (Bx17.7x17.7x0.74)	Conv. Japanese detail with steel tab	0.014	Fracture initiating from edge of weld
SB6Z7-Kn1 (AIJ, 1997)	Bu24x73 (Bx17.7x17.7x0.74)	Conv. Japanese detail with steel tab	0.038	Fracture initiating from edge of weld
SB6Z7-Kn2 (AIJ, 1997)	Bu24x73 (Bx17.7x17.7x0.74)	Conv. Japanese detail with steel tab	0.015	Fracture initiating from edge of weld
SB6Z3-Kn3 (AIJ, 1997)	Bu24x73 (Bx17.7x17.7x0.74)	Conv. Japanese detail with steel tab	0.033	Fracture initiating from edge of weld
SB6Z3-Kn4 (AIJ, 1997)	Bu24x73 (Bx17.7x17.7x0.74)	Conv. Japanese detail with steel tab	0.035	Fracture initiating from edge of weld
SB6Z7-Kn3 (AIJ, 1997)	Bu24x73 (Bx17.7x17.7x0.74)	Conv. Japanese detail with steel tab	0.043	Fracture initiating from edge of weld
SB6Z7-Kn4 (AIJ, 1997)	Bu24x73 (Bx17.7x17.7x0.74)	Conv. Japanese detail with steel tab	0.031	Fracture initiating from edge of weld
SB6Z3F-Kn5 (AIJ, 1997)	Bu24x73 (Bx17.7x17.7x0.74)	Conv. Japanese detail w/flux tab	0.042	Fracture initiating from edge of weld
SB6Z7F-Kn5 (AIJ, 1997)	Bu24x73 (Bx17.7x17.7x0.74)	Conv. Japanese detail w/ flux tab	0.042	Fracture initiating from edge of weld
SB6A3-Kn1 (AIJ, 1997)	Bu24x73 (Bx17.7x17.7x0.74)	Mod. A Japanese detail with steel tab	0.024	Fracture initiating from edge of weld
SB6A7-Kn1 (AIJ, 1997)	Bu24x73 (Bx17.7x17.7x0.74)	Mod. A Japanese detail with steel tab	0.024	Fracture initiating from edge of weld
SB6A3-Kn2 (AIJ, 1997)	Bu24x73 (Bx17.7x17.7x0.74)	Mod. A Japanese detail with steel tab	0.034	Fracture initiating from edge of weld
SB6A7-Kn2 (AIJ, 1997)	Bu24x73 (Bx17.7x17.7x0.74)	Mod. A Japanese detail with steel tab	0.042	Fracture in diaphragm initiating from edge of flange weld
SB6A3F-Kn3 (AIJ, 1997)	Bu24x73 (Bx17.7x17.7x0.74)	Mod. A Japanese detail with flux tab	0.026	Fracture in diaphragm initiating from edge of flange weld
SB6A3F-Kn4 (AIJ, 1997)	Bu24x73 (Bx17.7x17.7x0.74)	Mod. A Japanese detail with flux tab	0.052	Fracture initiating from edge of weld

**Table 4-4 Summary Table of Test Results with Box Columns (continued)**

SB6A7F-Kn3 (AIJ, 1997)	Bu24x73 (Bx17.7x17.7x0.74)	Mod. A Japanese detail with flux tab	0.044	Fracture initiating from edge of weld
SB6A7F-Kn4 (AIJ, 1997)	Bu24x73 (Bx17.7x17.7x0.74)	Mod. A Japanese detail with flux tab	0.062	Deterioration of Load - Local Buckling
SB6B3-Kn1 (AIJ, 1997)	Bu24x73 (Bx17.7x17.7x0.74)	Mod. B Japanese detail with steel tab	0.019	Fracture initiating from edge of weld
SB6B7-Kn1 (AIJ, 1997)	Bu24x73 (Bx17.7x17.7x0.74)	Mod. B Japanese detail with steel tab	0.017	Fracture in diaphragm initiating from edge of flange weld
SB6B3-Kn2 (AIJ, 1997)	Bu24x73 (Bx17.7x17.7x0.74)	Mod. B Japanese detail with steel tab	0.043	Fracture initiating from edge of weld
SB6B7-Kn2 (AIJ, 1997)	Bu24x73 (Bx17.7x17.7x0.74)	Mod. B Japanese detail with steel tab	0.033	Fracture initiating from edge of weld
SB6B3F-Kn3 (AIJ, 1997)	Bu24x73 (Bx17.7x17.7x0.74)	Mod. B Japanese detail with flux tab	0.035	Diaphragm fracture initiating from edge of flange weld
SB6B3F-Kn4 (AIJ, 1997)	Bu24x73 (Bx17.7x17.7x0.74)	Mod. B Japanese detail with flux tab	0.043	Fracture initiating from edge of weld
SB6B7F-Kn3 (AIJ, 1997)	Bu24x73 (Bx17.7x17.7x0.74)	Mod. B Japanese detail with flux tab	0.042	Fracture initiating from edge of weld
SB6B7F-Kn4 (AIJ, 1997)	Bu24x73 (Bx17.7x17.7x0.74)	Mod. B Japanese detail with flux tab	0.042	Fracture initiating from edge of weld
SB6Z3-Ky1 (AIJ, 1997)	Bu24x73 (Bx17.7x17.7x0.74)	Conv. Japanese detail with steel tab	0.033	Fracture initiating from edge of weld
SB6Z7-Ky1 (AIJ, 1997)	Bu24x73 (Bx17.7x17.7x0.74)	Conv. Japanese Detail with steel tab	0.037	Fracture initiating from edge of weld
SB6A3F-Ky1 (AIJ, 1997)	Bu24x73 (Bx17.7x17.7x0.74)	Mod. A Japanese detail with flux tab	0.043	Fracture initiating from edge of weld
SB6A7F-Ky1 (AIJ, 1997)	Bu24x73 (Bx17.7x17.7x0.74)	Mod. A Japanese detail with flux tab	0.043	Fracture initiating from edge of weld
SB6B3F-Ky1 (AIJ, 1997)	Bu24x73 (Bx17.7x17.7x0.74)	Mod. B Japanese detail with flux tab	0.041	Fracture initiating from edge of weld
SB6B7F-Ky1 (AIJ, 1997)	Bu24x73 (Bx17.7x17.7x0.74)	Mod. B Japanese detail with flux tab	0.043	Deterioration of Load - Local Buckling
SE6Z2-Os1 (AIJ, 1997)	Bu24x73 (Bx17.7x17.7x0.74)	Conv. Japanese detail with steel tab	0.02	Fracture from toe of access hole
SE6A2-Os1 (AIJ, 1997)	Bu24x73 (Bx17.7x17.7x0.74)	Mod. A Japanese detail with steel tab	0.033	Deterioration of Load - Local Buckling

**Table 4-4 Summary Table of Test Results with Box Columns (continued)**

SE6B2-Os1 (AIJ, 1997)	Bu24x73 (Bx17.7x17.7x0.74)	Mod. B Japanese detail with steel tab	0.034	Deterioration of Load - Local Buckling
FB6Z3-Os1 (AIJ, 1997)	Bu24x73 (Bx17.7x17.7x0.74)	Conv. Japanese detail with bolted web, field welded flange and steel tab	0.038	Fracture from toe of access hole
FB6Z7-Os1 (AIJ, 1997)	Bu24x73 (Bx17.7x17.7x0.74)	Conv. Japanese detail w/ bolted web, field welded flange and steel tab	0.039	Fracture from toe of access hole
FB6Z3F-Os2 (AIJ, 1997)	Bu24x73 (Bx17.7x17.7x0.74)	Conv. Japanese detail w/ bolted web, field welded flange and flux tab	0.025	Fracture initiating from edge of weld
FB6Z7F-Os2 (AIJ, 1997)	Bu24x73 (Bx17.7x17.7x0.74)	Conv. Japanese detail w/ bolted web, field welded flange and flux tab	0.043	Fracture initiating from edge of weld
FB6B3-Os1 (AIJ, 1997)	Bu24x73 (Bx17.7x17.7x0.74)	Modified detail B w/ bolted web splice, field welded flange and steel tab	0.038	Fracture from fillet weld at toe of weld access hole
FB6B7-Os1 (AIJ, 1997)	Bu24x73 (Bx17.7x17.7x0.74)	Modified detail B w/ bolted web splice, field welded flange and steel tab	0.039	Fracture from toe of access hole
FB6B3F-Os2 (AIJ, 1997)	Bu24x73 (Bx17.7x17.7x0.74)	Modified detail B w/ bolted web splice, field welded flange and flux tab	0.051	Fracture initiating from center of beam flange at weld
FB6B7F-Os2 (AIJ, 1997)	Bu24x73 (Bx17.7x17.7x0.74)	Modified detail B w/ bolted web splice, field welded flange and flux tab	0.042	Fracture initiating from center of beam flange at weld
FB6Z3F-Ok1 (AIJ, 1997)	Bu24x73 (Bx17.7x17.7x0.74)	Conv w/bolted web, field weld flng and flux tab	0.042	Fracture from toe of access hole
FB6Z3F-Ok2 (AIJ, 1997)	Bu24x73 (Bx17.7x17.7x0.74)	Conv. Japanese detail w/ bolted web, field flange weld, and flux tab	0.028	Diaphragm fracture initiating from edge of flange weld
FB6Z7F-Ok1 (AIJ, 1997)	Bu24x73 (Bx17.7x17.7x0.74)	Conv. Japanese detail w/ bolted web, field flange weld, and flux tab	0.031	Fracture from toe of access hole
FB6Z7F-Ok2 (AIJ, 1997)	Bu24x73 (Bx17.7x17.7x0.74)	Conv. Japanese detail w/ bolted web, field flange weld, and flux tab	0.01	Diaphragm fracture initiating from edge of flange weld
FB6B3F-Ok1 (AIJ, 1997)	Bu24x73 (Bx17.7x17.7x0.74)	Mod. B Japanese detail w/ bolted web splice, field flange weld, and flux tab	0.042	Diaphragm fracture initiating from edge of flange weld
FB6B3F-Ok2 (AIJ, 1997)	Bu24x73 (Bx17.7x17.7x0.74)	Mod. B Japanese detail w/ bolted web splice, field flange weld, and flux tab	0.036	Fracture initiating from edge of weld
FB6B7F-Ok1 (AIJ, 1997)	Bu24x73 (Bx17.7x17.7x0.74)	Mod. B Japanese detail w/ bolted web splice, field flange weld, and flux tab	0.026	Diaphragm fracture initiating from edge of flange weld

**Table 4-4 Summary Table of Test Results with Box Columns (continued)**

FB6B7F-Ok2 (AIJ, 1997)	Bu24x73 (Bx17.7x17.7x0.74)	Mod. B Japanese detail w/ bolted web splice, field flange weld, and flux tab	0.042	Fracture from fillet weld at toe of weld access hole
---------------------------	-------------------------------	------------------------------------------------------------------------------------	-------	------------------------------------------------------------

The issues of critical importance for the box column connection have already been discussed for other connection options earlier in this chapter. Therefore, they will be only briefly discussed here. Four issues of importance are noted. First, the longitudinal stress distribution for the flange at the welds for box column connections is comparable to that shown in Figure 4-6b. As a result, fracture for these connections initiates from the edge of the weld, and continuity plates or stiffeners are always required. Second, the web connection is consistently less effective in transferring bending moment and beam shear to the box column than it is for strong-axis-column-bending connections. As a result, many of the benefits through enhanced web connections for the welded-flange-welded-web and free-flange connections are not readily achieved with box column connections. Third, significant ductility for post-Northridge connections is sometimes provided by panel zone yield deformation, but excess panel zone deformation causes a potential for early connection fracture due to excess local inelastic deformation. Box columns have two "webs" which are effective in resisting panel zone shear, and the "web" thickness is usually the same as the flange thickness. As a consequence, panel zone yielding is less likely to occur, and doubler plates are less likely to be required with box columns. Plastic deformation in the panel zone is still possible, but panel zone yield strains are unlikely to be large, because the  $\frac{V_{pz}}{V_y}$  ratio is normally in the range of 0.5 to 0.7 for connections with box columns. This means that box columns have less concern with premature fracture due to large panel zone deformations, but connections with box columns may develop smaller plastic rotations, since the panel zones can contribute little to this deformation capacity. Fourth, the lateral support provided to the beam and beam-column connection by the column has been a concern in this chapter. These concerns were particularly significant for the weak-axis-column-bending and deep column connections. The box column connection is at the opposite extreme, since it has a large torsional stiffness compared to W12 and W14 wide flanges, and it does not rely upon warping torsion for this stiffness. As a result, box column connections should, on average, experience less deterioration due to lateral torsional buckling than do most other connection types.

Because of the large test database, and the generally good performance of connections with box columns in these past tests, box column connections are expected to provide good seismic performance if:

- continuity plates that are as thick as the beam flange are used inside the box and securely welded to all sides of the box,
- the connection detail employed in the design uses good detailing as defined for the connection type,
- the connection type does not rely heavily on the web connection for its connection ductility, and

- the connection type does not rely heavily on the panel zone yield deformation for the connection rotational capacity.

#### 4.9 Composite Slabs

Composite slabs increase the moment resistance of members and shift the neutral axis of the beam toward the concrete slab. Thus, the composite slab has been considered as the cause of connection fractures in some cases, and the protection against fracture in other cases.

Connection tests with a composite slab are expensive, because development of the maximum composite moment requires a cruciform type connection as illustrated in Figure 2-2.

Nevertheless, a number of tests performed with composite slabs are summarized in Table 4-5.

**Table 4-5 Summary of Composite Slab Test Results**

Specimen Identification	Beam (Column) Sizes	Information on Connection	Maximum Plastic Rotation Achieved	Outcome of test
UTA DBBWC (Engelhardt, et al., 2000)	Radius cut RBS bolted web	W36x150 (W14x398) 10-1"A490	0.05 (less than 80%) and 0.038 at fracture	south beam flange fractured near weld access hole at 0.038
UTA DBWPC (Engelhardt, et al., 2000)	Radius cut RBS with weak panel zone, bolted web	W36x150 (W14x283) 10-1"A490	0.05	Bottom Flange fracture in both beams at large deformations
TA&M DBWW-C (Engelhardt, et al., 2000)	Radius cut RBS with welded web – Limited lateral restraint to specimen	W36x150 (W14x398) 4-1" bolts with welded web	0.05 (less than 80%)	Rapid deterioration in resistance, tearing at buckle of both flanges at initial $\theta_p = 0.06$ cycle
TA&M DBWW SPZ-C (Engelhardt, et al., 2000)	Radius cut RBS with welded web – Limit lateral restraint to specimen	W36x150 (W14x398) 3/4" doubler both sides 4-1" bolts w/ welded web	0.05 with considerable deterioration	Less rapid deterioration than SPZ due to slab restraint - Test stopped due to out of plane buckling
UT-RBS-2 (NIST, 1998)	W30x99 (W12x279)	Pre-Northridge w/ radius cut RBS, bottom flange only, bolted web	0.021	K-line fracture
UCSD RBS-2 (NIST, 1998)	W36x150 (W14x426)	Pre-Northridge w/ radius cut, bottom flange only	0.01	Top flange weld fracture
UCSD RBS-2R (NIST, 1998)	W36x150 (W14x426)	Pre-Northridge w/ radius cut RBS, bottom flange Only	0.008	Top flange weld fracture

**Table 4-5 Summary of Composite Slab Test Results (continued)**

UCSD RBS-4 (NIST, 1998)	W36x150 (14x426)	Pre-Northridge w/ radius cut RBS, bottom flange only	0.03	k-area fracture
UM 2 (Leon, et al., 1998)	W27x94 (W14x211)	Pre-Northridge connection bolted webs w/ E70T-7 flange welds and partial (55%) composite	0.005	Bottom flange weld fracture
UM 3 (Leon, et al., 1998)	W27x94 (W14x211)	Pre-Northridge connection bolted webs w/ E70T-7 flange welds and partial (35%) composite	0.009	Bottom flange weld fracture
LU-C5 (Ricles, Mao, Lu and Fisher, 2000)	W36X150 (W27X398)	Welded-flange- welded-web connection	0.025 east beam fracture  0.046 at west beam fracture after east beam released	East beam fractured at shear stud weld approximately 9" from column face
UT Austin Specimen (Venti, and 2000) UTA-FF	W36x150 (W14x398)	Free-flange connection	0.034	Bottom flange of north beam fractured during the 4 <sup>th</sup> cycle at the maximum story drift

At first glance, the results summarized in Table 4-5 appear mixed, since some specimens had very large plastic rotations while others had small rotational capacity. However, a fairly consistent picture emerges as the details of the test programs are evaluated. Six of the specimens in Table 4-5 are pre-Northridge connections with relatively large beam sizes and with or without repair. These tests invariably had companion bare steel specimens. When one compares the composite specimens to the bare steel specimens, the composite specimens generally (Leon, et al., 1998) had slightly improved performance. They obtained slightly larger moment resistance and, on average, slightly larger plastic rotational capacity. Thus, the slab improved the performance slightly, but the improvement was not significant. Composite slabs move the neutral axis and increase the inelastic strain demands at some locations, but they also reduce strains at other locations and provide greater stability to the specimen. However, it must also be recognized that the composite slab does not make a significant contribution to the beam resistance for these deep beam specimens, because the slab is relatively thin and the beams are relatively deep, and the number of shear connectors usually results in partial composite action. Nevertheless, it appears from these tests that the composite slab may be a contributing cause for the reduced number of fractures in the top flange welds of pre-Northridge connections, since the slab makes its greatest reduction in strain demand at the top flange.

The remaining specimens are more ductile post-Northridge connections. These connections invariably attained significantly more ductility as both bare steel and composite connections.

The composite action again reduced the strain at some locations, and increased demands at other locations. The specimens with composite slabs consistently produced comparable maximum plastic rotations as their identical bare steel counterparts. The composite slab enhanced the stability of the specimens and reduced the deterioration noted with large plastic deformations. The Texas A&M specimens DBWW-C and DBWWSPZ-C very clearly illustrate this effect. These specimens were tested with less restraint at the supports than used in all other test programs, and as a consequence rapid deterioration was noted in the bare steel specimens due to the instability of the specimen. The slab greatly enhanced the specimen stability despite the limited support restraint, and much better performance was noted. Although it is difficult to compare the four Texas A&M specimens to other RBS tests because of these differences in the support conditions, these tests clearly demonstrate the added restraint and stiffness provided by the composite slab.

Additional tests on composite slabs were completed with the shear tab connection, and they will be described in Chapter 5. These specimens have shallower beams and much weaker bare steel connections, and so the composite slab provided a much larger increase in connection resistance for these connections than for the stronger connections tabulated in Table 4-5. Nevertheless, the observations with regard to connection ductility and rotational capacity are similar. The maximum rotation that was achieved with the composite specimens was nearly identical to that achieved with the bare steel specimens. The resistance at these rotations was nearly the same for both composite and bare steel specimens, because the composite action was lost at rotations well below the maximum rotation achieved by the specimens.

The prior analysis has shown that the contribution of the composite slab is generally positive or, at worst, neutral with regard to seismic performance of steel frame connections. However, Specimen LU-C5 shows a clear example of where composite action had negative effects. This specimen was a welded-flange-welded-web post-Northridge connection, and shear connectors were distributed throughout the beam length. The comparable bare steel welded-flange-welded-web specimens (LU-C1 and LU-C2) developed large rotational capacity and ductility as noted in Table 3-4. The plastic rotation for LU-C5 was comparable to the bare steel specimens, but Specimen LU-C5 fractured through the beam in the region of plastic deformation of the beam flange. The fracture started at a shear connector weld, and it occurred well away from the flange weld and weld access hole (in the order of  $\frac{d_b}{4}$  from the face of the column).

This fracture was an important observation, because shear connectors were deliberately excluded from the reduced section of RBS connections, because plastic deformation was expected to occur in that area. The pre-Northridge composite connections and the shear tab composite connections (described in Chapter 6) had shear connectors distributed over the beam length, but none of these connections developed significant plastic strain in the beams. The pre-Northridge connections had very little plastic rotation, and the shear tab connections developed their rotations within the connecting elements. Specimen LU-C5 was the only composite specimen that developed large plastic strains in beam flanges in the region where shear connectors were attached. Shear connector welds may introduce flaws and reduced toughness, which can contribute to early fracture of the beam. It is, consequently, recommended that shear connectors not be attached in these yield regions. The location of yielding may vary widely.

Welded-flange-welded-web connections and free-flange connections yield in the beam near the face of the column as depicted in Figure 2-10. Coverplate, haunch, and flange plate connections move the location of yielding further out into the beam as illustrated in Figure 4-7. The length of yielding can be quite long depending upon the ductility of the connection, the strain hardening, and the length of the beam specimen. It is recommended that shear connectors not be attached within a distance of  $d_b$  from the location where the maximum strain hardening moment develops in these ductile connections. This length,  $d_b$ , may not be large enough to avoid all yielding in the region where shear connectors are installed, but if this limit is satisfied, the plastic strains at any shear connector welds will be small, and they will develop only after large plastic rotations have occurred.

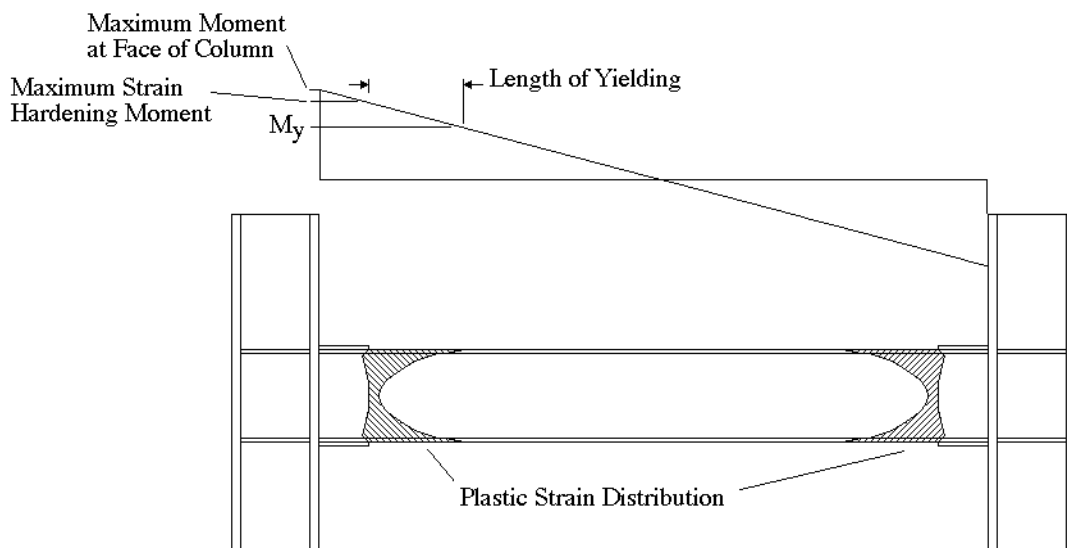


**Figure 4-7 Distribution of Plastic Strain in a Ductile Connection**

In summary, the research indicates that composite slabs:

- increase the stability and axial restraint of connections, and, as a consequence result in reduced deterioration of resistance during inelastic deformation,
- have little effect on the plastic rotational capacity of the connection,
- significantly increase the resistance of weaker and more flexible connections, but have very limited effect on the maximum resistance of deep beams with stiff, strong connections, and
- require that shear connectors be left out of regions of plastic strain in the beam for a distance,  $d_b$ , from the location of the maximum strain hardening moment in the beam.

#### 4.10 Temperature Effects

The discussion of connections in this report has placed considerable emphasis on the notch toughness of welds and material. It is well known (Barsom and Rolfe, 1987) that steel and weld

materials experience a transition temperature, where a significant reduction in the Charpy V-notch toughness must be expected for temperatures below this transition temperature. Steel moment frames are generally enclosed within the building envelope, and so it is unlikely that these connections will experience extremely low temperatures during earthquakes. However, steel moment frames are exposed during construction, and some moment frames are outside the building envelope. Further, earthquakes in cold climates such as Alaska may occur in low temperatures when these connections are subjected to earthquake loading. Tests have been completed in Japan evaluating the performance of connections tested at low temperatures ( $-23^{\circ}\text{C}$  or  $-10^{\circ}\text{F}$ ), and these tests are tabulated in Table 4-6. Comparison can be made between these test results and those included in Table 4-4. Direct one-to-one comparisons of several tests performed at low temperatures and identical tests performed at room temperature were made for six of the twelve specimens in the table, and the ratio of the experimental rotation for the low temperature test to the rotation achieved in the room temperature test is provided in parentheses in the last column of the table.

**Table 4-6 Summary of Test Results for Specimens Tested at Low Temperatures**

Specimen Identification	Beam (Column) Sizes	Information on Connection	Maximum Plastic Rotation Achieved	Outcome of test	Test Temperature, (Ratio of Rotation)
SE5Z3-Ch1 (AIJ, 1997)	Bu20x51 (Bx13.8x13.8x0.47)	Conv. Japanese Detail w/ steel runoff tab	0.02	Fracture from toe of access hole	$-23^{\circ}\text{C}$ (---)
SE5Z6-Ch1 (AIJ, 1997)	Bu20x51 (Bx13.8x13.8x0.47)	Conv. Japanese detail with steel runoff tab	0.02	Fracture initiating from edge of weld	$-23^{\circ}\text{C}$ (---)
SE5Z3F-Ch2 (AIJ, 1997)	Bu20x51 (Bx13.8x13.8x0.47)	Conv. Japanese detail w flux tab	0.04	Fracture from toe of access hole	$-23^{\circ}\text{C}$ (---)
SE5Z6F-Ch2 (AIJ, 1997)	Bu20x51 (Bx13.8x13.8x0.47)	Conv. Japanese detail w/flux tab	0.033	Fracture from toe of access hole	$-23^{\circ}\text{C}$ (---)
SE5A3-Ch1 (AIJ, 1997)	Bu20x51 (Bx13.8x13.8x0.47)	Mod. A Japanese detail with steel tab	0.038	Deterioration of Load – Local Buckling	$-23^{\circ}\text{C}$ (---)
SE5A6-Ch1 (AIJ, 1997)	Bu20x51 (Bx13.8x13.8x0.47)	Mod. A Japanese detail with steel tab	0.022	Fracture from toe of access hole	$-23^{\circ}\text{C}$ (---)
SE5A3F-Ch2 (AIJ, 1997)	Bu20x51 (Bx13.8x13.8x0.47)	Mod. A Japanese detail w/flux tab	0.06	Deterioration of Load – Local Buckling	$-23^{\circ}\text{C}$ (1.5)

**Table 4-6 Summary of Test Results for Specimens Tested at Low Temperatures  
 (continued)**

SE5A6F-Ch2 (AIJ, 1997)	Bu20x51 (Bx13.8x13.8x0.47)	Mod. A Japanese detail w/flux tab	0.041	Deterioration of Load – Local Buckling	-23°C (1.025)
SE5B3-Ch1 (AIJ, 1997)	Bu20x51 (Bx13.8x13.8x0.47)	Mod. B Japanese detail with steel tab	0.015	Fracture from fillet weld at toe of weld access hole	-23°C (0.375)
SE5B6-Ch1 (AIJ, 1997)	Bu20x51 (Bx13.8x13.8x0.47)	Mod. B Japanese detail with steel tab	0.038	Fracture from toe of access hole	-23°C (0.95)
SE5B3F-Ch2 (AIJ, 1997)	Bu20x51 (Bx13.8x13.8x0.47)	SE5B3F-Ch2 – Mod. B Japanese detail w/flux tab	0.06	Deterioration of Load – Local Buckling	-23°C (1.5)
SE5B6F-Ch2 (AIJ, 1997)	Bu20x51 (Bx13.8x13.8x0.47)	Mod. B Japanese detail w/flux tab	0.04	Deterioration of Load – Local Buckling	-23°C (1.0)
FW03 (Takanashi, 1997)	Bu8x75 (Stiff End Plate) - Also dynamic loading.	Field welded Japanese welded- flange-welded-web	Not defined in terms of rotation – Est. as > 0.03	Not defined	-40°C (0.7)
FW05 (Takanashi, 1997)	Bu8x75 (Stiff End Plate)	Field welded Japanese welded- flange-welded-web	Not defined in terms of rotation – Est. as > 0.01	Not defined	-80°C (0.3)
DW03 (Takanashi, 1997)	Bu8x75 (Stiff End Plate) - Also dynamic loading	Shop welded Japanese welded- flange-welded-web	Not defined in terms of rotation – Est. as > 0.03	Not defined	-40°C (1.0)
DW05 (Takanashi, 1997)	Bu8x75 (Stiff End Plate)	Shop welded Japanese welded- flange-welded-web	Not defined in terms of rotation – Est. as > 0.02	Not defined	-80°C (0.5)

The final four specimens of Table 4-6 are also Japanese (Takanashi, 1997) connection tests, but these tests had the combined goal of examining temperature effects as well as dynamic effects. Two of these tests were conducted at low temperatures with static loading while the other two were at low temperatures with dynamic loading. Comparisons of the plastic deformation achieved with these tests to comparable static tests at room temperature are provided in parenthesis in the last column. The room temperature comparison tests for these four specimens are not included in Table 4-4. These tests are performed at extremely low temperatures (-40°C and -80°C or -40°F and -112°F), and it can be seen that the plastic

rotational capacity is reduced significantly for these specimens. It should be noted that these last four specimens are also small.

The results clearly show that temperatures as low as  $-23^{\circ}\text{C}$  ( $-10^{\circ}\text{F}$ ) do not have a dramatic impact upon the plastic rotation and ductility achieved with moment resisting connections. Extremely low temperatures in the range of  $-40^{\circ}\text{C}$  and  $-80^{\circ}\text{C}$  clearly result in reduced connection ductility. On average, the plastic rotation achieved with the low temperature tests is about the same as achieved with the room temperature tests. Further, comparison of the failure modes suggests that fracture and deterioration due to buckling occur with similar frequency at room temperature and at  $-23^{\circ}\text{C}$  ( $-10^{\circ}\text{F}$ ). The low temperatures included in these tests are extremely low compared to the temperatures expected in most buildings during their normal service life. As a result, this comparison suggests that low temperatures should not be a primary concern when evaluating the expected ductility during seismic loading of steel moment frames. On the other hand,  $-23^{\circ}\text{C}$  ( $-10^{\circ}\text{F}$ ) is well above the low temperatures expected in exposed steel structures in very cold climates, and additional testing is needed before firm conclusions can be drawn for connections exposed to temperatures lower than  $-23^{\circ}\text{C}$  ( $-10^{\circ}\text{F}$ ).

#### 4.11 Dynamic Loading

The Northridge earthquake resulted in many acceleration records that produced high velocities and strain rates. It is well known (Manjoine, 1944) that rapid strain rates increase the apparent yield and tensile strength of steel and other materials. In addition, the toughness of welds and materials experiences a shift toward more brittle behavior with very rapid strain rates, and consequently, the rapid strain rates are believed to increase the potential for brittle fracture of steel frame connections. Research has been performed to address these issues.

The strain rates in a structure during an earthquake are highly localized, and they depend upon the dynamic properties of the structure and the acceleration record. Analyses were completed (Harrigan, 1996) of various steel frame buildings with a range of acceleration records, and these analyses showed that steel moment frames are likely to experience maximum local strain rates during severe earthquakes in the order of 0.05 to 0.15 in/in/sec. These maximum strain rates are very localized and occur for very short periods of time with only a few acceleration records. These strain rates are quite large, but they are significantly smaller (Manjoine, 1944) than strain rates that cause dramatic changes in material behavior. This same study performed tension tests on coupons taken from steel, weld metal, and base metal of steel moment-frame connections where the strain rate of the tests was at the rate of these maximum conditions as well as normal "static" strain rate conditions. The welds used in these tests were both E70T-4 and E7018 electrodes. The dynamic tests showed average increases of 5% to 15% in the tensile yield stress of the steel, and slight reductions in the ductility of the specimens. The dynamic testing had no apparent effect on the ultimate tensile stress of the coupons. In general, the effect of dynamic loading at the strain rates expected during severe earthquakes was not dramatic.

Crack propagation analyses were performed (Deierlein, 1998) with the goal of further understanding the strain rate effects on steel moment frame connection performance. This study considered the changes in the CVN notch toughness of steel and weld material with different

load rates as well as the strain rates expected during earthquake loading. It was again noted that earthquakes cause dynamic strains which are in the intermediate range rather than the static (approx. 0.0001 in/in/sec or smaller) or true dynamic (approx. 10 in/in/sec or larger) ranges. The analysis concluded that in general steels and welds with intermediate toughness will have the largest influence due to strain rate. Welds with low notch toughness such as the E70T-4 electrode will fracture at sufficiently small strains that the dynamic strain rate makes little difference to the performance. Tougher materials such as most structural steels and welds of E7018 electrodes have sufficient notch toughness that dynamic loading has little effect at these intermediate strain rates. As a result, the studies described appear to be consistent in suggesting that dynamic effects are not likely to play a significant role in the connection performance during earthquake loading.

Despite this observation, full sized dynamic connection tests have been performed, and the results of these tests are summarized in Table 4-7. None of these tests were performed in the SAC Steel Project, and most of the testing has been performed in Japan. However, on average, the results provide consistent support of the theoretical and coupon test observations noted above. In some cases, comparisons could be made between static tests and comparable dynamic tests, and these ratios are indicated in parentheses in the last column of the table.

**Table 4-7 Summary of Dynamic Connection Tests**

<b>Specimen Identification</b>	<b>Beam (Column) Sizes</b>	<b>Information on Connection</b>	<b>Maximum Plastic Rotation Achieved</b>	<b>Outcome of test</b>	<b>Approximate Load Rate and (Ratio of Rotation)</b>
Uang UCSD 4 (Uang, et al., 1998)	W30x99 (W14x176)	Pre-Northridge Connection	0.0	Beam flange Fracture	Est. 0.01 in/in/sec based on measured local strain (0.0 when compared to specimen 3)
Uang UCSD 5 (Uang, et al., 1998)	W30x99 (W14x176)	Pre-Northridge Connection	0.0 by SAC rules. Small one sided plastic rotation achieved for comparison in column 6	Beam flange Fracture	Same (1.0 when compared to specimen 1)
Uang UCSD 4R (Uang, et al., 1998)	W30x99 (W14x176)	Pre-Northridge Connection with Bottom only Haunch Repair	0.007	Beam flange Fracture	Approx. Same (0.25 when compared to 3R)
Uang UCSD 5R (Uang, et al., 1998)	W30x99 (W14x176)	Pre-Northridge Connection with Bottom Only Haunch Repair	0.007	Beam flange Fracture	Same (0.5 when compared to 1R)

**Table 4-7 Summary of Dynamic Connection Tests (continued)**

SB6Z3-Ky2D (AIJ, 1997)	Bu24x73 (Bx17.7x17.7x 0.74)	Conv. Japanese detail w/ steel tab	0.033	Fracture initiating from edge of weld	0.15 rad./sec or in the order of 0.1 in/in/sec (1.0)
SB6Z7-Ky2D (AIJ, 1997)	Bu24x73 (Bx17.7x17.7x 0.74)	Conv. Japanese detail w/ steel tab	0.031	Fracture initiating from edge of weld	0.15 rad./sec or in the order of 0.1 in/in/sec (0.84)
SB6Z3F-Ky3D (AIJ, 1997)	Bu24x73 (Bx17.7x17.7x 0.74)	Conv. Japanese detail w/ flux tab	0.043	Fracture initiating from edge of weld	0.15 rad./sec or in the order of 0.1 in/in/sec (1.02)
SB6Z7F-Ky2D (AIJ, 1997)	Bu24x73 (Bx17.7x17.7x 0.74)	Conv. Japanese detail w/ flux tab	0.042	Fracture initiating from edge of weld	0.15 rad./sec or in the order of 0.1 in/in/sec (1.0)
SB6A3F-Ky2D (AIJ, 1997)	Bu24x73 (Bx17.7x17.7x 0.74)	Mod. A Japanese detail w/ flux tab	0.034	Fracture initiating from edge of weld	0.15 rad./sec or in the order of 0.1 in/in/sec (0.78)
SB6A7F-Ky2D (AIJ, 1997)	Bu24x73 (Bx17.7x17.7x 0.74)	Mod. A Japanese detail w/ flux tab	0.043	Fracture initiating from edge of weld	0.15 rad./sec or in the order of 0.1 in/in/sec (1.0)
SB6B3F-Ky2D (AIJ, 1997)	Bu24x73 (Bx17.7x17.7x 0.74)	Mod. B Japanese detail w/ flux tab	0.043	Fracture initiating from edge of weld	0.15 rad./sec or in the order of 0.1 in/in/sec (1.05)
SB6B7F-Ky2D (AIJ, 1997)	Bu24x73 (Bx17.7x17.7x 0.74)	Mod. B Japanese detail w/ flux tab	0.043	Fracture initiating from edge of weld	0.15 rad./sec or in the order of 0.1 in/in/sec (1.0)
FW02 (Takanashi, 1997)	Bu8x75 (Stiff End Plate)	Field welded Japanese welded-flange- welded-web	Not defined in terms of rotation - Same as Static Est > 0.03	Not defined	0.3 to 0.5 rad./sec or in the order of 0.3 in/in/sec at 10°C (1.0)
FW04 (Takanashi, 1997)	Bu8x75 (Stiff End Plate)	Field welded Japanese welded-flange- welded-web	Not defined in terms of rotation - Failed on First Inelastic Excursion	Not defined	0.3 to 0.5 rad./sec or in the order of 0.3 in/in/sec at -80°C (approaching 0.0)

**Table 4-7 Summary of Dynamic Connection Tests (continued)**

DW02 (Takanashi, 1997)	Bu8x75 (Stiff End Plate)	Shop welded Japanese welded-flange- welded-web	Not defined in terms of rotation - Less as Static but Est > 0.03	Not defined	0.3 to 0.5 rad./sec or in the order of 0.3 in/in/sec  at 10 <sup>0</sup> C (1.0)
DW04 (Takanashi, 1997)	Bu8x75 (Stiff End Plate)	Shop welded Japanese welded-flange- welded-web	Not defined in terms of rotation - Est as > 0.01	Not defined	0.3 to 0.5 rad./sec or in the order of 0.3 in/in/sec  at -80 <sup>0</sup> C (0.5)

The first four tests shown in Table 4-7 were performed in the US (Uang et al., 1998) on pre-Northridge connections and pre-Northridge connections repaired with a bottom only haunch. The authors report an 18% increase in the weld flange forces due to dynamic loading, but this increased force is argued based upon hypothetical conditions because there clearly is not a significant increase in the moment shown in the moment-rotation curves for the dynamic tests. Comparison of the maximum rotations could suggest a significant difference in rotational capacity for dynamically tested specimens, but again this observation is not well supported. Three of the four pre-Northridge connections developed zero plastic rotation by the SAC (Clark, et al., 1997) definition, and the fourth developed only a small plastic rotation. Therefore, the ratios of 0.0 and 1.0 for these two specimens are arbitrary when considered in real terms. The haunch repairs on the two pre-Northridge connections suggest that the dynamic tests achieved consistently smaller plastic rotations than the static tests. This observation is also somewhat misleading since different repairs were used for each specimen, and it is not totally clear whether the differences in rotation capacity are caused by the dynamic testing or the differences in repair procedures. This study provides some evidence that dynamic testing reduces the plastic rotational capacity of repaired pre-Northridge connections, but the supporting evidence is mixed and not completely clear.

The next eight specimens of the table were part of a comprehensive Japanese study (AIJ, 1997) of connection performance, and one to one comparisons were possible as shown in the table. In general, it was noted that the plastic rotation was not adversely affected by dynamic strain. Two of the eight specimens developed larger plastic strains than the static tests, and two of the eight dynamic tests developed somewhat smaller plastic rotations. The Japanese research focuses on "skeleton curves" and accumulated ductility and energy dissipation, and when these terms are considered, they conclude that the dynamic tests provide slightly better seismic performance than do comparable static tests. These tests demonstrate a significant temperature build-up due to the heat development caused by plastic deformation during the dynamic tests. Yielding is always an irreversible process which develops heat in the specimen. With static testing, the heat has adequate time to dissipate, but the dynamic testing does not provide the time needed for the heat loss.

The final four specimens of Table 4-7 are also Japanese (Takanashi, 1997) connection tests, but these tests had the combined goal of examining temperature effects as well as dynamic effects. Six dynamic tests were completed, but only four had direct one to one comparisons at static loading, and these four dynamic specimens are included in the table. These tests showed that dynamic loading did not have a big effect on tests performed at room temperature. Some dynamically loaded specimens tolerated a larger number of cycles at the maximum deformation than did statically loaded specimens. Dynamic loading had a large effect on specimens tested at low temperature.

A number of tests and analyses have been completed, and the results of these studies lead to relatively consistent conclusions. Dynamic loading can clearly reduce the ductility and inelastic performance of connections, but the dynamic strain rate achieved during earthquake loading is sufficiently slow that the dynamic effects are clearly second-order effects. As a result, dynamic strain rates are not considered important in evaluating connection ductility during earthquake loading on ductile connections unless temperatures are low or unless strain rates are significantly larger than those discussed here. Dynamic loading may be detrimental to connection performance for connection systems with intermediate ductility.

## 5. FIELD-BOLTED CONNECTIONS FOR STEEL MOMENT FRAMES

### 5.1 Introduction

Chapters 1 through 4 focused on welded flange connections that could be approximated as rigid connections in the frame analysis. In addition, those connections were designed to develop the full plastic capacity of the beam, and they usually developed shear yielding in the panel zone. The behavior of those connections was dominated by the yield mechanisms and failure modes. These modes and mechanisms were considered for each connection type, and equations were developed to predict the resistance associated with each mode and mechanism. The conditions needed to balance the connection behavior to assure good connection performance were also investigated.

The evaluation and analysis methods used in Chapters 1 through 4 are continued in Chapter 5, but field-bolted connections are considered. These alternate connections sometimes cannot be approximated as rigid connections, and they sometimes may not develop the full plastic capacity of the connection. The yield mechanism and failure modes of these connections are sometimes different from those discussed in earlier chapters and often more complex. Nevertheless, large plastic rotations and good seismic performance can often be achieved with these connections. Chapter 5 will focus on the conditions necessary to achieve this good seismic performance.

### 5.2 PR Connections

The poor performance of the welded-flange-bolted-web pre-Northridge connection caused many engineers to consider alternate connections. These alternatives make increased use of bolting, and virtually all of them qualify as partially restrained (PR) connections under some conditions. PR connections may be partial stiffness connections, partial strength connections, or both. Partial stiffness PR connections usually have significant rotation within the connection before the connection develops its ultimate resistance. Flexibility and stiffness of PR connections vary greatly as illustrated in Figure 5-1. The figure shows the experimental moment-rotation envelope for four different connections with similar beam size but vastly different connection stiffness. Some of these connections are clearly partial strength connections, since they do not develop the full plastic capacity of the beam. The horizontal axis of this curve represents a pin connection, since the rotation increases freely with no rotational resistance. The vertical axis of this figure represents an idealized, fully restrained connection in that resistance develops with no elastic rotation. Real connections seldom achieve either of these idealized goals, as shown by the four experimental curves in the figure. Instead, they invariably develop some rotational resistance and some connection rotation, but the strength and stiffness of the connections vary widely.

Connection stiffness has considerable impact upon the structural behavior. Stiff connections such as the welded-flange-bolted-web connection shown in Figure 5-1 can usually be modeled as a rigid connection with no connection deformation. Nearly pinned connections such as the web-angle connection can normally be modeled as a pin connection, which develops no rotational resistance, with little loss of accuracy or reduction in the stability of the structure. However,

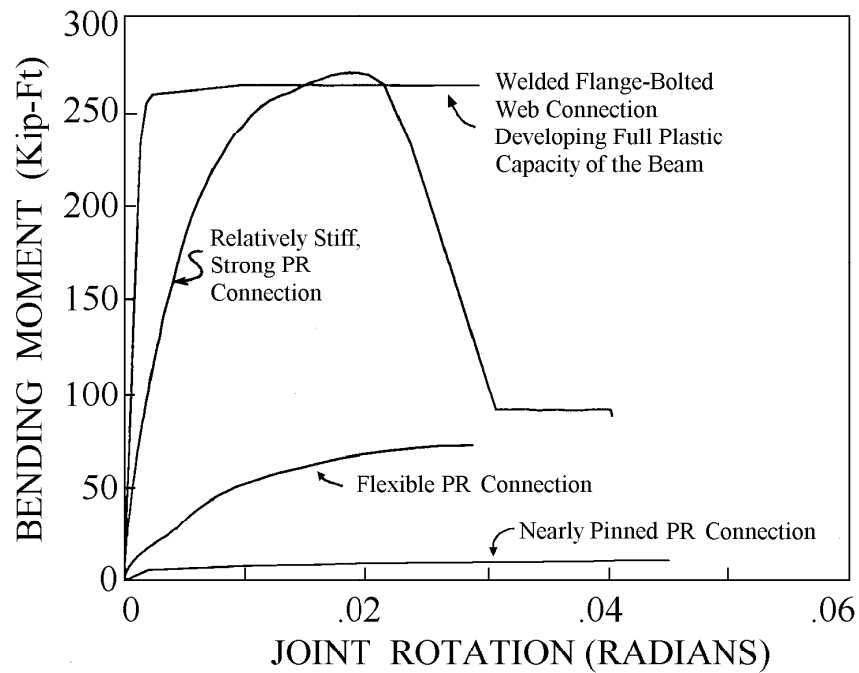


**Figure 5-1 Relative Strength and Stiffness of PR Connections**

partial stiffness connections with intermediate stiffness require a special computer model such as that illustrated in Figure 5-2. In this model, rotational spring stiffness of the joints must be considered in addition to the member stiffness of the beam and column. Because of the importance of the rotational spring stiffness,  $k_s$ , and the increased difficulty associated with completing a frame analysis such as illustrated in Figure 5-2, connections that require this special analysis are separated from those that do not. A wide range of connections can be categorized as PR connections. In this chapter, non-composite PR connections are discussed, and the connections are categorized as stiff PR connections, intermediate stiffness PR connections, and flexible PR alternatives. This division is used because somewhat different design and analysis procedures can be used for the different stiffness ranges. Stiff PR connections seldom require special analytical modeling such as illustrated in the figure. Nevertheless, some consideration of the connection stiffness is needed to assure that this simplification is valid. Flexible PR connections will always require special analysis such as depicted in Figure 5-2, or in many cases, their stiffness can conservatively be ignored. Intermediate stiffness connections may or may not require the special analytical modeling depending on the special conditions and relative stiffness of the connection.

This categorization, based upon the connection stiffness, is determined from experimental results combined with the simple analytical model illustrated in Figure 5-3. Figure 5-3 shows two frame subassemblies loaded with the same story shear with boundary conditions permitting moment frame sway deformation. The left frame has rigid (FR) connections, and the right frame has the same beam and column members with flexible PR connections and a connection rotational spring stiffness,  $k_s$ . The column deflections,  $\Delta$ , for both frames were computed based upon the elastic stiffness of the beam ( $EI_b$ ) and column ( $EI_c$ ) and the centerline member lengths.

For the FR connection,

$$\Delta_{FR} = \frac{V_c h}{12} \left\{ \frac{h^2}{EI_c} + \frac{L^2}{EI_b} \right\} \quad (5-1)$$

and for the PR connection

$$\Delta_{PR} = \frac{V_c h}{12} \left\{ \frac{h^2}{EI_c} + \frac{L^2}{EI_b} \right\} + \frac{V_c h^2}{2 k_s} \quad (5-2)$$

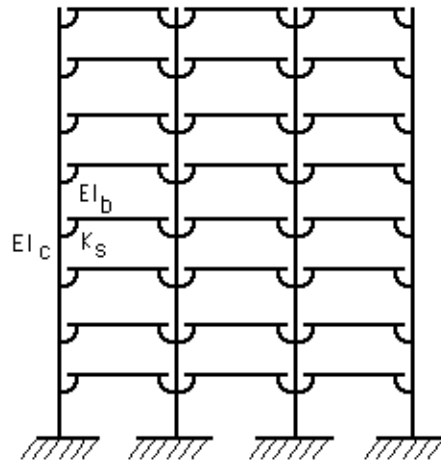


**Figure 5-2 Consequence of Connection Flexibility on Frame Behavior**

In general, it is not necessary to consider the spring stiffness in the structural analysis if it can be shown that the PR connection stiffness does not excessively increase frame story drifts or deformations. Therefore,  $\Delta_{FR}$  and  $\Delta_{PR}$  were compared to determine the relative magnitudes of these deflections. The increased deflection that is tolerable with PR connections without the more refined analysis is arbitrary, but a 10% increase was used as an approximate limit. Equation 5-3 defines the rotational spring stiffness necessary to ensure that PR connection frame story drifts are no more than 10% larger than story drifts in a rigid frame connection with the same loading and member properties.

$$k_s \geq \frac{60}{\left\{ \frac{h}{EI_c} + \frac{L^2}{h EI_b} \right\}} \quad (5-3)$$

It can be seen that the required stiffness depends upon the story height,  $h$ , and column spacing,  $L$ , in addition to the beam and column stiffness. This equation is used to evaluate approximately the stiffness of connections discussed in this chapter. Those connections that clearly satisfy this inequality are classed as full stiffness PR connections, while those that do not

remain as partial stiffness connections. The connections categorized as intermediate stiffness PR connections may or may not qualify as full stiffness connections according to Equation 5-3, depending upon the design details.

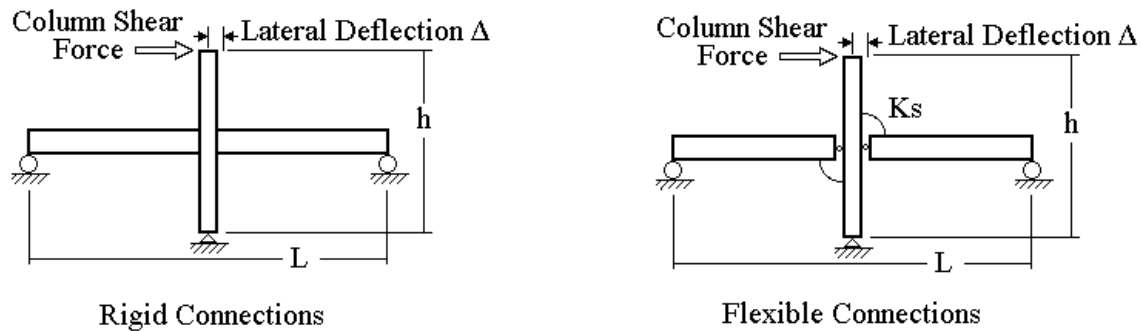


**Figure 5-3 Simplified Deflection Analysis for FR and PR Connections**

### 5.2.1 Modes of Failure, Yield Mechanisms, and Rotational Capacity of PR Connections

Seismic design requires a balance between the strength, stiffness, and ductility. The required strength, stiffness, and ductility (or the seismic demands) may vary widely depending upon the structural system and the local seismic hazard, and these demands are established by studies (Foutch, 2000; Krawinkler, 2000) that are beyond the scope of this report. However, the capacities are a major focus of this state of the art report, and there is a strong interrelation between the strength, stiffness, and ductility capacity of individual PR connections and the failure modes and yield mechanisms of each connection. Ductility is assured by verifying that a yield mechanism is fully developed before a brittle failure occurs. Given reliable information regarding the geometry of the connection and the material properties of members and connecting elements, ductile connection performance requires:

- accurate predictions of the yield mechanism and the mode of failure for each connection type,
- reliable estimates of the resistance associated with each mechanism and mode of failure, and
- reliable estimates of the ductility and deformational capacity of the connection for these various failure modes and yield mechanisms.

As with the welded flange connections, these diverse goals are achieved by examining yield mechanisms and failure modes for each connection type, and then predicting the resistance associated with each mechanism and each failure mode. A yield mechanism, which is capable of sustaining significant inelastic deformation, will provide ductile performance if its resistance is sufficiently smaller than the resistance associated with all failure modes that produce brittle failures. The failure mode, which is lower than all other failure modes, is the critical failure mode for the connection. However, closely spaced failure modes may jump ahead of one another because of the variability inherent in construction. The ductility and deformation capacity that can be achieved is a function of the yield mechanism and the critical failure mode for the connection, as well as the proximity of the resistances for these two conditions. In comparing failure modes and yield mechanisms, it is important to recognize that yielding or

failure may occur at different locations, and thus the comparisons of resistance must be normalized to a standard location on the connection. In this report, these comparisons will be made at the face of the column. Many different yield mechanisms and failure modes are possible for each connection type, and so a number of simple yet thorough equations are needed for each connection. These equations were developed from the analysis of the connection behavior and comparison of predicted behavior with experimental results. Basic concepts of force path, equilibrium, and elementary mechanics were used in the development of the models, but the tests of the reliability of the models were based upon their comparison to experimental results. The experimental results used for these comparisons include more than 850 connection experiments (Roeder, et al., 2000; Coons, 1999) performed prior to the SAC program, as well as the connection tests from the SAC Steel Project.

The ductility achieved with each connection type depends upon the yield mechanism and failure mode of the individual connection. Predicted ductility must also be determined for each individual case, and the ductility estimates are established based upon comparison with experimental results. As with the welded flange connections discussed in Chapters 2, 3, and 4, ductility is expressed in terms of two plastic rotations. The first plastic rotation,  $\theta_p$ , is the plastic rotation which can be achieved with a given yield mechanism and connection type without a sudden loss in resistance or deterioration in the behavior of the connection. The second plastic rotation,  $\theta_g$ , is the plastic rotation at which the connection is expected to lose its capacity to support gravity loads. These rotations are illustrated for a PR connection in Figure 5-4.

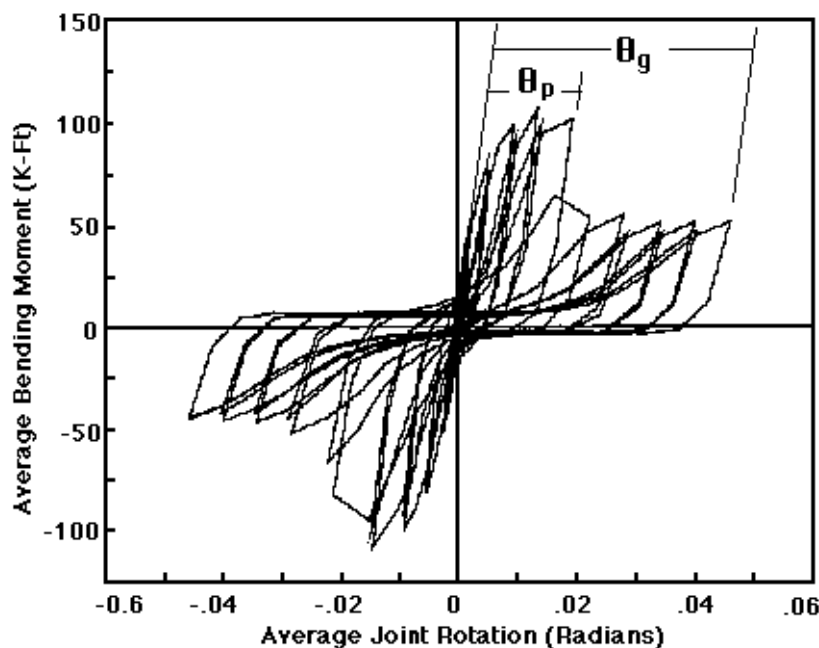


**Figure 5-4 Comparison of the Plastic Rotations,  $\theta_p$  and  $\theta_g$**

As noted in Chapters 2 and 3,  $\theta_p$  is more accurately determined than is  $\theta_g$ . This occurs because few experimental studies were conducted to deformation levels large enough to cause a



Simplified design models are developed for each of the major connection types. These models are developed from basic concepts of engineering mechanics, and the development is coupled with an evaluation of experiments performed on each connection type. Rotational limits are developed for preferred or controlling yield mechanisms, and they are based upon the rotations achieved in the experimental studies for connections which exhibit these yield mechanisms. Balance conditions are defined to ensure that connections are designed to achieve these controlling mechanisms. The rotational limits are average values based upon the available experimental data. Least squares regression analyses are performed on the experimental rotations to obtain unbiased estimates of the mean rotational capacity. The plastic rotation,  $\theta_p$ , is directly based upon experimental results, and standard deviations,  $\sigma_p$ , are computed. The plastic rotation at which loss of gravity load resistance is expected,  $\theta_g$ , and its standard deviation,  $\sigma_g$ , are more often based upon judgment and extrapolation of experimental results, since few experiments were conducted having deformations of the magnitude required for this level of behavior. As a result,  $\sigma_g$  values are often based upon the variability noted in  $\theta_p$ , and sometimes are not stated because of this limitation.

### 5.3 Stiff PR Connections

Connection resistance and stiffness are fundamentally different. Nevertheless, stiffer connections are usually also stronger connections, since they develop larger connection bending moments at smaller connection rotations. Stiff PR alternatives such as the extended-end-plate and the bolted-flange-plate connections are often stiff enough that their behavior is very close to that achieved by rigid connections. Further, they are often strong enough that they approach or achieve the full plastic capacity of the member. As a result, they may often be designed and analyzed by procedures similar to those used with FR connections. These stiff alternatives will be discussed first. Some engineers may prefer to class these stiff PR connections as FR connections, but it must be recognized that these connections can be approximated as FR connections only if certain design conditions are met. As a result, they are classed as stiff PR connections in this report.

#### 5.3.1 Extended-End-Plate Connections

The extended-end-plate connection illustrated in Figure 5-6 is a stiff, strong, PR connection, which has been used in steel structures for many years. More than 150 experiments have been performed on these connections with mixed results. Most of these past experiments are not directly related to seismic design in that they evaluate monotonic loading only, or they utilize members or elements which cannot develop significant inelastic deformation.

Several studies (Tsai and Popov, 1988; Johnstone and Walpole, 1981; Whittaker and Walpole, 1982; Murray and Kukreti, 1988; Sherbourne, 1961; Murray and Meng, 1996) focused on the seismic behavior of these connections. In general, the hysteretic behavior of end-plate connections can be good or relatively poor depending upon the mode of failure. Figures 5-7, 5-8, and 5-9 show typical hysteresis curves obtained during past cyclic load tests. These three experiments are for members of comparable, modest size, but different yield mechanisms and failure modes were achieved in each test. Figure 5-7 shows the moment-rotation curve where the bolts between the end-plate and the column face fractured. Figure 5-8 is the moment-rotation

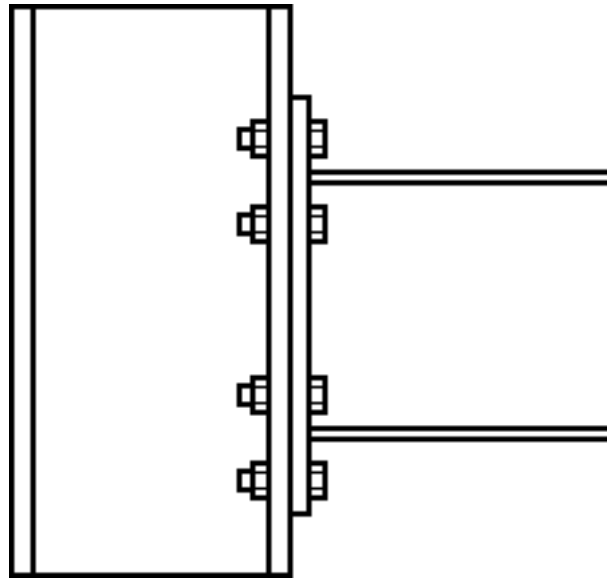


**Figure 5-6 Typical Extended-End-Plate Connection**

behavior that occurs when yielding occurs in the end-plate. Figure 5-9 shows the good energy dissipation and inelastic performance achieved if the connection is strong enough to ensure formation of a plastic hinge in the beam. This specimen has a stiffened end-plate, which ensured beam yielding. Comparison of these figures shows that relatively little ductility is achieved if bolt failure occurs, but large ductility can be developed if flexure of the end-plate (Figure 5-8) or plastic bending of the beam (Figure 5-9) controls the capacity. End-plate connections are often categorized in terms of thick end-plates or thin end-plates. Thin end-plates are those where the plate is thin enough to have yielding of the plate, and thick end-plates are those that develop yielding in the members. While thin end-plates may provide good ductility and inelastic deformation capacity, they do not develop the full plastic capacity of the beam. The above observations suggest that thick end-plates have desirable attributes for seismic design. Stiffened end-plates are also used to ensure that excess yield and deformation of the end-plate does not occur. Ideally stiffened end-plate connections result in flexural yield of the member and good hysteretic behavior.

Many other failure modes have been noted in past end-plate connection experiments. Some experiments produced energy dissipation through local flexural yielding of the column flange. Other failure modes are bolt failure (including prying forces) and tensile fracture of the weld between the end-plate and the beam. Fillet welds have been used to join the beam and end-plate (Johnstone and Walpole, 1981; Whittaker and Walpole, 1982), and a number of fillet weld failures with poor connection performance were noted. Complete penetration welds have also been tested, and it has been suggested (Murray and Meng, 1996) that good performance is achieved with CJP welds if the flange weld access hole is eliminated. This flange weld is a shop weld, and it can always be completed in a flat, downhand weld position. Fracture of the welds between the beam and the end-plate may result in significantly less ductility, energy dissipation, and inelastic rotational capacity than the other failure modes. The plastic rotation and deformation achieved when tensile bolts fail may be quite limited, and these capacities depend upon a number of factors such as the prying force, the bolt grip, and thread length of the bolt.

These failure modes are illustrated in Figure 5-10. There may be interrelation and coupling between these different behavioral modes.

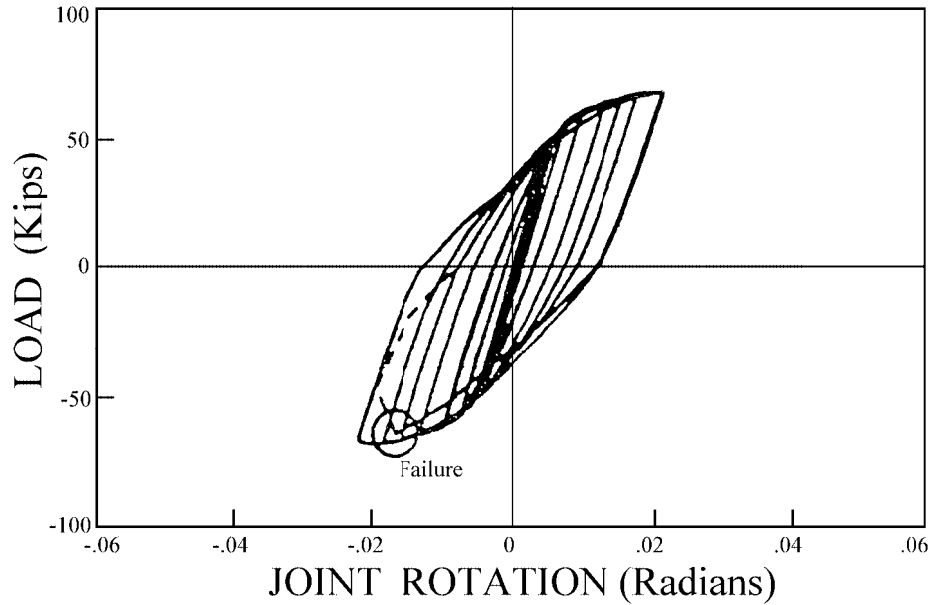


**Figure 5-7** Moment-Rotation Behavior for Extended-End-Plate Connection With Bolt Fracture

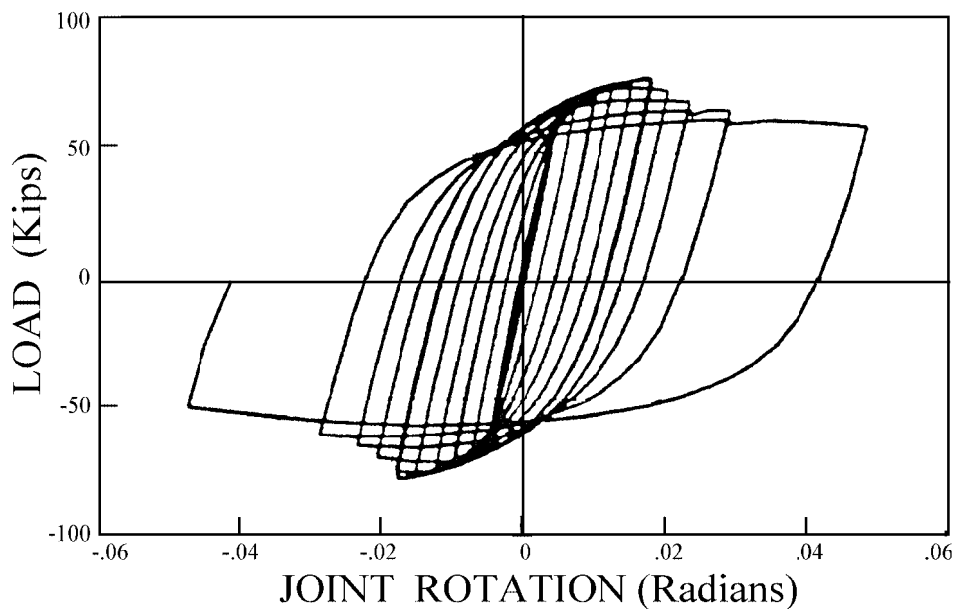


**Figure 5-8** Moment-Rotation Behavior for Extended-End-Plate Connection With Plastic Deformation in the End-Plate

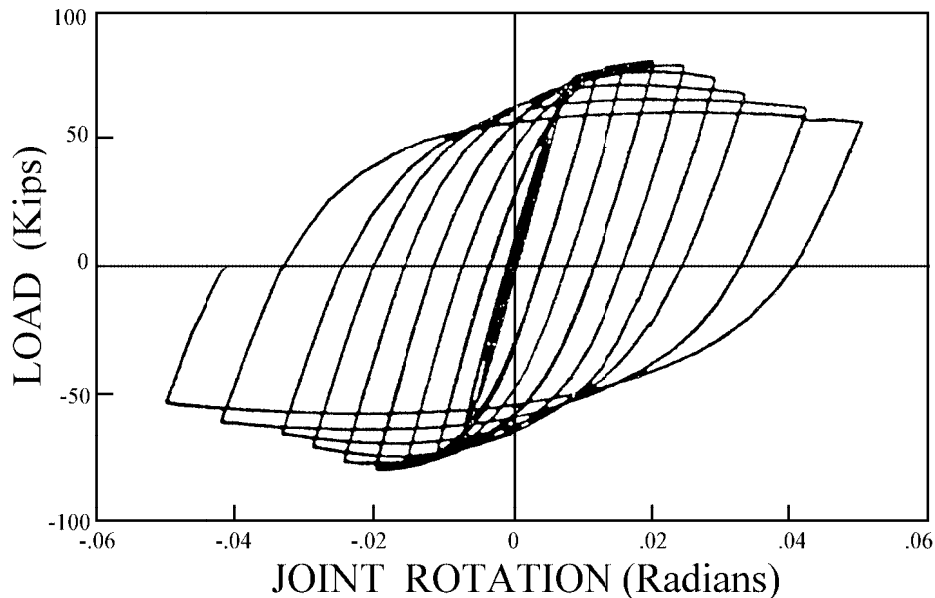


**Figure 5-9 Moment-Rotation Behavior for Stiffened Extended-End-Plate Connection With Plastic Deformation in the Beam**

AISC proposes methods (AISC, 1994; Murray, 1990) for the design and analysis of end-plate connections, however review of references (Tsai and Popov, 1988; Johnstone and Walpole, 1981; Whittaker and Walpole, 1982) suggests that this method is not always adequate for assuring good seismic performance. The AISC method does not consider the plastic rotation of the connection, nor does it always restrict the use of failure modes and yield mechanisms that may result in reduced rotational capacity. Further, there is room for debate (Coons, 1999; Murray and Sumner, 2000) as to whether some equations used in the AISC procedure are the most accurate indicators of yield and failure resistance.

It must be recognized that the behavior noted in the extended-end-plate connection qualifies it as among the most complex of all connections. The complexity of the prying forces in the bolts and the large number of failure modes are attributes which induce much of this complexity. The yield mechanisms that are possible with extended-end-plate connections are illustrated in Figure 5-10. Yield mechanisms include flexural yielding of the beam, flexural yielding of the end-plate, and shear yielding of the panel zone of the column. Column flange, web, and stiffener deformations and buckling deformations may contribute to the connection rotational capacity, but they are not illustrated in the figure because they are not likely to be a dominant or reliable source of plastic rotation. Figure 5-5 clearly shows that plastic rotational limits depend upon the yield mechanism and the failure mode. The yield mechanism and failure modes are dependent upon the geometry and material properties of the members and components of the connection.

As part of the SAC Program, eleven experiments were performed (Murray and Sumner, 2000) on extended-end-plate connections to address these yield mechanisms and failure modes and to finalize design recommendations. Table 5-1 summarizes the results of these tests. Previous discussion has noted that significant plastic rotation could be achieved with extended-end-plate connections which yield through flexural yielding of the beam and through plastic

bending of the plate, and these two yield mechanisms were emphasized in these tests. Shear yielding of the panel zone is also an attractive method of achieving plastic rotations. However, as will be discussed later in this section, panel zone yielding is more difficult to predict with the extended-end-plate connection than it is with the welded flange connections described in Chapters 2, 3, and 4. The behavior of the extended-end-plate connection is severely complicated by the many design options (for example, stiffened or unstiffened, 4-bolt or 8-bolt) possible with the extended-end-plate connections. Some of these options are illustrated in Figure 5-11, and these options were another focus of the experimental research. The experiments performed during the SAC Phase 2 research (Murray, et al., 2000) were intended to determine which options provided predictable behavior and good seismic performance, and to develop design guidelines for the extended-end-plate connection.

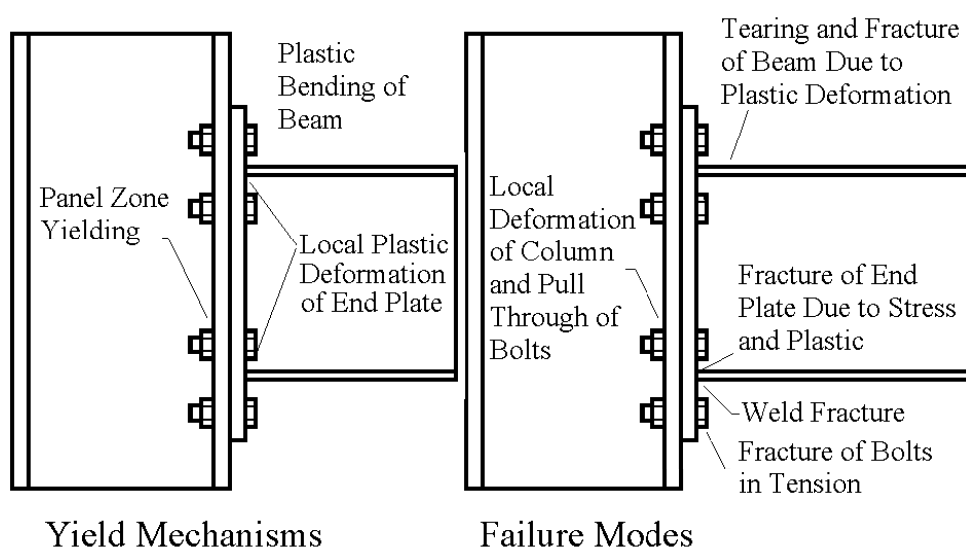


**Figure 5-10 Primary Yield Mechanisms and Common Failure Modes for Bolted Extended-End-Plate Connections**

The extended-end-plate connection is limited by the tensile capacity of the bolts. The stiffened and unstiffened 4-bolt configurations are suitable for smaller beams, but the 4-bolt configurations generally do not provide enough tensile capacity to develop the full plastic bending capacity of heavier beam sections. As a result, 4-bolt-wide and the stiffened 8-bolt configuration are intended for deeper beams and beams with heavier flanges. The 4-bolt-wide configuration has eight bolts per flange as shown in Figure 5-11, but “4 bolt wide” is a commonly used descriptor of that configuration.

Since the tensile force is a limiting factor for these connections, prying forces in the bolts are a major concern. Prying forces can be large with the extended-end-plate connection, and research has shown that prying forces are difficult to predict with accuracy. However, the research also shows that prying forces remain negligibly small (Murray and Sumner, 2000) with thick end-plate designs. Thick end-plates remain essentially elastic throughout large inelastic

**Table 5-1 Summary Table of Extended-End-Plate Connection Tests**

Specimen Identification	General Information	Beam (Column) Sizes	Tensile Bolts Per Flange & End-plate Thickness	Plastic Rotation @ Initial Failure	Plastic Rotation due to Panel Zone	Plastic Rotation due to End-plate	Failure Mode	Initial Failure Moment / $M_p$
1-Thick	Four bolt unstiffened	W24x68 (W14x120)	4 --1 1/4 " A490 w/ 1 1/2" plate	0.044	0.008	0.004	Primarily Flange Buckling	1.18
1-Thin	Four bolt unstiffened - thinner end-plate than 1 - Appears that most deformation is in end pl	W24x68 (W14x120)	4 --1 1/4 " A325 w/ 1 1/8" plate	0.02 (0.031 on first excursion)	0.005	<b>0.01</b>	Tensile Bolt Fractures	1.12
2-Thick	Stiffened 8 bolt (4 rows of 2 bolts per flange)	W30x99 (W14x193)	8 --1 1/4 " A490 w/ 1 3/4" plate	0.040	0.003	0.000	Primarily Flange Buckling	1.15 @ face 1.07 @ end of stiff
2-Thin	Stiffened 8 bolt (4 rows of 2 bolts per flange)	W30x99 (W14x193)	8 --1 1/4 " A325 w/ 1" plate	0.049	0.007	0.004	Primarily Flange Buckling	1.22 @ face 1.15 @ end of stiff
3-Thick	Stiffened 8 bolt (4 rows of 2 bolts per flange) - primary yield in beam at end of stiffener - little panel zone yield	W36x150 (W14x257)	8 --1 1/4 " A490 w/ 2 1/2" plate	0.045 not balanced SAC cycles	0.006	0.002	Primarily Flange Buckling	1.23 @ face 1.14 @ end of stiff
3-Thin	Stiffened 8 bolt (4 rows of 2 bolts per flange)	W36x150 (W14x257)	8 --1 1/4 " A325 w/ 1 1/4" plate	0.011	0.004	0.001	Bolt Fracture	1.03 @ face 0.97 @ end of stiff
4-Thick	Four bolt wide (8 bolts per flange) unstiffened	W30x99 (W14x193)	4 --1 1/4 " A325 w/ 1 1/4" plate	0.031	0.007	0.001	Bolt Rupture and End-plate Tear	1.13
4-Thin	Four bolt wide (8 bolts per flange) unstiffened	W30x99 (W14x193)	4 --1 1/4 " A325 w/ 1" plate	0.021	0.010	0.010	Bolt Rupture and End-plate Tear	1.05

**Table 5-1 Summary Table of Extended-End-Plate Connection Tests (continued)**

5-Thick	Four bolt wide (8 bolts per flange) unstiffened	W36x150 (W14x257)	4 -1 <sup>1</sup> / <sub>4</sub> " A325 w/ 1 <sup>3</sup> / <sub>8</sub> " plate	0.019	0.008	0.009	Bolt Rupture and End-plate Tear	1.03
5-Thin	Four bolt wide (8 bolts per flange) unstiffened	W36x150 (W14x257)	4 -1 <sup>1</sup> / <sub>4</sub> " A325 w/ 1 <sup>1</sup> / <sub>4</sub> " plate	0.018	0.007	0.008	Bolt Rupture and End-plate Tear	1.02

## Notes:

1. This summary is obtained from Murray and Sumner (2000).
2. Note that the numbering is not the same as used by Murray and Sumner (2000). This numbering was used because the primary difference in specimens is that Thin specimens are designed for thin plate behavior (plate deformation and bolt fracture) while Thick specimens are designed to approach thick plate behavior (plastic bending of the beam).
3. Bending moment is at the face of the column.

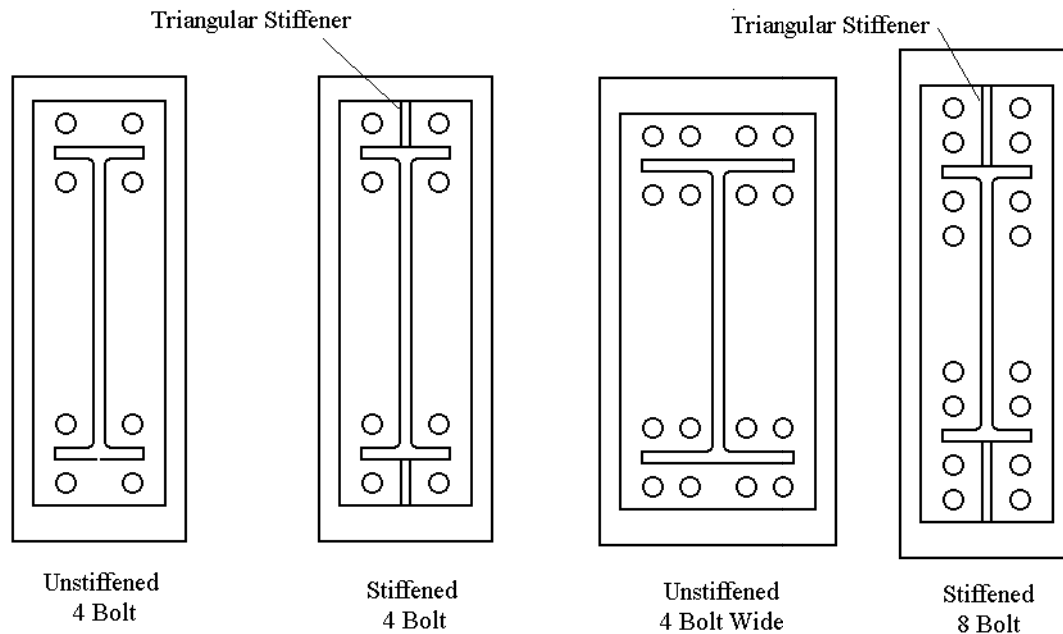


**Figure 5-11 Typical Extended-End-Plate Configurations**

rotations. On the other hand, prying forces can be large and relatively unpredictable with thin end-plates. Thin end-plates may develop significant plastic rotation, but they are unsuitable for seismic design because of their lack of control over prying forces and the potential for tension bolt fracture when large prying forces occur. As a result, design recommendations in this report are provided only for thick end-plates. Additional research is needed before thin end-plates are suitable for seismic design.

Figure 5-12 shows a moment-rotation curve for an unstiffened 4-bolt extended-end-plate connection with a W24 beam. The specimen attained significant plastic rotation of approximately 0.04 radians, and ultimately the test was stopped with severe local buckling of the beam flanges. This W24x68 section is approaching the largest section that can effectively be used with an unstiffened 4-bolt extended-end-plate connection. Therefore, the stiffened end-plate and unstiffened 4-bolt-wide configurations were tested to evaluate the extended-end-plate connections for larger beams. Table 5-1 shows that the stiffened end-plate details also provided relatively good ductility with the thick plate designs, but the unstiffened 4-bolt-wide configuration provided erratic performance. The 4-bolt stiffened connection offers only limited advantages over the 4-bolt unstiffened connection, and so no design procedure is proposed for that connection here. As a result, design methods are proposed only for the 8-bolt stiffened connection and the unstiffened 4-bolt configuration.

Examination of past experimental research results shows that extended-end-plate connections may use relaxed panel zone and continuity plate design requirements over those required for most other full-strength connections. The extended-end-plate distributes the beam flange forces over a greater effective beam depth and over a greater length of the column flange as illustrated in Figure 5-13. As a result, the continuity plate requirement should be based upon the combined

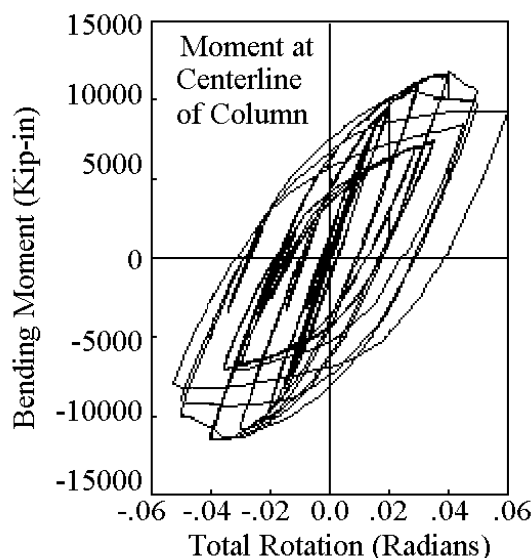


**Figure 5-12 Moment-Rotation Curve for an Unstiffened 4-Bolt Extended-End-Plate Connection**

column flange and end-plate thickness because of this effect. Therefore, different continuity plate requirements are defined for the extended-end-plate connection than for the connections discussed in Chapters 2, 3, and 4. Past experiments (Coons, 1999) also demonstrate that it is conservative to use the effective depth,  $d_{eff}$ , as the distance from the edge of the end-plate to the opposite beam flange as shown in the figure in the evaluation of panel zone yielding. These factors are reflected in the yield mechanism and failure mode equations provided in Tables 5-2, 5-3, and 5-4. Table 5-2 shows yield mechanism calculations for both the 4-bolt unstiffened end-plate and the 8-bolt stiffened end-plate. Table 5-3 provides the equations for the failure modes of the 4-bolt unstiffened end-plate connection, and Table 5-4 shows the failure mode equations for the 8-bolt stiffened end-plate configuration. All three tables are for connections designed as thick plate connections where the end-plate is designed to be strong enough to assure yielding in the beam, since this has been shown to provide reasonable ductility in past experiments. End-plate yielding is evaluated by yield line theory in Tables 5-3 and 5-4, however, the 4-bolt unstiffened equations are developed from a more direct application of yield line theory, while the 8-bolt stiffened connection equations are more empirical in their development. In both the 4-bolt unstiffened and 8-bolt stiffened end-plate connections, thick plate behavior is assured by the balance conditions in the last line of Table 5-2. Significant differences in equations for these two connection configurations result in the separate failure mode tables for unstiffened 4-bolt and stiffened 8-bolt connections (Tables 5-3 and 5-4). For stiffened end-plates, the minimum thickness of the stiffener must be equal to the thickness of the beam web. The design method for both the stiffened and unstiffened end-plate require that the bolt pattern be symmetric about both beam flanges and about the beam itself. Further, the end-plate width should not extend more than 1" beyond the tips of the beam flanges for both the stiffened and unstiffened configurations. Figure 5-14 defines the geometry needed to use some of the equations in these tables.

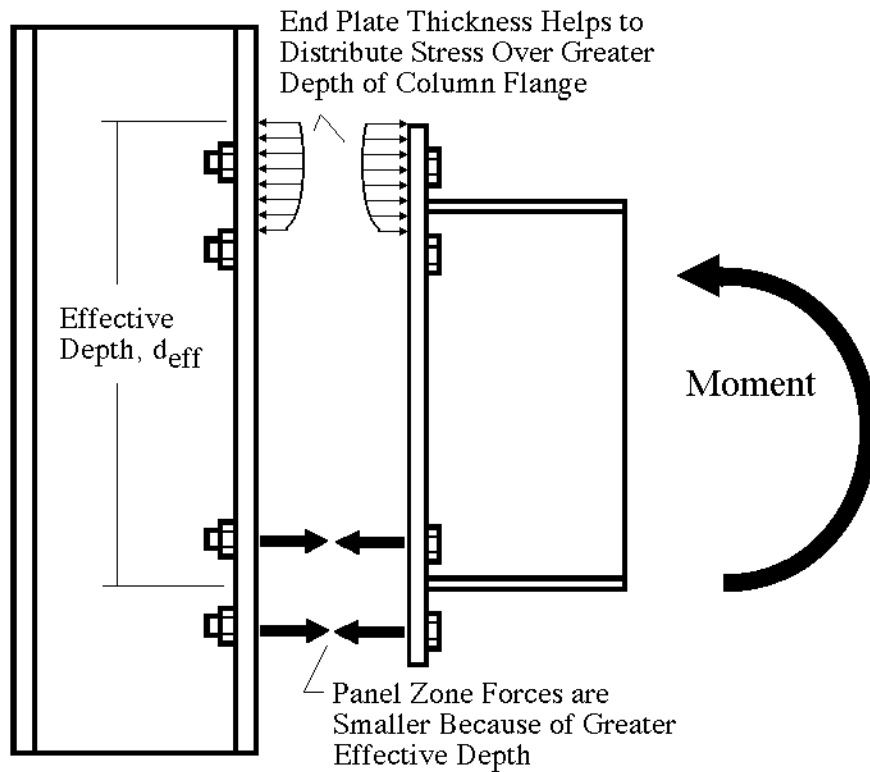


**Figure 5-13 Schematic of Bending Moment Flange Force Distribution for Extended-End-Plate Connection**

The panel zone yield balance conditions for the unstiffened end-plate are similar to those derived for the unreinforced pre-Northridge and post-Northridge welded flange connections in Figure 2-11, and those for the stiffened end-plate are comparable to the haunch connection in Figure 3-14. However, the relative importance of panel zone yielding may be different for the extended-end-plate connection than for the welded flange connections described in Chapters 2 and 3, because the local stiffness at the beam flange weld is dramatically different.

The plastic rotations obtained with the thick plate, 4 bolt unstiffened and 8 bolt stiffened connections were consistent with the rotations obtained in past thick plate extended-end-plate connection tests and illustrated in Figure 5-5. The plastic rotations that can be achieved with the extended-end-plate are quite large, but they are strongly dependent upon the beam depth as illustrated in Figure 5-5. A regression analysis of test results shows that the plastic rotational capacity is:

$$\theta_{p\text{mean}} = 0.0607 - 0.0013 d_b, \quad (5-4a)$$

and the standard deviation is

$$\sigma_p = 0.006 - 0.0003 d_b. \quad (5-4b)$$

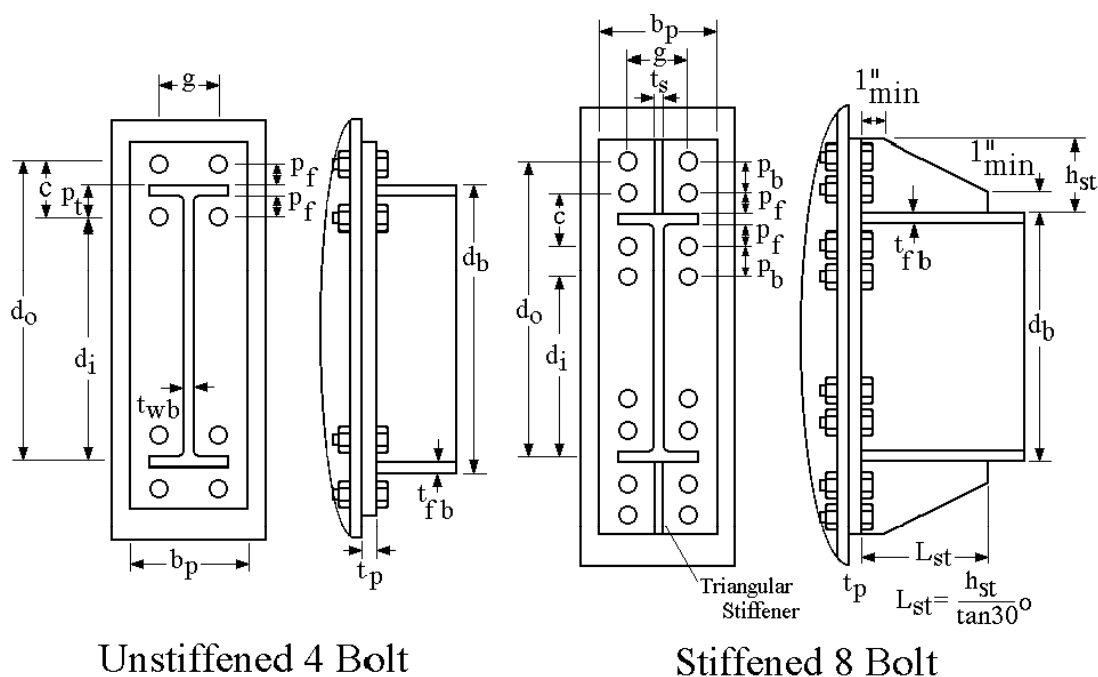


**Figure 5-14 Geometry Needed to Define End-Plate Resistance Models**

The rotation and standard deviation are in radians, and the beam depth is in inches. It should be noted that the number of test results for the extended-end-plate connection are quite large, and so the standard deviation is small compared to that achieved with other connection types. Not one extended-end-plate connection was continued to a deformation, which would allow rational determination of the maximum rotation for supporting gravity loads,  $\theta_g$ . Further, some failure modes of the extended-end-plate connection do not offer the same redundancy for the gravity load support as noted for some other connections. In particular, bolt fracture would cause a rapid loss in both moment capacity and gravity load shear capacity. It is clear that  $\theta_g$  cannot be smaller than  $\theta_p$ , but it is difficult to ensure that  $\theta_g$  is significantly larger than  $\theta_p$ . The design procedure is intended to prevent bolt fracture, and so  $\theta_g$  is estimated as being 0.01 radians larger than  $\theta_p$ .

$$\theta_{g\text{mean}} = \theta_{p\text{mean}} + 0.01 = 0.0707 - 0.0013 d_b. \quad (5-5)$$

These rotation limits are based upon a column spacing of approximately 25 ft, and they are restricted to 4 bolt unstiffened and 8 bolt stiffened extended-end-plates, which are designed by thick plate yield mechanisms (see bottom line of Table 5-2) so that plastic bending of the beam is the dominate yield mechanism. Longer column spacing will produce somewhat larger rotations, but significantly smaller rotations are possible with significantly shorter beam spans. The tensile capacity of the bolts limit the resistance of extended-end-plate connections. As a result, the unstiffened 4 bolt end-plate is unlikely to develop the full plastic capacity for beams bigger than

the lightest W24 or W27 sections. The 8 bolt stiffened end-plate is similarly limited to modest weights of W30 and W36 sections.

**Table 5-2 Yield Mechanisms for Both 4-Bolt Unstiffened and 8-Bolt Stiffened Extended-End-Plate Connections**

Yield Mechanism	Equation to Define Yield Mechanism Moment Resistance at the Face of the Column
Flexural Yielding of Beam	for unstiffened end-plate --- $M_{\text{yield Flexure}} = S F_{yb}$ for stiffened end-plate --- $M_{\text{yield Flexure}} = S F_{yb} \frac{L - d_c}{L - d_c - 2 L_{st}}$
Panel Zone Yielding	$V_y = 0.55 d_b F_{yc} d_{eff} t_{wc}$ and $\Sigma M_{\text{yield Panel Zone}} = 0.55 d_b F_{yc} d_{eff} t_{wc} \left( \frac{L-d_c}{L} \right) \left( \frac{h}{h - d_{eff}} \right)$ Note that $t_{wc}$ includes the thickness of any doubler plate.
Balance of Panel Zone Yielding and Flexural Yielding	$0.55 d_b F_{yc} d_{eff} t_{wc} \left( \frac{L-d_c}{L} \right) \left( \frac{h}{h - d_{eff}} \right) < 0.9 (\Sigma M_{\text{yield Flexural}})$ but preferably $0.55 d_b F_{yc} d_{eff} t_{wc} \left( \frac{L-d_c}{L} \right) \left( \frac{h}{h - d_{eff}} \right) \geq \frac{2}{3} (\Sigma M_{\text{yield Flexural}})$
Requirements for Balance of Failure Modes to Ensure Ductility	$M_{\text{fail-Beam Flexure}} \leq M_{\text{fail-Bolt Tension}}$ and $M_{\text{fail-Beam Flexure}} \leq 0.8 M_{\text{fail-Plate Bending}}$ and $F_{fu} = \frac{R_y M_{\text{fail-Beam Flexure}}}{(d_b - t_{bf})} < R_{\text{All Limit States}}$ All yield and tensile stresses are expected stresses, and $R_y$ is not commonly used in this report. However, the balance conditions of the extended-end-plate required separation of failure modes to ensure ductile behavior, and $R_y$ was selected as an appropriate value for this separation.

Note: All material properties provided in this table are expected values rather than minimum values.

**Table 5-3 Failure Modes for 4-Bolt Unstiffened Extended-End-Plate Connections**

Failure Mode	Equation for Failure Moment at the Face of the Column	Related Issues
Plastic Deformation of Beam	$M_{\text{fail Beam Flexure}} = Z_b \frac{F_{yb} + F_{ub}}{2}$ <p>This moment need not exceed <math>63.3 Z_b</math> for steels with minimum specified yield stress less than 50 ksi.</p>	
Tensile Fracture of Bolts	$M_{\text{fail Bolt Tension}} = N T_b \frac{d_o + d_i}{2}$ <p>where <math>N</math> is 4 for 4 bolt unstiffened connection; <math>d_o</math> and <math>d_i</math> are the distances defined in Figure 5-14; and <math>T_b = 90 A_{bt}</math> for A325 bolts or <math>113 A_{bt}</math> for A490 bolts</p>	This model requires thick plate design so that prying forces can be neglected.
Plastic Bending of End-plate	$M_{\text{fail-Plate Bending}} = t_p^2 F_{yp} \left\{ (d_b - p_t) \left( \frac{b_p}{2} \left( \frac{1}{p_f} + \frac{1}{s} \right) + (p_f + s) \frac{2}{g} \right) + \frac{b_p}{2} \left( \frac{d_b}{p_f} + \frac{1}{2} \right) \right\}$ <p>where <math>s = \frac{1}{2} \sqrt{b_p g}</math>.</p>	Based on yield line analysis with dimensions given in Figure 5-14
Shear Yielding and Rupture of End-Plate	<p>Plate thickness, <math>t_p</math>, must satisfy</p> $\frac{F_{fu}}{2} < 0.55 F_{yp} b_p t_p$ <p>and</p> $\frac{F_{fu}}{2} < 0.45 F_{up} (b_p - 2(d_{bt} + 0.125)) t_p$	Checks to ensure that the plate is not too thin to develop yield line mechanism.
Shear Capacity	<p>Shear force, <math>V</math>, at the face of the column is based upon plastic bending at each end of beam and must be designed so that it does not control the capacity of the connection. For unstiffened 4 bolt connection</p> $\frac{2M_{\text{fail Beam Flexure}}}{L - d_c} + V_g < 3 F_v A_{bt}$ <p>where <math>F_v</math> and <math>A_{bt}</math> are the nominal bolt shear strength by AISC LRFD and the bolt area, respectively. Note that bearing capacity of bolts in bolt holes must also be checked for both the end-plate and the column flange.</p>	Equation assumes shear is carried by bolts in compression.
Column Flange Thickness Requirements for No Stiffener to the Beam Tension Flange	<p>For column flanges without stiffeners or continuity plates, the minimum thickness of column, <math>t_{cf}</math>, must be greater than</p> $t_{cf} > \sqrt{\frac{F_{fu} \left( \frac{g}{2} - k_1 \right)}{2 F_{yc} c}}$ <p>Stiffeners required to carry the unbalanced portion of the force, <math>F_{fu}</math>, if the column flange thickness does not satisfy this requirement.</p>	The dimensions are defined in the figure except that $k_1$ is distance from centerline of column web to flange toe of fillet.

**Table 5-3 Failure Modes for 4-Bolt Unstiffened Extended-End-Plate Connections (continued)**

<p>Plastic Bending Capacity of Stiffened Column Flanges</p>	<p>The column flange thickness, <math>t_{fc}</math>, must be larger than</p> $t_{fc} > \sqrt{\frac{F_{fu}}{0.8 F_{yc} Y_c}}$ <p>where</p> $Y_c = \left(\frac{c}{2} + s\right) \left(\frac{1}{\frac{b_{fc} - g}{2} + \frac{g}{2} - k_1}\right) + \left(\frac{b_{fc} - g}{2} + \frac{g}{2} - k_1\right) \left(\frac{4}{c} + \frac{2}{s}\right)$ <p>and</p> $s = \sqrt{\frac{\left(\frac{g}{2} - k_1\right) \frac{b_{fc} - g}{2}}{b_{fc} - \frac{g}{2} - k_1}} (2b_{fc} - 4k_1)$	<p>Yield line theory of bending of column flanges. Dimensions defined in Figure 5-14. <math>F_{fu}</math> is defined above.</p>
<p>Column Stiffener Requirements for Beam Compression Flange</p>	<p>No Stiffener required if</p> $F_{fu} < (6k + 2t_{pl} + t_{bf}) F_{yc} t_{wc}$ <p>Stiffeners required to carry the unbalanced portion of the force, <math>F_{fu}</math>, if the column flange thickness does not satisfy this requirement. This equation recognizes the greater spreading of beam flange force to the column web provided by the end-plate.</p>	<p><math>k</math> is the column fillet distance from the extreme fiber of column flange to the web toe of fillet.</p>
<p>Weld Fracture</p>	<p>Experiments have shown that E71T-1 Gas Shielded FCAW welds will prevent weld fracture if the following conditions are met. Flange welds are full penetration with no weld cope, but the under side of beam flange must be sealed with <math>\frac{3}{8}</math>" fillet weld. The complete penetration groove weld is placed against fillet weld seal after initial backgouging into the sealing fillet weld. Webs may be full penetration or fillet welds.</p>	
<p>Flange Buckling for both Beam and Column</p>	<p>for flange - <math>\frac{b_f}{2t_f} \leq \frac{52}{\sqrt{F_y}}</math></p>	
<p>Web Buckling for both Beam and Column</p>	<p>controlled if <math>\frac{d_b}{t_w} \leq \frac{418}{\sqrt{F_y}}</math></p>	<p>See discussion in Chapter 4</p>
<p>Lateral Torsional Buckling</p>	<p><math>L_b &lt; \frac{2500 r_y}{F_y}</math></p> <p>where <math>L_b</math> is the unsupported length.</p>	<p>Equation from AISC LRFD Seismic Provisions</p>
<p>Strong Column Weak Beam</p>	$1.1 < \frac{\sum Z_c \left(F_{yc} - \frac{P_{uc}}{A_g}\right)}{\sum Z_b \frac{F_{yb} + F_{ub}}{2}}$	<p>Significant strain hardening occurs with this connection, and the proposed limit reflects this fact.</p>

Note: All material properties provided in this table are expected values rather than minimum values.

**Table 5-4 Failure Modes for 8-Bolt Stiffened Extended-End-Plate Connections**

Failure Mode	Equation for Failure Moment at the Face of the Column	Related Issues
Plastic Deformation of Beam	$M_{\text{fail-Beam Flexure}} = Z_b \frac{F_{yb} + F_{ub}}{2} \frac{L - d_c}{L - 2L_{st} - d_c}$ <p>and</p> $F_{fu} = \frac{R_y M_{\text{fail-Beam Failure}}}{(d_b - t_{bf})}$ <p>The term <math>\frac{F_{yb} + F_{ub}}{2}</math> need not exceed 63.3 ksi for steels with minimum tensile yield stress of less than 50 ksi.</p>	The plastic moment occurs at the end of the stiffener.
Tensile Fracture of Bolts	$T_b > \frac{0.00002305 p_f^{0.591} F_{fu}^{2.583}}{t_p^{0.885} d_{bt}^{1.909} t_s^{0.327} b_p^{0.965}} + T_p$ <p>where <math>T_b = F_t A_{bt}</math></p> <p><math>F_t</math> is the minimum bolt tensile stress as defined in the AISC LRFD Specification, and <math>A_{bt}</math> is the nominal area of the bolt. <math>T_p</math> is minimum bolt pretension as defined in AISC LRFD Specification. Note that this requirement assumes there is no tension on the connection, and this additional force must be considered if present.</p>	Dimensions defined in Figure 5-14. $F_{fu}$ is defined above.
Required End-Plate Stiffener Thickness	$t_s > \frac{F_{yb}}{F_{ys}} t_{wb}$	This equation assures that the stiffener has comparable resistance to the beam web.
Plastic Bending of End-Plate	<p>For 8-bolt stiffened connection, the end plate must be designed to have a minimum thickness of</p> $t_p > \frac{0.00442 p_f^{0.873} g^{0.577} F_{fu}^{0.917}}{d_{bt}^{0.924} t_s^{0.112} b_p^{0.682}}$ <p>and</p> $t_p > \frac{0.00297 p_f^{0.257} g^{0.148} F_{fu}^{1.017}}{d_{bt}^{0.719} t_s^{0.162} b_p^{0.319}}$ <p>where <math>d_{bt}</math> is the bolt diameter.</p>	Equations are empirical but are based upon regression analysis. The dimensions are given in Figure 5-14. $F_{fu}$ is defined above.
Shear Capacity of Connection	<p>Shear force, <math>V</math>, at the face of the column is based upon plastic bending at each end of beam and must be designed so that it does not control the capacity of the connection. For 8 bolt stiffened connection</p> $\frac{2M_{\text{fail Beam Flexure}}}{L - d_c} + V_g < 6 F_v A_{bt}$ <p>where <math>F_v</math> and <math>A_{bt}</math> are the nominal shear strength by AISC LRFD and the bolt area, respectively, Note that bearing capacity of bolts on bolt holes must also be checked for both end-plate and column flange.</p>	Equation assumes shear is carried by bolts in compression.

**Table 5-4 Failure Modes for 8-Bolt Stiffened Extended-End-Plate Connections (continued)**

<p>Column Flange Thickness                  Stiffener Requirements at Beam Tension Flange</p>	<p>For column flanges without stiffeners or continuity plates, the minimum thickness of column, <math>t_{cf}</math>, is</p> $t_{fc} > \sqrt{\frac{\alpha_m F_{fu} \left( \frac{g}{2} - \frac{d_{bt}}{4} - k_1 \right)}{0.9 F_{yc} (3.5 p_b + c)}}$ <p>where</p> $\alpha_m = C_a \left( \frac{A_f}{A_w} \right)^{1/3} \left( \frac{\frac{g}{2} - \frac{d_{bt}}{4} - k_1}{d_{bt}} \right)^{1/4}$ <p><math>C_a</math> is 1.45 and 1.31 for A325 bolts and <math>F_{yp}</math> of 36 and 50 ksi, respectively. <math>C_a</math> is 1.48 and 1.33 for A490 bolts and <math>F_{yp}</math> of 36 and 50 ksi, respectively. The above values assume <math>F_{yb}</math> is 50 ksi, and modifications are required for different beam steel. If the column flange thickness does not satisfy the above requirement, tension stiffeners are required. The stiffeners must have enough capacity to reduce the flange force, <math>F_{fu}</math>, to a level where the required flange thickness is less than that provided.</p>	<p>Dimensions defined in the figure. <math>F_{fu}</math> is defined above.</p>
<p>Column Stiffener Requirements for Beam Compression Flange</p>	<p>No stiffener required if</p> $F_{fu} \frac{L - d_c}{L - d_c - 2 L_{st}} < (6k + 2t_p + t_{fb}) F_{yc} t_{wc}$ <p>Stiffeners required to carry the unbalanced portion of the force, <math>F_{fu}</math>, if the column flange thickness does not satisfy this requirement. This equation recognizes the greater spreading of beam flange force to the column web provided by the end-plate.</p>	<p><math>k</math> is the column fillet distance from the extreme fiber of column flange to the web toe of fillet.</p>
<p>Bending of Stiffened Column Flange</p>	$t_{fc} \geq t_p$ $t_{wc} \geq \frac{t_{wb}}{2}$	<p>The stiffened column flange has similar geometry to the end-plate, and a <math>t_{fc}</math> greater than <math>t_p</math> assures adequate flange resistance.</p>
<p>Weld Fracture</p>	<p>Experiments have shown that E71T-1 Gas Shielded FCAW welds will prevent weld fracture if the following conditions are met. Flange welds are full penetration with no weld cope, but the under side of beam flange must be sealed with <math>3/8</math>" fillet weld. The complete penetration groove weld is placed against fillet weld seal after initial backgouging in the fillet weld. Web welds may be full penetration or fillet welds.</p>	
<p>Flange Buckling for both Beam and Column</p>	<p>for flange - <math>\frac{b_f}{2 t_f} \leq \frac{52}{\sqrt{F_y}}</math></p>	

**Table 5-4 Failure Modes for 8-Bolt Stiffened Extended-End-Plate Connections  
(continued)**

Web Buckling for both Beam and Column	Controlled if $\frac{d_b}{t_w} \leq \frac{418}{\sqrt{F_y}}$	See discussion in Chapter 4
Lateral Torsional Buckling	$L_b < \frac{2500 r_y}{F_y}$ $L_b$ is the unsupported length.	Equation from AISC LRFD Seismic Provisions
Strong Column Weak Beam	$1.1 < \frac{\sum Z_c \left( F_{yc} - \frac{P_{uc}}{A_g} \right)}{\sum Z_b \frac{F_{yb} + F_{ub}}{2} \frac{L - d_c}{L - d_c - 2 L_{st}}}$	Based on plastic moment capacity of beam at end of stiffener

Note: All material properties provided in this table are expected values rather than minimum values.

### 5.3.2 Bolted-Flange-Plate Connections

Bolted-flange-plate connections such as shown in Figure 5-15 also have been used in steel structures for a number of years, but they are less widely used than the extended-end-plate connection. Welded variations of the flange-plate connection have also been employed, and were described in Chapter 3. Past tests on bolted-flange-plate connections are limited (Hoit, 1997), but most existing tests include cyclic loading of the connections. One study (Popov and Pinkney, 1969) reported tests on both bolted and welded-flange-plate connections. Four bolted and six welded-flange-plate connections were tested. Three of the four bolted-flange-plate tests fractured the net section of the beam flange. This net section failure invariably occurred near the last row of bolts (away from the column), since this is the region with the largest tensile force in the beam flange. The fourth specimen fractured in the flange-plate near the weld to the column face. This failure and several others appeared to be influenced by the local buckling occurring in the plate or flange. Two of these specimens had connections which were strong enough to develop significant flexural yield of the beam, but the failures still occurred in the connection as noted above.

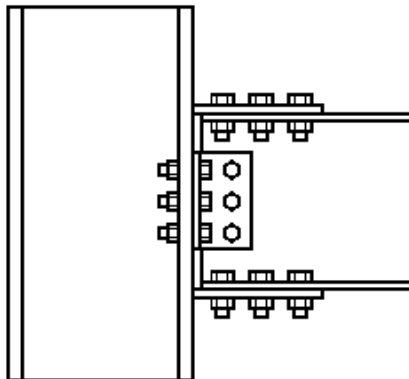


**Figure 5-15 Typical Bolted-Flange-Plate Connection**

A second study (Harriot and Astaneh, 1990) reported the results of three tests on bolted-flange-plate connections. All three of these more recent bolted-flange-plate tests fractured in the net section on the bolted flange plate in the row of bolts nearest the column, since the tensile force in the plate is largest at this location. Figures 5-16 and 5-17 present two of the moment-rotation curves, which represent the extremes of behavior achieved in this study. The beams in these tests are of modest size (W18) and are comparable to the end-plate connections shown in Figures 5-7 through 5-9. Comparison of these figures suggests that the best behavior attained with the extended-end-plate connection is comparable with that best behavior obtained with the bolted-flange-plate connection. However, the end-plate connections produce full hysteresis curves with more energy dissipation. The hysteresis curves obtained with flange-plate connections are pinched because of connector slip, local buckling, or local yield of the plate or flange around the connector. Flange-plate connections may have significant energy dissipation and rotation capacity as shown in Figure 5-17, or they may have very limited energy dissipation with small inelastic rotations as suggested by Figure 5-16. The difference again depends upon the yield mechanism and failure mode. Net section fracture of the beam or flange-plate or fracture of the flange weld appear to be common modes of failure. These modes of failure can be brittle with limited inelastic deformation capacity unless they are delayed while plastic rotation occurs at other locations.

The flange-plate connection uses a full penetration weld between the flange-plates and the column face. Thus, some of the same concerns noted with the FR connections can also be applied to the flange-plate connection, but the flange-plate welds are shop welds rather than the field welds used with connections described in Chapters 2 and 3. In addition, the flange plate connection can be more flexible than the FR bolted web-welded flange connection because of deformation of the flange-plate. The connection stiffness depends upon the size and length of the flange-plate, the number and size of bolts, and the fit of the bolts in their bolt holes. The increased flexibility may affect the frame stiffness, but it may also have an effect on connection fracture and failure mode.

The range of yield mechanisms and failure modes that is possible with bolted-flange-plate connections is illustrated in Figure 5-18. Yield mechanisms include flexural yielding of the beam, tensile yield of the flange-plate, and shear yielding of the panel zone of the column. In addition, there may be permanent deformation due to local column flange and web deformation, connection slip, and local buckling, which are not illustrated in the figure since their contribution is small. Bolt hole elongation is illustrated in the figure because it can contribute significant rotation, but it is difficult to control and design. Different amounts of plastic deformation are possible depending upon the yield mechanism, the geometry and material properties of the connection, and the relationship of the yield resistance to the failure resistance. Failure modes include net section fracture of either the flange-plate or beam flange, fracture of shear bolts between the flange-plate and the beam, elongation of bolt holes and pull out of bolts, and fracture of the weld between the flange-plate to the column. Block shear and several other modes of failure must be considered, but are not included in the figure; however, the evidence suggests that block shear will also permit modest ductility from the connection. Clearly there may be interrelation and coupling between these different failure modes and yield mechanisms, but ductile behavior is again achieved when the resistance associated with a reliable yield mechanism is sufficiently smaller than the critical failure moment.

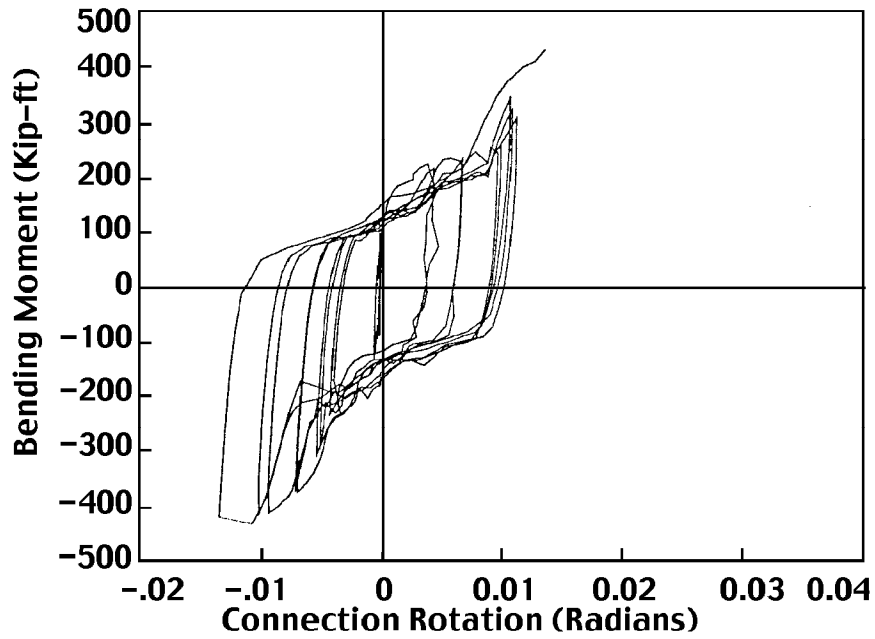


**Figure 5-16** Moment-Rotation of Bolted-Flange-Plate Connection With Limited Rotation Capacity

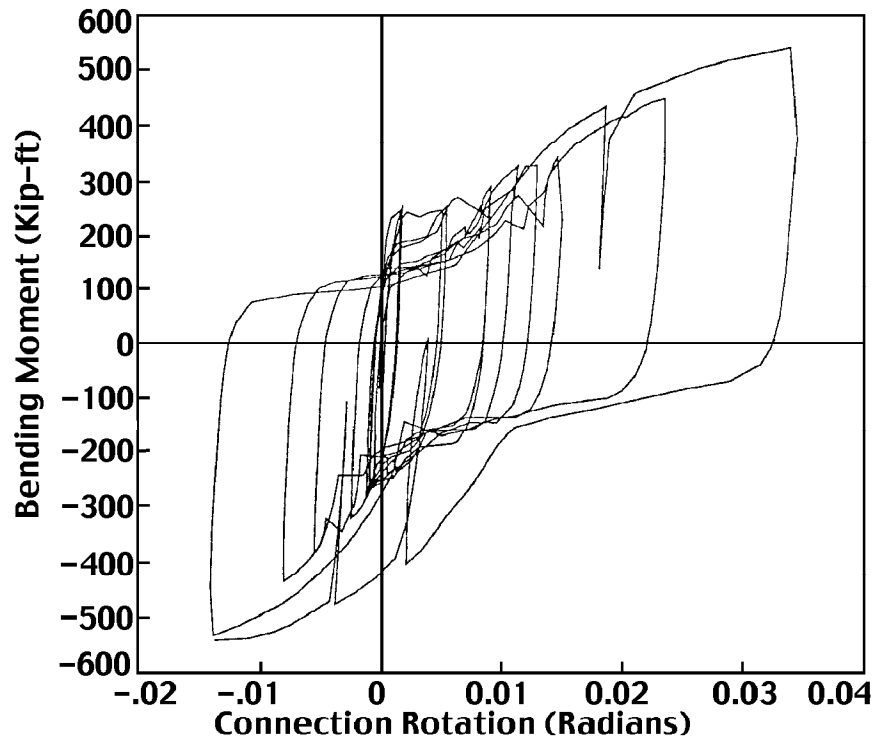


**Figure 5-17** Moment-Rotation of Bolted-Flange-Plate Connection With Large Rotation Capacity

A series of eight experiments was performed (Schneider and Teeraparbong, 1999) on bolted-flange-plate connections to address these yield mechanisms and failure modes. Table 5-5 summarizes the results, and Figure 5-19 is a typical moment-rotation curve obtained from these tests. It can be seen that these connections all achieved large plastic rotations. Three types of yield mechanisms are significant for the bolted-flange-plate connection as illustrated in Figure 5-18. Table 5-5 shows that the plastic rotation achieved in these SAC tests is well distributed among the three major yield mechanisms.

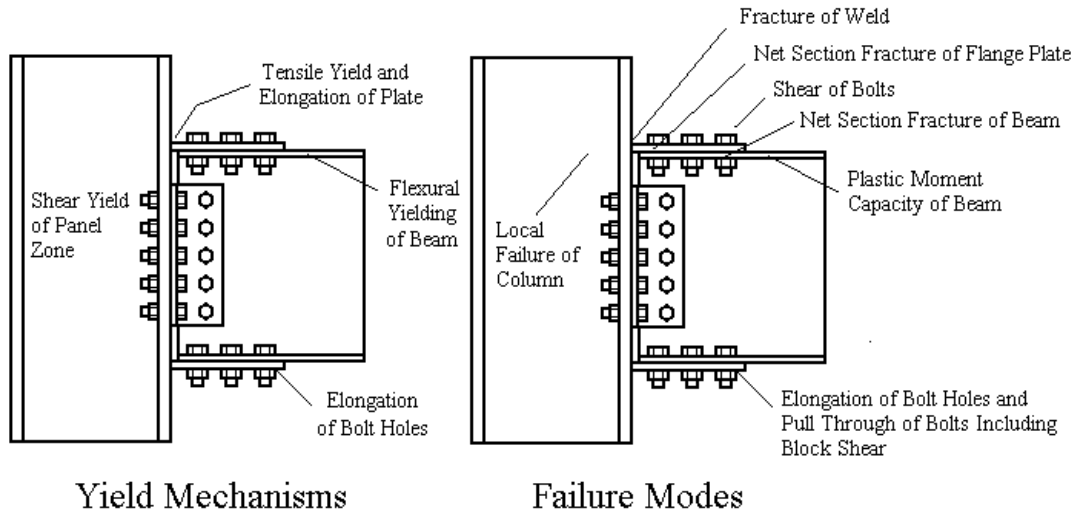


**Figure 5-18 Primary Yield Mechanisms and Common Failure Modes for Bolted-Flange-Plate Connections**

Ductility is achieved if a significant yield mechanism develops at loads and deformations well below those associated with all failure modes. Yield or fracture occur at different locations in the connection as illustrated in Figure 5-18, but these predicted yield and failure moments are all converted to a moment at the face of the column in Tables 5-6 and 5-7. Figure 5-20 defines the geometric terms needed to interpret some of these moment equations. The SAC Phase 2 tests (Schneider and Terraparbong, 1999) showed that the best ductility was achieved in connections with balanced yielding in all three mechanisms. Therefore, the best ductility is likely to be achieved when the equations are approximately balanced so that:

- the moment causing initial shear yield of the panel zone is approximately equal to but slightly smaller than the flexural yield moment of the beam, and
- the moment causing tensile yield of the plate is slightly larger than flexural yield moment of the beam when moments are all computed at a consistent location.

The balanced yield mechanisms occur with yielding in three different steel components. Each of these components has uncertainty and variability in their material properties. Balance of the yield mechanisms with the expected material properties as noted above assures that, when one element has properties which are at a statistic extreme, other mechanisms pick up the slack and contribute more to the plastic rotation. These balance conditions are mathematically stated in the last line of Table 5-6. If this balance is achieved, bolted-flange-plate connections provided

among the largest reliable plastic rotations observed in this entire research program for connections with moderately large member sizes. Table 5-5 shows that large rotations were attained for beam sizes up to W30x99. Engineers normally avoid very long bolt groups, and the shear capacity of the bolts combined with the tolerable length of the bolted connection establish the upper size limits for this connection. When these factors are considered, it is likely that the bolted-flange-plate connection will provide adequate seismic performance for the lighter W36 sections, but it is unlikely to be suitable for heavier sections.

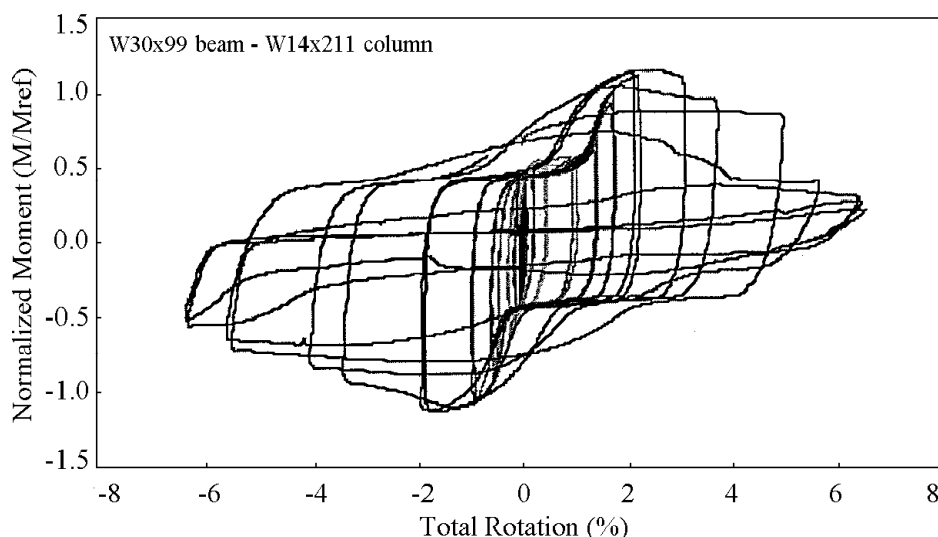


**Figure 5-19 Moment-Rotation Behavior of a Bolted-Flange-Plate Connection**

To prevent fracture of the connection before the yield deformation is achieved, it is necessary to ensure that the moments at the face of the column associated with the critical failure modes are larger than the yield moments which contribute to the plastic rotation. A simple inequality is undesirable here due to uncertainty of material properties and because of the separation needed between yielding and fracture. As a result, the balance condition illustrated in the last line of Table 5-6 is recommended to provide the opportunity for developing the maximum plastic rotation. Table 5-7 supplies the predicted moments at the face of the column associated with the failure modes of the bolted-flange-plate connection. Again, these moments are defined at the face of the column, even though the failures often occur at other locations. The geometric corrections included in the equations of Table 5-7 are essential for providing comparison between the different moments and assuring good seismic performance.

The panel zone yield balance conditions for the bolted flange plate are similar to those derived for the coverplated connection in Figure 3-22. However, the relative importance of panel zone yielding may be different for the bolted-flange-plate connection than for the welded flange connections described in Chapters 2 and 3, because the local stiffness at the beam flange weld is dramatically different. It would appear that the bolted-flange-plate connection should be less susceptible to early fracture due to large panel-zone deformations than the welded flange connections. However, further research is needed to verify this fact.

**Table 5-5 Summary of Bolted-Flange-Plate Test Results**

Test Specimen	General Description and Information	Beam and (Column) Sizes	Flange Plate and (Bolts)	Maximum Total Plastic Rotation	Plastic Rotation Due to Beam Flexure	Plastic Rotation Due to Plate Deformation	Plastic Rotation Due to Panel Zone Yielding
BFP01	Designed to emphasize flange-plate yielding. Fracture of flange-plate in heat affected zone.	W24x68 (W14x120)	1"x10" (18-1"A490 Oversize Holes)	0.051	0.001	0.023	0.027
BFP02	Designed to emphasize flange-plate yielding. Fracture of flange-plate in heat affected zone.	W24x68 (W14x120)	1"x11" (10-1"A490 Std Holes)	0.054	0.01 (0.04 in late cycles after buckling)	0.013	0.03
BFP03	Designed to have flexural yielding of beam at end of flange-plate. Flange buckling and beam flange fracture at net section.	W30x99 (W14x211)	1 <sup>3</sup> / <sub>8</sub> "x14" (16-1"A490 Std Holes)	0.04	0.027	.007	0.015
BFP04	Designed to have balanced flexural yield of beam and yield of flange-plate. Flange buckling and beam flange fracture.	W24x68 (W14x120)	1"x12" (12-1"A490 Std Holes)	0.05	0.02 (0.05 in late cycles after buckling)	0.007	.033
BFP05	Same as BFP03 except enlarged holes and washer plate. Flange and web buckling and beam flange fracture at the net section.	W30x99 (W14x211)	1 <sup>3</sup> / <sub>8</sub> "x14" (16-1"A490 Std Holes w/washer pl)	0.04	0.02	0.02 (significant only in late cycles)	0.016
BFP06	Designed to primarily have flange-plate yielding. Lot of deformation due to bolt slip. Buckling and fracture of beam flange.	W24x68 (W14x120)	1"x10" (10-1"A490 Oversize Holes)	0.057	0.01 (0.03 after local buckling)	0.037	0.015
BFP07	Same as BFP02 except enlarged holes and washer plate. Lot of deformation due to bolt slip. Flange and web buckling and beam flange fracture at end of washer pl.	W24x68 (W14x120)	1"x11" (10-1"A490 Std Holes w/washer pl)	0.058	0.007 (larger in late cycles after buckling)	0.03	0.015

**Table 5-5 Summary of Bolted-Flange-Plate Test Results (continued)**

BFP08	Designed to primarily have flange-plate yielding rated capacity of flange-plate 95% of $M_p$ of beam. However balanced behavior resulted. Tested to two cycles of $\theta_p$ of 0.052 with no fracture or deterioration. Doubler plate added and retested. Repeat test stopped due to severe local and LTB distortion.	W24x68 (W14x145)	1"x11"x27" Flange-plates w/reduced section to 6" width and 5"length	0.052 initial test 0.038 in repeated test at 80% 0.055 at conclusion	0.014 initial test 0.019 repeat test	0.007 initial test 0.018 repeat test	0.033 initial test 0.004 repeat test
-------	------------------------------------------------------------------------------------------------------------------------------------------------------------------------------------------------------------------------------------------------------------------------------------------------------------------------	---------------------	------------------------------------------------------------------------------------	----------------------------------------------------------------------------------------	-----------------------------------------------	-----------------------------------------------	-----------------------------------------------

## Notes:

1. Plastic rotations are rotations prior to significant loss of resistance or initial fracture of the connection.
2. All web shear tab connections used oversized holes.
3. W24 beam all had  $\frac{3}{8}$ "x4  $\frac{1}{2}$ " shear tab with 6 -  $\frac{3}{4}$ " A490 bolts. W24 beam all had  $\frac{1}{2}$ "x4  $\frac{1}{2}$ " shear tab with 8-1" A490 bolts. All shear tab bolts had oversized holes.
4. A lot of plate rotation was slip but some yield occurred on BFP06 and possibly BFP05.
5. These summarized test results are from Schneider and Teeraparbong (1999).

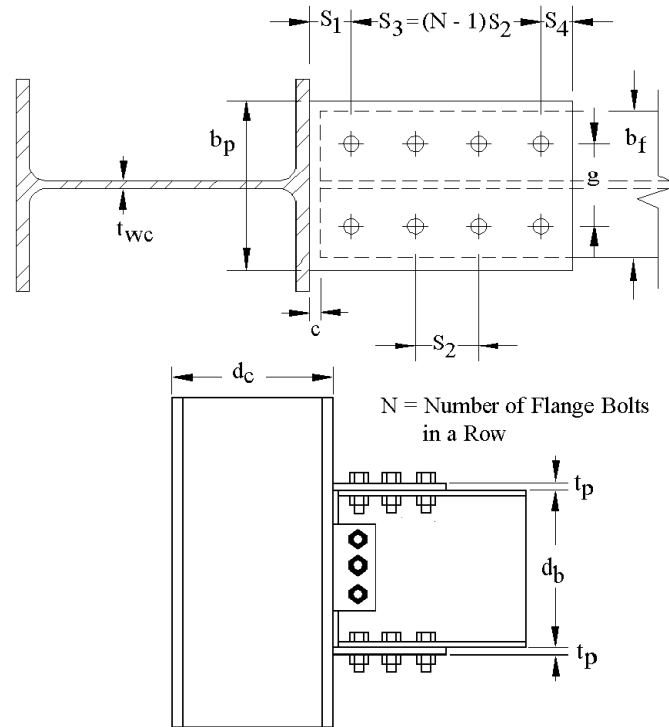


**Figure 5-20 Definition of Geometry of the Bolted-Flange-Plate Equations**

Connection stiffness for bolted-flange-plate connections was evaluated (Schneider and Teeraparbong, 1999) to determine whether special analysis such as depicted in Figure 5-2 is required. The connection is very stiff prior to bolt slip, but the secant modulus value  $k_s$  decreases when slip occurs, and then increases again after larger inelastic deformations are noted. The moment at slip is variable, but initial slip generally occurs at a moment in the range of 40% of the ultimate moment capacity, and the stiffness of the connection is well within the limit defined by Equation 5-3 in this range. After slip, the connection secant stiffness approaches the stiffness implied by Equation 5-3, but it appears that the connection is within the 10% limit up to moments of approximately 60% of the ultimate moment capacity. As a result, this connection may be analyzed as a full stiffness connection for most practical conditions. A reduced stiffness may be appropriate, however, for estimating nonlinear deflections or deflections at higher loads. The effective secant stiffness changes rapidly after initial slip, and so a unique estimate of the stiffness for this region is not possible. If a rotational spring stiffness analysis of the type illustrated in Figure 5-2 is employed, it would appear that a minimum spring stiffness,  $k_s$ , of

$$k_s \geq \frac{40}{\left\{ \frac{h}{EI_c} + \frac{L}{h} \frac{L}{EI_b} \right\}} \quad (5-6)$$

would establish a reasonable bound on the elastic behavior.

**Table 5-6 Yield Mechanisms for Bolted-Flange-Plate Connection**

Yield Mechanism	Equation to Define Yield Mechanism Moment Resistance at the Face of the Column
Flexural Yielding of Beam	$M_{\text{yield Flexure}} = S F_{yb} \frac{L - d_c}{L - d_c - 2(S_1 + S_3)}$
Tensile Yield of Flange-plate	$M_{\text{yield Flange-Plate}} = F_{yp} t_{pl} b_p (d_b + t_{pl}) \frac{L - d_c}{L - d_c - S_1}$ <p>This equation is restricted to the case where the top and bottom flange plates have the same thickness.</p>
Panel Zone Yielding	$V_{\text{yield}} = 0.55 d_b F_{yc} d_c t_{wc}$ <p>and</p> $\Sigma M_{\text{yield Panel Zone}} = 0.55 d_b F_{yc} d_c t_{wc} \left( \frac{L - d_c}{L} \right) \left( \frac{h}{h - d_b} \right)$ <p>Where <math>t_{wc}</math> includes the thickness of the column web and any doubler plate attached to the panel zone.</p>
Balance of Panel Zone Yielding and Flexural Yielding	$(0.9) 0.55 d_b F_{yc} d_c t_{wc} \left( \frac{L - d_c}{L} \right) \left( \frac{h}{h - d_b} \right) > (\Sigma M_{\text{yield Flexural}})$ <p>but preferably</p> $0.55 d_b F_{yc} d_c t_{wc} \left( \frac{L - d_c}{L} \right) \left( \frac{h}{h - d_b} \right) > \frac{3}{2} (\Sigma M_{\text{yield Flexural}})$ <p>Where <math>t_{wc}</math> includes the thickness of the column web and any doubler plate attached to the panel zone.</p>
Balance Requirement Between Yield Mechanisms and Failure Modes for Ductility	$1.2 M_{\text{yield beam flexure}} < M_{\text{fail}}$ <p>for bolt shear failure and plate and beam net section fracture failure modes, and</p> $M_{\text{yield Panel Zone}} \approx (\Sigma 0.9 M_{\text{yield Flexural}})$ <p>and</p> $M_{\text{yield Flange-Plate}} = F_{yp} t_{pl} b_p (d_b + t_{pl}) \frac{L - d_c}{L - d_c - S_1} \approx 1.1 M_{\text{yield Flexural}}$

Note: All material properties provided in this table are expected values rather than minimum values.

**Table 5-7 Failure Modes for Bolted-Flange-Plate Connections**

Failure Mode	Equation for Failure Moment at the Face of the Column	Related Issues
Plastic Deformation of Beam	$M_{\text{fail-Beam Flexure}} = Z_b \frac{F_{yb} + F_{tb}}{2} \frac{L - d_c}{L - d_c - 2(S_1 + S_3)}$	Plastic moment occurs at the end of flange-plate.
Fracture of Shear Bolts	$M_{\text{fail-Bolt Shear}} = 2 N F_v A_{bt} d_b \frac{L - d_c}{L - d_c - (2 S_1 + S_3)}$ <p>where <math>N</math>, <math>F_v</math> and <math>A_{bt}</math> are the number of bolts in one row, the nominal shear strength by AISC LRFD and the bolt area, respectively,</p>	Geometry defined in Figure 5-20.
Net Section Fracture of Flange-Plate	$M_{\text{fail-Net Section Plate}} =$ $= 0.85 F_{tp} (b_p - 2 (d_{\text{bthole}} + .062)) t_p (d_b + t_p) \frac{L - d_c}{L - d_c - 2 S_1}$ <p>where <math>t_p</math> is the thickness of the top and bottom flange plate. This equation is valid only for the case where the top and bottom flange-plates have the same width and thickness.</p>	Note that $d_{\text{bthole}}$ is the actual diameter of the bolt hole.
Net Section Fracture of Beam	$M_{\text{fail-Net Section of Beam}} =$ $= F_{ub} \{Z_b - 2 (d_{\text{bthole}} + .062)) t_{fb} (d_b - t_{fb})\} \frac{L - d_c}{L - d_c - 2(S_1 + S_3)}$ <p><math>Z_b</math> is the plastic section modulus of the beam about the major axis (x-axis) of the beam.</p>	Note that $d_{\text{bthole}}$ is the actual diameter of the bolt hole.
Minimum Resistance of Web Connection	$V_{\text{web}} > \frac{Z_b (F_{yb} + F_{tb})}{L - d_c} \frac{L - d_c}{L - d_c - 2(S_1 + S_3)} + V_g$ <p>where <math>V_g</math> is the shear force due to gravity load and <math>V_{\text{web}}</math> is the minimum required shear strength of the web shear connection.</p>	
Weld Fracture	Experiments have shown that E71T-1 Gas Shielded FCAW welds with appropriate inspection and quality control will avoid weld fracture.	
Block Shear	AISC LRFD Block Shear criteria including bolt pull-through must be applied to the block shear patterns of the flange plate and beam flange illustrated in Figure 5-21.	

**Table 5-7 Failure Modes for Bolted-Flange-Plate Connections (continued)**

Flange Buckling for Both Beam and Column	for flange, $\frac{b_f}{2 t_f} \leq \frac{52}{\sqrt{F_y}}$	
Web Buckling for Both Beam and Column	for web, $\frac{d_b}{t_w} \leq \frac{418}{\sqrt{F_y}}$	See discussion in Chapter 4.
Lateral Torsional Buckling	$L_b < \frac{2500 r_y}{F_y}$ <i>L<sub>b</sub></i> is the unsupported length.	Equation from AISC LRFD Seismic Provisions
Continuity Plate	$t_{fc} \geq 0.4 \sqrt{\frac{P_{bf}}{F_{yc}}}$ where $P_{bf} = 1.8 t_p b_p F_{yp}$	Based on area of flange plate
Strong Column Weak Beam	$1.1 < \frac{\sum Z_c (F_{yc} - \frac{P_{uc}}{A_g})}{\sum Z_b \frac{F_{yb} + F_{tb}}{2} \frac{L - d_c}{L - d_c - 2(S_1 + S_3)}}$	Based on plastic moment capacity of the beam at the last row of bolts.

Note: All material properties provided in this table are expected values rather than minimum values.

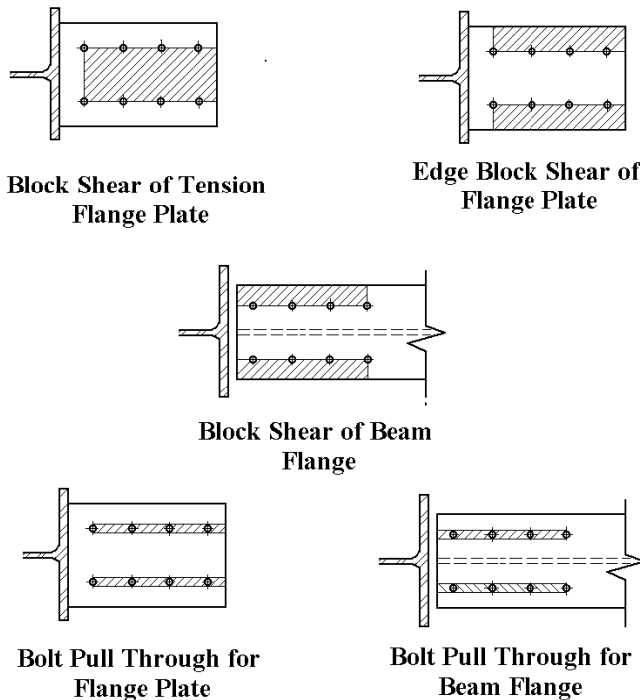


**Figure 5-21 Possible Block Shear and Bolt Pull-Through Mechanisms for Bolted-Flange-Plate Connection**

Ductility achieved by the bolted-flange-plate connection is significant as illustrated in the moment-rotation curve of Figure 5-19 and data summary of Table 5-5. The figure reveals that these connections exhibit a somewhat pinched hysteretic behavior, but they can develop the full plastic capacity of the beam and are capable of sustaining large plastic rotations even for large member sizes. A regression analysis of test results show that:

$$\theta_{p\text{mean}} = 0.11 - 0.00233 d_b, \quad (5-7a)$$

and the standard deviation is

$$\sigma_p = 0.0114 + 0.00044 d_b. \quad (5-7b)$$

The rotation and standard deviation are in radians, and the beam depth is in inches.

The maximum rotations,  $\theta_g$ , for supporting gravity loads were estimated using the two methods described in Chapter 2. A regression analysis was completed for these estimated rotations and

$$\theta_{g\text{mean}} = 0.091 - 0.00108 d_b, \quad (5-8a)$$

and the standard deviation is

$$\sigma_g = 0.0219 + .00085 d_b. \quad (5-8b)$$

Equation 5-8 results in smaller  $\theta_g$  values than  $\theta_p$  values for shallow beam depths. This anomaly will occur only with beam depths less than W16 sections. This occurs because the tests were all conducted on large beam sizes. The rotation,  $\theta_g$ , can never be smaller than  $\theta_p$ , and so  $\theta_g$  should conservatively be set to  $\theta_p$  for W14 beams and smaller.

These rotations require that the shear tab be designed for the shear force associated with the full estimated failure moment at the face of the column due to the plastic moment capacity of the beam as shown in Table 5-7. The bolt holes in the shear tab (and preferably the flange plates) must be 1/8" larger than the bolt diameter, and the connection should be designed to achieve a balanced shear yield, flexural yield, and tensile flange-plate yield as closely approximating those noted in Table 5-6. The specified rotations are based upon tests on connections with beams up to W30 sections. The rotations proposed here are appropriate for column spacing of 25 ft. or more. Significantly smaller plastic rotations should be expected with significantly shorter beam spans.

#### 5.4 PR Connections with Intermediate Stiffness

Figures 5-1 and 5-2 illustrate the wide variation in connection stiffness that is possible with PR connections and the special analysis procedures required if the connection stiffness has a significant impact on the structural response and story drift. The relatively stiff PR connections described earlier will usually develop a resistance exceeding the plastic capacity of the members to be connected, and they can often be analyzed without resorting to the connection stiffness models illustrated in Figure 5-2. The design procedures proposed in these earlier sections were

all based upon the concept that these connections were full strength, full or nearly full stiffness connections.

A number of other more flexible PR connections are available. These connections usually require consideration of the connection stiffness in the structural analysis, and they often have a resistance which is less than the plastic capacity of the member. These flexible PR connections are discussed in later sections of this chapter.

This section considers connections that are intermediate to the stiff, strong connections described in Section 5-3 and the weaker, more flexible connections described later in this chapter. The T-stub connection is significantly stiffer and stronger than the double-flange-angle, the web-angle, the shear tab connection, or a whole range of composite PR connections. The bolted T-stub connection is more viable for seismic design than the more flexible options. As a result, this bolted T-stub connection is the only connection included in this intermediate grouping.

#### **5.4.1 T-Stub Connection**

T-stub connections as illustrated in Figure 5-22 have had a long history. They were used extensively in riveted structures between about 1920 and 1960. They have been used with both high-strength and mild steel bolts since riveted connections faded from construction practice. A number of major buildings were constructed with high-strength bolted T-stub connections in seismically active parts of the US during the 1960s and early 1970s. Bolted T-stub connections are still commonly used in the less seismically active portions of the country. However, they have not been commonly used for seismic design since the early 1970s. The reasoning and rationale behind this change were discussed in Chapters 1 and 2. Bolted T-stub connections will often be comparable to the bolted-flange-plate connection and extended-end-plate connection described earlier. That is, they can develop the full plastic capacity of the beam and their stiffness is such that they can be analyzed as rigid or nearly rigid connections. At the same time, the moment capacity of these connections may be as small as 60% to 70% of the full plastic capacity of the beam, and their stiffness may be small enough to require analyses such as depicted in Figure 5-2. While T-stub connections are clearly PR connections, they are stiffer and stronger than some other PR connection alternatives discussed later in this chapter.

A number of past tests (Roeder et al., 1994; Hechtmann and Johnston, 1947; Batho, et al., 1934, 1936, and 1938) on T-stub connections are available. Most of the data deals with riveted connections and monotonic behavior, but some tests examine cyclic inelastic behavior and high-strength bolts. Many of the riveted connections were encased in concrete for fire protection in these past test programs, since this practice was common prior to 1960. The concrete encasement may increase the strength and stiffness of the connection by as much as 30-50%, but the general behavior, including modes of failure and deformation limits, was unchanged.

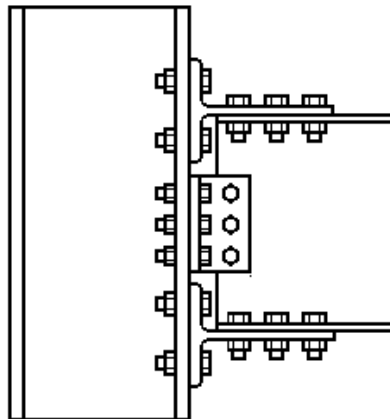


**Figure 5-22 Typical T-Stub Connection**

The cyclic moment-rotation behavior of T-stub connections is pinched as shown in Figure 5-23. Figure 5-23 is the moment-rotation curve for a specimen with tight fitting mild steel bolts which were designed to simulate rivets. Shear yielding of the bolts connecting the beam flange to the stem of the T-section was the yield mechanism, and shear fracture of the bolts was the failure mode for this test. It can be seen that the connection had limited rotational capacity with this behavior. Figure 5-24 is the comparable specimen where the yield mechanism is flexural yield of the flanges of the T-section and the ultimate failure is tensile fracture of the high strength bolts between the flange of the T-section and the column. Very large inelastic rotations are noted with this connection. Both Figure 5-23 and 5-24 are partial strength connections since yielding and ultimate failure occur within the connecting elements. Flexural yield of the flanges of the T-section leads to greater ductility and rotational capacity than shear yield of beam flange bolts. Yield and early fracture of the tension bolts between the flange of the T-section and the column flange will usually lead to less ductility than other modes of failure.

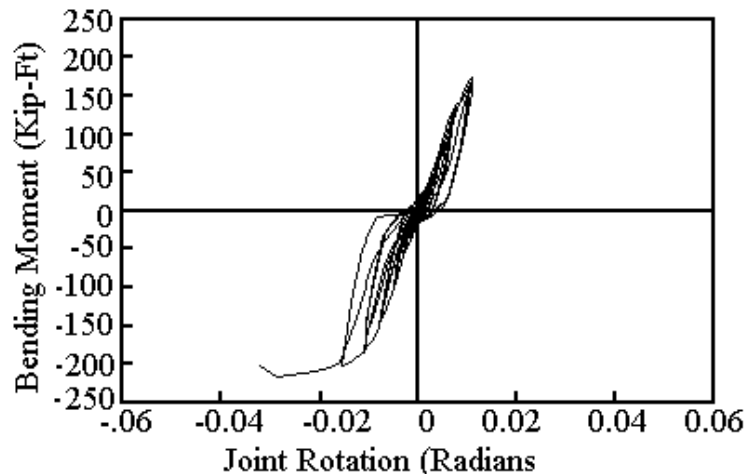


**Figure 5-23 Moment-Rotation Behavior of T-Stub Connection with Shear Yield of Shear Connectors Between the Stem of T-Section and the Beam Flange**

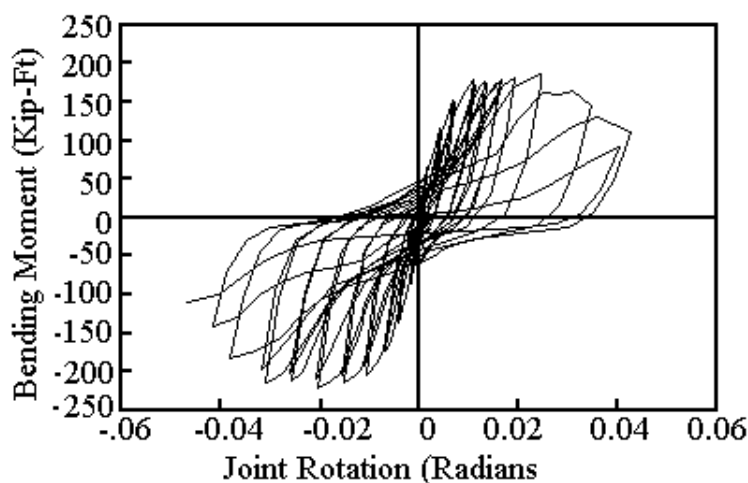


**Figure 5-24 Moment-Rotation Behavior of T-Stub Connection with Flexural Yield of Flanges of T-Section**

Some T-stub connections were tested with high strength bolts. Comparison of the results for high strength bolts to the results achieved with rivets and mild steel bolts shows many common features in the behavior of all bolt types. In general, the maximum inelastic deformation prior to initial fracture and the hysteretic behavior are about the same for all bolts for a given mode of failure. However, there are differences between the behavior obtained with rivets and high-strength bolts (Roeder et al., 1994). High-strength bolts result in less pinching of the hysteresis curves than suggested by Figures 5-23 and 5-24, because the frictional resistance during slip is larger. High strength bolts sometimes develop slightly larger rotational capacity than comparable riveted connections due to looseness and elongation of the bolt holes, whereas riveted connections have snug tight fit of the rivets in the holes. High-strength bolts are unlikely to yield during plastic deformation, since bolt hole elongation is likely to occur first. Further, the bolt proof load may be maintained reasonably well if bolt yielding is avoided, and so considerable energy dissipation is achieved by the friction caused by slip with high-strength bolts. Thus, high strength bolts increase the probability that flexural yielding of the flanges of the T-section will occur, and this is one of the more ductile yield mechanisms of partial strength connections. On the other hand, high strength bolts are less ductile than rivets or mild steel bolts under direct shear or tension loading. They are much more susceptible to the uncertainties of prying action than their mild steel counterparts. As a result, fracture of tension or shear bolts is even less desirable for connections with high strength bolts than it is for riveted connections.

The T-stub connection is one of the few connections which can be fully bolted without any shop or field welding. The bolting offers a distinct advantage in construction, and the use of these connections should increase the redundancy of steel moment frame buildings, since the bolted connections are likely to be used at all beam-column connections. However, the connection is relatively difficult to design because of the diverse yield mechanisms and failure modes, which are illustrated in Figure 5-25. The yield mechanisms include shear yielding of the panel zone, flexural yielding of the beam, tensile yielding of the stem of the T-section, and local flexural yielding of the flange of the T-section. Full strength connections are limited to beam flexural yielding and panel zone yielding, while partial strength connections will generally be limited to tensile elongation of the stem of the T-stub and local flexural yielding of the flanges of

the T-section. Additional rotation can be achieved through elongation of the bolt holes, plastic elongation of the tensile bolts, and plastic shear deformation of the shear bolts. These secondary mechanisms are not included in the figure because the ductility of the mechanism is limited or the calculations for prediction of the mechanism are uncertain. The failure modes of the T-stub connection are even more complex, as illustrated in the figure. Net section fracture of the stem of the T-section and the beam flange, fracture of the tensile bolts, fracture of the flange of the T-section due to plastic deformation, fracture of the shear bolts, elongation of the bolt holes and block shear failure, and failure due to local buckling and excessive deformation of the beam and column are all possible failure modes. Several of these failure modes are influenced by the uncertainty in the tensile forces in the bolts due to prying action. An extensive research program (Leon et al., 1999) of 58 push-pull type tests such as illustrated in Figure 5-26 was developed to better understand prying action and the interrelation between the different failure modes. These tests were used to develop a basic understanding of the different failure modes and simplified models for predicting local connection behavior. These simple models were then used to predict global connection behavior. Twelve additional full connection tests were employed to verify the global connection behavior and verify the validity of the models used to predict the behavior. Table 5-8 summarizes the results of these full connection tests.

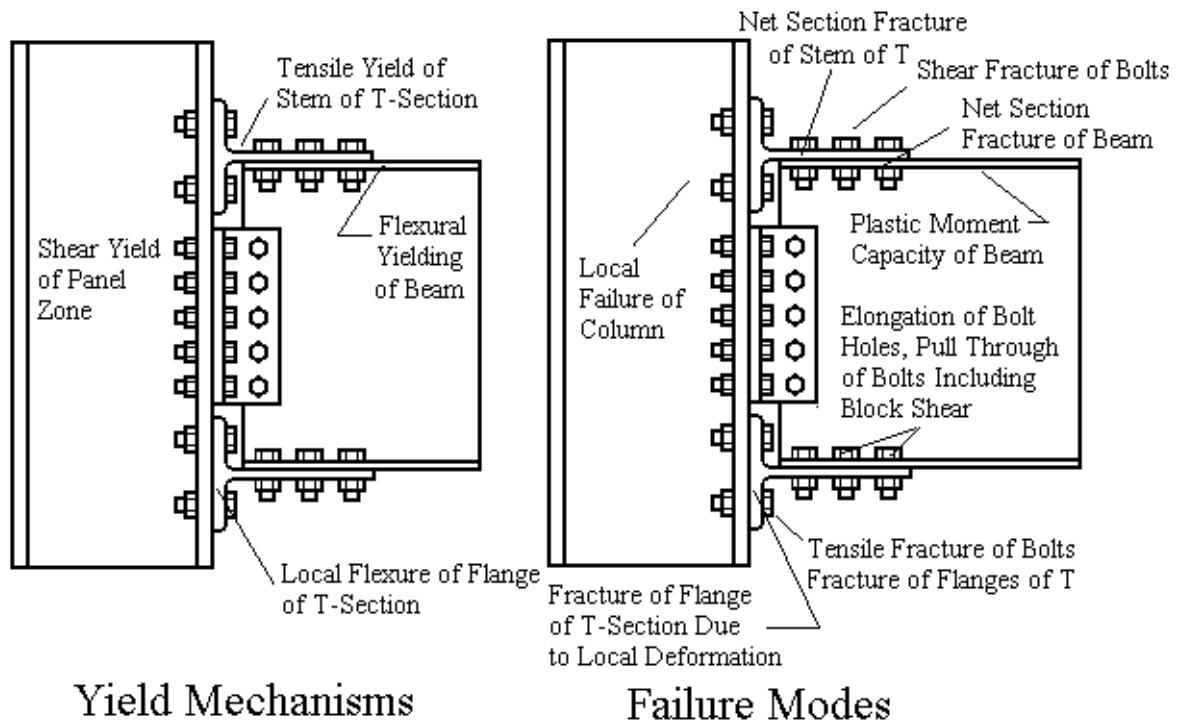


**Figure 5-25 Primary Yield Mechanisms and Common Failure Modes for Bolted T-Stub Connections**

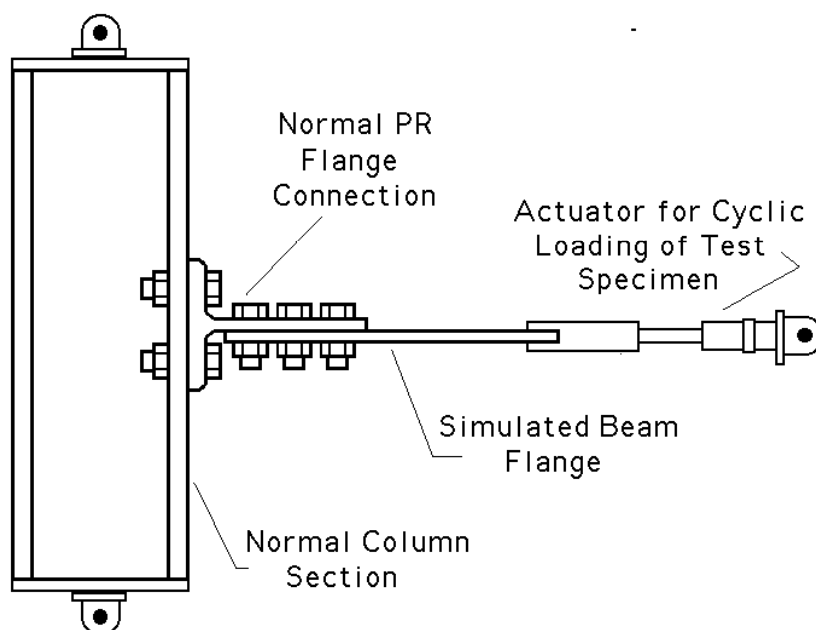


**Figure 5-26 Typical Pull Test Configuration**

The experiments showed that the bolted T-stub connection is a versatile connection for seismic design, and it is capable of developing substantial plastic rotation and resistance. Figure 5-27 illustrates a typical moment vs. plastic rotation curve for a full strength T-stub connection with a W24 beam. The research ultimately led to improved equations for estimating the resistance associated with each yield mechanism and mode of failure, and the research produced methods for balancing the yield mechanisms and failure modes to provide reasonable seismic design models and seismic performance for both full strength and partial strength bolted T-stub connections. Table 5-9 supplies the recommended equations for the yield mechanisms of the bolted T-stub connection, and the bottom four lines of the table give the balance conditions necessary to ensure that the connections will perform within the desired limits. Table 5-10 provides the recommended equations for the failure modes. Figures 5-28 and 5-29 summarize the geometric dimensions needed to use many of the equations in these tables.

As with the bolted-flange-plate connection, yield and failure occur at different locations on the beam, the column, and the connecting elements. As a result, geometric corrections are required for the yield and failure resistance equations of Tables 5-9 and 5-10 to provide comparable moments at the face of the column. The yield mechanism with the lowest resistance is expected to be the mechanism providing most of the connection ductility, and significant ductility is expected to be achieved if this yield mechanism has a resistance significantly lower than that required for the failure modes. Balance conditions are given in Table 5-9 to aid in assuring ductile behavior for both full strength and partial strength connections. Full strength bolted T-stub connections are designed so that the full plastic capacity of the beam and the panel zone shear deformation are the sources of the plastic deformation. The third line of Table 5-9 provides the recommended balance in failure resistance needed to assure this behavior. For full strength connections, the resistance associated with all failure modes must be larger than the

**Table 5-8 Summary of Bolted T-Stub Connection Tests**

Specimen Identification	General Information	Beam (Column) Sizes	Shear Bolts & T-Section	Web Connection	Tensile Bolts	Plastic Rotation @ Initial Failure	Failure Mode	Initial Failure Moment / $M_p$
FS-01	Flange angle connection	W18x40 (W14x145)	4 - 7/8" A490 w/L8x6x1	5/16" Shear Tab w/ 3 - 7/8" A490	2 - 7/8" A490 Bolts	0.015 and 0.025 initial cycle	Tensile bolt fracture	0.88
FS-02	Flange angle connection - FS-01 w/ longer portion of upstanding leg of L	W18x40 (W14x145)	4 - 7/8" A490 w/L8x6x1	5/16" Shear Tab w/ 3 - 7/8" A490	2 - 7/8" A490 Bolts	.025	Tensile bolt fracture	0.76
FS-03	No doubler plate or slab. Fairly significant yielding in T-stem.	W21x44 (W14x145)	8 - 7/8" A490 w/T cut from W16x45	3/8" Shear Tab w/ 3 - 7/8" A490	8 - 7/8" A490 Bolts	0.038	T-Stem Net Section & Beam Flange Buckling	0.978
FS-04	No doubler plate or slab. Significant T-stub yielding.	W21x44 (W14x145)	8 - 1" A490 w/T cut from W16x45	3/8" Shear Tab w/ 3-1" A490	8 - 1" A490 Bolts	0.04	Net Section of stem of T	1.002
FS-05	1/2" doubler plate, 1/2" continuity plate but no slab. Little yielding of T-stub.	W24x55 (W14x145)	10 - 7/8" A490 w/ T cut from W16x100	3/8" Shear Tab w/ 4 - 7/8" A490	8 - 7/8" A490 Bolts	0.033	Flange Buckling of Beam	1.060
FS-06	1/2" doubler plate, 1/2" continuity plate but no slab. Little yielding of T-stub.	W24x55 (W14x145)	8 - 1" A490 w/T cut from W16x100	3/8" Shear Tab w/ 4 - 1" A490	8 - 1" A490 Bolts	0.05	Flange Buckling of Beam	0.978
FS-07	1/2" doubler plate, 1/2" continuity plate but no slab. Little yielding of T-stub.	W24x55 (W14x145)	10 - 7/8" A490 w/ T cut from W21x93	3/8" Shear Tab w/ 4 - 7/8" A490	8 - 7/8" A490 Bolts	0.047	Beam Net Section & Flange Buckling	1.042

**Table 5-8 Summary of Bolted T-Stub Connection Tests (continued)**

FS-08	1/2" doubler plate, 1/2" continuity plate but no slab. Little yielding of T-stub.	W24x55 (W14x145)	10 - 1" A490 w/T cut from W21x93	3/8" Shear Tab w/ 4 - 1" A490	8 - 1" A490 Bolts	0.046	Flange Buckling of Beam	1.047
FS-09	1/2" doubler plate both sides, 1/2" continuity plate but no slab.	W27x84 (W14x145)	12 - 7/8" A490 w/T cut from W33x169	1/2" Shear Tab w/ 5 - 7/8" A490	8 - 7/8" A490 Bolts	0.02	Tensile Bolt Fracture	1.20
FS-10	1/2" doubler plate both sides, 1/2" continuity plate but no slab.	W27x84 (W14x145)	12 - 1" A490 w/T cut from W33x169	9/16" Shear Tab w/ 5 - 1" A490	8 - 1" A490 Bolts	0.02 and 0.03 on return cycle	Beam Flange and Web Buckle	1.25

Notes:

1. Moment evaluated at last row of bolts.
2. Plastic moment capacity determined by mill certification yield stress. For FS-03 and FS-04,  $M_p$  is 5533; for FS-05, FS-06, and FS-07,  $M_p$  is 8174; for FS-08 it is 7209.
3. This test summary is from Leon, et al. (1999).

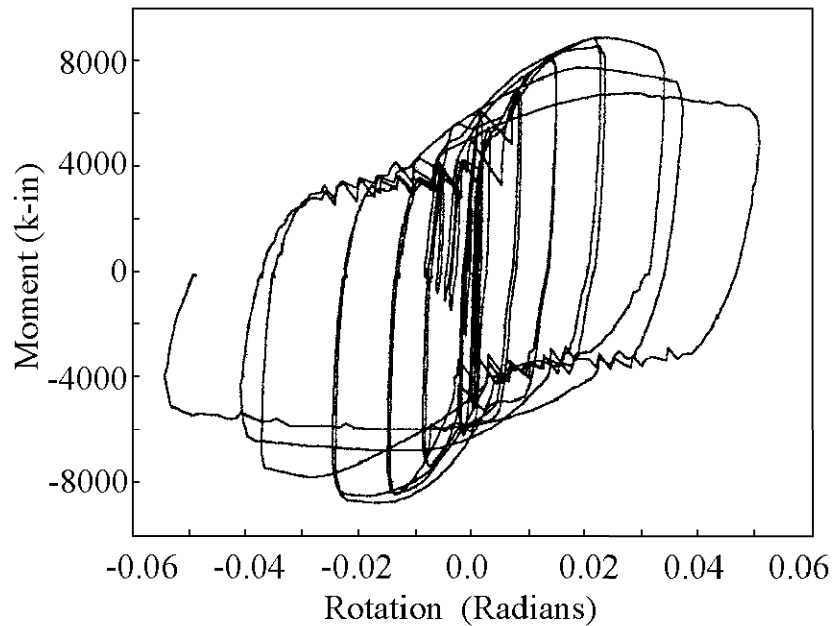


**Figure 5-27** Typical Moment-Rotation Curve for Bolted T-Stub Connection

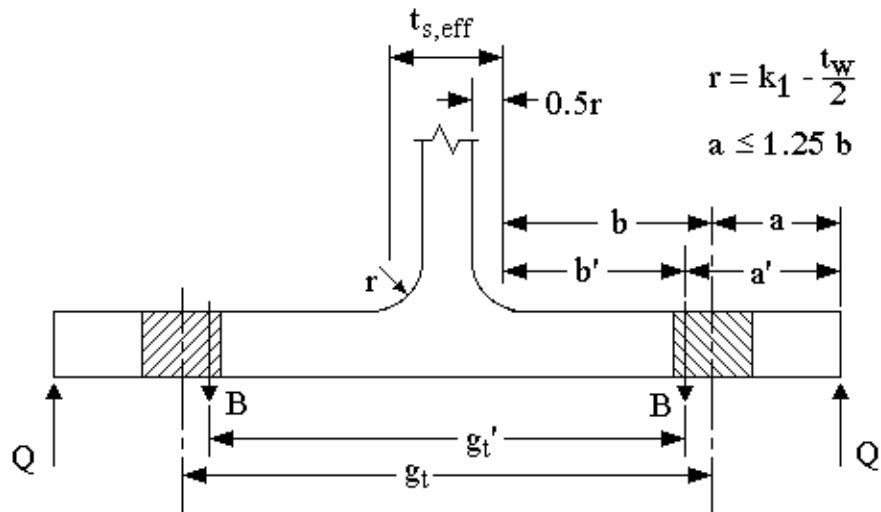


**Figure 5-28** Geometry for Prying Forces and Bending of T-Section Flanges

yield mechanism resistance, and line four of the table provides this balance condition. As with the extended-end-plate and the bolted-flange-plate connections, the panel zone balance connection developed for the welded flange connections are employed for the bolted T-stub connection. However, the smaller concentration of local stiffness in these bolted connections suggests that these connections may tolerate much larger amounts of panel zone yield deformation.

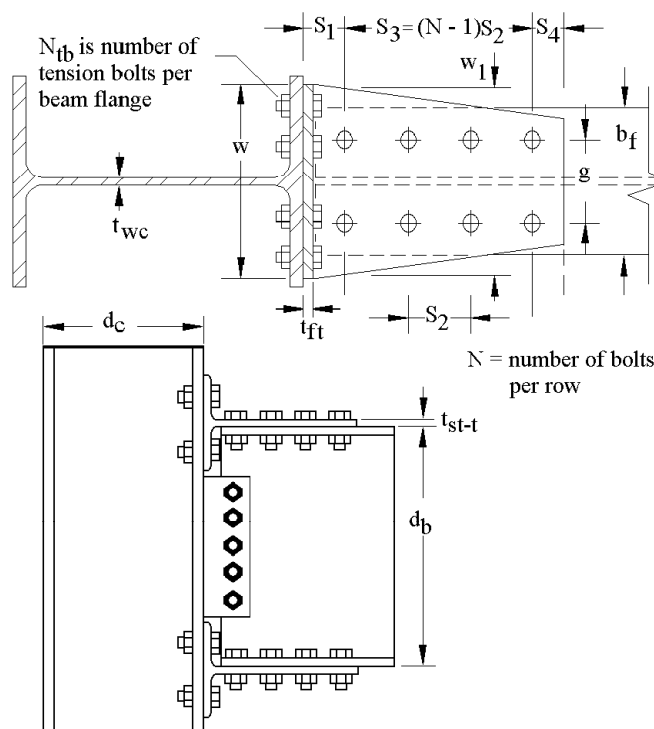


**Figure 5-29 Geometry for Other T-Stub Failure Modes**

**Table 5-9 Yield Mechanisms for Bolted T-Stub Connection**

Yield Mechanism	Equation to Define Yield Mechanism Moment Resistance at the Face of the Column
Flexural Yielding of Beam	$M_{yield} = S F_{yb} \frac{L - d_c}{L - d_c - 2(S_1 + S_3)}$
Panel Zone Yielding	$M_{yield} = 0.55 d_b F_{yc} d_c t_{wc} \left( \frac{L - d_c}{L} \right) \left( \frac{h}{h - d_b} \right)$
Balance of Flexural and Panel Zone Yielding	$(\Sigma M_{yield} \text{ Flexural}) < (0.9) 0.55 d_b F_{yc} d_c t_{wc} \left( \frac{L - d_c}{L} \right) \left( \frac{h}{h - d_b} \right)$ but preferably $0.55 d_b F_{yc} d_c t_{wc} \left( \frac{L - d_c}{L} \right) \left( \frac{h}{h - d_b} \right) < \frac{3}{2} (\Sigma M_{yield} \text{ Flexural})$
Balance of Yield Mechanisms and Failure Modes Needed for Ductile Performance	Experiments have shown that ductile behavior of the connection with full strength connection behavior can be achieved if 1.1 $M_{yield} < \phi M_{fail}$ for T-section, bolt tension, and beam net section failure modes
Balance of T-section Flange Flexural Capacity for Control of Prying Forces	The prying forces in partial strength connections must be limited to no more than 30% of bolt force associated with the failure moment acting alone.
Balance Requirement for partial strength connections using the rotational capacity given in Equation 5-12a	$M_{fail}$ – stem of T must be within 15% of $M_{fail}$ – flange of T in flexure

Note: All material properties provided in this table are expected values rather than minimum values.

**Table 5-10 Failure Modes for Bolted T-Stub Connections**

Failure Mode	Equation for Failure Moment at the Face of the Column	Related Issues
Fracture of Shear Bolts	$M_{\text{fail-Bolt Shear}} = 2 N F_v A_{bt} d_b \frac{L - d_c}{L - d_c - (2 S_1 + S_3)}$ <p>where <math>N</math>, <math>F_v</math> and <math>A_{bt}</math> are the number of bolts in one row, the nominal shear strength by AISC LRFD and the bolt area, respectively.</p>	Geometry defined in Figure 5-29.
Net Section Fracture of Stem of T-Section	$M_{\text{fail-Net Section T}} = F_{ut} (W - 2 (d_{bt} + .125) t_{st-t}) \frac{L - d_c}{L - d_c - 2 S_1}$ <p>where <math>W</math> is lesser of <math>W \leq W_I</math> and <math>W \leq g + S_3 \tan \theta_{eff}</math>. where <math>g</math> is the gage spacing of the bolts in the beam flange as illustrated in Figure 5-29.</p>	$d_{bt}$ is the bolt diameter and $\theta_{eff} = 60 t_{\text{stem-t}}$ except $15^\circ < \theta_{eff} < 30^\circ$
Plastic Capacity of Flanges of T-Section	$M_{\text{fail-Flexure T-Flanges}} = \frac{2 (2a' - \frac{d_{bt}}{4}) W F_{yt} t_f^2 (d_b + t_{st-t})}{4a' b' - d_{bt} (b' + a')}$	Geometry is defined in Figure 5-28. $a' = a + \frac{d_{bt}}{2}$ and $b' = b - \frac{d_{bt}}{2}$ as shown in figure.
Tension Capacity of Bolts Including Prying Force	$M_{\text{fail-Bolt Tension}} = N t_b (d_b + t_{st-t}) \left\{ T_b + \frac{p F_{yt} t_f^2}{4 a'} \right\} \frac{a'}{a' + b'}$ <p>This calculation is valid only for connections with four tension bolts per row in two rows as depicted in Figure 5-29.</p>	$T_b$ is nominal tensile resistance of bolts and $p = \frac{2 W}{8}$
Net Section Fracture of Beam	$M_{\text{fail-Net Section}} = F_{ub} \left\{ Z_b - 2 (d_{bt} + .125) t_{fb} (d_b - t_{fb}) \right\} \frac{L - d_c}{L - d_c - 2 (S_1 + S_3)}$	$A_{bm}$ is cross sectional area of beam.
Block Shear	AISC LRFD Block Shear criteria must be applied to the block shear and bolt pull-through patterns illustrated in Figure 5-21.	See Figure 5-21 for geometry.
Continuity Plate Requirements	Continuity plates are required if $t_{fc} < 1.5 t_{ft}$ or if $\frac{1.1 R_y F_{yb} Z_b}{d_b - t_{bf}} > (6 k + t_{st-t} + 5 t_{ft}) F_{yc} t_{wc}$ Continuity plate must carry the unbalanced portion of the force, $\frac{1.1 R_y F_{yb} Z_b}{d_b - t_{bf}}$ .	$k$ is the column fillet distance from the extreme fiber of column flange to the web toe of fillet.
Required Column Flange Thickness with Continuity Plate	If continuity plates are required, the minimum column flange thickness is $t_{fc} < 1.0 t_{ft}$	

**Table 5-10 Failure Modes for Bolted T-Stub Connections (continued)**

Flange Buckling for both Beam and Column	for flange, $\frac{b_f}{2 t_f} \leq \frac{52}{\sqrt{F_y}}$	
Web Buckling for both Beam and Column	Buckling controlled if $\frac{d_b}{t_w} \leq \frac{418}{\sqrt{F_y}}$	See discussion in Chapter 4.
Lateral Torsional Buckling	$L_b < \frac{2500 r_y}{F_y}$ $L_b$ is the unsupported length.	Equation from AISC LRFD Seismic Provisions
Strong Column Weak Beam	$1.1 < \frac{\sum Z_c (F_{yc} - \frac{P_{uc}}{A_g})}{\sum Z_b \frac{F_{yb} + F_{ub}}{2} \frac{L - d_c}{L - d_c - 2(S_1 + S_3)}}$	Based on plastic moment capacity of beam at the last bolt of T-section

Note: All material properties provided in this table are expected values rather than minimum values.

Partial strength connections are also possible for the bolted T-stub connection, and they develop their plastic deformation within the T-section. The 58 push-pull tests show that significant plastic deformation can occur within this connecting element, but the best performance is likely to be achieved with plastic flexural deformations of the flanges of the T-section coupled with tensile elongation of the stem of the T-section. If flexural yielding of the flanges of the T-section occurs, it is essential to control the prying forces in the tension bolts, since the prying forces will be significant, and bolt fracture leads to reductions in connection ductility. It is important that these prying forces not be too large, or it will be difficult to control the ductility of partial strength connections. For this partial strength connection to occur, the failure moment,  $M_{fail}$ , for local flexure of the flanges of the T-section and local failure of the stem of the T-section must be smaller than all other failure moments, and should be approximately equal. The bottom two lines of Table 5-9 provide balance conditions needed to assure ductility of these partial strength T-stub connections.

Fractures in the k-area have been noted in fabricated members (Tide, 2000) and in some recent steel frame connection tests. Research completed in another part of this research program (Frank, 2000) has shown that the notch toughness attained in the k-area of rotary straightened hot rolled wide flange sections is significantly less than that normally expected in steel members. Fractures in the k-area of bolted T-stub connections have been claimed, but have not been documented in the literature. The k-area issue is potentially important to the bolted T-stub connection, because large stress and deformation demands are placed upon the k-area. However, it should be noted that no k-area fractures were noted in the 58 push-pull tests or in the 12 full connection tests included in this research program. As a result of the lack of documentation of k-area fractures in T-stub connections and the complete lack of failures noted in the T-stub connection research program, no limitations or recommendations regarding the k-area resistance of T-stub connections are included in this report. However, this is an ongoing concern with these connections.

The stiffness of the bolted T-stub connection depends upon many parameters including elongation of the tensile bolts, local flexural deformation of the flanges of the T-section, tensile elongation of the stem of the T-section, shear deformation of bolts, elongation of bolt holes, deformation of the column flanges, and slip of bolts in their bolt holes, in addition to other common sources such as panel zone deformation. These various components of deformation have been combined into a series of springs for a connection stiffness model as illustrated in Figure 5-30. Detailed models (Leon et al., 1999) of these different behaviors were developed based upon the 58 push-pull tests described earlier and their correlation to the full connection tests summarized in Table 5-8. These models permit reasonable prediction of the connection stiffness, but they are much too complex for practical connection design and evaluation. A simplified model for predicting the connection rotational spring stiffness,  $k_s$ , is

$$k_s = \frac{d_b M_{fail}}{0.375} \quad (5-9)$$

where  $M_{fail}$  is the failure moment that controls the resistance of the connection, from Table 5-10, and  $d_b$  is beam depth in inches. It should be noted that  $k_s$  has units of kip-inches per radian, and  $M_{fail}$  must be provided in kip-inches and  $d_b$  in units of inches. In some cases, this spring stiffness may be large enough that the connections can be analyzed as a rigid connection frame, but it can not generally be assumed that the T-stub connections will meet the connection stiffness criteria of Equation 5-3. As a result, the bolted T-stub connection must be regarded as a partial stiffness connection, which requires special frame analysis such as that illustrated in Figure 5-2.

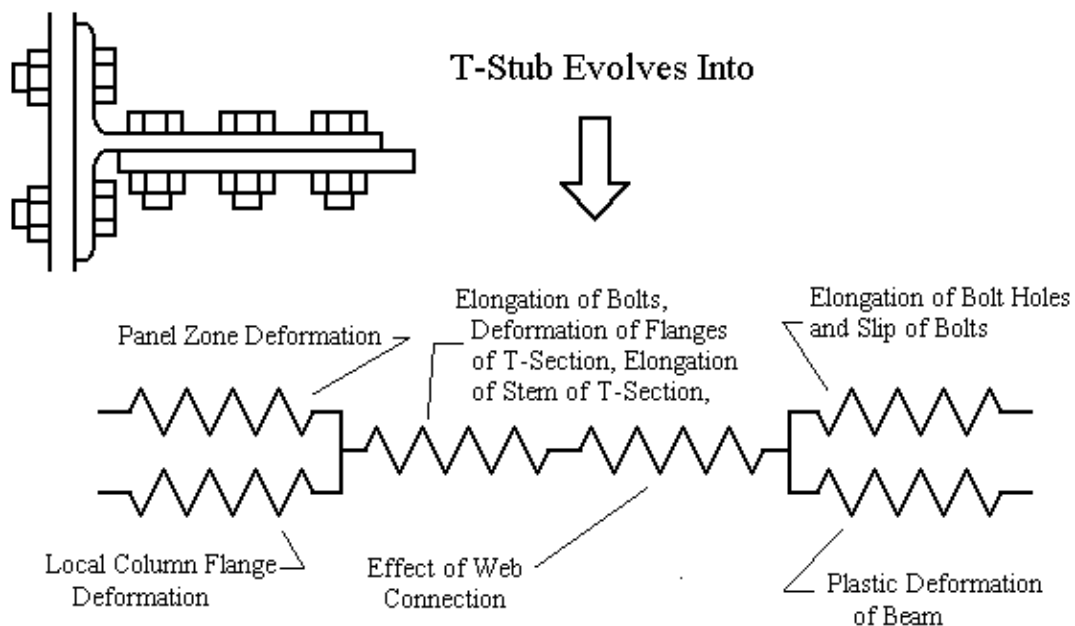


**Figure 5-30 Detailed Stiffness Model for T-Stub Connection**

The plastic rotations obtained with the full strength bolted T-stub connection were determined as:

$$\theta_{p\text{mean}} = 0.11 - 0.0032 d_b, \quad (5-10a)$$

and the standard deviation is

$$\sigma_p = 0.04 - 0.0016 d_b. \quad (5-10b)$$

The test results for high-strength bolts are not directly comparable to the results for riveted connections, and so the reliable test data for obtaining the rotational limit are all based upon W21 through W27 beam sections included in the SAC Research Program. As with the extended-end-plate connection, the moment resistance of the bolted T-stub connection depends upon the tensile capacity of the bolt, the prying forces, and the bending of the flanges of the T-section. The combined effect of these parameters limit the use of the bolted T-stub connection to modest sized members, and it is unlikely that a full strength bolted T-stub connection could be designed with beam members much heavier than modest sized W27 beam sections. None of the bolted T-stub connection tests were continued to a deformation which would allow rational determination of the maximum rotation for supporting gravity loads,  $\theta_g$ . However, the bolted T-stub connection has redundancy for the gravity load support, since both beam flange connections and the web connection are usually capable of supporting dead load. In addition, the bolted T-stub is less sensitive to large rotations than many other connections. It is clear that  $\theta_g$  cannot be smaller than  $\theta_p$ , and the redundancy and reduced sensitivity to large rotations suggest that  $\theta_g$  should consistently be in the order of 0.02 radians larger than  $\theta_p$ . As a result,  $\theta_g$  is estimated as

$$\theta_{g\text{mean}} = 0.13 - 0.0032 d_b. \quad (5-11)$$

The rotations and standard deviation are in radians, and the beam depth is in inches.

These rotation limits are based upon a column spacing and beam span of approximately 25 ft, and they are restricted to full strength bolted T-stub connections so that plastic bending of the beam and panel zone yield of the column are the dominate yield mechanisms. Longer column spacing will produce somewhat larger rotations, but significantly smaller rotations are possible with significantly shorter beam spans.

Partial strength connections will not develop the full plastic capacity of the beam. The plastic rotations of these connections are limited by local flexure of the flanges of the T-section combined with tensile yield of the stem of the T-section. The yield mechanisms require the balance conditions shown in Table 5-9. The plastic rotation achievable with the partial strength connection depends on the comparison of the failure resistances,  $M_{\text{fail}}$ , due to local plastic flexure of T-section flange and due to net section fracture of the stem of the T-section.

So that

$$\theta_{p\text{mean}} = \frac{0.9-1.4 \left\{ \frac{\text{ABS} \{ M_{\text{fail-TFlngFlex}} - M_{\text{fail-TStem}} \}}{M_{\text{fail-TFlngFlex}} + M_{\text{fail-TStem}}} \right\}}{d_b} \quad (5-12a)$$

and the standard deviation is

$$\sigma_p = \frac{0.156''}{d_b} \quad (5-12b)$$

As a lower bound on  $\theta_p$

$$\theta_{\text{lower bound}} = \frac{0.6-1.4 \left\{ \frac{\text{ABS} \{ M_{\text{fail-TFlngFlex}} - M_{\text{fail-TStem}} \}}{M_{\text{fail-TFlngFlex}} + M_{\text{fail-TStem}}} \right\}}{d_b} \quad (5-12c)$$

The above limits are based upon statistical evaluation of the push-pull tests, and they reflect the failure of the individual T-stub section. As a result, this value of  $\theta_p$  is a more severe condition than that noted for the full strength T-stub connection. Clearly,  $\theta_g$  is no smaller than  $\theta_p$ , but it is unlikely that  $\theta_g$  is much larger than the plastic rotation provided in Equation 5-12, because of the reduced redundancy noted with failure in the connecting elements. As a result,  $\theta_g$  is estimated as

$$\theta_{g\text{mean}} = \theta_{p\text{mean}} + 0.01 \quad (5-13)$$

The rotation limits for partial strength connections are strongly dependent upon beam depth, but these rotation limits do not depend upon span length because all of the plastic deformation is concentrated in the connecting elements. Therefore, these rotation limits are applicable to all span lengths.

## 5.5 Flexible PR Connections

Flexible PR connections will always require consideration of the connection spring stiffness,  $k_s$ , and frame models such as illustrated in Figure 5-2. In addition, the more flexible PR connections will only be able to develop a small portion of the plastic moment capacity of the beam. As a result, they are all partial strength, partial stiffness connections. Bolted flange-angle, bolted web-angle, and shear tab connections are discussed in this section. Several similar composite connections are described in Chapter 6.

### 5.5.1 Double-Flange-Angle Connections

Double-flange-angle connections (Roeder et al., 1994) such as illustrated in Figure 5-31 have a nearly identical history to T-stub connections. They were first used as riveted connections from approximately 1920 through 1960. During this period, their usage was typically in shorter

buildings or the top stories of tall buildings. As with T-stub connections, they were often encased in concrete for fire protection prior to about 1960. The concrete increases the strength and stiffness of the connection by several times because of the low stiffness and reduced resistance of the double-flange-angle connection. High-strength bolted connections were used since approximately 1960, but double-flange-angle connections have not been used in seismic-resistant lateral-load frames since about 1970. Double-flange-angle connections are weaker and more flexible than the T-stub connection. They usually develop no more than 30% to 70% of the plastic bending capacity of the beam. They are still used as moment-resisting connections in less seismically active zones, and their usage is limited for many applications by their low strength and stiffness. Double-flange-angle connections have many similarities with seated beam connections except that seated beam connections usually have a heavy bottom flange angle and a light top flange angle, while double-flange-angle connections would normally have the same for the top and bottom. In addition, the double-flange-angle connection will usually have a web angle to carry the shear force. Seated beam connections are normally treated as pinned connections, but they are known (Chasten, et al., 1989; Dailey and Roeder, 1989) to have some rotational resistance.

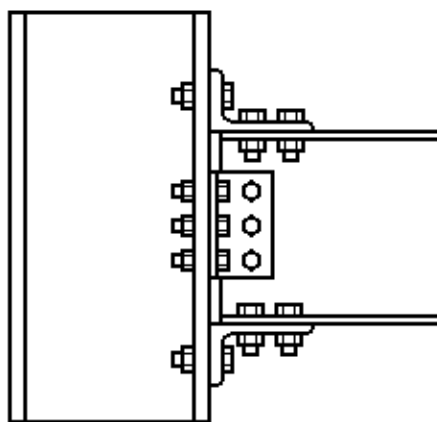


**Figure 5-31 Typical Double-Flange-Angle Connection**

Double-flange-angle connections also have severely pinched hysteresis curves, and the curves depend heavily upon the failure modes. Figures 1-10 and 1-11 are moment-rotation curves for double-flange-angle connections. Figure 1-10 shows the behavior of a connection with flexural yielding of the upstanding leg of the double-flange-angle but ultimate tensile fracture of the bolts between the upstanding leg of the angle and the column flange. Figure 1-11 shows the behavior of a connection with tensile yield and ultimate fracture of the bolts between the upstanding leg of the angle and the column flange. This behavior is very similar to that noted with the T-stub connections. The largest ductility and rotational capacity is achieved with the local flexural yielding of the vertical leg of the angle, and the smallest rotational capacity is achieved with tensile fracture of the bolts (Roeder, Leon, and Preece, 1994; Hechtmann and Johnston, 1947; Batho, et al., 1934, 1936 and 1938). Many tests of these connections were done with rivets or mild steel bolts, but a substantial number of double-flange-angle connections (Azizinamini and Radziminski, 1989) with high strength bolts have been tested. Nevertheless, most of this testing stops short of seismic cyclic load conditions. The observations of the behavior of these connections and concerns with respect to seismic design are similar to those

noted for the T-stub connection. The yield mechanisms and failure modes of this connection are as illustrated in Figure 5-32. The inelastic deformation occurs within the connecting elements since these are partial strength connections. Failure modes are also similar to those noted with the T-stub connection, but failure of the beam due to local buckling, excessive plastic deformation, or net section fracture of the beam is unlikely with this weaker, more flexible connection.

Due to the limited resistance of these connections, their applications in seismic design are limited. They may be suitable for applications where the required seismic resistance is low. They may be beneficial in repair or retrofit of existing buildings, since simple shear tab connections can be converted to double-flange-angle connections in existing structures. Because of the limited applications, limited research was performed on these connections in the SAC Phase 2 research program. Ten of the 58 push-pull specimens illustrated in Figure 5-26 were double-flange-angle connections. Two of the bolted connections summarized in Table 5-8, and two of the shear tab tests (Astaneh and Liu, 2000) described later in this chapter and in Chapter 6 employed double-flange-angle connections. In addition, a review of past research studies (Coons, 1999) accumulated a summary of past experimental data on these connections.

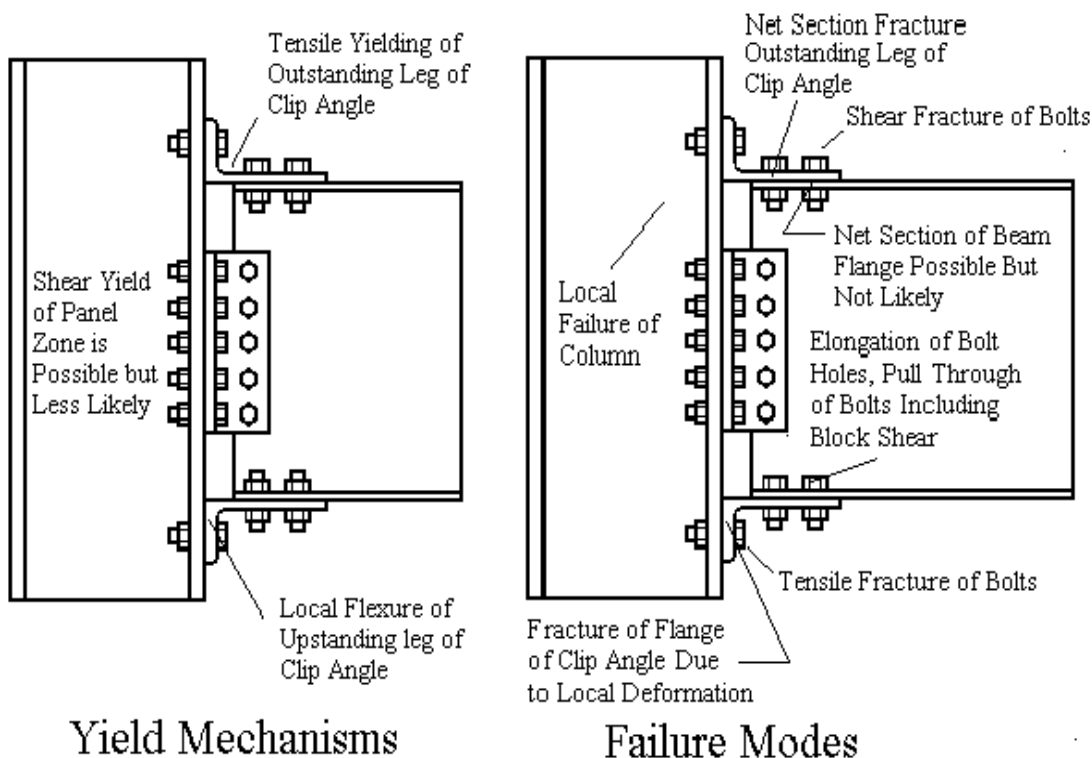


**Figure 5-32 Primary Yield Mechanisms and Common Failure Modes for the Bolted Double-Flange-Angle Connection**

Table 5-11 provides recommended equations for the failure modes for the bolted double-flange-angle connections. The moment capacity of these connections is limited, and is unlikely to exceed 30% to 70% of the plastic capacity of the beam unless the beam is very small. Flexural yielding of the upstanding leg of the double-flange-angle is the only reliable yield

mechanism for this connection when high-strength bolts are used. Other yield mechanisms may provide some plastic rotation, but this rotational capacity is small. As a result, it is proposed that resistance associated with different failure modes be compared for this connection. The equations for predicting individual failure modes are primarily based (Roeder et al., 1994) upon riveted connections or connections with mild steel bolts, but they were adapted to high-strength bolts through reasoning regarding the differences in their behavior. There are fundamental differences between rivets and high strength bolts. Rivets provide moderate ductility against tensile and shear fracture of the rivets, while high strength bolts offer virtually no plastic deformability in these failure modes. On the other hand, high-strength bolts may develop some rotational capacity due to looseness of the bolt holes and elongation of these bolt holes, while rivets would normally develop neither of these effects.

The rotational spring stiffness of the bolted double-flange-angle connection can be estimated as

$$k_s < \frac{M_{\text{fail}}}{0.01} \quad (5-14)$$

where  $M_{\text{fail}}$  is the critical failure mode for the connection from Table 5-11. As with other connections described in this chapter, this stiffness is not the maximum connection stiffness. It is generally a secant stiffness for deformations at which the resistance achieves 50% to 75% of the maximum capacity. At this stiffness level, small amounts of inelastic deformation are assumed, but the behavior is still primarily elastic. This spring stiffness will always be below the limit of Equation 5-3, and so the connection stiffness must be considered in the analysis in methods such as illustrated in Figure 5-2.

Given the above proposed equations, good rotational capacity can be achieved if plastic bending of the upstanding leg of the angle controls the capacity of the connection. This condition is stated in the balance condition in the bottom line of Table 5-11. Plastic bending of the leg of the angle induces prying forces in the bolts, and these prying forces are estimated in the capacity equations of the table. However, tensile fracture of the bolts results in small rotational capacity, and so the tensile force in the bolt is limited to the proof load to avoid this brittle failure mode. If these conditions are met, the plastic rotational capacity,  $\theta_p$ , is

$$\theta_p < \frac{0.50}{d_b} \quad (5-15)$$

Experiments show that  $\theta_g$  is significantly larger than  $\theta_p$ , because both flange angles and web-angle are capable of supporting dead loads, and so  $\theta_g$  can be conservatively estimated as

$$\theta_g < \frac{0.50}{d_b} + 0.02 \quad (5-16)$$

These rotations require both flange angles for bending resistance and web angles or shear tabs for shear resistance. This rotational limit is strongly dependent upon beam depth, but is

largely independent of span length, since all of the deformation occurs within the connecting element.

**Table 5-11 Failure Modes for Bolted Double-Flange-Angle Connections**

Failure Mode	Moment at the Face of the Column	
Plastic Bending Capacity of Upstanding Leg of the Angle	$M_{fail} = \frac{.5 w t_a^2 F_{ya}}{d' - \frac{t_a}{2}} (d_b + d')$	See geometry of Figure 5-33.
Shear Fracture of Bolts Between Outstanding Leg of Angle and Beam Flange	$M_{fail} = 2 N T_b (d_b + t_a) \frac{L - d_c}{L - d_c - (S_1 + S_3)}$ Where $T_b = 90 A_{bt}$ for A325 bolts and $T_b = 113 A_{bt}$ for A490 bolts	$A_{bt}$ is the cross sectional area of bolt.
Fracture of Tension Bolts	$M_{fail} = T_p (d + d') - \frac{0.25 w t_a^2 F_{ya}}{a}$ where $a = l_a - d'$ $d' = b - .425 d_{bh}$ and $T_p$ = minimum required proof load of the high strength bolt by AISC LRFD provisions.	Prying force is needed to plastically deform angle. Bolt force limited to proof load. Dimensions are defined in Figure 5-33.
Net Section Fracture of Outstanding Leg of Angle	$M_{fail} = F_{ta} (W - 2 (d_{bt} + .125)) t_a (d_b + t_a) \frac{L - d_c}{L - d_c - 2 S_1}$ where $W$ is lesser of $W \leq W_I$ and $W \leq g + S_3 \tan \theta_{eff}$ . Because both legs of the angle have the same thickness, this is less likely to control the capacity than the other modes.	$d_{bt}$ is the bolt diameter and $\theta_{eff} = 60 \tan^{-1} \frac{t}{g}$ except $15^\circ < \theta_{eff} < 30^\circ$ .
Bolt Elongation, Bolt Pull Through, and Block Shear	Block shear, bolt hole elongation, and bolt pull through must be checked by normal AISC criteria, but they are less likely to control the design of these connections than the bolted T-stub or other connections.	
Other Issues	Balance of panel zone stress state, continuity plates and flange and web slenderness requirements would apply to these connections, but are unlikely to affect the design since the connection develops a moment capacity sufficiently small that the members are unlikely to receive high enough stress to cause problems in these areas. Weak-beam-strong-column requirements may be a problem even with the relatively small moments in the beams and connections because of the large axial loads in the columns due to gravity load.	
Recommended Balance Condition	$M_{fail-Flexure \text{ of angle leg}} < 1.1 M_{fail-All \text{ other modes}}$ Other modes include tension fractures of bolts, shear fracture of bolts, and net section fracture of outstanding leg.	

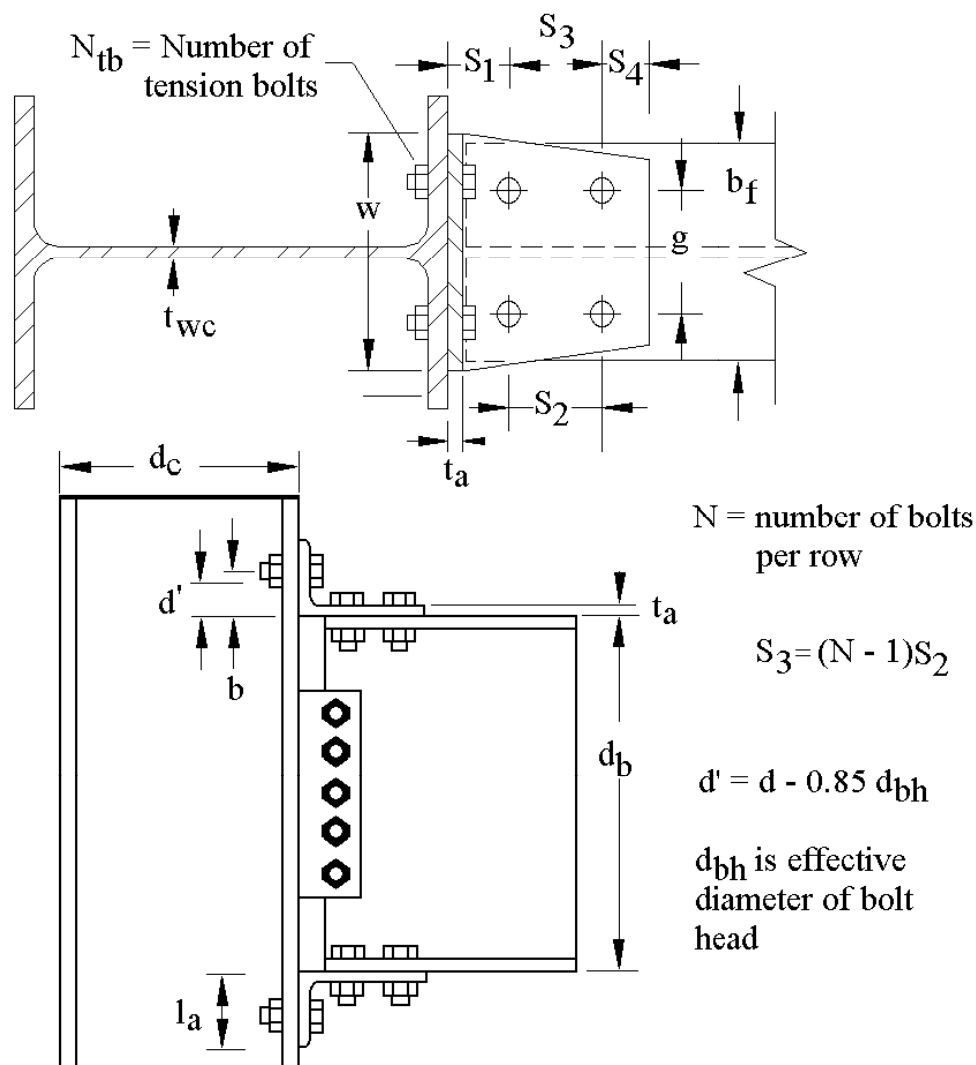


**Figure 5-33 Geometry for Failure Mode Evaluation of Double-Flange-Angle Connections**

### 5.5.2 Web-Angle Connections, Shear Tab Connections, and Other Web-Only Connections

Some PR connections are so flexible that they are commonly treated as pinned connections. These connections clearly have some stiffness and rotational resistance, but the resistance and stiffness are small enough that they are commonly neglected in the design of new structures. The web-angle connection shown in Figure 5-34 and the shear tab connection shown in Figure 5-35 are both connections of this type. They are both normally designed as pinned, shear connections. However, they are both known to have some rotational resistance. The maximum rotational resistance is typically in the order of 10% to 25% of the plastic capacity of the beam, and the rotational stiffness of both connections is relatively low. However, these connections may provide supplemental stiffness and resistance to existing buildings. The supplemental stiffness and resistance are all additive to the basic structural system, since these flexible connections were not considered in the original design. Further, there are often many of these

web-only connections, and the addition of their stiffness and resistance may help to reduce the cost of repair or retrofit of existing structures. As a consequence, both these connections are discussed here.

The web-T connection illustrated in Figure 5-36 has also been used and investigated (Astaneh and Nader, 1990). The web-T connection has not been as widely used in seismic design as the shear tab and the web-angle connections, and so the discussion of this connection is limited in this report. The T-section may be either bolted to the column as shown in the figure or welded to the column with fillet welds at the tips of the flange of the T-section. The resistance and stiffness of the web-T connection are not dramatically different from those noted for the web-angle and shear tab connections. However, the stem of the T-section permits the use of multiple rows of bolts to the beam web, and this may increase the stiffness and resistance of the bolt group over that discussed here. The reader is referred elsewhere (AISC, 1994; Astaneh and Nader, 1990) for details on this connection.

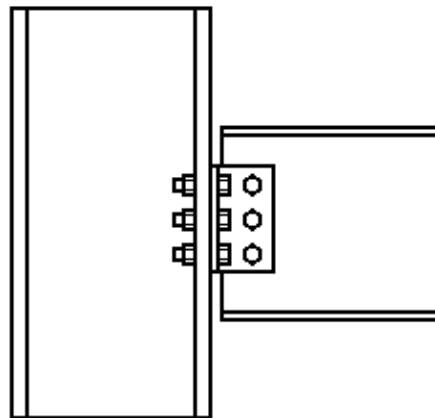


**Figure 5-34 Typical Bolted Web-Angle Connection**

The web-angle connections use bolted angles to transfer the shear between the beam web and the column as illustrated in Figure 5-34. The shear tab connection shown in Figure 5-35 uses a small plate or shear tab which is shop welded to the column and field riveted or bolted to the web of the beam. As noted earlier, both connections are designed for shear only, but they are both known to have some rotational resistance. There have been extensive tests for the web-angle connections (Lewitt et al., 1965; Munse et al., 1959; Lipson, 1977) and for the shear tab connections (Richard et al., 1980; Astaneh et al., 1989).

The web-angle connection was commonly used as a riveted connection prior to 1960. These were commonly used as beam-to-beam connections since virtually all beam-to-column connections used T-stub or double-flange-angle connections. Since the 1960s, both the web-angle and shear tab connections have had continued use as beam-to-beam connections with high-strength bolts. However, in recent years, these connections have also been widely used in beam-to-column connections. This has occurred because fewer welded-flange-bolted-web connections were used in recent steel moment frames, and nominal pinned connections were used at all other locations because of their simplicity and reduced cost.

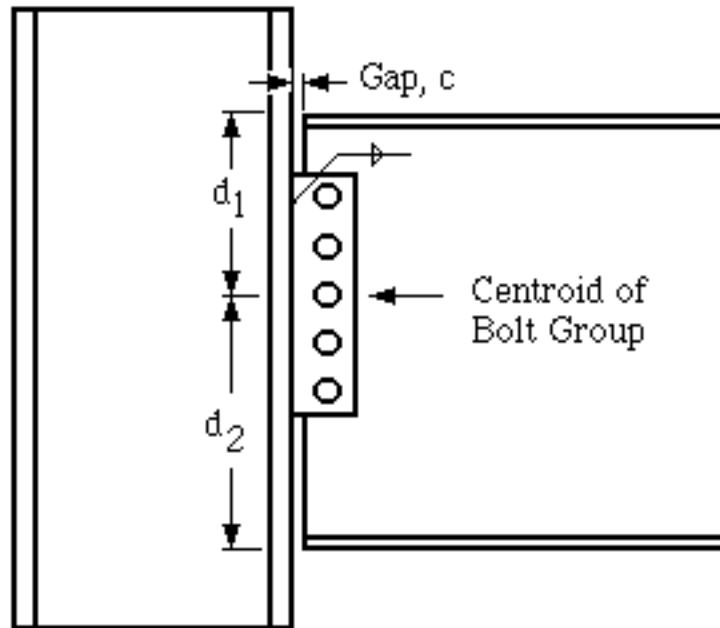


**Figure 5-35 Typical Bolted Shear Tab Connection**

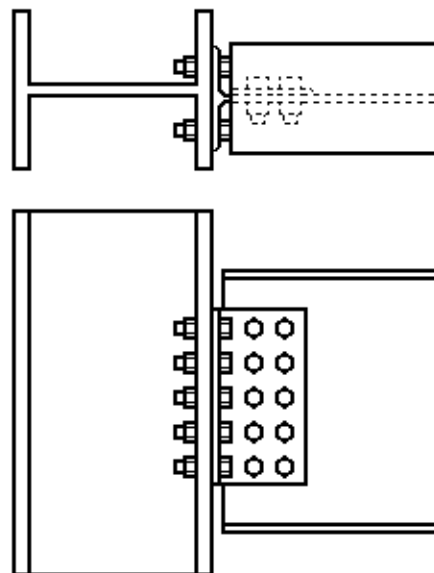


**Figure 5-36 Bolted Web-T Connection**

Figure 5-37 illustrates the moment-rotation behavior under monotonic loading for a web-angle connection of comparable beam depth to the T-stub, end-plate and flange-plate connections described earlier. By comparison, the moment capacity of the web-angle connection is much smaller than that shown in Figures 1-10, 1-11, 5-23 and 5-24. However, the rotational capacity for

this moderate beam depth is quite large. The connections are quite flexible, and this resistance can be activated only at relatively large rotations. The rotational capacity can be very large, but it depends upon the number of bolts and the geometry of the connection. Deeper connections cannot tolerate as large a rotation as shallower connections because of the large binding effect on the top and bottom bolts and because of the limited clearance distance. The plastic deformation is concentrated in the connection and so the rotation that is achievable with this connection decreases with increasing depth but is unaffected by beam span length.

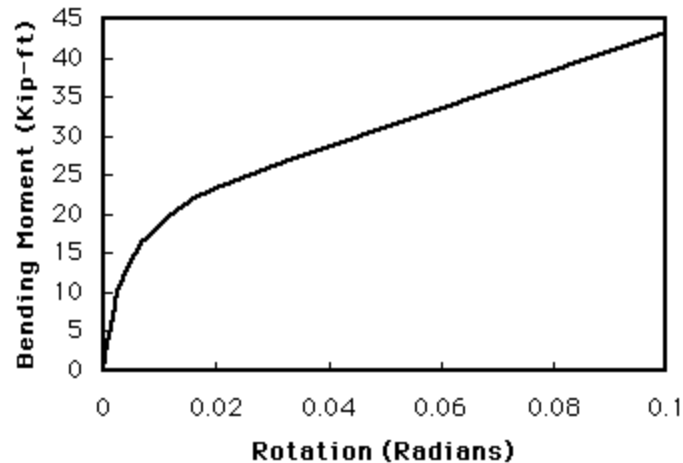


**Figure 5-37 Moment-Rotation Behavior for Bolted Web-Angle Connection**

Research (Liu and Astaneh-Asl, 2000) was performed on these connections as part of the SAC Program to provide a better understanding of the stiffness and resistance of the shear tab connections at different deformation levels. Table 5-12 summarizes the results of these tests. The tests were directed toward examining the effects of the composite slab (including lightweight and normal weight concrete), of older and newer design methods, of different reinforcement methods (rebar or wire mesh, and transverse and longitudinal metal deck placement), and of different column orientations on the strength, stiffness, and rotational capacity of the bolted shear tab connection. The discussion of the composite connections is deferred to Chapter 6. Four of these connection tests were bare steel connections, since they were performed to provide control specimens for the research program, and these four specimens are discussed in this section along with the historic test results.

The large rotational capacity of the bolted web-angle and bolted shear tab connections (as illustrated in Figures 5-37 and 5-38) reduces the need for the yield mechanism and failure mode reasoning that was applied to other stiffer and stronger connections. There is usually enough rotational capacity in these bolted connections to fully develop the stiffer and stronger connections in the building without a need for detailed calculations or balanced behavior. Evaluation of the bolted web-angle and bolted shear tab connections then becomes a question of connection stiffness and resistance. The limiting rotations are relevant because they show the deformation needed to develop the resistance of the connection. Further, they provide limits on the rotation,  $\theta_g$ , at which the beam can no longer support its gravity load based on the size and detailing of the connection.

Figure 5-38 shows a moment-rotation curve for the four SAC shear tab connections. The moment-rotation curves are often non-symmetric, and there are two primary reasons for this. First, the initial moment in the connection due to gravity load makes the connection appear weaker in one direction, since the applied seismic deformation immediately increases the moments in one direction while initially decreasing the moments in the other. This differential can be seen in Table 5-12, where the average maximum moment from the two connections in one direction is noted and the average maximum in the reverse direction is noted in parenthesis. This difference in apparent strength is most significant in the composite connections, and will be discussed in Chapter 6. Another part of the apparent difference in the positive and negative moment resistance is caused by binding action illustrated in Figure 5-39. Figure 5-38 shows that the connection is much stronger in the negative moment direction than in the positive moment direction at rotations larger than about 0.06 radians. This additional strength comes only at very large rotations, and it is caused by binding between the steel beam flange and the column flange as illustrated in Figure 5-39. This added resistance is not seen in all tests. As a result, this extra resistance was physically deducted from the moment capacities tabulated in Table 5-12, and this resistance is not considered in the resistance estimates provided later in this section. This resistance must be neglected because it depends on variables such as the clearance gap shown in Figure 5-35. This gap varies from beam to beam and from fabricator to fabricator. Consequently, it may or may not occur on a given connection. Due to this uncertainty, the extra resistance cannot be considered an inherent characteristic of the connection, and is therefore deleted from this discussion.

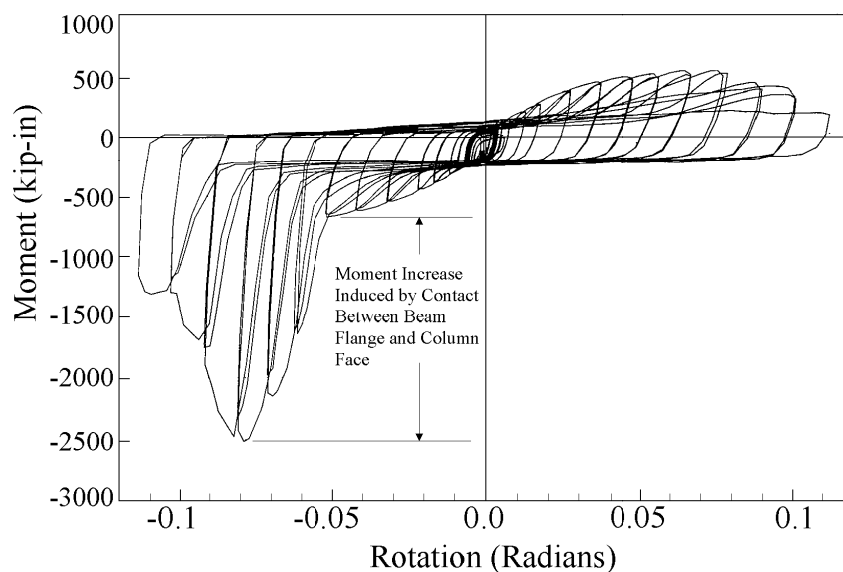


**Figure 5-38 Moment-Rotation Curve for the Bolted Shear Tab Connection**

The shear tab connection has substantial rotational capacity. The rotation is limited by the binding action and depth of the bolt group,  $d_{bg}$ , illustrated in Figure 5-39, and the connection clearance,  $c$ , and the binding moment arms,  $d_1$  and  $d_2$ , illustrated in Figure 5-35. Figure 5-40 shows the rotations that were achieved with the bare steel shear tab connection and several rotations noted for the web-angle connection. The rotations are separated into rotations,  $\theta_p$ , likely to cause a reduction in moment capacity and the rotation,  $\theta_g$ , at which the beam is unlikely

to continue to support gravity loading. All these rotations are plastic rotations: rotations in excess of the elastic rotation where elastic behavior is defined to be the resistance at approximately 60% of the ultimate capacity of the connection. Figure 5-40 shows that there is little apparent difference between the rotations achieved with web-angle connections or shear tab connections. The rotations are large, but they decrease significantly with increasing depth,  $d_{bg}$ , of the bolt group. This decrease is caused by the increased binding action noted with these deeper connections.

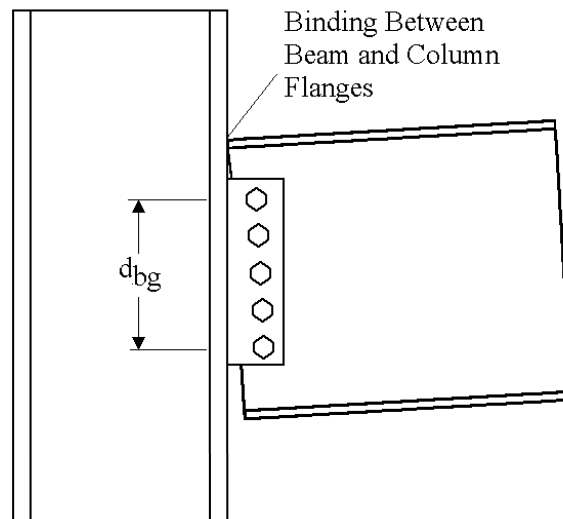


**Figure 5-39 Deformation and Binding of Shear Tab Connection**

The rotations  $\theta_p$  are usually smaller than  $\theta_g$ . However, the difference is small for these non-composite connections, and so  $\theta_p$  has little value to structural engineers, since the primary concern is the point at which the gravity load capacity of the connection is lost. As will be discussed further in Chapter 6,  $\theta_g$  for the bare steel bolted shear tab specimens is consistent with  $\theta_g$  for the composite specimens. As a result, the combined data were used to obtain the best estimate of  $\theta_g$  with the lowest standard deviation. These measured rotations were used in a regression analysis to predict connection rotational capacity, and the plastic rotation capacity,  $\theta_g$ , is

$$\theta_{g\text{mean}} = 0.15 - 0.0036 d_{bg} \quad (\text{radians, with } d_b \text{ in inches}) \quad (5-17a)$$

and

$$\sigma_g = 0.015 - 0.0011 d_{bg} \quad (5-17b)$$

where  $d_{bg}$  is in inches, and the rotation and standard deviation are in radians.

**Table 5-12 Summary of Bolted Shear Tab Connection Tests**

Test Specimen	Slab, Reinforcement and other details	Beam Size and Web Connection	Normalized Connection Stiffness Ks/ (EI/L)	Max Connection Moment (Reversed Cycle)	Plastic Rotation at Loss of Max. Resistance	Avg. Max. Resistance / Mp	Connection Moment Prior to Fracture (Reversed Cycle)	Plastic Rotation at Fracture	Avg. Resistance Prior to Fracture /Mp
1A	No Slab	W18x35 3/8" pl w/4 7/8"A325N	0.87	270 (710)	0.07 (0.19)	0.135	200 (550)	0.13	0.054 (0.15)
2A	No Slab	W24x55 3/8" pl w/6 7/8"A325N	1.22	600 (1600)	0.086 (0.23)	0.183	500 (1500)	0.08	0.071 (0.21)
3A	Transverse Ribs w/wire mesh, 3/4" studs @ 24", lightweight concrete	W18x35 3/8" pl w/4 7/8"A325N	0.92	1650 (850)	0.03	0.47 (0.24)	800 (350)	0.12	0.23 (.099)
4A	Transverse Ribs w/ wire mesh, #5 reinforcing @ 12", 3/4" studs @ 24", lightweight concrete	W18x35 3/8" pl w/4 7/8"A325N	1.47	1600 (1200)	0.015	0.46 (0.35)	800 (500)	0.125	0.23 (0.14)
5A	Transverse Ribs w/ wire mesh, #3 reinforcing @ 12", 3/4" studs @ 24", lightweight concrete, bottom stiffened seat added	W18x35 w/Stiffened Seat	2.37	2300 (1300)	0.053	0.67 (0.38)	2300 (800)	0.053	0.67 (0.23)
6A	Longitudinal Ribs w/ wire mesh, #3 transverse bars @ 12", 3/4" studs @ 12", lightweight concrete	W24x55 3/8" pl w/6 7/8"A325N	1.76	4100 (1600)	0.027	0.59 (0.23)	0 (900)	0.10	0.0 (0.13)
7A	Longitudinal Ribs w/ wire mesh, #3 transverse bars @ 12", 3/4" studs @ 12", lightweight concrete, no concrete in web cavity	W24x55 3/8" pl w/6 7/8"A325N	0.64	2850 (1650)	0.026	0.41 (0.24)	750 (750)	0.09	0.11 (0.11)

**Table 5-12 Summary of Bolted Shear Tab Connection Tests (continued)**

8A	Longitudinal Ribs w/ wire mesh, #3 transverse reinforcing @ 12" & 3/4" studs @ 12", lightweight concrete, bottom flange angle added	W24x55 3/8" pl w/6 7/8"A325N	1.83	4700 (4000)	0.03	0.67 (0.57)	2200 (2000)	0.08	0.51 (0.29)
1B	No Slab - Old Shear Tab Detail	W18x35 1/2" pl w/ 3 1" A325N	0.10	350 (350)	0.125	0.127	350 (350)	0.125	0.127
2B	No Slab-Old Shear Tab Detail	W24x55 1/2" pl w/4 1" A325N	0.08	750 (500)	0.06	0.33 (0.07)	1200 (300)	0.10	0.17 (0.043)
3B	Identical to 3A except normal weight concrete	W18x35 3/8" pl w/4 7/8"A325N	1.09	2100 (800)	0.035	0.61 (0.23)	750 (200)	0.13	0.22 (0.06)
4B	More heavily reinforced slab but similar to 6B.	W24x55 3/8" pl w/6 7/8"A325N	1.10	3500 (2400)	0.028	0.50 (0.34)	0 (1000)	0.085	0.0 (0.14)
5B	Longitudinal Ribs w/wire mesh, #3 transverse reinforcing @ 12" & 3/4" studs @ 12", normal weight concrete	W24x55 1/2" pl w/4 1" A325N	0.52	3000 (1500)	0.028	0.43 (0.21)	500 (1500) excludes binding Moment	0.10	0.071 (0.21)
6B	Identical to 6a except normal weight concrete	W24x55 3/8" pl w/6 7/8"A325N	0.76	3600 (2200)	0.028	0.51 (0.31)	0 (1200)	0.12	0.0 (0.17)
7B	Longitudinal Ribs w/ wire mesh, #3 transverse reinforcing @ 12" & 3/4" studs @ 8", normal weight concrete	W33x118 3/8" pl w/8 7/8"A325N	0.31	5300 (3300)	0.024	0.21 (0.13)	1200 (2800)	0.073	0.048 (0.11)

**Table 5-12 Summary of Bolted Shear Tab Connection Tests (continued)**

8B	Flange angles top and bottom with longitudinal Ribs w/wire mesh, #3 transverse reinforcing @ 12" & 3/4" studs @ 12", normal weight concrete	W24x55 No web connection	1.35	5600 (3700)	0.034	0.80 (0.53)	5600 (3700)	0.04	0.80 (0.53)
----	---------------------------------------------------------------------------------------------------------------------------------------------	-----------------------------	------	----------------	-------	----------------	----------------	------	----------------

## Notes:

1. Average moment at connection determined from moment at centerline of column adjusted for location at face of the column. This is 60 times load for W18 specimens and  $60 \times (150-7)/150 = 0.953 \times 60$ . The moment was also corrected for the horizontal component of force induced by the gravity load actuators.
2. Plastic moment capacity,  $M_p$ , equals 3697 kip-in for 1A, 3511 kip-in for 3A, 3451 kip-in for 4A, 5A, 1B, and 3B, 6995 kip-in for 2A, 6A, 7A, 8A, 2B, 4B, 5B, 6B and 8B, and 24900 kip-in for 7B.
3. Note that moment capacity is normalized by plastic bending moment of the bare steel beam. The connection stiffness is normalized by the  $EI/L$  of the bare steel beam with the clear span half span length (approximately 12.5 ft.) used in the test.
4. Stiffness,  $K_s$ , is a secant stiffness appropriate for development of approximately one half the maximum capacity.
5. This summary is from Lui and Astaneh-Asl (2000).

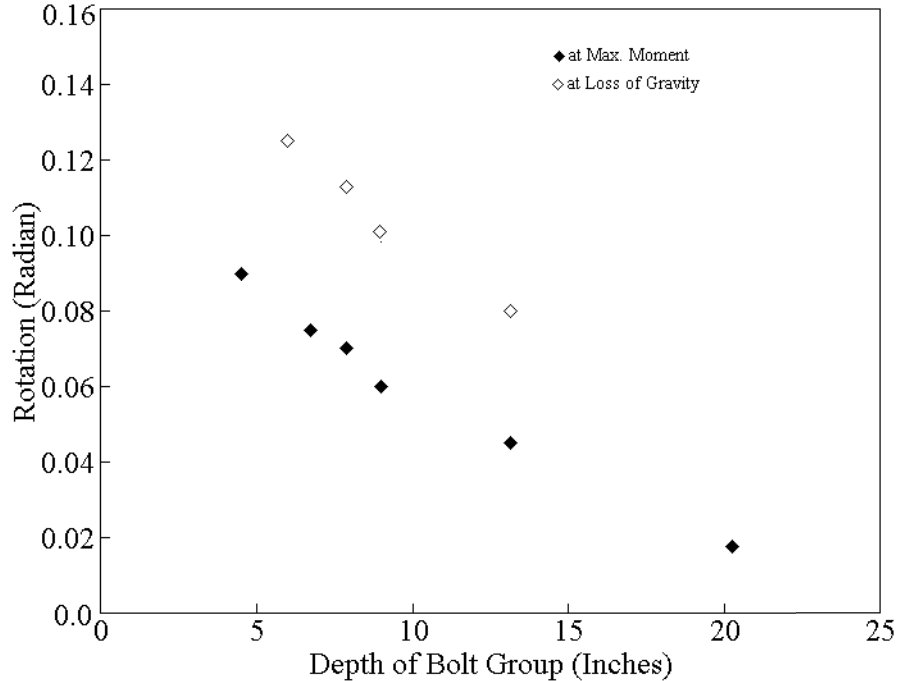


**Figure 5-40 Rotational Capacity of Shear Tab and Web-Angle Connections**

It has been correctly noted (Liu, and Astaneh-Asl, 2000) that the above equation does not consider the gap,  $g$ , between the end of the beam and the binding distances,  $d_1$  and  $d_2$ , noted in Figure 5-35. As a result, a second rotational limit was proposed, and the maximum rotation,  $\theta_g$ , should be the smaller of that estimated by Equations 5-17 or 5-18.

$$\theta_g = \frac{g}{d_{max}} - 0.02 \quad (5-18)$$

where  $d_{max}$  is the larger of  $d_1$  and  $d_2$ . The rotation and standard deviation are in radians, and  $g$  and  $d_{max}$  are in inches.

The stiffness of the connection also depends upon the depth of the bolt group, since deeper bolt groups provide increased connection stiffness as shown in Figure 5-41. Table 5-12 shows that the connection stiffness may be very low, since the rotational spring stiffness of the connection,  $k_s$ , is sometimes as low as 10% of  $EI/L$ . As a result, these connections must always be analyzed as flexible connections with rotational springs as depicted in Figure 5-2. Figure 5-41 demonstrates that the connection stiffness increases approximately linearly with the depth of the bolt group, and a linear regression produced

$$k_s = 28000 (d_{bg} - 5.6") \quad (5-19)$$

where  $k_s$  is in units of kip-in/radian and  $d_{bg}$  is in inches.

This stiffness is not the maximum stiffness of the connection. It is a secant stiffness to the rotation at which 50% to 75% of the maximum resistance is achieved. This stiffness has a limited amount of permanent deformation, but the deformation is not large, and it provides more realistic indications of building performance. The spring stiffness is variable and sensitive to small changes in the connection (for example, tightness of bolts, and the size and alignment of bolt holes). However, because these connections are used for supplemental stiffness and resistance, the variability will not adversely affect the results. Equation 5-19 should then provide a good indication of elastic connection behavior.

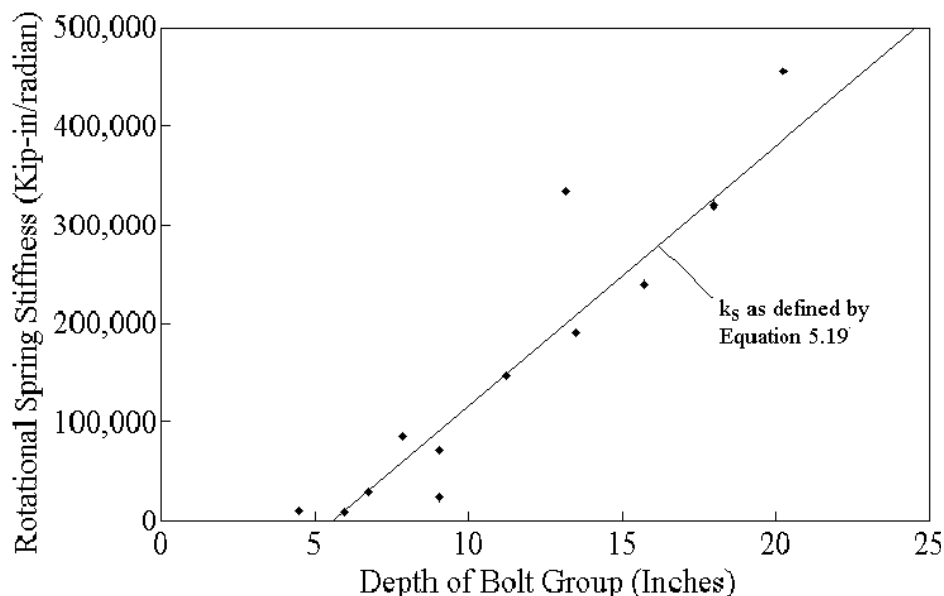


**Figure 5-41 Stiffness of Shear Tab and Web-Angle Connection**

The rotational resistance of the connection is also an important consideration. The moment resistance of the bolt group can conservatively be estimated by assuming each bolt develops its maximum plastic shear capacity as illustrated in Figure 5-42. The moment resistance achieved in this research suggests that the plastic resistance of the bolt may be taken as the shear resistance of the bolt with threads excluded without a resistance factor. However, bearing of the bolts and edge distance requirements must be verified to assure that this limit is appropriate. The estimated moment resistance of the bolt group,  $M_{bg}$ , underestimated the maximum resistance obtained in the experiments summarized in Table 5-12 for all specimens. Nevertheless, the estimation was within 10% of the maximum in all cases.

The bolt group moment resistance,  $M_{bg}$ , is illustrated in Figure 5-43, and the maximum shear force on the bolt group is also illustrated in the figure. The shear tab plate and weld (or the web angle and its bolts or welds) must be strong enough to fully develop the bolt group moment if the rotations given in Equations 5-17 and 5-18 are to be achieved. The moment carried by the shear tab and the weld is the moment at the face of the column,  $M_{fc}$ , rather than  $M_{bg}$ . The difference between these moments may appear to be small, but it can be larger than expected. First, the eccentricity,  $e$ , can be large with some weak axis column bending connections. Second, the total shear force,  $V$ , is large compared to  $M_{bg}$ , and so the change in moment can be significant over the

short distance. The reader is referred to the AISC LRFD provisions (AISC, 1994) and other references (Liu, and Astaneh-Asl, 2000) for design limits for the plate and weld.

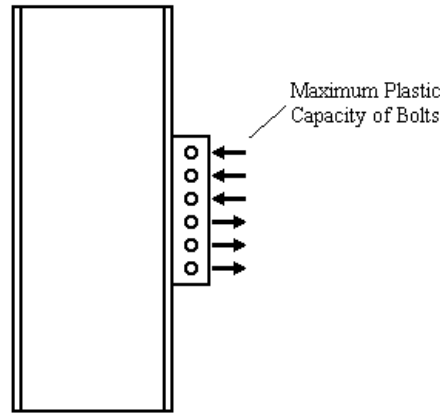


**Figure 5-42 Evaluation of Moment Capacity of Shear Tab Bolt Group Connection**

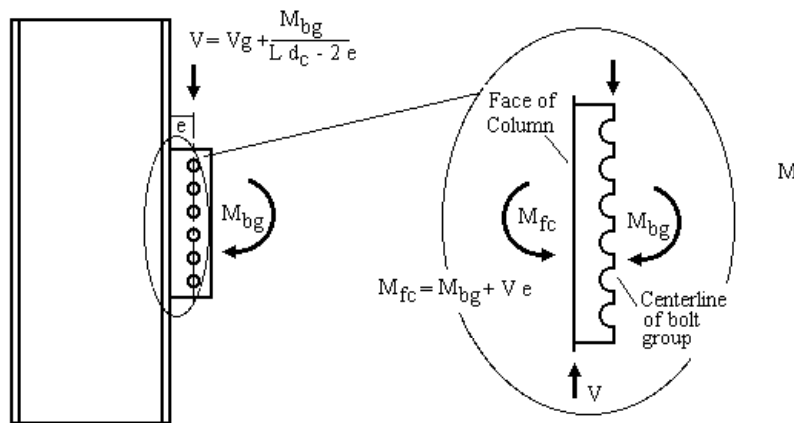


**Figure 5-43 Equilibrium Conditions for Evaluating Shear Tab Plate and Weld**

As noted earlier, the stiffness and resistance defined for these connections are primarily beneficial as supplemental resistance and stiffness for repair and retrofit of existing buildings. The columns used for these connections were normally designed for gravity load only. Therefore, it is necessary to check to see if the columns have enough resistance to support their full gravity load in addition to the moments at the column as illustrated in Figure 5-43 and the shear force due to the lateral load moments accepted by these connections. The specimens summarized in Table 5-12 did not have the axial loads due to the multistory gravity loads on them, and so the behavior observed in these experiments does not include this effect.

## 6. SUPPLEMENTAL AND OTHER CONNECTIONS

### 6.1 General Discussion of Concept

This chapter is somewhat different from the preceding chapters, since it primarily deals with connections that relate to supplemental resistance and energy dissipation. Supplemental stiffness and resistance for lateral loads may be provided by structural elements that are often not considered in the design of lateral load resistance of new buildings, but this resistance and stiffness may aid in economical repair and retrofit of existing buildings. In most cases, this supplemental stiffness and resistance is relatively small, but it is distributed through many locations of the building. Supplemental damping or energy dissipation may also be provided to reduce the seismic demands on both new and existing buildings.

In addition, partial descriptions of several connection alternatives are presented. This is done for several reasons. First, partial descriptions are furnished because some connection alternatives are patented systems, and complete data and documented information on the systems are not available. In other cases, partial descriptions are provided because more complete and comprehensive information is available in another single publication. Finally, some connections have been developed or expressed in concept, but the research necessary to bring that connection up to the level of other connections discussed in this report is incomplete.

### 6.2 Supplemental Connections - Composite PR Connections

Composite PR connections are presented as supplemental connections in this report because their stiffness and resistance are too small for most seismic design applications. However, they may be suitable for adding stiffness and resistance to an existing building. Two types of composite connections are discussed. The composite-shear-tab connection discussion is a follow-up of the discussion started in Chapter 5 on the bolted web-angle and shear tab connection. The effect of the composite action on the strength, stiffness, and ductility of the connection will be noted. There is also an extensive body of information on composite-double-flange-angle or composite-seated beam connections, and this will be discussed in a separate section. It will be shown that these connections are suitable for enhancing an existing building with deficient connections, and they may be suitable for new buildings with low seismic demands. However, composite-double-flange-angle connections lack the large resistance and deformation capacity required for the most demanding seismic requirements. A separate overview of this work will be presented, but detailed recommendations will not be made since there is a comprehensive AISC design manual on these connections.

#### 6.2.1 Composite-Shear-Tab Connections

Shear tab connections are used extensively at beam column connections that are not considered part of the lateral load frame. The beams are commonly designed for composite action for gravity load. As shown earlier, shear tab connections have significant strength and stiffness, which may possibly be used to reduce the cost of repair and retrofit of existing structures. The composite versions of these connections, as illustrated in Figure 6-1, may offer even greater stiffness and moment resistance. Composite connections are expected to be most suitable as supplemental strength and stiffness for damaged or deficient buildings.

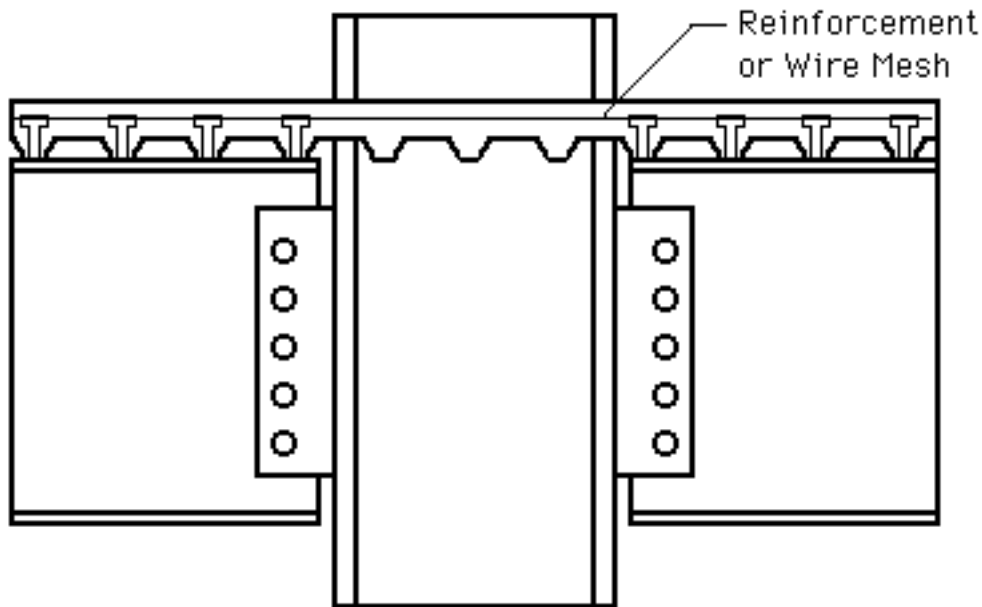


**Figure 6-1 Typical Composite-Shear-Tab Connection**

As noted for the bare shear tab connection in Chapter 5, the composite-shear-tab connection is not evaluated by the yield mechanism and failure mode approach as used for most other connections. This was done because the rotations are sufficiently large that the connection will normally retain its ability to support gravity loads long beyond the  $\theta_g$  of most other steel moment frame connections. The rotation of these connections is inherently caused by plastic deformation of the shear tab, elongation of bolt holes, and slip of bolts in the connection. Brittle fracture with limited rotational capacity is possible if the shear tab and beam web are too thick to permit these local inelastic deformations, or if the shear tab welds do not have adequate capacity. During the SAC Phase 2 research program, 11 tests (Liu and Astaneh-Asl, 2000) were performed on shear tab connections with concrete slabs. Figure 6-2 shows a typical moment rotation curve for these connections. Table 5-12 summarizes the test results. The moment rotation curves are invariably non-symmetric, and there are two primary reasons for this. First, the initial moment in the connection due to gravity load makes the connection appear weaker in one direction than in the other. This occurs because the initial moments due to gravity load are not known nor can they be measured in the experiments. As a result, the applied seismic deformation immediately increases the moments in one direction while initially decreasing the moments in the other direction from this unknown initial state. Second, the connection is also stronger in one direction than in the other. The composite slab increases the moment capacity significantly when the bending moment causes compression in the concrete at the face of the column. However, the composite slab has very little effect when the moment acts in the other direction. This difference in strength is very significant, as can be seen in Figure 6-2. As a result, the strength of composite steel shear tab connections cannot be averaged between the forward and reversed directions as can the bare steel connections. Instead it is appropriate to compute the moment capacity of the composite section in one direction, and the moment capacity of the bare connection (as discussed in Chapter 5) in the other direction. Composite-shear-tab connections may also develop increased bending moment at large rotations due to binding between the beam

and column flanges as discussed in Chapter 5 and as illustrated in Figures 5-38 and 5-39. Again, this binding action does not provide an increase in resistance that can be effectively used in seismic design. This additional strength comes only at very large rotations. It occurs only after the composite stiffness and resistance provided by the connection is lost, and it usually results in fracture of the connection at slightly larger deformations.

The composite action of the connection is lost at rotations that are well below those achievable by the bare steel shear tab connection. The estimated rotation for this loss of composite action is stated as  $\theta_p$  in this section and in this report. After the rotation  $\theta_p$  is reached, the increased resistance provided by the composite slab is effectively lost, and the connection resistance approaches that of the bare steel connection discussed in Chapter 5. As with the bare steel shear tab connection, the maximum rotational capacity of the composite-shear-tab connection is limited by the binding action, the clearances between the ends of beam flanges, and the face of the column as illustrated in Figures 5-35 and 5-38, and the depth,  $d_{bg}$ , of the bolt group. The binding action causes a significant increase in the moment resistance, and fracture of the connection occurs shortly thereafter because of the large tensile forces developed in the shear tab. This additional resistance cannot be relied upon for seismic design, and it is excluded from the tabulated moment capacities listed in Table 5-12 and the moment capacity predictions included in this section. As with the bare steel connection, deep bolt groups also cause larger moments. Deep bolt groups also reduce the rotational capacity of the connection because the top and bottom bolts of the group cause increased binding action with large bolt forces. Interior bolts in the group may not be able to develop their full yield force because top and bottom bolts may fracture at a smaller rotation than needed to fully develop the interior bolts. Figure 6-3 shows the rotations that were achieved with the composite-shear-tab connection. In addition, rotations achieved with bare steel web-angle and shear tab connections are also plotted in the figure. The rotations are separated into rotations,  $\theta_p$ , which are likely to cause a reduction in composite moment capacity and the rotation,  $\theta_g$ , at which the beam is unlikely to continue to support gravity loading. All of these rotations are plastic rotations. Comparison of these rotations shows that  $\theta_p$  of the composite connection is generally smaller than that seen with the bare steel connection. However,  $\theta_g$  of the composite connection is essentially the same as that achieved with the bare steel connections. Further, the bare steel connection moment resistance is retained until the connection deforms to near this larger rotation. The rotations are large, but they decrease significantly with increasing depth,  $d_{bg}$ , of the bolt group. The permanent deformation is concentrated in the connection elements and the slab near the face of the column, and so the beam span length has little effect on the rotational capacity.

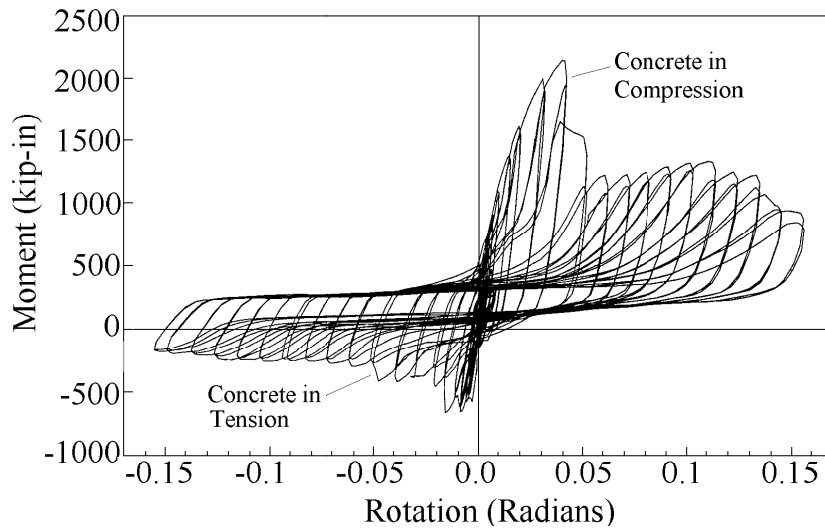


**Figure 6-2 Moment-Rotation Curve for the Composite-Shear-Tab Connection**

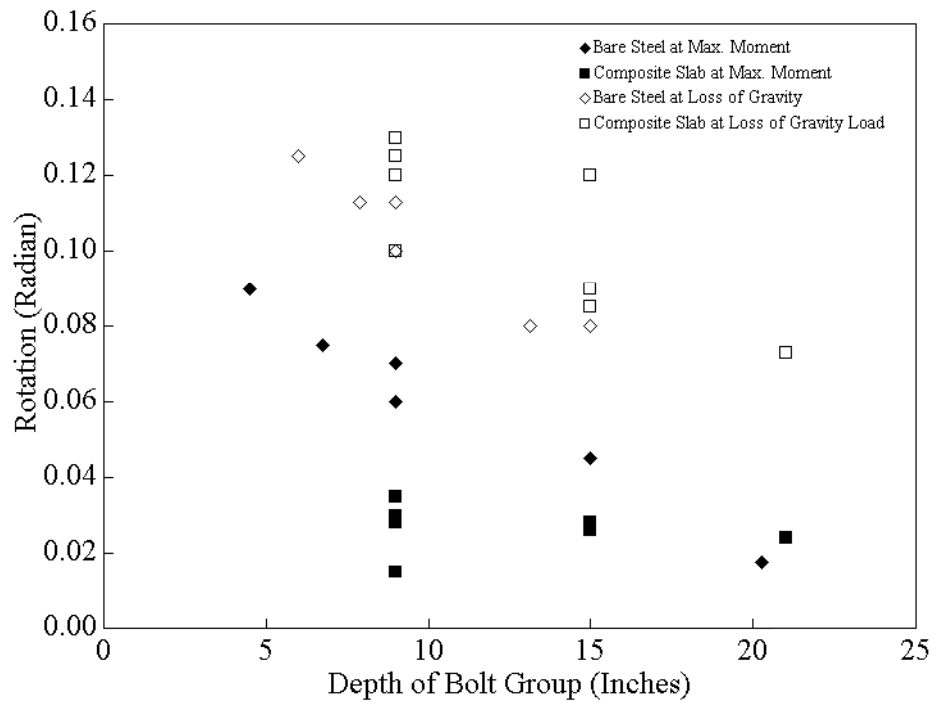


**Figure 6-3 Rotational Capacity of Composite-Shear-Tab Connections**

These measured rotations were used in a regression analysis to predict connection rotational capacity, and the plastic rotation capacity,  $\theta_p$ , is

$$\theta_{p\text{mean}} = 0.029 - 0.0002 d_{bg} . \tag{6-1a}$$

The standard deviation,  $\sigma_p$ , of  $\theta_p$  is

$$\sigma_p = 0.0067 + 0.0006 d_{dg}. \quad (6-1b)$$

The extra moment provided by composite action of the slab is lost when the plastic rotation exceeds  $\theta_p$ . However, the moment resistance provided by the bare steel shear tab connections continues to be developed until a much larger rotation,  $\theta_g$ . This larger rotation is approximately the same as the maximum rotation for supporting gravity loads,  $\theta_g$ , and

$$\theta_{g\text{mean}} = 0.15 - 0.0036 d_{bg}, \quad (6-2a)$$

and the standard deviation,  $\sigma_g$ , of  $\theta_g$  is

$$\sigma_g = 0.015 - 0.0011 d_{bg} \quad (6-2b)$$

where the rotations and standard deviations of the rotations are in radians, and  $d_{bg}$  is in inches.

The maximum rotation,  $\theta_g$ , is significantly larger than  $\theta_p$ . This rotation is identical to the rotation noted for the bare steel shear tab connection in Equation 5-17, since the data for composite and bare steel connections were statistically similar for the large rotations and were combined to provide a larger database. As noted (Liu and Astaneh-Asl, 2000) with the bare steel shear tab, Equation 6-2 does not consider the gap,  $g$ , between the end of the beam and the binding distances,  $d_1$  and  $d_2$ , noted in Figure 5-35. As a result, a second rotational limit was proposed, and the maximum rotation,  $\theta_g$ , should be the smaller of that estimated by Equations 6-2 or 6-3.

$$\theta_g = \frac{g}{d_{\text{max}}} - 0.02, \quad (6-3)$$

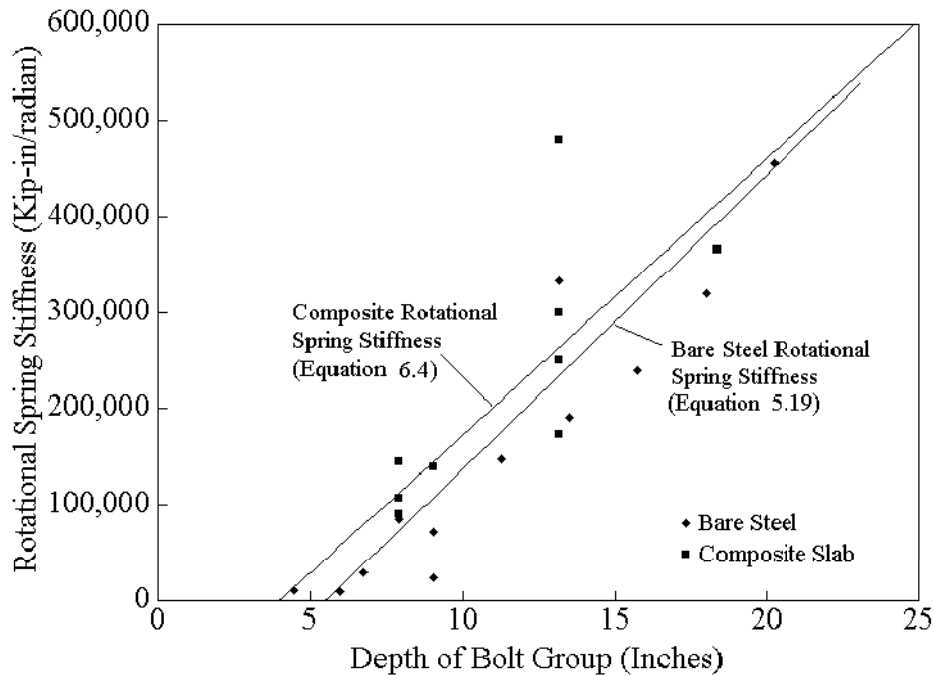
Note that  $d_{\text{max}}$  is the larger of  $d_1$  and  $d_2$  as defined in Figure 5-35. The dimensions  $d_{\text{max}}$  and  $g$  are in units of inches.

Figure 6-4 provides a comparison of the measured rotational spring stiffness for the composite shear tab connections to that of the bare steel shear tab connections. The stiffness of the composite shear tab connection also depends upon the depth of the bolt group and the moment arm to the slab in compression. Deeper bolt groups and deeper sections provide increased connection moment and stiffness. The rotational spring stiffness of these composite connections is larger than that provided by the bare steel shear tab connections, but the increase is not as large as one may expect. This can be seen by comparing the test data for bare steel and composite specimens and by comparing the least squares regression fit estimates of their stiffness in the figure. Table 5-12 shows that the connection stiffness may still be relatively low, since the rotational spring stiffness of the connection,  $k_s$ , is commonly between 30% and 150% of  $EI/L$ . As a result, these connections also must be analyzed as flexible connections with rotational springs as depicted in Figure 5-2. Figure 6-4 shows that the connection stiffness

increases approximately linearly with the depth of the bolt group, and so a linear regression of this was also computed so that

$$k_s = 28000 (d_{bg} - 3.3) \quad (6-4)$$

where  $k_s$  is in units of kip-in/radian and  $d_{bg}$  is in units of inches.



**Figure 6-4 Comparison of Stiffness of Composite and Bare Steel Shear Tab Connection**

The rotational resistance of the connection is also an important consideration. To the extent that the failure of these connections is brittle, the resistance should be computed (Liu, and Astanteh-Asl, 2000) based upon an assumption of linear elastic behavior. The resistance at loss of composite action clearly appears to be more brittle than the failure of the bare steel connections. This can be noted by the smaller rotation at this loss of composite action in Figure 6-2 as compared to Figure 5-40, and by examination of Table 5-12. Nevertheless, the ultimate moment capacity is achieved at relatively large rotations compared to the rotations achieved with most moment frame connection types. Figure 6-5 provides a schematic of the proposed evaluation procedure for determining the maximum moments in these composite connections. With this proposed procedure, the connection on the left hand side of the column in the figure is treated as a bare steel shear tab connection as discussed in Chapter 5, since the slab is assumed to have no stress with this part of the model. The opposite side of the column has compression in the composite slab, and the total magnitude of this compressive force is limited by the smaller of:

- the compressive capacity of the concrete in contact with the face of the column, or
- the maximum tensile capacity that can be developed by shear in the bolts.

Comparison of various simplified models of predicting composite resistance shows that the resistance was conservatively estimated by assuming each bolt develops its maximum capacity as illustrated in Figure 6-5 until the compressive capacity of the concrete on the face of the column reaches its maximum compressive capacity. On this composite side of the connection, the bolts, which are furthest from the composite slab, develop their maximum plastic capacity. The moment computed by this method is considered the composite moment capacity,  $M_{comp}$ , as illustrated in Figure 6-6.

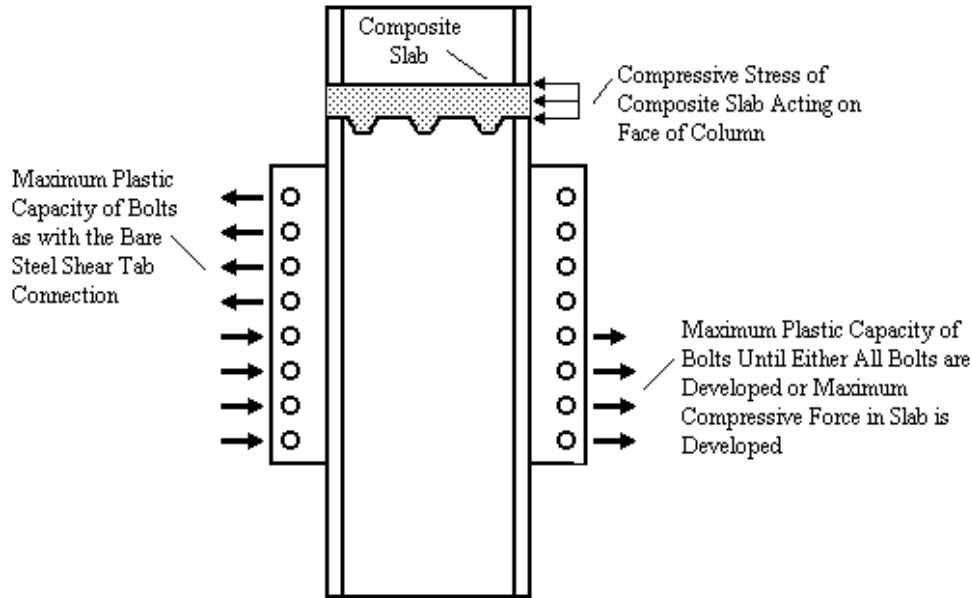


**Figure 6-5 Evaluation of Moment Capacity of Connection**

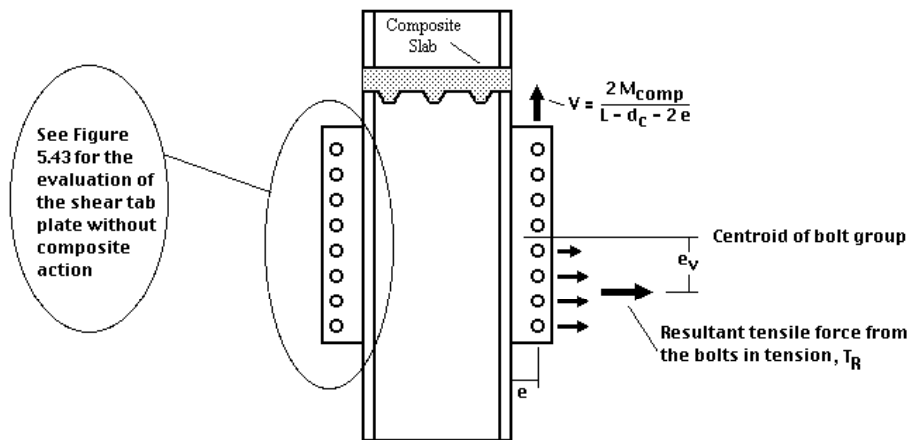


**Figure 6-6 Forces Applied to the Shear Tab Plate and Weld**

As with the bare steel connection in Chapter 5, the shear tab plate and the shear tab weld must be strong enough to develop fully this composite action if the rotational capacity indicated

in Equations 6-1 and 6-2 are to be achieved. The connection with tensile stress at the top of the connection must be evaluated by the procedures discussed in Chapter 5 and summarized in Figure 5-43. The connection with compression in the concrete slab must be evaluated as illustrated in Figure 6-6. The shear tab plate and weld are subjected to a resultant tensile force,  $T_R$ , and this force has an eccentricity,  $e_v$ , as shown in the figure. The shear force,  $V$ , acting on the plate is caused by the connection moment only, since the gravity load shear force,  $V_g$ , would reduce this connection shear. Thus, the plate and the weld must be strong enough to resist the resultant tensile force, the shear,  $V$ , and the moment at the face of the column caused by  $V$  and  $T_R$  with their respective eccentricities. Permissible capacities for the plate and the weld can be established according to the AISC LRFD provisions (AISC, 1994). The reader is referred to (Liu and Astaneh-Asl, 2000) for a somewhat different and more detailed design procedure.

As noted for the bare steel shear tab connection, the stiffness and resistance defined for these composite shear tab connections is primarily beneficial as supplemental resistance and stiffness for repair and retrofit of existing buildings. The columns used for these connections were normally designed for gravity load only. Therefore, it is necessary to check to see if the columns have enough resistance to support their full gravity load in addition to the moments at the column as illustrated in Figures 5-43 and 6-6 and the shear force due to the lateral load moments accepted by these connections. It should be noted that the specimens summarized in Table 5-12 did not have the axial loads due to the multi-story gravity loads on them, and so the behavior observed in these experiments does not include this effect.

### 6.2.2 Other Composite PR Connections

Other flexible connections such as the double-flange-angle connection and seated beam connection have been used in steel frames for many years. The stiffness and resistance of these flexible connections are typically ignored in the structural design. However, it is well known that these PR connections have some rotational stiffness and resistance, and the stiffness and resistance may be much larger when the connection is used in conjunction with a composite floor slab as illustrated in Figures 6-7 and 6-8.

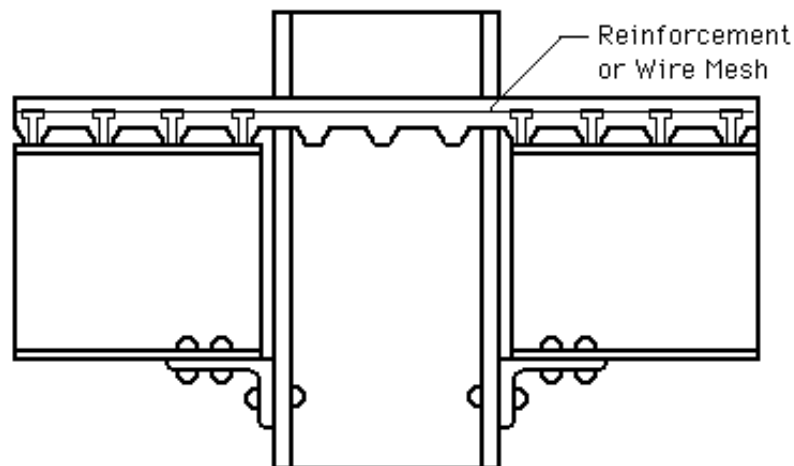


**Figure 6-7 Typical Composite-Seated-Beam Connection**

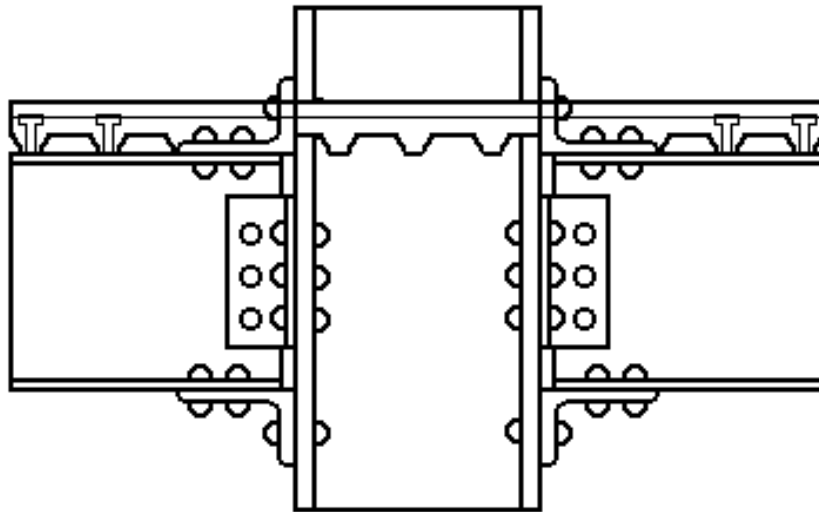


**Figure 6-8 Typical Composite-Double-Flange-Angle Connection**

Composite PR connections have been studied in a number of research programs (Leon, 1994; Ammerman, and Leon, 1987; Leon et al., 1987; Bernuzzi et al., 1991; Nethercot, 1991; Davison et al., 1990; Puhali et al., 1990). Further, the research has been primarily directed to gravity loads with tests under monotonic loading. However, a few cyclic tests (Ammerman, and Leon, 1987; Leon et al., 1987; Bernuzzi et al., 1991) have been performed to evaluate lateral load behavior. In addition, many of the tests were completed in Europe with different detailing standards and seismic performance expectations from those of the US. Figures 6-9 and 6-10 show typical moment-rotation hysteresis curves obtained from these cyclic tests. It can be seen that the hysteretic curves are pinched and deteriorating. The strength of the connections is usually smaller than the plastic bending capacity of the steel beam. The plastic rotations can be quite large if the proper yield mechanism is achieved, but they can also be relatively small as shown in Figure 6-10. There are clearly not enough cyclic experimental results to fully evaluate the behavior of these composite PR connections, but when the experimental data for monotonic loading is added, a reasonable assessment can be made. Further, there are a large number of failure modes, and some of the modes are complex and difficult to compute.

The behavior of composite PR connections depends on whether they are interior connections or exterior connections. This would seem likely because compressive stress between the concrete slab and the steel column must develop to obtain composite behavior with cyclic rotational resistance, and compression cannot develop on both sides with a one-sided connection. A larger contact area between the steel and concrete is available when the concrete fills the inside of the flanges, and so better behavior is sometimes noted under these conditions. While the resistance obtained with the composite PR connections may not be large, it is not insignificant, and moderate rotational capacities are possible. However, as noted in Chapter 4, the increased stiffness and resistance provided by the composite slab will be relatively less as the beam depth increases, because the thin deck slab cannot shift the neutral axis as much with deeper beam sections. The energy dissipation is also quite limited as can be seen in Figures 6-9 and 6-10, but the energy dissipation is probably no smaller than the energy dissipated by many other PR connections discussed in Chapter 5. Their behavior is variable, and related to the mode

of failure. Researchers (Bernuzzi et al., 1991) tabulated and summarized test results on approximately 44 tests (mostly monotonic) on PR composite connections. Some of these specimens failed through local yielding and web crippling of the column due to the large compressive stress that may develop at the bottom flange connection, and these specimens obtained rotations in the order of 0.035 to 0.065 radians before failure occurred. Other specimens failed through fracture of the reinforcement of the deck slab, and these specimens obtained rotations in the order of .01 to .045 radians. Still other specimens developed yielding in the bottom clip angle and shear fracture of the bolts connecting the bottom flange to the angle or restraining element, and these had rotations in the order of .03 radians. Finally, a few specimens developed the full yielding of the beam. The composite slab raised the neutral axis of the beam to a level near the top flange. This beam yielding caused increased strains in the bottom flange and local buckling of the bottom flange was noted. These specimens had rotations of 0.025 to 0.045 before failure occurred. These rotations were obtained with modest sized specimens (normally W21 or less), and so reduced rotational capacity must be expected as the beam depth is increased.

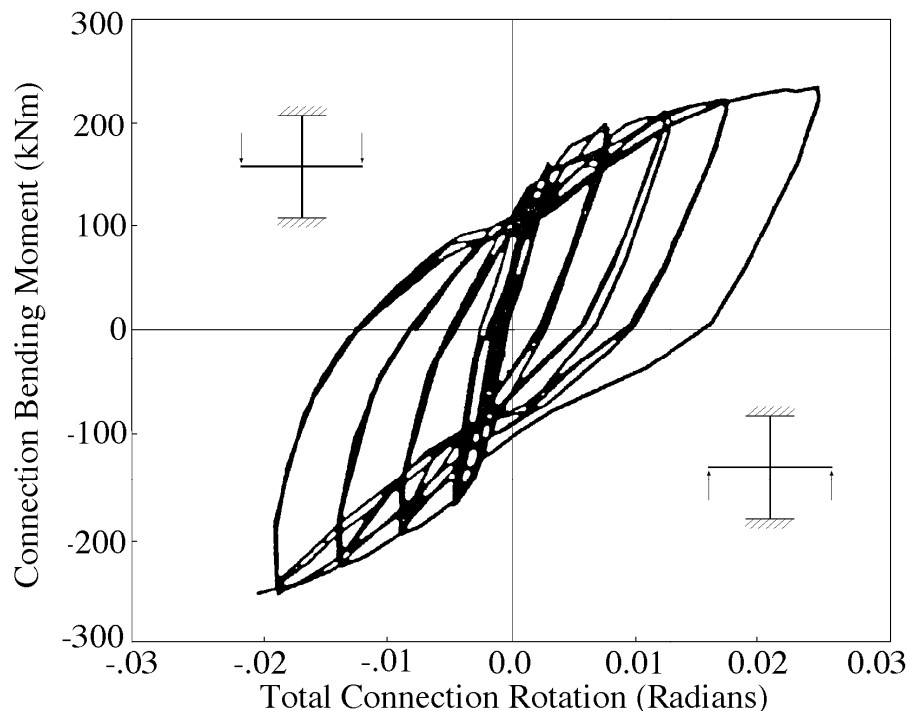


**Figure 6-9 Typical Moment Rotation Curve for Composite PR Connection**

The benefit of composite action is most significant with connections that are relatively flexible, but research (Daniels et al., 1970) has shown that even welded flange connections may be stiffened or strengthened by the addition of a composite slab to the connection. Again, the depth of the beam is important. This can be observed from the discussion on composite slabs in Chapter 4, because the post-Northridge connections discussed in that section had relatively deep beams, and little increase in strength and stiffness due to the addition of composite slabs could be observed in those tests. It should be recognized that the monotonic test results are again

likely to produce upper bounds on the rotational capacity achievable with cyclic tests. Therefore the lower range of the rotations achieved with monotonic tests may be used to establish approximate rotation limits for cyclic loading. The rotation at yield is also difficult to predict for these connections, since the connections have very rounded force-deflection curves. They are stiff at low stress levels, but the tangent stiffness decreases rapidly with increasing load. This is similar to the behavior noted for the T-stub and double-flange-angle connections, and therefore stiffness modeling similar to that used for these other connections in Chapter 5 (Sections 5.4 and 5.5) is appropriate.

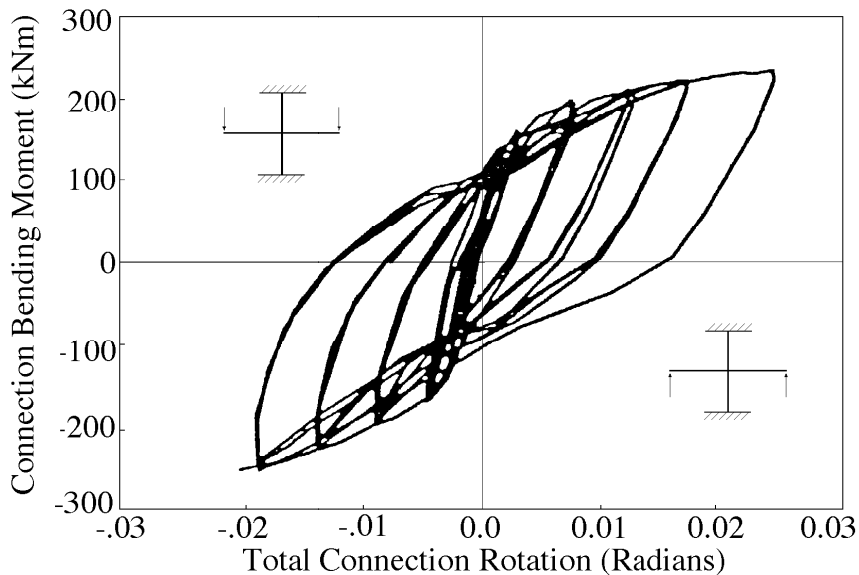


**Figure 6-10 Typical Composite Moment Rotation Curve**

As mentioned earlier, relatively few of these connections are designed and built to be PR composite connections. However, many connections may still behave in this manner even though they were not designed to achieve this composite resistance. This true behavior may benefit in the seismic rehabilitation of some structures, since additional seismic resistance is achieved through calculation of the true behavior with minimal addition cost. This composite action may also have been a contributing factor to the limited damage to steel frame buildings with fractured connections after the Northridge earthquake. However, several conditions are important for these connections. These include:

- The behavior of interior and exterior joints are inherently different because of the contact between the concrete slab and the column face on one or both sides of the column.
- The concrete slab must make bearing contact on the column face.
- The slab must have some tensile reinforcing provided by reinforcing bar or welded wire fabric. Some tests suggested inferior performance with welded wire fabric over that achieved with rebar.
- There must be a shear transfer mechanism between the steel beam and the reinforced concrete slab.

- The stiffness and moment capacity for individual connections will be different in positive and negative bending as noted for the composite-shear-tab connection in the previous section.

If these conditions are satisfied and appropriate strength and failure mode calculations are made, PR composite connections may provide some benefit to the seismic performance. They may be useful as secondary or supplemental seismic resistance. It is questionable, however, whether these connections have the strength, stiffness, and ductility necessary to provide the primary seismic resistance for steel moment frames. The calculations required to predict the behavior of these composite PR connections can be complex. The tests performed to date suggest the greatest ductility and inelastic behavior occurs if the connection develops the plastic capacity of the steel beam, or with yielding of angles and other connecting elements. The least ductility may be achieved with tensile yielding of the connections between the seat angle and the column flange or tensile yield and fracture of the deck reinforcement. A number of other yield mechanisms and failure modes are possible, and they may produce intermediate ductility levels. It should be noted that the rotational limits discussed in this section are equivalent to  $\theta_p$  rotations, because these rotations coincide with reaching the first failure mode and sustaining a significant loss of resistance. Most of these composite PR connections may still develop relatively large  $\theta_g$  rotations, since gravity loads can often be supported as large deformations occur.

Several issues are likely to be important with these connections. These include:

- A wide range of failure modes and yield mechanisms are possible. The ductility, energy dissipation, and rotational capacity are likely to be dependent upon these modes of behavior, and so models are needed to predict the strength, stiffness, and ductility with the different mechanisms.
- Some of the variations of these composite PR connections, such as illustrated in Figures 6-7 and 6-8, may develop prying action in the bolted connections. Prying behavior must be understood for seismic design of these connections.
- Energy dissipation and rotational capacity are likely to depend upon the inherent looseness and flexibility in the steel connection.
- The major goal of these connections may be modifications to existing structures, but research (Leon, et al., 1996) has shown that the best performance of these connections is achieved when the slab is properly reinforced to aid in the development of the connection. Existing slabs are unlikely to have that amount of reinforcement, and this may limit the utility of the connection.

This discussion has provided an overview of the behavior of composite PR connections. It can be seen that these connections are not likely to have the moment resistance or rotational capacity required for the most demanding seismic applications. They are likely to be able to tolerate large rotations while supporting gravity loads, but their stiffness and resistance due to composite behavior will be reduced at much smaller rotations. In general, they will not be able to develop the full plastic capacity of the beams, and their stiffness will be well below that of a rigid connection as defined by Equation 5-3. Further, the benefits of these composite

connections will be most significant with modest sized members where the composite connections are at every beam-to-column connection distributed throughout the building. Nevertheless, composite PR connections may be beneficial in upgrading or repairing an existing building, since the supplemental strength and stiffness may reduce the cost of these structural modifications. This report does not provide the details of utilizing these composite PR connections, because a comprehensive document (Leon, et al., 1996) on these connections has already been published by AISC. The reader is referred to this document for this more detailed information.

### 6.3 Supplemental Connections – Weld Overlay Connections

Many steel moment-frame connections were damaged during the Northridge earthquake. repair and retrofit of these existing connections are concerns that were partially addressed in earlier chapters and sections, and are also more comprehensively addressed in an AISC Design Guide (Gross, et al., 1999). However, some research has attempted to develop more economical methods of repair and retrofit than those described earlier in this report. The weld overlay method as depicted in Figure 6-11 has been proposed as one means of economically improving the performance of some pre-Northridge connections. Research (Anderson, et al., 1995; Simon, et al., 1999; Anderson, et al., 2000) has been performed on this method through past NSF research, through volunteer efforts of researchers and engineers, and through the SAC program (Anderson, et al., 2000). Table 6-1 summarizes these connection experiments. Note that the #1 and #2 specimens from the table were tested outside (Simon, et al., 1999) this research program.

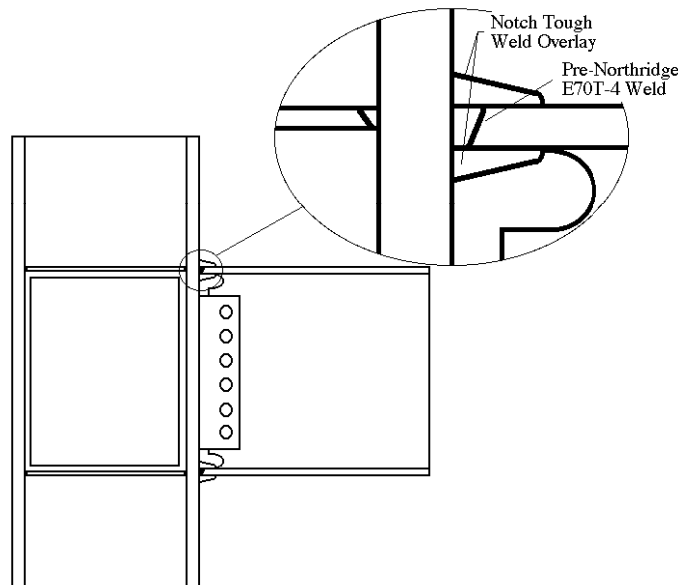


**Figure 6-11 Schematic of Weld Overlay Method**

The overlay method employs a significant weld overlay made with notch tough weld electrodes to strengthen the weld, reduce the stresses in the pre-Northridge weld, and provide a significant increase in the level of toughness of the welded flange connection. The weld overlay increases the tensile area at the face of the column, but it also extends well out on the beam

flange base metal as shown in the figure. A number of questions are raised by this practice. These include:

- This connection alternative mixes weld metal from E70T-4 electrode with tough electrodes such as E7018 or E71T-8. Research (Johnson, 2000) has been completed to address the effect of intermixed weld metal on the CVN notch toughness. It was shown that mixing of E7018 weld metal with E70T-4 root metal caused some (possibly significant) reduction of the CVN toughness over that provided by E7018 electrodes alone. Mixing of E71T-8 electrode with E70T-4 root electrode had a smaller effect. In general, it appears that the toughness of the intermixed weld metal was significantly greater than that typically provided by E70T-4 electrode acting alone.
- This connection effectively fills the weld access hole region with the overlay weld metal. Therefore, the quality of the weld metal may be affected by the reduced clearance in this region. In other cases, field cutting in the weld access hole area is needed to obtain the full overlay required of the connection. Field cutting may improve the surface finish and transition geometry of the weld access hole as it enters the beam flange. Much depends upon the grinding or finish that is applied to the cut surface. At the same time, field cutting may introduce roughness and irregularities in the weld access hole region and in the transition of the weld access hole to the beam flange. These irregularities may promote crack development. Several specimens of Table 6-1 had cracking into the k-area from the weld access hole region. This cracking may be affected by flaws introduced by the limited space available for completing the weld at the toe of the overlay and by flaws introduced during cutting of the weld access hole.
- Large quantities of overlay metal are required, and the volume should increase significantly with increasing beam flange area. At the same time, a given inelastic rotation demand places greater strain demands on deeper connections. Thus, the economy and practicality of this connection will vary depending upon the beam size, and it is necessary to establish appropriate limits for this connection alternative. However, it should also be recognized that the weld overlay method requires minimal backgouging of existing metal, and this helps to reduce the cost of the modification as well as minimizing the disturbance to the existing material. In addition, the weld overlay does not dramatically strengthen or reinforce the connection as do the coverplate and haunch methods described in Chapter 4. Consequently, the weld overlay method does not increase the demands on the panel zone or the column for strong-column-weak-beam criteria.

A series of tests was performed to develop a design method for this connection and to address issues such as those noted above. Figure 6-12 is a moment-rotation curve from one of these tests. A number of the moment-rotation curves (including Figure 6-12) showed specimen slip during the testing that was not removed from the reported research results. This slip causes discontinuities in the moment rotation behavior as illustrated in the figure, and leads to slight overestimates of the specimen rotation. The rotation estimates included in Table 6-1 remove the rotation contributed by the slip, since this cannot be expected in real buildings, and so rotation estimates are sometimes slightly different from those reported by the authors (Simon, et al., 1999; Anderson, 2000). Examination of Table 6-1 shows that all tests were completed on modest sized beams, and that the method significantly improved the inelastic rotational capacity over that expected for recent pre-Northridge connections. At the same time, the rotations

**Table 6-1 Summary of Weld Overlay Connection Test Results**

Test Specimen	General Description and Information	Beam and (Column) Sizes	Plastic Rotation at Failure	Failure Mode
# 1 (Simon, et al., 1999)	Tested as damaged construction with bottom flange weld fractured – the weld overlays were applied over a 3/8" crack - no doubler plate – 1/2" specified (11/16" measured) Class A Weld Overlays on both top and bottom sides of bottom flange and the bottom side only of top flange with E7018 electrode	W21x68 (W16x77)	.033	Top beam flange cracked and k-area crack at bottom flange of beam
# 2 (Simon, et al., 1999)	Tested as undamaged construction - with doubler plate - 3/8" specified (9/16" to 11/16" measured) Class C Weld Overlays on both top and bottom sides of both flanges with E7018 electrode	W21x68 (W16x77)	0.028	Horizontal crack at top k-area leading to flange fracture
SAC 1 (Anderson, et al., 2000)	Tested as undamaged construction - no doubler plate - Class C Weld Overlays on both top and bottom sides of both flanges with E71T-8 electrode - overlay extended 1/4" beyond web cope on outer sides	W21x68 (W16x77)	0.04	Crack in beam flange in front of overlay.
SAC 2 (Anderson, et al., 2000)	Tested as undamaged construction - Minimum required of Class C Weld Overlay, with doubler plate - 9/16" overlays on both top and bottom sides of both flanges with E71T-8 electrode - overlay extended 1/4" beyond web cope on outer sides	W21x68 (W16x77)	0.03	k-area crack propagating through bottom flange of beam
SAC 3 (Anderson, et al., 2000)	Tested as undamaged construction - Minimum required 5/16" Class C overlay on top and bottom sides of bottom flange and 5/8" Class A overlay on bottom sides of top flange with E71T-8 electrode - overlay extended 1/2" beyond web cope on outer sides	W21x68 (W16x77)	0.038	k-area crack propagating through bottom flange of beam
SAC 4 (Anderson, et al., 2000)	Tested as undamaged construction - Minimum required Class C Weld Overlay - 5/16" overlays on both top and bottom sides of both flanges with E71T-8 electrode - overlay extended 1/2" beyond web cope on outer sides	W30x99 (W14x176)	0.027	k-area crack propagating through bottom flange of beam
SAC 5 (Anderson, et al., 2000)	Tested as bottom flange damaged with 1/8" crack but top flange undamaged - Class A Weld Overlay - 5/8" overlays on both top and bottom sides of bottom flange but on only bottom side of top flange with E71T-8 electrode - overlay extended 1/2" beyond web cope on outer sides	W30x99 (W14x176)	0.012	Fracture of top flange of beam

Notes:

1. Plastic rotations are rotations prior to significant loss of resistance or initial fracture of the connection and are story drift rotations.
2. All flange welds are E70T-6 full penetration welds. All bottom flange backing bars removed, backgouged, and reinforced with 1/4" fillet of E71-T8.
3. For DC-1, DC-2, Dc-3, CW-1, and CW-2 moment at face of column determined graphically, yield stress assumed to be nominal 50 ksi, and dimensions inferred from test setup for LS-2.

achieved with the weld overlay connection are significantly smaller than those achieved with most of the post-Northridge connections described in Chapter 3. Thus, the weld overlay improves the expected performance of undamaged pre-Northridge connections, but it does not bring the behavior up to the same standards that are possible with new connections. Further, the limited rotational capacity achieved with modest sized specimens in this research program suggests that the method may not provide adequate improvement to the seismic performance of large members and connections that are often used in modern steel moment frames. However, weld overlays offer considerable promise for small and moderate sized members.

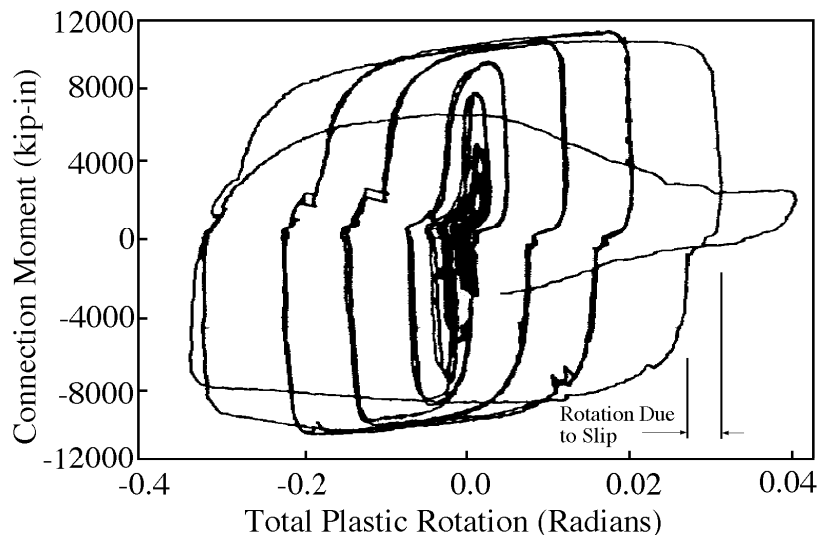


**Figure 6-12 Typical Moment-Rotation Curve for Weld Overlay Connection**

The overlay method is considered as both a method of repair of cracked welds and a retrofit of undamaged pre-Northridge connections. Specimens # 1 and SAC 5 are initially damaged specimens, and # 2 and SAC 1, 2, 3, and 4 are initially undamaged specimens. Class designations are used to correlate the modification method to the initial condition of the connection. Class A repairs are repairs primarily intended for connections where less than 50% of the flange capacity is assured, and class C modifications are those intended for the case where more than 50% of flange capacity can be assured. Several other classes are proposed, but they are not discussed here since there was no experimental effort to verify these other classes of connection.

Two design procedures have been proposed for the weld overlay connection, but unfortunately neither of the proposed procedures have been experimentally verified since all of the specimens have slight variations in their design and none of the test specimens were designed by either procedure. The simplified procedure (Anderson, et al., 2000) incorporates the basic procedures of the more complex method. For the simplified method, the connection shear force,  $V$ , is computed assuming that the plastic hinge develops a distance  $d/2$  from the face of the column. The weld overlay is designed for the full yield tensile force of the flange, and one half the shear force is distributed to each flange weld as depicted in Figure 6-13 for a class A connection. For a class C connection, the existing flange weld is assumed to be at least 50%

effective, and the forces are decreased proportionally. In both cases, the weld is sized at an effective throat as illustrated in the figure. This simplified method provides a basis for sizing the weld overlay, but provides no guidance on how long the overlay should be. All tests were run with weld overlays that extended to (and often beyond on the outer flange side) the intersection of the weld access hole with the beam flange. This simplified design method does not satisfy equilibrium, since it assumes different moments at the face of the column when determining the tensile force,  $T$ , and the shear force,  $V$ , but it ignores the shear capacity (not the moment capacity) of the web connection.

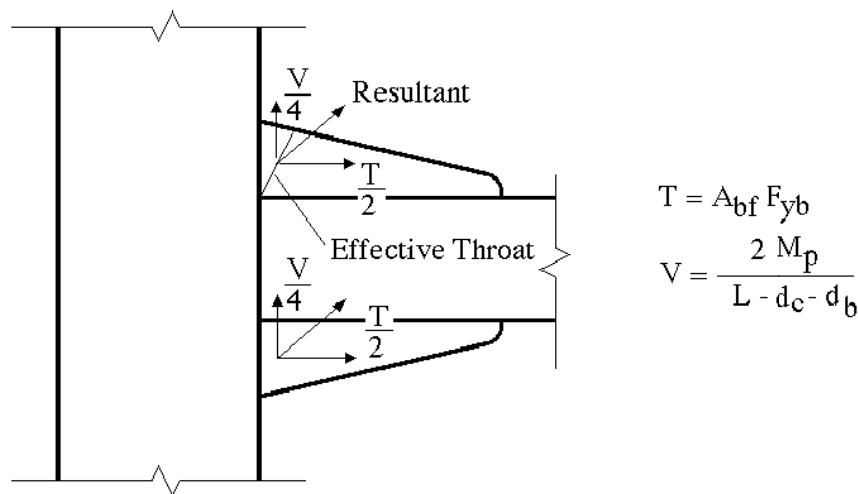


**Figure 6-13 Schematic of Simplified Overlay Design Method**

The second design method (Maranian, 1999) is different, more complete, and more complex than the simplified method. The method addresses the concern that a large part of the shear force is transferred by the flange welds. This second method has some similarities to the design methods for the seated beam connection (Garrett, and Brockenbrough, 1986). In this proposed method, the excess shear not assumed to be carried by the shear tab connection is distributed to the beam flange as depicted in Figure 6-14, and the excess shear is transmitted to the column through bending and shear of the weld overlays. The beam flange is used to help carry these combined loads with class C connections. The weld overlay (and beam flange in the case of class C connection) are checked for the combined bending, shear, and tensile yield force at the face of the column. The beam flange is checked for the combined bending, shear, and tensile force at the toe of the overlay. The excess shear is given a parabolic distribution to the flange as depicted in the figure, but the length of the distribution is limited by the yield stress on the beam web, which is similar to the seated beam design procedure. As with the seated beam analogy, local bending moments and shear in the beam flange and overlay are computed by equilibrium. This proposed method results in relatively high computed local stress, and stresses are limited based upon the properties of the materials. Restrained conditions are assumed in the steel, since restraint increases the apparent yield stress under tension. This helps the steel to tolerate the large computed local stresses. The justification for this restraint is not provided, nor does it appear to be well justified at the edge of the weld overlay, since a three-dimensional stress state is difficult to hypothesize at this location. As noted earlier, neither design method was used to

design any of the test specimens, and, as a result, the design methods were not verified in the research program. They are presented here only for information regarding the present thinking of the developers of this connection. The reader is referred elsewhere (Maranian, 1999) for further details on this design method.

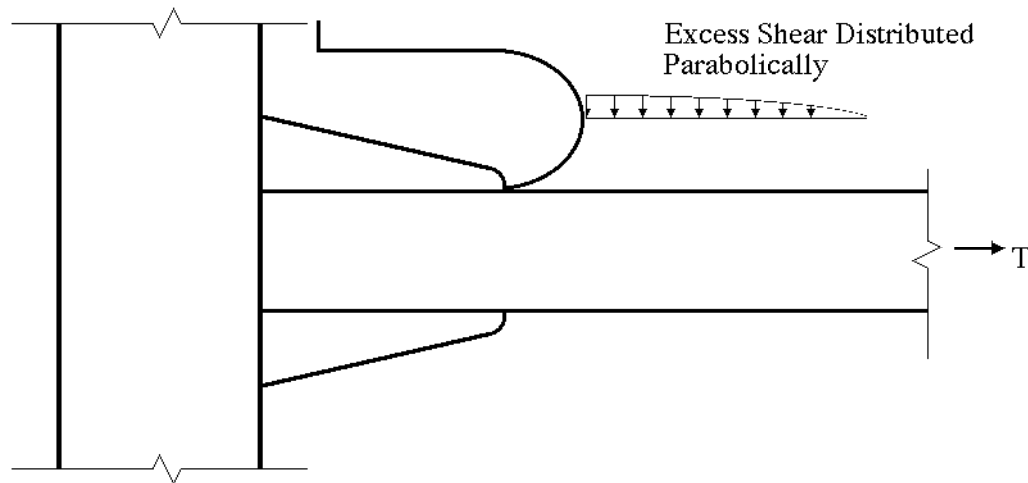


**Figure 6-14 Schematic of the Overlay Weld Loading with the More Complex Proposed Design Method**

The overlay looks promising as a possible repair and retrofit method for modest or intermediate sized pre-Northridge connections. Table 6-1 shows that it provided reasonably good ductility for small and modest sized specimens, but other research clearly shows that it is more difficult to achieve ductility from larger specimens. Thus, it is not clear that the weld overlay will provide a significant benefit for large specimens. The research shows that the method is capable of developing improved plastic rotational capacity, but the performance of these connections is also a step below that obtained with many post-Northridge connections described in Chapter 3. The overlay weld connection results in considerable interference of the inner welds with the beam flange copes, and horizontal cracks developed in most of the test specimens in the k-area region initiating from this interference region.

The connection is not included as a prequalified connection in the guidelines developed through this research, because there is not a documented and substantiated design method for the connection. It is required of all prequalified connections that sufficient testing be completed so that all failure modes are understood and design models and procedures be verified with the test program. The weld overlay research has been somewhat disconnected and haphazard, as is common with new connection developments. This occurs because researchers tend to modify the next test to reduce problems seen in the previous test. The unfortunate consequence of this is that none of the test specimens have been designed by the proposed design procedures. Further research is needed to develop the design method and to understand fully the behavior of this connection.

## 6.4 Supplemental Connections – Connections with Friction and Damping

Supplemental damping has also been considered as a method of improving the seismic performance of moment frame connections. Passive damping through visco-elastic dampers or friction-based dampers has been extensively researched (Grigorian, and Popov, 1994; Reinhorn, and Li, 1995; Li, and Reinhorn, 1995), and they offer considerable potential for seismic design of new buildings and repair or retrofit of existing buildings. Seismic design specifications (ICBO, 1997) and seismic rehabilitation guidelines (FEMA 273, 1997) recognize the benefit of this passive damping on the seismic performance, and these damping devices have been used in a number of new and existing buildings. Most of these applications have been at selected locations between flexible frames and stiff and strong walls or braced frames. Frequently, these stiff elements have limited ductility, and the damping devices limit the forces on these potentially brittle elements.

Friction-based dampers can provide stable inelastic resistance through many cycles of large deformation, and these devices were judged a promising method of improving the seismic performance of steel moment-frame connections. This method was considered during this research program, and the bolted flange plate connection (as discussed in Chapter 5) was viewed as an ideal candidate for this application. Initial research (Schneider, 1998) examined the use of these connections with brass or bronze friction plates placed between the steel interfaces. Design studies were performed to examine the possible use of passive friction dampers in test specimens, and it became clear that the space required to place the damping devices was a dominant concern. Design proposals were discussed with design engineers and steel fabricators, and ultimately the connection option illustrated in Figure 6-15 became the option with the only real promise for steel moment-frame connection design. With this choice, new construction would be completed with "Christmas tree columns" typical of Japanese construction with connections as illustrated in Figure 3-4. However, a much larger number of bolts was required for the friction connection, since the connection moment capacity was controlled by friction bolts and the friction acted in single shear. This led to a long connection. Fewer bolts and shorter flange plates could be employed if double shear were developed with flange plates and bronze plates on the inside and outside of both beam flanges, but this results in a large number of pieces for each connection splice. In addition, long slotted holes and beam gaps are required to achieve the required rotational capacity. The gap and the elongated slot must be large with deep beams of large rotational capacity. For example, a 0.04 radian rotational capacity and a W36 beam requires that the slot be approximately 1.5" longer than its width. The large number of bolts and the long slotted holes result in very long connections, and the long connection forces the connection rotation well out into the beam span. Rotations within the beam span require larger amplitudes to achieve a given frame story drift, and this further increases the connection length, since larger connection rotations are required. In addition, serious questions were raised regarding the long-term friction characteristics at the bronze-steel interface. Material specialists noted that long-term contact while waiting for earthquake occurrence can result in freezing or bonding of the two dissimilar materials so that the slip required for connection rotation may not occur with these friction base dampers. This would result in brittle fracture of the connection since there were no locations for inelastic deformation to occur. There is a basis for arguing this conclusion, because some researchers (Grigorian and Popov, 1995) have noted that the frictional slip is really gouging and fretting of the softer material rather than a pure friction. Nevertheless, it is equally clear that properties of materials do change over time. Finally, it was noted that this

type of connection requires opening and closing of the floor slab during major earthquakes. This raises additional questions regarding the expected performance of the connection and the suitability of the concept for steel moment frames.

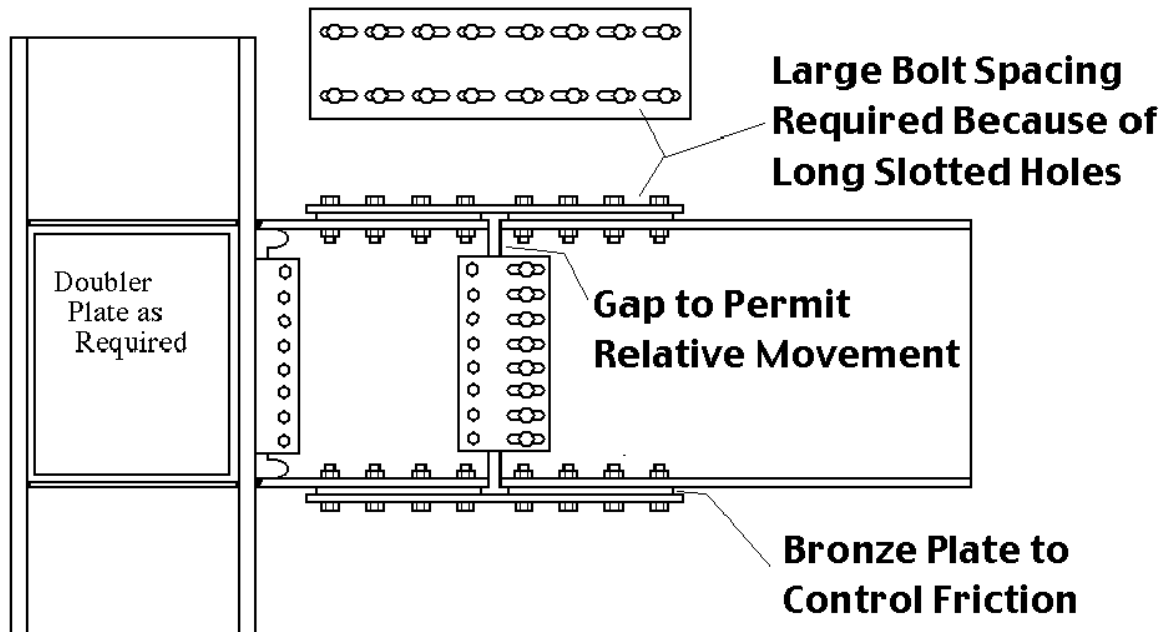


**Figure 6-15 Schematic of Proposed Friction Damper Connection**

In view of these factors, practicing engineers and fabricators on the Connection Performance Technical Advisory Committee determined that friction-based passive damping as discussed above was impractical for application in steel moment frames with the present technology. As a result, no connections of this type were tested, and no recommendations regarding the design of these connections are made in this report or in the design guidelines.

An ongoing research program (Clifton, and Butterworth, 2000; Butterworth, and Clifton, 2000) in New Zealand is evaluating connections with friction-based dampers. The connections are similar to those considered above. The connections have been tested for modest sized members, and the performance to date has been good.

## 6.5 Other Connections

This report has attempted to provide a complete picture of the connections that are available for seismic design of steel moment frames. However, the report has included only those connections where adequate data and information was available to understand the connection behavior. Several patented or proprietary connections are available for seismic design of steel moment frames. The connections are designed by methods developed by the patent holders, and the complete test results and the complete evaluation methods are not publicly available for review and interpretation. No recommendations or design guidelines are developed for these connections in this report.

## 7. SUMMARY, CONCLUSIONS, AND UNRESOLVED ISSUES

### 7.1 Summary

This report has provided a comprehensive state of the art review of the seismic performance of steel moment-frame connections. The goal of the work was to understand fully the seismic performance of the connections at all levels of demand, with particular emphasis on the strength, stiffness, and rotational capacity of each connection type. The yield mechanisms and failure modes of each connection type were the primary emphasis of the research, because these modes and mechanisms dominate the seismic performance of all connections. Yield mechanisms provide a location and source of yield deformation where large plastic rotations can occur before fracture or deterioration of connection resistance can develop. Failure modes result in fracture and loss of resistance. Many different failure modes are possible for each connection type. Ductility is assured for each connection by predicting the resistance associated with each yield mechanism and each failure mode, and by ensuring that the resistance associated with a viable yield mechanism is significantly lower than that resistance associated with all failure modes. Simplified design models were developed and tabulated for each connection. These design models predict the resistance associated with each yield mechanism and each failure mode. In addition, balance conditions are provided to ensure that there is adequate separation between desirable yield mechanisms and undesirable failure modes so that good connection performance can be achieved.

Analytical and experimental studies were completed. These studies were used to develop the simplified design models and to determine the balance conditions that are required to ensure desirable connection performance. In addition, data from hundreds of other past connection studies were evaluated to provide a comprehensive picture of the connection performance for both existing and new connections. These studies are summarized, and the results are used to establish the capabilities and limits for each connection. Design models and the balance conditions were developed, based upon the path of forces and moments through the connection, upon equilibrium, and upon concepts of basic engineering mechanics. These models were then verified against the experimental results. The most desirable combination of yield mechanism and the appropriate separation between this yield mechanism and the critical failure modes was determined for each connection. The balance conditions were established to achieve this separation and to ensure that these desirable conditions can be achieved in practice.

Given that the connection is designed to achieve this desirable connection performance, the plastic rotational capacity and the estimated statistical variation of the connection performance are estimated for each connection type. The plastic rotations are of two types. The first plastic rotation,  $\theta_p$ , is estimated as the rotation at which initial fracture or significant loss of resistance is expected in the connection. Significant loss of resistance is considered a resistance which is less than 80% of the nominal plastic capacity of the connection, based upon the expected yield and tensile properties of the steel. The second rotational capacity is the rotation,  $\theta_g$ , which is expected to produce adequate damage to the connection so that the beam and the connection may be unable to support the full gravity load. The resistance of the connections both at initial yielding and ultimate load are estimated by simplified models. Finally, connection stiffness is relevant for some connection types, and where connection stiffness must be considered,

estimated connection stiffness is provided. Therefore, this report provides the information needed to assess connection behavior at all levels of performance.

This report is comprehensive. Chapters 2 through 6 provide summaries of performance of all relevant connection types, discussion of past research results, and recommended models for predicting and controlling connection performance. A wide range of connections are described in these chapters, including:

- pre-Northridge welded-flange-bolted-web connections,
- improved unreinforced post-Northridge welded-flange-bolted-web connections,
- unreinforced post-Northridge welded-flange-welded-web connections including the improved welded-web connection with the improved weld access hole and the free-flange connection,
- reduced-beam-section (RBS) connections,
- reinforced connections including the haunch and coverplated connections,
- welded-flange-plate connections where the flange-plate is welded directly to the column but the beam flange is not,
- stiff bolted connections that can normally be approximated as rigid connections, including the extended-end-plate and the bolted-flange-plate connections,
- intermediate stiffness bolted T-stub connections that can usually, but not always, be approximated as rigid connections,
- flexible partially restrained (PR) connections that always require consideration of the connection stiffness, and that include the double-angle, web-angle, and shear tab connections,
- composite connections including the composite shear tab and the composite-double-angle connections, and
- economical connection retrofit methods such as the weld overlay.

Finally, a range of general issues that relate to many connections is evaluated. The reader is referred to Chapters 2 through 6 for details on each of these connection types.

## 7.2 Conclusions

The large number of important conclusions provided throughout this report are too numerous to itemize here. However, several points are worthy of note.

1. The pre-Northridge welded-flange-bolted-web connection is capable of providing good seismic performance under some conditions, but the design and construction methods that were used for this connection are not adequate for guaranteeing this behavior. The work has shown that a number of factors contributed to the damage these connections experienced during the Northridge earthquake. These include:
  - the low notch toughness of the E70T-4 electrode;

- the flaws introduced by leaving backing bars and runoff tabs in place on the pre-Northridge connection;
- the reduced ductility resulting from the greater depth and weight of beams and columns used in modern structures;
- the reduced ductility resulting from changes in the yield stress and properties of the steel that have evolved over past years;
- the limited contribution of the bolted web to the shear and moment resistance of the connection;
- the effect of panel zone yielding and panel zone deformation (these clearly have an impact on the performance of the connection, but their contribution appears to be variable and not completely clear).

Other factors such as the continuity plates and local buckling requirements also have had some impact.

2. The welded-flange-bolted-web connection with removed runoff tabs, removed backing bars, and notch tough weld electrodes resulted in improved seismic performance, since brittle fractures of the weld were avoided. However, the overall connection performance and rotational capacity of the tested specimens were only slightly improved above the pre-Northridge connection, because fracture occurred in the beam flange near the toe of the weld access hole at inelastic deformations only slightly larger than those noted for the pre-Northridge connection. The research has shown that the geometry and transition of the weld access hole and the strength and stiffness of the web connection must be improved to provide significant enhancement of the connection performance.
3. The welded-flange-welded-web connections provided good ductility and connection performance if certain conditions were satisfied. Two alternatives, the welded-web connection with both improved weld access hole geometry and notch tough electrodes, and the free-flange connection, were presented in Chapter 3. Both of these alternatives provided large plastic rotations, but they both required:
  - a relatively stiff, strong web attachment,
  - improved transition of the geometry at the weld access hole,
  - notch tough electrodes, and
  - improved backing bar details.

These connections clearly showed greater sensitivity to panel zone yield deformation. Panel zone yield deformation was desirable in that it provided significant plastic rotation in these connections, but excessive panel zone deformation led to fracture into the web connection or the column and reduced connection ductility. These observations regarding panel zone yielding led to improved balance conditions for ensuring the maximum connection ductility.

4. Reinforced connections including the haunch and coverplated connection can provide large plastic rotations and good seismic performance. However, both connections have disadvantages. The haunch connection is a costly alternative, which probably limits its use to repair and retrofit of existing structures. The coverplate connection is more economical and may be useful for new construction, but it requires that the resistance of various

components of the connection be properly balanced to avoid fracture of the beam or the column. Both alternatives require consideration of the fact that plastic deformation occurs at a location well out into the beam span.

5. The RBS connection provided very good seismic performance through many tests. However, the tests are concentrated into a very narrow range of beam depths and column spans. This connection is clearly one of the most robust connections suitable for use in the heavier framing used in modern steel construction.
6. Several bolted connections have been evaluated. Bolted connections provide good seismic performance, and they may develop the full plastic capacity of the beam. The extended-end-plate connection, the bolted-flange-plate, and the bolted T-stub connections provided very good seismic performance, although their use may be somewhat restricted by size limits. The 4-bolt unstiffened end-plate and the 8-bolt stiffened end-plate connections which are designed by the thick-plate design model provide good connection ductility and overall seismic performance. However, these connections are restricted in beam size by the tensile capacity of the bolts. The bolted-flange-plate connections consistently provided the largest plastic rotations achieved with any of the tests completed during this research program, but this ductility requires a careful balance between three different yield mechanisms. This connection is prequalified up to some W30 beams, but further testing may well show adequate performance up to lighter W36 sections, since the shear capacity of the bolts and the tolerable length of the bolt group are factors which limit the size of these connections. The bolted T-stub connection can be a full strength or a partial strength connection, and as a consequence it can also be a full stiffness or reduced stiffness connection. It provided good rotational capacity, but its size limits are restricted to approximately W27 sections or less because of the available T-sections combined with prying action and the tensile capacity of the bolts. These bolted alternatives offer considerable attraction for seismic design, but seismic design of the connections is usually more complex because of the added failure modes and yield mechanisms.
7. Flexible PR connections such as the flange-angle connection, web-angle connection, and shear-tab connection have also been evaluated. These connections require consideration of the connection stiffness, and the maximum resistance is much smaller than the full plastic capacity of the beam. The shear-tab connections and web angle connections were evaluated with the goal of providing supplemental stiffness and resistance in existing buildings with a large number of these connections. The resistance and stiffness of these connections are neglected in new building design because these connections are primarily used at beam connections to gravity-load columns. Nevertheless, it may be possible to use this supplemental stiffness and resistance to repair and retrofit existing structures economically. The stiffness of these connections is low, and the resistance is well below the plastic bending capacity of the beams entering the connection. However, the total plastic rotational capacity for these connections is large, and the connection resistance is retained through nearly all of this rotation. Models are provided for predicting the resistance, rotational capacity, and stiffness of these connections. The columns for these connections may be a weak link, however, because they were not normally designed to support the bending moments that are transferred from the connections, in addition to their gravity loads.

8. Composite PR connections were also considered. Particular emphasis was placed upon composite slabs with shear tab connections, since these are commonly used in modern steel-frame buildings. This supplemental stiffness may also reduce the cost of repair and retrofit of existing steel-frame buildings. The stiffness and resistance provided by these connections are limited, but they are significantly larger than noted for the bare steel connections. This added stiffness and rotation is lost at rotations well below the maximum rotation tolerated by the bare steel connection, and connection behavior reverts to the non-composite behavior for these large rotations. Models are provided for estimating the composite resistance, the composite stiffness, the rotation at which the composite action is lost, as well as the behavior noted in Item 7.
9. Connection repair has been a consideration of this research. The haunch and coverplated connections are available for repair of existing connections, but they are costly and also have limitations. The weld overlay method is also available, but the design procedures for this method have not been fully verified. Experiments indicate that this repair method is promising for moderate sized members, but the information available at this time is not adequate to document fully the performance of this connection.
10. A wide range of other connections and other issues are addressed. Refer to Chapters 2 through 6 for recommendations and conclusions on these other topics. The report also contains extensive references to more detailed and comprehensive reports on individual connection types.

### **7.3 Unresolved Issues**

The SAC steel project has resolved many issues regarding the seismic performance of steel moment-frame connections. This report contains recommendations for a wide range of connection types, and it addresses many related issues. However, connection tests and analyses are expensive, and definitive answers could not be established for all connections nor all issues. The following items require additional research to develop fully rational design guidelines.

1. The free-flange connection and the weld overlay are two connection alternatives that have had limited testing in this program. Both of these connections have provided good seismic performance. Both test programs were limited in scope, and the connection failure modes and the models for predicting the behavior of the connection are not fully developed. The existing free-flange connection tests permit development of design models, but the connection is restricted to moderate beam depths for special moment frames in areas with high seismic demands. Testing, which was directed toward better understanding the failure modes of the connection and better defining the required resistance and design of the web attachment, could significantly extend the range of applicability of this connection. For the weld overlay, some tests also have provided good seismic performance. Unfortunately, each test was slightly different, and the tests were not designed by a consistent design procedure. It is not possible to verify design models under these conditions. Therefore, additional tests that were conducted with a consistent goal of evaluating the failure modes and the design or prediction models could result in significant increases in the range of applicability of this repair method. Similar comments could be made about other connections, but these two examples are particularly apparent because of their limited test programs.

2. Lateral torsional buckling results in deterioration of resistance of steel moment-frame connections, and lateral support is employed to control lateral buckling and the rapid deterioration in resistance that results from it. This report provided evidence that the present lateral support requirements for seismic design are conservative. Further, reduced bracing requirements were argued for the RBS connection based upon this work. Lateral bracing can be expensive, and liberalized bracing lengths could offer significant economic advantage. Unfortunately, this study of lateral bracing in this report was not comprehensive enough to develop, by rational methods, improved unbraced length requirements. Research is needed in this area.
3. Continuity plate requirements are also important to seismic design, but the results of research summarized in this report show that existing limits have not been chosen by rational methods and may be conservative. Continuity plates are expensive, and research has shown that they are not always necessary. At the same time, they are clearly needed in some connections because they help provide a more uniform stress and strain distribution to the beam flange weld and they reduce the potential for damage to the column flange and web. Research is required in this area, and work (Dexter, et al., 1999) has started with funding by AISC.
4. Panel-zone yielding is an important yield mechanism for a large number of connections, but this report has shown that excessive panel-zone yield deformation causes early fracture in many connections. Balance conditions have been rationally developed in this report to assure a balance between these desirable and undesirable attributes. However, these balance conditions probably should not be the same for all types of connection. The balance should depend upon the postyield stiffness of the panel zone and the local stiffness of the individual connection type. The postyield stiffness of panel zones is not well understood. Many models have been developed, and they are all highly empirical. They fit some data well and other data poorly. As a result, the frame deflection and deformation due to panel-zone yielding are not consistently well predicted, nor are the local deformations that accompany this panel-zone deformation accurately estimated. As a consequence, the effect of the panel zone on connection performance is only approximately understood. Further research is needed to improve the understanding of panel yield behavior and the post-yield stiffness of these connections.
5. This report has shown that bolted connections offer substantial advantages for seismic design. They can be economical and their construction methods may be less sensitive to flaws and errors. However, the failure modes and yield mechanisms of bolted connections are more complex than most welded-flange connections. Further, most past bolted connection research has focused on strength-based design which had minimal concerns of connection ductility. As a consequence, the models for predicting connection performance and balancing connection behavior are not as well defined as the models used for welded-flange connections, and they also are more complex. Further research into the seismic performance of bolted connections is desirable in fully understanding the yield mechanisms and failure modes of these connections as well as balancing the connection performance to achieve maximum ductility from the connections.

## REFERENCES, FEMA REPORTS, SAC REPORTS, NOTATION, AND ACRONYMS

### References.

- AIJ, 1997, *Full-Scale Test on Plastic Rotation Capacity of Steel Wide-Flange Beams Connected With Square Tube Steel Columns*, Kinki Branch of the Architectural Institute of Japan, Steel Committee, Osaka (in Japanese with attached abridged English version).
- AIJ, 1996, *Technical Recommendations for Steel Construction for Buildings (Part I Guide to Steel-Rib Fabrication)*, 4th Ed., the Architectural Institute of Japan, Tokyo (in Japanese).
- AISC, 1994, *Load and Resistance Factor Design Manual of Steel Construction*, Second Edition, Volume II, *Connections*, Part 10, American Institute of Steel Construction, Chicago, Illinois.
- AISC, 1928, *Steel Construction*, 1<sup>st</sup> Edition, American Institute of Steel Construction, New York, New York.
- AISC, 1997, *Seismic Provisions for Structural Steel Buildings*, American Institute of Steel Construction, Chicago, Illinois.
- Almudhafar, S., and Chambers, J.J., 2000, "Stiffness Implications of Beams with Reduced Flanges," *Proceedings of US-Japan Workshop on Seismic Fracture Issues in Steel Structures*, San Francisco, California.
- Ammerman, D.J., and Leon, R., 1987, "Behavior of Semi-Rigid Composite Connections," *Engineering Journal*, Vol. 24, No. 2, American Institute of Steel Construction, Chicago, Illinois.
- Anderson, J., Duan, J., Maranian, P., and Xiao, Y., 2000, *Improvement of Welded Connections Using Fracture Tough Overlays*, SAC Report 00/20, SAC, Sacramento, California.
- Astaneh, A., Call, S.M., and McMullin, K.M., 1989, "Design of Single Plate Shear Connections," *Engineering Journal*, Vol. 26, No. 1, American Institute of Steel Construction, Chicago, Illinois.
- Astaneh, A., and Nader, M.N., 1990, "Experimental Studies and Design of Steel Tee Shear Connections", *ASCE, Journal of Structural Engineering*, Vol. 116, No. 10.
- Astaneh, A., Nader, M.N., and Malik, L., 1989, "Cyclic Behavior of Double Angle Connections," *ASCE, Journal of Structural Engineering*, Vol. 115, No. 5.
- AWS, 1994, *Structural Welding Code - Steel*, AWS D1.1-94, American Welding Society, Miami, Florida.
- Azizinamini, A., and Radzinski, J.B., 1989, "Static and Cyclic Performance of Semirigid Steel Beam-to-Column Connections," *ASCE, Journal of Structural Engineering*, Vol. 115, No. 12.
- Barsom, J. M., and Pellogrino, J.V., 2000, *Failure Analysis of Welded Beam-to-Column Connections*, Report SAC/BD-99/23, SAC Joint Venture, Sacramento, California.
- Batho, C., 1938, "The Effect of Concrete Encasement on the Behaviour of Beam and Stanchion Connections," *The Structural Engineer*, pp. 427-447.
- Batho, C., Lash, S.D., 1936, "Further Investigations on Beam and Stanchions Connections, Including Connections Encased in Concrete; Together with Laboratory Investigations on a Full-Scale Steel Frame," *Final Report of the Steel Structures Research Committee*, pp 276-363, Department of Scientific and Industrial Research, His Majesty's Stationery Office, London.

- Batho, C., Rowan, H.C., 1934, "Investigations on Beam and Stanchions Connections," *Second report of the Steel Structures Research Committee*, pp 61-137, Department of Scientific and Industrial Research, His Majesty's Stationery Office, London.
- Bernuzzi, C., Noe, S., and Zandonini, R., 1991, "Semi-Rigid Composite Joints: Experimental Studies," *Connections in Steel Structures II: Behavior, Strength and Design*, edited by R. Bjorhovde, A. Colson, G. Haaier and J. Stark, pp 189-200, American Institute of Steel Construction, Chicago, Illinois.
- Bertero, V.V., Krawinkler, H., and Popov, E.P., 1973, *Further Studies on Seismic Behavior of Steel Beam-to-Column Subassemblages*, EERC Report 73-27, University of California, Berkeley.
- Bonowitz, D., and Youssef, N., 1995, *SAC Survey of Steel Moment-Resisting Frame Buildings Affected by the 1994 Northridge Earthquake*, Technical Report 95-06: Surveys and Assessment of Damage to Buildings Affected by the Northridge Earthquake of January 17, 1994, SAC Joint Venture, pp. 2-1 to 2-169.
- Bjorhovde, R., Goland, L.J., and Bensch, D.J., 1999, *Tests of Full-Scale Beam-to-Column Connections*, unpublished report to Steel Shape Producers Council.
- Butterworth, J.W., and Clifton, C.G.C., "Performance of Hierarchical Friction Dissipating Joints in Moment Resisting Steel Frames", Paper 0718, *Proceedings 12<sup>th</sup> World Conference on Earthquake Engineering*, Auckland, New Zealand, 2000.
- Castiglioni, C.A., Bernuzzi, C., and Agatino, M.R., 1998, "Design and Damage Assessment of Structural Steel Components Under Seismic Actions," *Proceedings of the NEHRP Conference and Workshop on Research on the Northridge, California Earthquake of January 17, 1994*, CUREe, Berkeley, California.
- Chasten, C.P., Fleishman, R.B., Driscoll, G.C., and Lu, L.W., 1989, *Top-and-Seat-Angle Connections and End-Plate Connections: Behavior and Strength Under Monotonic and Cyclic Loading*, ATTLSS Report No. 89-05, Lehigh University, Bethlehem, Pennsylvania.
- Chen, S.J., 1996, "A Simple and Effective Retrofit Method for Steel Beam-to-Column Connections," *Seventh US-Japan Workshop on the Improvement of Structural Design and Construction Practices*, Applied Technology Council, Redwood City, California.
- Chen, S.J., 1999, "Design of Ductile Steel Beam-to-Column Connections for Seismic Resistance," *Workshop on Design Technologies of Earthquake-Resistant Moment Resisting Connections*, Taipei, Taiwan.
- Chi, W.M., Deierlein, G.G., and Ingrassia, A.R., 1997, *Finite Element Fracture Mechanics Investigation of Welded Beam-Column Connections*, Report No. SAC/BD-97/05, SAC Joint Venture.
- Choi, J., Stojadinovic, B., and Goel, S.C., 2000, *Parametric Tests on the Free Flange Connection*, Report SAC/BD-00/02, SAC Joint Venture.
- Clark, P., Frank, K., Krawinkler, H., and Shaw, R., 1997, *Protocol for Fabrication, Inspection, Testing, and Documentation of Beam-Column Connection Tests and Other Experimental Specimens*, SAC Report SAC/BD-97/02, SAC Joint Venture.
- Clifton, C.G., and Butterworth, J.W., 2000, "Moment-Resisting Seismic-Resistance Systems with Semi-Rigid Connections," Paper 1602, *Proceedings 12<sup>th</sup> World Conference on Earthquake Engineering*, Auckland, New Zealand.
- Coons, R.G., *Seismic Design and Database of End-Plate and T-Stub Connections*, 1999, A thesis submitted in partial fulfillment of the Master of Science in Civil Engineering Degree, University of Washington, Seattle, Washington.

- Dailey, R., and Roeder, C.W., 1989, "Web Crippling of Seated Beam Connections," *Engineering Journal*, Vol. 3, No. 26, American Institute of Steel Construction, Chicago, pp. 90-95.
- Daniels, J.H., Kroll, G.D., and Fisher, J.W., 1970, "Behavior of Composite-Beam to Column Joints," *ASCE, Journal of Structural Division*, Vol. 96, No. ST3.
- Davison, J.H., Lam, D., and Nethercot, D.A., 1990, "Semi-Rigid Action of Composite Joints," *Structural Engineer*, Vol. 68, No. 24, pp. 489-499.
- Deierlein, G.G., and Chi, W.M., 1999, *SAC TASK 5.3.3 - Integrative Analytical Investigations on the Fracture Behavior of Welded Moment Resisting Connections*, Final Report, John A. Blume Earthquake Engineering Center, Dept. of Civil and Environmental Engineering, Stanford University, Palo Alto, California.
- Dexter, R.J., Hajjar, J.F., Cotton, S.C., Prochnow, S.D., and Ye, Y., 1999, *Reassessment of Design Criteria and New Alternatives for Column Transverse Stiffeners (Continuity Plates) and Web Doubler Plates: Interim Report*, Structural Engineering Report ST-99-3, Dept of Civil Engineering, U. of Minnesota, Minneapolis, Minnesota.
- Engelhardt, M.D., 1998, *Design Recommendations for Radius Cut Reduced Beam Section Moment Connections*, unpublished report based on presentation to AISC Annual Convention.
- Engelhardt, M.D., 2000, *Brief Report of Steel Moment Connection Test Specimen UTA-FF*, Dept. of Civil Engineering, U. of Texas, Austin, Texas.
- Engelhardt, M.D., Fry, G., Johns, S., Venti, M., and Holliday, S., 2000, *Behavior and Design of Radius-Cut, Reduced Beam Section Connections*, SAC Report 00/17, SAC Joint Venture.
- Engelhardt, M.D., and Husain, A.S., 1993, "Cyclic Loading Performance of Welded Flange-Bolted Web Connections," *ASCE, Journal of Structural Engineering*, Vol. 119, No. 12.
- Engelhardt, M.D., and Sabol, T.A., 1998, "Reinforcing of Steel Moment Connections with Cover Plates: Benefits and Limitations," *Engineering Structures*, Vol. 20, No. 4-6, pp. 510-20, Elsevier, London.
- Engelhardt, M.D., Winneberger, T., Zekany, A.J., and Potyraj, T.J., 1996, "The Dogbone Connection: Part II," *Modern Steel Construction*, Vol. 36, No. 8, American Institute of Steel Construction, Chicago, Illinois.
- Engelhardt, M.D., Winneberger, T., Zekany, A.J., and Potyraj, T.J., 1998, "Experimental Investigation of Dogbone Moment Connections," *Engineering Journal*, Vol. 35, No. 4, American Institute of Steel Construction, Chicago, Illinois.
- Englekirk, P.E., 1999, "Extant Panel Zone Design Procedures for Steel Frames are Questioned," *Earthquake Spectra*, Vol. 15, No.2, Earthquake Engineering Research Institute, Oakland, California.
- FEMA 267, 1995, *Interim Guidelines: Evaluation, Repair, Modification and Design of Welded Steel Moment Frame Structures*, Reports FEMA 267 and 267A, Federal Emergency Management Agency, Washington, DC.
- FEMA 273, 1997, *NEHRP Guidelines for the Seismic Rehabilitation of Buildings*, Reports FEMA 273 and Commentary FEMA 274, Federal Emergency Management Agency, Washington, DC.
- Gilton, C.S., Chi, B., and Uang, C.M., 2000a, *Cyclic Testing of a Free Flange Moment Connection*, SAC Report 00/19, SAC Joint Venture.
- Gilton, C.S., Chi, B., and Uang, C.M., 2000b, *Cyclic Testing of RBS Moment Connections: Weak Axis Configuration and Deep Column Effects*, SAC Report 00/23, SAC Joint Venture.

- Goel, S.C., Stojadinovic, B., and Lee, K.H., 1997, "Truss Analogy for Steel Moment Connections," *Engineering Journal*, Vol. 34, No. 2, American Institute of Steel Construction, Chicago, Illinois.
- Grigorian, C.E., and Popov, E.P., 1994, *Energy Dissipation with Slotted Bolted Connections*, EERC Report 94/02, University of California, Berkeley.
- Gross, J., Englehardt, M.D., Uang, C.M., Kasai, K., and Iwankiw, N., 1999, *Modification of Existing Steel Welded Moment Frame Connections for Seismic Resistance*, AISC Steel Design Guide Series 12, American Institute of Steel Construction, Chicago, Illinois.
- Grubbs, K.V., 1997, *The Effect of the Dogbone Connection on the Elastic Stiffness of Steel Moment Frames*, a thesis submitted in partial fulfillment of the degree of Master of Science in Engineering, University of Texas, Austin, Texas.
- Harrigan, P., 1996, *Possible Cause of Cracking in Steel Moment Resistant Frames During the 1994 Northridge Earthquake*, a thesis submitted in partial fulfillment of the requirements for the degree of Master of Science in Civil Engineering, University of Washington, Seattle, Washington.
- Harriott, J.D., and Astaneh, A., 1990, *Cyclic Behavior of Steel Top-and-Bottom Plate Moment Connections*, EERC Report 90-19, University of California, Berkeley.
- Hechtman, R.A., and Johnston, B.C., 1947, *Riveted Semi-Rigid Beam-to-Column Building Connections*, Progress Report No. 1, Committee of Steel Structures Research, American Institute of Steel Construction, Chicago, Illinois.
- Hoit, M., 1997, *An Investigation into the Seismic Design of Flange Plated Moment Resistant Connections*, Master's Thesis, University of Washington, Seattle, Washington.
- ICBO, 1988, *Uniform Building Code*, 1988 Edition, International Conference of Building Officials, Whittier, California.
- ICBO, 1997, *Uniform Building Code*, 1997 Edition, International Conference of Building Officials, Whittier, California.
- Iwankiw, N.R., and Carter, C.J., 1996, "The Dogbone: A New Idea to Chew on," *Modern Steel Construction*, Vol. 36, No. 1., American Institute of Steel Construction, Chicago, Illinois.
- Johnson, M., 1999, Edison Electric Progress Report.
- Johnson, M., 2000, *State of the Art Report on Welding and Inspection*, FEMA 355B, Federal Emergency Management Agency, Washington, DC.
- Johnstone, N.D. and Walpole, W.R., 1981, *Bolted End-Plate Beam to Column Connections Under Earthquake Type Loading*, Research Report 81-7, Dept of Civil Engineering, Univ. of Canterbury, Christchurch, New Zealand.
- Kaufmann, E.J., and Fisher, J.W., 1995, *A Study of the Effects of Material and Welding Factors on Moment Frame Weld Joint Performance Using a Small-Scale Tension Specimen*, SAC Report 95-08, SAC, Sacramento, California.
- Kim, T., Whittaker, A.S., Bertero, V.V., and Gilani, A.S.J., 2000 *Steel Moment-Resisting Connections Reinforced with Cover and Flange Plates*, Report SAC/BD-00/27, SAC Joint Venture.
- Krawinkler, H., 1978, "Shear Design of Steel Frame Joints", AISC, *Engineering Journal*, Vol. 15, No. 3, pp 82-91.

- Krawinkler, H., 2000, *State of the Art Report on Systems Performance of Moment Steel Frame Buildings in Earthquakes*, FEMA 355C, Federal Emergency Management Agency, Washington, DC.
- Krawinkler, H., Bertero, V.V., and Popov, E.P., 1971, *Inelastic Behavior of Steel Beam-to-Column Subassemblages*, EERC Report 71-7, University of California, Berkeley.
- Krawinkler, H., Gupta, A., Medina, R., and Luco, N., 2000, *Loading Histories for Seismic Performance Testing of SMRF Components and Assemblies*, SAC Report 00/10, SAC Joint Venture.
- Kwasniewski, L., Stojadinovic, B., and Goel, S.C., 1999, *Local and Lateral-Torsion Buckling of Wide Flange Beams*, Report SAC/BD-99/20, SAC Joint Venture.
- Lee, K.H., Stojadinovic, B., Goel, S.C., Margarian, A.G., Choi, J., Wongkaew, A., Rayher, B.P., Lee, D.Y., 2000, *Parametric Tests on Unreinforced Connections*, Report SAC/BD-00/01, SAC Joint Venture.
- Leon, Roberto, 1994, "Composite Semi-Rigid Construction", *Engineering Journal*, AISC, Vol 31, No. 2, Chicago, IL.
- Leon, Roberto, Ammerman, D.J., and McCaule, R.D., 1987, "Semi-Rigid Composite Steel Frames", *Engineering Journal*, AISC, Vol 24, No. 4, Chicago, IL.
- Leon, R.T., Hajjar, J., Gustafson, M.A., and Shield, C.M., 1998, "Seismic Response of Composite Moment-Resisting Connections, I: Performance, II: Behavior", *ASCE, Journal of Structural Engineering*, Vol. 124, No. 8.
- Leon, R.T., Hoffman, J.J., and Singer, T., 1996, *Partially Restrained Composite Connections*, AISC Steel Design Guide Series 8, American Institute of Steel Construction, Chicago, IL.
- Leon, R.T., Swanson, J.A., and Smallidge, J.M., 1999, *SAC Steel Project - Subtask 7.03: Results and Data CD*, Georgia Institute of Technology, Atlanta, GA.
- Lewitt, C.W., Chesson, E., and Munse, W.H., 1965, *Restraint Characteristics of Flexible Riveted and Bolted Beam-to-Column Connections*, *Engineering Experiment Station Bulletin 500*, University of Illinois, Urbana, IL.
- Li, C., and Reinhorn, A.M., 1995, *Experimental and Analytical Investigation of Seismic Retrofit of Structures with Supplemental Damping: Part II – Friction Devices*, Report NCEER-95-0009, Multidisciplinary Center for Earthquake Engineering Research, State University of New York at Buffalo, Buffalo, New York.
- Lipson, S.L., 1977, "Single-Angle Welded-Bolted Connections", *ASCE, Journal of Structural Engineering*, Vol 103, No. ST3.
- Liu, J., and Astaneh-Asl, A., 2000, *Cyclic Tests on Simple Connections Including Effects of the Slab*, Report SAC/BD-00/03, SAC Joint Venture.
- Manjoine, M.J., 1944, "Influence of Rate of Strain and Temperature on Yield Stresses of Mild Steel", *Transactions*, ASME, 66, pp. A211, 18.
- Munse, W.H., Bell, W.G., and Chesson, E., 1959, "Behavior of Riveted and Bolted Beam to-Column Connections", *Journal of Structural Division*, ASCE, No. ST3, Vol. 85, pp 29-51.
- Murray, T.M., 1990, *Extended End Plate Moment Connections*, AISC Steel Design Guide Series 4, Chicago, IL.
- Murray, T.M., and Sumner, E., 1999, *Cyclic Testing of Bolted Moment End-Plate Connections*, Report SAC/BD-00/21, SAC Joint Venture

- Murray, T.M., and Kukreti, A.R., 1988, "Design of 8-bolt Stiffened Moment End Plate, AISC, *Engineering Journal*, Vol 25, No 2,.
- Meng, R.L., and Murray, T. M., 1996, *Moment End-Plate Connections for Seismic Loading*, Report CE-VPI-ST 96/04, Virginia Polytechnic Institute and State University, Blacksburg, VA.
- Nakashima, M, and Sawaizumi, S., 1999, "Effect of Column-to-Beam Strength Ratio on Earthquake Responses of Steel Moment Frames, Parts 1 and 2", *Journal of Steel Construction Engineering*, Vol. 6, No 4 (in Japanese).
- Nakashima, M., Roeder, C.W., and Maruoka, Y., 1999, "Steel Moment Frames for Earthquakes in the United States and Japan", ASCE, *Journal of Structural Engineering*, submitted for publication review.
- Nethercot, D.A., 1991, "Tests on Composite Connections", *Connections in Steel Structures II: Behavior, Strength and Design*, Edited by R. Bjorhovde, A. Colson, G. Haaier and J. Stark, AISC, Chicago, IL, pp 177-188.
- NIST, 1998, *Modification of existing Welded Steel Moment Frame Connections for Seismic Resistance*, Draft Report, National Institute for Standards and Testing, Gaithersburg, MD.
- Noel, S., and Uang, C.M., 1996, *Cyclic Testing of Steel Moment Connections for the San Francisco Civic Center Complex*, Report TR-96/07, Division of Structural Engineering, U. of California, San Diego, CA.
- Plumier, A., 1990, "New Idea for Safe Structure in Seismic Zones", *IABSE Symposium*, Brussels, Belgium.
- Popov, E.P., Amin, N.R., Louie, J.J., and Stephen, R.M., 1986, "Cyclic Behavior of Large Beam-column Assemblies," *Engineering Journal*, AISC, Chicago, IL.
- Popov, E.P., Bertero, V. V., and Chandramouli, S., 1975, *Hysteretic Behavior of Steel Columns*, Report EERC 75-11, University of California, Berkeley, CA.
- Popov, E. P., Blondet, M., Stepanov, L., and Stojadinovic', B., 1996, *Full-Scale Steel Beam-Column Connection Tests*, SAC 96-01, Part 2, SAC Joint Venture.
- Popov, E.P., and Pinkney, R.B., 1969, "Cyclic Yield Reversals in Steel Building Connections", ASCE, *Journal of Structural Engineering*, Vol. 95, No. ST3, pp 327-353.
- Popov, E.P., and Stephen, R.M., 1970, *Cyclic Loading of Full Size Steel Connections*, EERC Report 70-3, University of California, Berkeley,.
- Popov, E.P., Yang, T.S., and Chang, S.P., 1998, "Design of Steel MRF Connections Before and After 1994 Northridge Earthquake", *Engineering Structures*, Vol. 20, No. 12, Elsevier, London.
- Puhali, R., Smotlak, I., and Zandonini, R., 1990, "Semi-Rigid Composite Action: Experimental Analysis and a Suitable Model", *Journal of Constructional Steel Research*, Vol. 15, pp 121-151.
- Reinhorn, A.M., and Li, C., 1995, *Experimental and Analytical Investigation of Seismic Retrofit of Structures with Supplemental Damping: Part I – Fluid Viscous Damping Devices*, Report NCEER-95-0001, Multidisciplinary Center for Earthquake Engineering Research, State University of New York at Buffalo, Buffalo, New York.
- Richard, R.M., Gillett, P.E., Kriegh, J.D., and Lewis, B.A., 1980, "The Analysis and Design of Single Plate Framing Connections," AISC, *Engineering Journal*, Vol. 17, No. 2.

- Ricles, J.M., Mao, C., and Lu, L.W., 2000, *Dynamic Tension Tests of Simulated Welded Beam Flange Connections*, SAC BD 00-07, SAC Joint Venture.
- Ricles, J.M., Mao, C., Lu, L.W., and J. Fisher, J.W., 2000, *Development and Evaluation of Improved Details for Ductile Welded Unreinforced Flange Connections*, SAC BD 00-24, SAC Joint Venture.
- Roeder, C.W., 1996, *Summary Report of SAC Phase I- Task 7 Experimental Studies*, SAC 96-01, Part 1, SAC Joint Venture
- Roeder, C.W., and Foutch, D.A., 1996, "Experimental Results for Seismic Resistant Steel Moment Frame Connections", ASCE, *Journal of Structural Engineering*, No. 6, Vol. 122.
- Roeder, C.W., Knechtel, B, Thomas, E., Vaneaton, Anne, Leon, R.T., and Preece, F.R., 1996, "Seismic Behavior of Older Steel Structures," *ASCE Journal of Structural Engineering*, Vol 122, No. 4.
- Roeder, C.W., Leon, R.T., and Preece, F.R., 1994, *Strength, Stiffness and Ductility of Older Steel Structures Under Seismic Loading*, SGEM Report 94-4, Dept. of Civil Engineering, University of Washington, Seattle, WA.
- SAC, 1996, *Technical Report: Experimental Investigations of Beam-Column Subassemblages*, SAC 96-01, Parts 1 and 2, SAC Joint Venture.
- SAC DATABASE, A computer data base of test results developed during the SAC Steel Project and maintained on <http://quiver.eerc.berkeley.edu:8080>.
- Schneider, S.P., Roeder, C.W., and Carpenter, J.E., 1993, "Seismic Behavior of Moment-Resisting Steel Frames," Analytical Study and Experimental Investigation," ASCE, *Journal of Structural Engineering*, Vol. 119, No. 6.
- Schneider, S.P., 1998, "Progress Report on Task 7.09," *Connection Performance TAP Meeting*, Los Angeles, CA., SAC Joint Venture
- Schneider, S. P., and Teeraparbwong, I., 2000, *Bolted Flange Plate Connections*, Report SAC/BD-00/05, SAC Joint Venture.
- Shen, J., and Astaneh-Asl, A., "Hysteretic behavior of bolted-angle connections", *Journal of Constructional Steel Research*, Vol 51, Elsevier, London, pgs 201-218.
- Sherbourne, A.N., 1961, "Bolted Beam-to-Column Connections", *The Structural Engineer*, Vol 39, pp 203-210.
- Shuey, B.D., Englehardt, M.D., and Sabol, T.A., 1996, *Testing of Repair Concepts for Damaged Steel Moment Connections*, SAC 96-01, Part 2, SAC Joint Venture.
- Swanson, J., Leon, R.D., and Smallridge, J., 2000, *Tests on Bolted Connections*, Report SAC/BD-00/04, SAC Joint Venture.
- Tide, R.H.R., 2000, "Evaluation of steel properties and cracking in k-area of W shapes", *Engineering Structures*, Vol. 22, No. 2, Elsevier Science, Ltd., Oxford, UK, p128-34.
- Tide, R.H.R., Nugent, W.J., and Freeman, S.A., *Structural Repairs of Complete Penetration Welds at 6300 and 6320 Canoga Avenue, Woodland Hills, California*, Los Angeles, CA, Building Permit File, Wiss, Janey, Elstner Associates, Inc., Northbrook, IL, February 18, 1994.
- Tremblay, R., Tchegotarev, N, and Filliatrault, A., 1997, "Seismic Performance of RBS Connections for Steel Moment Resisting Frames: Influence of Loading Rate and Floor Slab," *Proceedings of STESSA Conference*, Kyoto, Japan,.

- Tsai, K.C., and Popov, E.P., 1988, *Steel Beam-Column Joints in Seismic Moment Resisting Frames*, EERC Report 88/19, University of California, Berkeley, CA.
- Uang, C.M., and Bondad, D., 1998, "Cyclic Performance of Haunch Repaired Steel Moment Connections: Experimental Testing and Analytical Modeling," *Engineering Structures*, Vol. 20, No.4-6, pgs 552-61, Elsevier.
- Uang, C.M., and Fan, C.C., 1999, *Cyclic Instability of Steel Moment Connections with Reduced Beam Section*, Report SAC BD-99/19, SAC Joint Venture
- Uang, C.M., Qi-Song, Y, and Bondad, D., 1998, "Dynamic Testing of Pre-Northridge and Haunch-Repaired Steel Moment Connections," *Proceedings of the NEHRP Conference and Workshop on Research on the Northridge, California Earthquake of January 17, 1994*, Vol III, CUREe, Richmond, California, pgs 730-37.
- Venti, M., and Engelhardt, M.D., 2000, *Test of a Free Flange Connection with a Composite Floor Slab*, SAC Report 00/18, SAC Joint Venture.
- Whittaker, A.S., and Gilani, A., 1996, *Washington High School Reconstruction - Cyclic Testing of Steel Beam-Column Connections*, Report No. EERCL-STI/96-04, Earthquake Engineering Research Center, University of California, Berkeley, CA.
- Whittaker, D., and Walpole, W.R., 1982, *Bolted End-Plate Connections for Seismically Designed Steel Frames*, Research Report 82-11, Dept of Civil Engineering, Univ. of Canterbury, Christchurch, New Zealand.
- Xue, M., Kaufmann, E.J., Lu, L.W., and Fisher, J.W., 1996, "Achieving Ductile Behavior of Moment Connections : Part I and Part II," *Modern Steel Construction*, AISC, Chicago, IL.
- Youssef, N., Bonowitz, D., and Gross, J., 1995, *A Survey of Steel Moment-Resisting Frame Buildings Affected by the 1994 Northridge Earthquake*, Report NISTIR 5626, NIST, US Dept. of Commerce, Gaithersburg, MD.
- Yu, Q.S., Gilton, C., and Uang, C.M., 2000, *Cyclic Response of RBS Moment Connections: Loading Sequence and Lateral Bracing Effects*, SAC Report 00/22, SAC Joint Venture.
- Zekioglu, A, Mozaffarian, H., Chang, K.L., Uang, C.M., and Noel, S., 1997, "Designing after Northridge," *Modern Steel Construction*.

### **FEMA Reports.**

FEMA reports are listed by report number.

FEMA-178, 1992, *NEHRP Handbook for the Seismic Evaluation of Existing Buildings*, developed by the Building Seismic Safety Council for the Federal Emergency Management Agency, Washington, DC.

FEMA-267, 1995, *Interim Guidelines, Inspection, Evaluation, Repair, Upgrade and Design of Welded Moment Resisting Steel Structures*, prepared by the SAC Joint Venture for the Federal Emergency Management Agency, Washington, DC. Superseded by FEMA 350 to 353.

FEMA-267A, 1996, *Interim Guidelines Advisory No. 1*, prepared by the SAC Joint Venture for the Federal Emergency Management Agency, Washington, DC. Superseded by FEMA 350 to 353.

FEMA-267B, 1999, *Interim Guidelines Advisory No. 2*, prepared by the SAC Joint Venture for the Federal Emergency Management Agency, Washington, DC. Superseded by FEMA 350 to 353.

- FEMA-273, 1997, *NEHRP Guidelines for the Seismic Rehabilitation of Buildings*, prepared by the Applied Technology Council for the Building Seismic Safety Council, published by the Federal Emergency Management Agency, Washington, DC.
- FEMA-274, 1997, *NEHRP Commentary on the Guidelines for the Seismic Rehabilitation of Buildings*, prepared by the Applied Technology Council for the Building Seismic Safety Council, published by the Federal Emergency Management Agency, Washington, DC.
- FEMA-302, 1997, *NEHRP Recommended Provisions for Seismic Regulations for New Buildings and Other Structures, Part 1 – Provisions*, prepared by the Building Seismic Safety Council for the Federal Emergency Management Agency, Washington, DC.
- FEMA-303, 1997, *NEHRP Recommended Provisions for Seismic Regulations for New Buildings and Other Structures, Part 2 – Commentary*, prepared by the Building Seismic Safety Council for the Federal Emergency Management Agency, Washington, DC.
- FEMA-310, 1998, *Handbook for the Seismic Evaluation of Buildings – A Prestandard*, prepared by the American Society of Civil Engineers for the Federal Emergency Management Agency, Washington, DC.
- FEMA-350, 2000, *Recommended Seismic Design Criteria for New Steel Moment-Frame Buildings*, prepared by the SAC Joint Venture for the Federal Emergency Management Agency, Washington, DC.
- FEMA-351, 2000, *Recommended Seismic Evaluation and Upgrade Criteria for Existing Welded Steel Moment-Frame Buildings*, prepared by the SAC Joint Venture for the Federal Emergency Management Agency, Washington, DC.
- FEMA-352, 2000, *Recommended Postearthquake Evaluation and Repair Criteria for Welded Steel Moment-Frame Buildings*, prepared by the SAC Joint Venture for the Federal Emergency Management Agency, Washington, DC.
- FEMA-353, 2000, *Recommended Specifications and Quality Assurance Guidelines for Steel Moment-Frame Construction for Seismic Applications*, prepared by the SAC Joint Venture for the Federal Emergency Management Agency, Washington, DC.
- FEMA-354, 2000, *A Policy Guide to Steel Moment-Frame Construction*, prepared by the SAC Joint Venture for the Federal Emergency Management Agency, Washington, DC.
- FEMA-355A, 2000, *State of the Art Report on Base Metals and Fracture*, prepared by the SAC Joint Venture for the Federal Emergency Management Agency, Washington, DC.
- FEMA-355B, 2000, *State of the Art Report on Welding and Inspection*, prepared by the SAC Joint Venture for the Federal Emergency Management Agency, Washington, DC.
- FEMA-355C, 2000, *State of the Art Report on Systems Performance of Steel Moment Frames Subject to Earthquake Ground Shaking*, prepared by the SAC Joint Venture for the Federal Emergency Management Agency, Washington, DC.
- FEMA-355D, 2000, *State of the Art Report on Connection Performance*, prepared by the SAC Joint Venture for the Federal Emergency Management Agency, Washington, DC.
- FEMA-355E, 2000, *State of the Art Report on Past Performance of Steel Moment-Frame Buildings in Earthquakes*, prepared by the SAC Joint Venture for the Federal Emergency Management Agency, Washington, DC.
- FEMA-355F, 2000, *State of the Art Report on Performance Prediction and Evaluation of Steel Moment-Frame Buildings*, prepared by the SAC Joint Venture for the Federal Emergency Management Agency, Washington, DC.

## SAC Joint Venture Reports.

SAC Joint Venture reports are listed by report number, except for SAC 2000a through 2000k; those entries that do not include a FEMA report number are published by the SAC Joint Venture.

SAC 94-01, 1994, *Proceedings of the Invitational Workshop on Steel Seismic Issues, Los Angeles*, September 1994, prepared by the SAC Joint Venture for the Federal Emergency Management Agency, Washington, DC.

SAC 94-01, 1994b, *Proceedings of the International Workshop on Steel Moment Frames, Sacramento*, December, 1994, prepared by the SAC Joint Venture for the Federal Emergency Management Agency, Washington, DC.

SAC 95-01, 1995, *Steel Moment Frame Connection Advisory No. 3*, prepared by the SAC Joint Venture for the Federal Emergency Management Agency, Washington, DC.

SAC 95-02, 1995, *Interim Guidelines: Evaluation, Repair, Modification and Design of Welded Steel Moment Frame Structures*, prepared by the SAC Joint Venture for the Federal Emergency Management Agency, Report No. FEMA-267, Washington, DC.

SAC 95-03, 1995, *Characterization of Ground Motions During the Northridge Earthquake of January 17, 1994*, prepared by the SAC Joint Venture for the Federal Emergency Management Agency, Washington, DC.

SAC 95-04, 1995, *Analytical and Field Investigations of Buildings Affected by the Northridge Earthquake of January 17, 1994*, prepared by the SAC Joint Venture for the Federal Emergency Management Agency, Washington, DC.

SAC 95-05, 1995, *Parametric Analytic Investigations of Ground Motion and Structural Response, Northridge Earthquake of January 17, 1994*, prepared by the SAC Joint Venture for the Federal Emergency Management Agency, Washington, DC.

SAC 95-06, 1995, *Technical Report: Surveys and Assessment of Damage to Buildings Affected by the Northridge Earthquake of January 17, 1994*, prepared by the SAC Joint Venture for the Federal Emergency Management Agency, Washington, DC.

SAC 95-07, 1995, *Technical Report: Case Studies of Steel Moment-Frame Building Performance in the Northridge Earthquake of January 17, 1994*, prepared by the SAC Joint Venture for the Federal Emergency Management Agency, Washington, DC.

SAC 95-08, 1995, *Experimental Investigations of Materials, Weldments and Nondestructive Examination Techniques*, prepared by the SAC Joint Venture for the Federal Emergency Management Agency, Washington, DC.

SAC 95-09, 1995, *Background Reports: Metallurgy, Fracture Mechanics, Welding, Moment Connections and Frame Systems Behavior*, prepared by the SAC Joint Venture for the Federal Emergency Management Agency, Report No. FEMA-288, Washington, DC.

SAC 96-01, 1996, *Experimental Investigations of Beam-Column Subassemblages, Part 1 and 2*, prepared by the SAC Joint Venture for the Federal Emergency Management Agency, Washington, DC.

SAC 96-02, 1996, *Connection Test Summaries*, prepared by the SAC Joint Venture for the Federal Emergency Management Agency, Report No. FEMA-289, Washington, DC.

SAC 96-03, 1997, *Interim Guidelines Advisory No. 1 Supplement to FEMA-267 Interim Guidelines*, prepared by the SAC Joint Venture for the Federal Emergency Management Agency, Report No. FEMA-267A, Washington, DC.

- SAC 98-PG, *Update on the Seismic Safety of Steel Buildings – A Guide for Policy Makers*, prepared by the SAC Joint Venture for the Federal Emergency Management Agency, Washington, DC.
- SAC 99-01, 1999, *Interim Guidelines Advisory No. 2 Supplement to FEMA-267 Interim Guidelines*, prepared by the SAC Joint Venture, for the Federal Emergency Management Agency, Report No. FEMA-267B, Washington, DC.
- SAC, 2000a, *Recommended Seismic Design Criteria for New Steel Moment-Frame Buildings*, prepared by the SAC Joint Venture for the Federal Emergency Management Agency, Report No. FEMA-350, Washington, DC.
- SAC, 2000b, *Recommended Seismic Evaluation and Upgrade Criteria for Existing Welded Steel Moment-Frame Buildings*, prepared by the SAC Joint Venture for the Federal Emergency Management Agency, Report No. FEMA-351, Washington, DC.
- SAC, 2000c, *Recommended Postearthquake Evaluation and Repair Criteria for Welded Steel Moment-Frame Buildings*, prepared by the SAC Joint Venture for the Federal Emergency Management Agency, Report No. FEMA-352, Washington, DC.
- SAC, 2000d, *Recommended Specifications and Quality Assurance Guidelines for Steel Moment-Frame Construction for Seismic Applications*, prepared by the SAC Joint Venture for the Federal Emergency Management Agency, Report No. FEMA-353, Washington, DC.
- SAC, 2000e, *A Policy Guide to Steel Moment-Frame Construction*, prepared by the SAC Joint Venture for the Federal Emergency Management Agency, Report No. FEMA-354, Washington, DC.
- SAC, 2000f, *State of the Art Report on Base Metals and Fracture*, prepared by the SAC Joint Venture for the Federal Emergency Management Agency, Report No. FEMA-355A, Washington, DC.
- SAC, 2000g, *State of the Art Report on Welding and Inspection*, prepared by the SAC Joint Venture for the Federal Emergency Management Agency, Report No. FEMA-355B, Washington, DC.
- SAC, 2000h, *State of the Art Report on Systems Performance*, prepared by the SAC Joint Venture for the Federal Emergency Management Agency, Report No. FEMA-355C, Washington, DC.
- SAC, 2000i, *State of the Art Report on Connection Performance*, prepared by the SAC Joint Venture for the Federal Emergency Management Agency, Report No. FEMA-355D, Washington, DC.
- SAC, 2000j, *State of the Art Report on Past Performance of Steel Moment-Frame Buildings in Earthquakes*, prepared by the SAC Joint Venture for the Federal Emergency Management Agency, Report No. FEMA-355E, Washington, DC.
- SAC, 2000k, *State of the Art Report on Performance Prediction and Evaluation*, prepared by the SAC Joint Venture for the Federal Emergency Management Agency, Report No. FEMA-355F, Washington, DC.
- SAC/BD-96/01, *Selected Results from the SAC Phase 1 Beam-Column Connection Pre-Test Analyses*, submissions from B. Maison, K. Kasai, and R. Dexter; and A. Ingrassia and G. Deierlein.
- SAC/BD-96/02, *Summary Report on SAC Phase 1 - Task 7 Experimental Studies*, by C. Roeder (a revised version of this document is published in Report No. SAC 96-01; the original is no longer available).
- SAC/BD-96/03, *Selected Documents from the U.S.-Japan Workshop on Steel Fracture Issues*.

- SAC/BD-96/04, *Survey of Computer Programs for the Nonlinear Analysis of Steel Moment Frame Structures*.
- SAC/BD-97/01, *Through-Thickness Properties of Structural Steels*, by J. Barsom and S. Korvink.
- SAC/BD-97/02, *Protocol for Fabrication, Inspection, Testing, and Documentation of Beam-Column Connection Tests and Other Experimental Specimens*, by P. Clark, K. Frank, H. Krawinkler, and R. Shaw.
- SAC/BD-97/03, *Proposed Statistical and Reliability Framework for Comparing and Evaluating Predictive Models for Evaluation and Design*, by Y.-K. Wen.
- SAC/BD-97/04, *Development of Ground Motion Time Histories for Phase 2 of the FEMA/SAC Steel Project*, by P. Somerville, N. Smith, S. Punyamurthula, and J. Sun.
- SAC/BD-97/05, *Finite Element Fracture Mechanics Investigation of Welded Beam-Column Connections*, by W.-M. Chi, G. Deierlein, and A. Ingrassia.
- SAC/BD-98/01, *Strength and Ductility of FR Welded-Bolted Connections*, by S. El-Tawil, T. Mikesell, E. Vidarsson, and S. K. Kunnath.
- SAC/BD-98/02, *Effects of Strain Hardening and Strain Aging on the K-Region of Structural Shapes*, by J. Barsom and S. Korvink.
- SAC/BD-98/03, *Implementation Issues for Improved Seismic Design Criteria: Report on the Social, Economic, Policy and Political Issues Workshop* by L. T. Tobin.
- SAC/BD-99/01, *Parametric Study on the Effect of Ground Motion Intensity and Dynamic Characteristics on Seismic Demands in Steel Moment Resisting Frames* by G. A. MacRae.
- SAC/BD-99/01A, *Appendix to: Parametric Study on the Effect of Ground Motion Intensity and Dynamic Characteristics on Seismic Demands in Steel Moment Resisting Frames* by G. A. MacRae.
- SAC/BD-99/02, *Through-Thickness Strength and Ductility of Column Flange in Moment Connections*, by R. Dexter and M. Melendrez.
- SAC/BD-99/03, *The Effects of Connection Fractures on Steel Moment Resisting Frame Seismic Demands and Safety*, by C. A. Cornell and N. Luco.
- SAC/BD-99/04, *Effects of Strength/Toughness Mismatch on Structural and Fracture Behaviors in Weldments*, by P. Dong, T. Kilinski, J. Zhang, and F.W. Brust.
- SAC/BD-99/05, *Assessment of the Reliability of Available NDE Methods for Welded Joint and the Development of Improved UT Procedures*, by G. Gruber and G. Light.
- SAC/BD-99/06, *Prediction of Seismic Demands for SMRFs with Ductile Connections and Elements*, by A. Gupta and H. Krawinkler.
- SAC/BD-99/07, *Characterization of the Material Properties of Rolled Sections*, by T. K. Jaquess and K. Frank.
- SAC/BD-99/08, *Study of the Material Properties of the Web-Flange Intersection of Rolled Shapes*, by K. R. Miller and K. Frank.
- SAC/BD-99/09, *Investigation of Damage to WSMF Earthquakes other than Northridge*, by M. Phipps.
- SAC/BD-99/10, *Clarifying the Extent of Northridge Induced Weld Fracturing and Examining the Related Issue of UT Reliability*, by T. Paret.
- SAC/BD-99/11, *The Impact of Earthquakes on Welded Steel Moment Frame Buildings: Experience in Past Earthquakes*, by P. Weinburg and J. Goltz.

- SAC/BD-99/12, *Assessment of the Benefits of Implementing the New Seismic Design Criteria and Inspection Procedures*, by H. A. Seligson and R. Eguchi.
- SAC/BD-99/13, *Earthquake Loss Estimation for WSMF Buildings*, by C. A. Kircher.
- SAC/BD-99/14, *Simplified Loss Estimation for Pre-Northridge WSMF Buildings*, by B. F. Maison and D. Bonowitz.
- SAC/BD-99/15, *Integrative Analytical Investigations on the Fracture Behavior of Welded Moment Resisting Connections*, by G. G. Deierlein and W.-M. Chi.
- SAC/BD-99/16, *Seismic Performance of 3- and 9- Story Partially Restrained Moment Frame Buildings*, by B. F. Maison and K. Kasai.
- SAC/BD-99/17, *Effects of Partially-Restrained Connection Stiffness and Strength on Frame Seismic Performance*, by K. Kasai, B. F. Maison, and A. Mayangarum.
- SAC/BD-99/18, *Effects of Hysteretic Deterioration Characteristics on Seismic Response of Moment Resisting Steel Structures*, by F. Naeim, K. Skliros, A. M. Reinhorn, and M. V. Sivaselvan.
- SAC/BD-99/19, *Cyclic Instability of Steel Moment Connections with Reduced Beam Section*, by C.-M. Uang and C.-C. Fan.
- SAC/BD-99/20, *Local and Lateral-Torsion Buckling of Wide Flange Beams*, by L. Kwasniewski, B. Stojadinovic, and S. C. Goel.
- SAC/BD-99/21, *Elastic Models for Predicting Building Performance*, by X. Duan and J. C. Anderson.
- SAC/BD-99/22, *Reliability-Based Seismic Performance Evaluation of Steel Frame Buildings Using Nonlinear Static Analysis Methods*, by G. C. Hart and M. J. Skokan.
- SAC/BD-99/23, *Failure Analysis of Welded Beam to Column Connections*, by J. M. Barsom and J. V. Pellegrino.
- SAC/BD-99/24, *Weld Acceptance Criteria for Seismically-Loaded Welded Connections*, by W. Mohr.
- SAC/BD-00/01, *Parametric Tests on Unreinforced Connections, Volume I – Final Report*, by K.-H. Lee, B. Stojadinovic, S. C. Goel, A. G. Margarian, J. Choi, A. Wongkaew, B. P. Reyher, and D.-Y. Lee.
- SAC/BD-00/01A, *Parametric Tests on Unreinforced Connections, Volume II – Appendices*, by K.-H. Lee, B. Stojadinovic, S. C. Goel, A. G. Margarian, J. Choi, A. Wongkaew, B. P. Reyher, and D.-Y. Lee.
- SAC/BD-00/02, *Parametric Tests on the Free Flange Connections*, by J. Choi, B. Stojadinovic, and S. C. Goel.
- SAC/BD-00/03, *Cyclic Tests on Simple Connections Including Effects of the Slab*, by J. Liu and A. Astaneh-Asl.
- SAC/BD-00/04, *Tests on Bolted Connections, Part I: Technical Report*, by J. Swanson, R. Leon, and J. Smallridge.
- SAC/BD-00/04A, *Tests on Bolted Connections, Part II: Appendices*, by J. Swanson, R. Leon, and J. Smallridge.
- SAC/BD-00/05, *Bolted Flange Plate Connections*, by S. P. Schneider and I. Teeraparbong.
- SAC/BD-00/06, *Round Robin Testing of Ultrasonic Testing Technicians*, by R. E. Shaw, Jr.

- SAC/BD-00/07, *Dynamic Tension Tests of Simulated Welded Beam Flange Connections*, by J. M. Ricles, C. Mao, E. J. Kaufmann, L.-W. Lu, and J. W. Fisher.
- SAC/BD-00/08, *Design of Steel Moment Frame Model Buildings in Los Angeles, Seattle and Boston*, by P. Clark.
- SAC/BD-00/09, *Benchmarking of Analysis Programs for SMRF System Performance Studies*, by A. Gupta and H. Krawinkler.
- SAC/BD-00/10, *Loading Histories for Seismic Performance Testing of SMRF Components and Assemblies*, by H. Krawinkler, A. Gupta, R. Medina, and N. Luco.
- SAC/BD-00/11, *Development of Improved Post-Earthquake Inspection Procedures for Steel Moment Frame Buildings*, by P. Clark.
- SAC/BD-00/12, *Evaluation of the Effect of Welding Procedure on the Mechanical Properties of FCAW-S and SMAW Weld Metal Used in the Construction of Seismic Moment Frames*, by M. Q. Johnson.
- SAC/BD-00/13, *Preliminary Evaluation of Heat Affected Zone Toughness in Structural Shapes Used in the Construction of Seismic Moment Frames*, by M. Q. Johnson and J. E. Ramirez.
- SAC/BD-00/14, *Evaluation of Mechanical Properties in Full-Scale Connections and Recommended Minimum Weld Toughness for Moment Resisting Frames*, by M. Q. Johnson, W. Mohr, and J. Barsom.
- SAC/BD-00/15, *Simplified Design Models for Predicting the Seismic Performance of Steel Moment Frame Connections*, by C. Roeder, R. G. Coons, and M. Hoit.
- SAC/BD-00/16, *SAC Phase 2 Test Plan*, by C. Roeder.
- SAC/BD-00/17, *Behavior and Design of Radius-Cut, Reduced Beam Section Connections*, by M. Engelhardt, G. Fry, S. Jones, M. Venti, and S. Holliday.
- SAC/BD-00/18, *Test of a Free Flange Connection with a Composite Floor Slab*, by M. Venti and M. Engelhardt.
- SAC/BD-00/19, *Cyclic Testing of a Free Flange Moment Connection*, by C. Gilton, B. Chi, and C. M. Uang.
- SAC/BD-00/20, *Improvement of Welded Connections Using Fracture Tough Overlays*, by James Anderson, J. Duan, P. Maranian, and Y. Xiao.
- SAC/BD-00/21, *Cyclic Testing of Bolted Moment End-Plate Connections*, by T. Murray, E. Sumner, and T. Mays.
- SAC/BD-00/22, *Cyclic Response of RBS Moment Connections: Loading Sequence and Lateral Bracing Effects*, by Q. S. Yu, C. Gilton, and C. M. Uang.
- SAC/BD-00/23, *Cyclic Response of RBS Moment Connections: Weak Axis Configuration and Deep Column Effects*, by C. Gilton, B. Chi, and C. M. Uang.
- SAC/BD-00/24, *Development and Evaluation of Improved Details for Ductile Welded Unreinforced Flange Connections*, by J. M. Ricles, C. Mao, L.-W. Lu, and J. Fisher.
- SAC/BD-00/25, *Performance Prediction and Evaluation of Steel Special Moment Frames for Seismic Loads*, by K. Lee and D. A. Foutch.
- SAC/BD-00/26, *Performance Prediction and Evaluation of Low Ductility Steel Moment Frames for Seismic Loads*, by S. Yun and D. A. Foutch.
- SAC/BD-00/27, *Steel Moment Resisting Connections Reinforced with Cover and Flange Plates*, by T. Kim, A. S. Whittaker, V. V. Bertero, A. S. J. Gilani, and S. M. Takhirov.

SAC/BD-00/28, *Failure of a Column K-Area Fracture*, by J. M. Barsom and J. V. Pellegrino.

SAC/BD-00/29, *Inspection Technology Workshop*, by R. E. Shaw, Jr.

SAC/BD-00/30, *Preliminary Assessment of the Impact of the Northridge Earthquake on Construction Costs of Steel Moment Frame Buildings*, by Davis Langdon Adamson.

### Notation.

- $A_b$  Area of beam flange for the weld overlay connection. (See Figure 6-13)
- $A_{bt}$  Nominal cross sectional area of a bolt.
- $A_g$  Gross area of the column.
- $C_{GeometricCorrection}$  Geometric correction to account for the fact that the moment at the connection is larger than the plastic moment capacity for weak column-strong beam evaluation.
- $C_{ffst}$  Nominal compressive force used to design the web connection for the free flange connection. See Figure 3-10.
- $Ei_b$  Elastic modulus multiplied by the moment of inertia of the beam.
- $El_c$  Elastic modulus multiplied by the moment of inertia of the column.
- $F_{fu}$  Flange force caused by bending moment in bolted connections (See Tables 5-3 and 5-4).
- $F_{StrainHardeningStress}$  Estimated stress due to strain hardening for the weak-column-strong-beam evaluation criteria.
- $F_t$  Expected tensile strength of the steel. Median value expected from a large test program. Also used as the minimum bolt tensile strength (as defined by the AISC LRFD Specification in Tables 5-3 (where values are given), 5-4 and 5-10 (where it is used in  $T_b$ )).
- $F_{ta}$  Expected tensile strength of the steel in the angle used in double angle connection. Median value expected from a large test program.
- $F_{tb}$  Expected tensile strength of the beam steel. Median value expected from a large test program.
- $F_{tc}$  Expected tensile strength of the column steel. Median value expected from a large test program.
- $F_{tp}$  Expected tensile strength of the plate steel used in extended end plate of flange plate connections. Median value expected from a large test program.
- $F_v$  Nominal bolt shear strength from the AISC LRFD Provisions. (Used in Chapters 5 and 6)
- $F_y$  Expected yield stress of the steel. Median value expected from a large test program.
- $F_{yb}$  Expected yield stress of the beam steel. Median value expected from a large test program.
- $F_{yc}$  Expected yield stress of the column steel. Median value expected from a large test program.
- $F_{yp}$  Expected yield stress of the plate steel used in extended end plate of flange plate connections. Median value expected from a large test program.
- $F_{ub}$  Nominal tensile resistance of a bolt as defined by AISC LRFD Provisions.
- $L$  Beam span length from the center of one column to the center of the adjacent column.

---

$L_b$	Unsupported length of the beam.
$L_{cp}$	Length of the coverplate in coverplated connections.
$L_b$	Length of the flange plate in bolted and welded flange-plate connections.
$L_{eff}$	Effective clear length of the free flange in free-flange connection as illustrated in Figure 3.10.
$L_{fp}$	Length of the flange plate in flange-plate connections as defined in Figure 3-29.
$L_h$	Length of the haunch as defined in Figure 3-15.
$L_{RBS}$	Length from the face of the column to the center of the reduced beam section for the RBS connection.
$L_{st}$	Length of the stiffener for the stiffened end-plate connection. Defined in Figure 5-14.
$M_{bg}$	Moment at the bolt group for the bolted shear-tab connection. (See Figure 5-43)
$M_{fail}$	Resistances computed for all classes of failure modes for connections in this report.
$M_{fc}$	Moment in the weld and shear tab at the face of the column for the bolted shear tab connection. (See Figure 5-43)
$M_{yield}$	Resistances computed for all classes of yield mechanisms for connections in this report.
$M_y$	Bending moment at initial yielding of the wide-flange section.
$M_p$	Plastic moment capacity of a wide-flange section.
$N$	Number of shear bolts for various bolted connections. Defined differently for extended end plate (see Tables 5-3 and 5-4), bolted T-Stub (see Figure 5-29) and the bolted flange plate (see Figure 5-20) connections.
$N_{tb}$	Number of tension bolts for various bolted connections.
$P_{bf}$	Nominal design force historically used to design continuity plates in Equations 2-6 and 2-7.
$P_{uc}$	Factored compressive load on the column.
$R_y$	Ratio of the expected yield stress to the nominal yield stress of the steel. All yield and tensile stress included in this report are expected stresses, and $R_y$ is not commonly used in this report. However, the balance conditions of the extended end plate required separation of failure modes to ensure ductile behavior, and $R_y$ was selected as an appropriate value for this separation. (Used only in Tables 5-3 and 5-4)
$S$	Elastic section modulus.
$S_{RBS}$	Elastic section modulus of the beam at the reduced beam section for radiused RBS connection.
$S_b$	Elastic section modulus of the beam.
$S_c$	Elastic section modulus of the column.
$S_1$	Bolt spacing dimension. Defined in Fig 5-20 for bolted flange plate and Figure 5-29 for bolted T-stub connection.
$S_2$	Bolt spacing dimension. Defined in Fig 5-20 for bolted flange plate and Figure 5-29 for bolted T-stub connection.
$S_3$	Bolt spacing dimension. Defined in Fig 5-20 for bolted flange plate and Figure 5-29 for bolted T-stub connection.

---

---

$S_4$	Bolt spacing dimension. Defined in Fig 5-20 for bolted flange plate and Figure 5-29 for bolted T-stub connection.
$T$	Tensile force for the weld overlay induced by the bending moment. (See Figure 6-13)
$T_b$	Tensile resistance of bolts included for failure mode resistance calculations of bolted connections.
$T_{ffst}$	Nominal tensile force used to design the web connection for the free flange connection. See Figure 3-10.
$T_p$	Minimum bolt pretension.
$V$	Shear in the shear-tab connection caused by gravity load and the earthquake moments. Shear force in the weld overlay connection. (See Figure 6-13)
$V_c$	Shear in the column.
$V_{ffst}$	Nominal shear force used to design the web connection for the free flange connection. See Figure 3-10.
$V_{ffw}$	Total connection shear force considered in the free-flange connection design and assigned to the web attachment.
$V_g$	Shear force caused by gravity load in the design of some bolted connections.
$V_{pz}$	Shear force in the panel zone defined by equilibrium and caused by bending moments in the beam.
$V_{pzMy}$	Shear force in the panel zone caused by the yield moment, $M_y$ , at the location where flexural yielding is expected in the beam.
$V_p$	Plastic shear capacity of the panel zone after significant strain hardening as defined by Equation 2-3.
$V_{pAISC}$	Plastic shear capacity of the panel zone after significant strain hardening as defined by the present AISC <i>Seismic Design Provisions</i> and Equation 2-4.
$V_{web}$	Minimum web shear capacity required in the design of certain bolted connections.
$V_y$	Yield shear capacity of the panel zone as defined by Equation 2-1.
$V_{yAISC}$	Yield shear capacity of the panel zone based upon the AISC nominal shear yield stress and as defined by Equation 2-2.
$Y_c$	Arbitrary dimension used as one step in the failure mode resistance calculations of the end-plate connection.
$Z$	Plastic section modulus.
$Z_{RBS}$	Plastic section modulus of the beam at the reduced beam section for radiused RBS connection.
$Z_b$	Plastic section modulus of the beam. Unless otherwise noted, $Z_b$ is the plastic section about the x-axis or the major axis of bending.
$Z_c$	Plastic section modulus of the column. This term is used only in the strong-column-weak-beam design requirements, and the axis of orientation should be the axis orthogonal to the plane of the connection.
$a$	Free flange clearance (See Figure 3-10)
$a'$	Dimension for defining prying moments in bolted T-stub connection. (See Figure 5-28)

---

---

$b$	Clearance between web plate and beam flange for free flange connection (See Figure 3-10)
$b'$	Dimension for defining prying moments in bolted T-stub connection. (See Figure 5-28)
$b_{RBS}$	Minimum flange width of wide flange section at the reduced beam section of the radiused RBS connection.
$b_f$	Flange width of wide-flange sections.
$b_{fb}$	Flange width of the beam for continuity plate evaluation.
$b_p$	Width of the end plate for the extended end-plate connection. Defined in Figure 5-14.
$c$	Bolt spacing for the stiffened extended end-plate connection as defined in Figure 5-14. Clearance for bolted flange plate connection (see Figure 5-20), bolted T-stub (see Figure 5-29), and web angle and shear tab connection (see Figure 5-35)
$d$	Distance from the center of the bolt to the heel of the angle in double flange angle connections. (See Figure 5-33)
$d'$	Bolt spacing dimension used in the double flange angle connection. Defines the location of plastic deformation on the upstanding leg of the angle. (See Figure 5-33)
$d_b$	Depth of the wide-flange section for the beam.
$d_{bg}$	Depth of bolt group for bolted shear tab connection. See Figure 5-38.
$d_{bt}$	Diameter of the bolt.
$d_c$	Depth of the wide-flange section for the column.
$d_{eff}$	Effective depth for panel-zone yielding of several connection alternatives. Defined in Figure 3-15 for haunch connection, and Figure 5-13 for the extended end plate connection.
$d_i$	Distance from the center of the beam flange to the inner row of bolts for the far flange with extended end-plate connection. Defined in Figure 5-14.
$d_o$	Distance from the center of the beam flange to the outer row of bolts for the far flange with extended end-plate connection. Defined in Figure 5-14.
$d_{max}$	Maximum value of $d_1$ and $d_2$ .
$d_1$	Distance from the centroid of a shear-tab bolt group to the extreme top fiber of the beam. (See Figure 5-35)
$d_2$	Distance from the centroid of a shear-tab bolt group to the extreme lowest fiber of the beam. (See Figure 5-35)
$e$	Eccentricity between the centerline of the bolts and the face of the column in the shear tab connection. (See Figure 5-43)
$g$	Bolt gage spacing for bolted connections. Defined in Figure 5-14 for extended end plate connection, Fig 5-20 for bolted flange plate connection and Figure 5-29 for bolted T-stub connection.
$h$	Story height defined as the distance between the centers of the appropriate beams.
$h_{seff}$	Weld segment length for free flange connection (See Figure 3-10).
$k_s$	Rotational spring stiffness of partial stiffness connections discussed in Chapters 5 and 6.

---

---

$k_l$	Horizontal fillet distance from the center of the web of a wide flange to the toe of the fillet on the flange, as defined in the AISC LRFD <i>Steel Construction Manual</i> .
$l_a$	Length of the upstanding leg of the angle for double-flange-angle connections. (See Figure 5-33)
$p_b$	Bolt spacing for the stiffened end-plate connection as illustrated in Figure 5-14.
$p_t$	Distance from center of inner row of bolts to the outside of the adjacent beam flange in the 4-bolt unstiffened extended end-plate connection. See Figure 5-14.
$p_f$	Distance from the near surface of the beam flange to the center of the adjacent row of bolts in the extended end-plate connection as defined in Figure 5-14.
$r_y$	Radius of gyration about the weak axis (y axis) of the wide-flange section.
$t_f$	Flange thickness of wide-flange sections.
$t_{fb}$	Flange thickness of wide-flange section for the beam.
$t_{fc}$	Flange thickness of wide-flange section for the column.
$t_{ft}$	Flange thickness of the T-section used in the T-stub connection.
$t_s$	Thickness of the stiffener for the stiffened end-plate connection as illustrated in Figure 5-14.
$t_{fs-t}$	Thickness of the stem of the T-section used in the T-stub connection.
$t_w$	Web thickness of wide-flange sections.
$t_{wb}$	Web thickness of wide-flange section for the beam.
$t_{wc}$	Web thickness of wide-flange section for the column.
$s$	Arbitrary dimension used as one step in the failure mode resistance calculations of the end-plate connection.
$\alpha$	Relative length of free flange to the flange thickness for free-flange connection
$\Delta_{FR}$	Column deflection or story drift of a single story subassembly with fully restrained connections. See Figure 5-3.
$\Delta_{PR}$	Column deflection or story drift of a single story subassembly with partially restrained connections. See Figure 5-3.
$\theta_{eff}$	Angle for defining the Whitmore net section for bolted T-stub and bolted double-flange-angle connection.
$\theta_g$	Plastic rotation at which the connection may not be able to support the gravity loads.
$\theta_{gmean}$	Mean value of the plastic rotation at which the connection may not be able to support the gravity loads based upon the test results.
$\theta_p$	Plastic rotation of the connection.
$\theta_{pmean}$	Mean value of the plastic rotation of the connection based upon the test results.
$\sigma_g$	Standard deviation of the rotation at which the connection may not be able to support the gravity loads.
$\sigma_p$	Standard deviation of the plastic rotation.

---

**Acronyms.**

2-D, two-dimensional	CAC-A, air carbon arc cutting
3-D, three-dimensional	CAWI, Certified Associate Welding Inspector
A, acceleration response, amps	CGHAZ, coarse-grained HAZ
A2LA, American Association for Laboratory Accreditation	CJP, complete joint penetration (weld)
ACAG, air carbon arc gouging	CMU, concrete masonry unit, concrete block
ACIL, American Council of Independent Laboratories	COD, crack opening displacement
AE, acoustic emission (testing)	“COV,” modified coefficient of variation, or dispersion
AISC, American Institute for Steel Construction	CP, Collapse Prevention (performance level)
AISI, American Iron and Steel Institute	Connection Performance (team)
AL, aluminum	Cr, chromium
ANSI, American National Standards Institute	CSM, Capacity Spectrum Method
API, American Petroleum Institute	CTOD, crack tip opening dimension or displacement
ARCO, Atlantic-Richfield Company	CTS, controlled thermal severity (test)
As, arsenic	Cu, copper
ASD, allowable stress design	CUREe, California Universities for Research in Earthquake Engineering
ASME, American Society of Mechanical Engineers	CVN, Charpy V-notch
ASNT, American Society for Nondestructive Testing	CWI, Certified Welding Inspector
ASTM, American Society for Testing and Materials	D, displacement response, dead load
ATC, Applied Technology Council	DMRSF, ductile, moment-resisting, space frame
AWS, American Welding Society	DNV, Det Norske Veritas
B, boron	DRAIN-2DX, analysis program
BB, Bolted Bracket (connection)	DRAIN-3DX, analysis program
BD, background document	DRI, direct reduced iron
BF, bias factor	DST, Double Split Tee (connection)
BFO, bottom flange only (fracture)	DTI, Direct Tension Indicator
BFP, Bolted Flange Plates (connection)	EAF, electric-arc furnace
BM, base metal	EBT, eccentric bottom tapping
BO, Boston, Massachusetts	EE, electrode extension
BOCA, Building Officials and Code Administrators	EERC, Earthquake Engineering Research Center, UC Berkeley
BOF, basic oxygen furnace	EGW, electrogas welding
BSEP, Bolted Stiffened End Plate (connection)	ELF, equivalent lateral force
BSSC, Building Seismic Safety Council	EMS, electromagnetic stirring
BUEP, Bolted Unstiffened End Plate (connection)	ENR, Engineering News Record
C, carbon	ESW, electroslag welding
CA, California	EWI, Edison Welding Institute
	FATT, fracture appearance transition temperature
	fb, fusion boundary

---

FCAW-G, flux-cored arc welding – gas-shielded	LTH, linear time history (analysis)
FCAW-S or FCAW-SS, flux-cored arc welding – self-shielded	LU, Lehigh University
FEMA, Federal Emergency Management Agency	M, moment
FF, Free Flange (connection)	MAP, modal analysis procedure
FGHAZ, fine-grained HAZ	MAR, microalloyed rutile (consumables)
FL, fusion line	MCE, Maximum Considered Earthquake
FR, fully restrained (connection)	MDOF, multidegree of freedom
GBOP, gapped bead on plate (test)	MMI, Modified Mercalli Intensity
gl, gage length	Mn, manganese
GMAW, gas metal arc welding	Mo, molybdenum
GTAW, gas tungsten arc welding	MRF, steel moment frame
HAC, hydrogen-assisted cracking	MRS, modal response spectrum
HAZ, heat-affected zone	MRSF, steel moment frame
HBI, hot briquetted iron	MT, magnetic particle testing
HSLA, high strength, low alloy	N, nitrogen
IBC, <i>International Building Code</i>	Nb, niobium
ICBO, International Conference of Building Officials	NBC, <i>National Building Code</i>
ICC, International Code Council	NDE, nondestructive examination
ICCGHAZ, intercritically reheated CGHAZ	NDP, Nonlinear Dynamic Procedure
ICHAZ, intercritical HAZ	NDT, nondestructive testing
ID, identification	NEHRP, National Earthquake Hazards Reduction Program
IDA, Incremental Dynamic Analysis	NES, National Evaluation Services
IMF, Intermediate Moment Frame	NF, near-fault, near-field
IO, Immediate Occupancy (performance level)	Ni, nickel
IOA, Incremental Dynamic Analysis	NLP, nonlinear procedure
ISO, International Standardization Organization	NLTH, nonlinear time history (analysis)
IWURF, Improved Welded Unreinforced Flange (connection)	NS, north-south (direction)
L, longitudinal, live load	NSP, Nonlinear Static Procedure
LA, Los Angeles, California	NTH, nonlinear time history (analysis)
LACOTAP, Los Angeles County Technical Advisory Panel	NVLAP, National Volunteer Laboratory Accreditation Program
LAX, Los Angeles International Airport	O, oxygen
LB, lower bound (building)	OHF, open hearth furnace
LBZ, local brittlezone	OMF, Ordinary Moment Frame
LDP, Linear Dynamic Procedure	OTM, overturning moment
LEC, Lincoln Electric Company	P, axial load
LMF, ladle metallurgy furnace	P, axial load, phosphorus
LRFD, load and resistance-factor design	Pb, lead
LS, Life Safety (performance level)	PGA, peak ground acceleration
LSP, Linear Static Procedure	PGV, peak ground velocity
	PIDR, pseudo interstory drift ratio
	PJP, partial joint penetration (weld)
	PPE, Performance, Prediction, and Evaluation (team)
	PQR, Performance Qualification Record
	PR, partially restrained (connection)

---

---

PR-CC, partially restrained, composite connection	SPC, Seismic Performance Category
PT, liquid dye penetrant testing	SRSS, square root of the sum of the squares
PWHT, postweld heat treatment	SSPC, Steel Shape Producers Council
PZ, panel zone	SSRC, Structural Stability Research Council
QA, quality assurance	SUG, Seismic Use Group
QC, quality control	SW, Slotted Web (connection)
QCP, Quality Control Plan, Quality Certification Program	SwRI, Southwest Research Institute
QST, Quenching and Self-Tempering (process)	T, transverse
RB, Rockwell B scale (of hardness)	TBF, top and bottom flange (fracture)
RBS, Reduced Beam Section (connection)	Ti, titanium
RCSC, Research Council for Structural Connections	TIGW, tungsten inert gas welding
RT, radiographic testing	TMCP, Thermo-Mechanical Processing
S, sulphur, shearwave (probe)	TN, Tennessee
SAC, the SAC Joint Venture; a partnership of SEAOC, ATC, and CUREe	TT, through-thickness
SAV, sum of absolute values	TWI, The Welding Institute
SAW, submerged arc welding	UB, upper bound (building)
SBC, <i>Standard Building Code</i>	UBC, <i>Uniform Building Code</i>
SBCCI, Southern Building Code Congress International	UCLA, University of California, Los Angeles
SCCGHAZ, subcritically reheated CGHAZ	UM, University of Michigan
SCHAZ, subcritical HAZ	URM, unreinforced masonry
SCWB, strong column, weak beam	US, United States of America
SCWI, Senior Certified Welding Inspector	USC, University of Southern California
SDC, Seismic Design Category	USGS, US Geological Survey
SDOF, single degree of freedom	UT, ultrasonic testing
SE, Seattle, Washington	UTA, University of Texas at Austin
SEAOC, Structural Engineers Association of California	UTAM, Texas A & M University
SFRS, seismic-force-resisting system	V, vanadium
Si, silicon	VI, visual inspection
SMAW, shielded metal arc welding	w/o, without
SMF, Special Moment Frame	WBH, Welded Bottom Haunch (connection)
SMRF, special moment-resisting frame (in 1991 UBC)	WCPF, Welded Cover Plate Flange (connection)
SMRF, Steel Moment Frame	WCSB, weak column, strong beam
SMRSF, special moment-resisting space frame (in 1988 UBC)	WF, wide flange
SN, strike-normal, fault-normal	WFP, Welded Flange Plate (connection)
Sn, tin	WFS, wire feed speed
SP, Side Plate (connection)	WPQR, Welding Performance Qualification Record
SP, strike-parallel, fault-parallel	WPS, Welding Procedure Specification
SP, Systems Performance (team)	WSMF, welded steel moment frame
	WT, Welded Top Haunch (connection)
	WTBH, Welded Top and Bottom Haunch (connection)
	WUF-B, Welded Unreinforced Flanges – Bolted Web (connection)

---

WUF-W, Welded Unreinforced Flanges –  
Welded Web (connection)

**SAC PHASE II PROJECT PARTICIPANTS****FEMA Project Officer**

Michael Mahoney  
Federal Emergency Management Agency  
500 C St. SW, Room 404  
Washington, DC 20472

**FEMA Technical Advisor**

Robert D. Hanson  
Federal Emergency Management Agency  
DFO Room 353  
P.O. Box 6020  
Pasadena, CA 91102-6020

**Joint Venture Management Committee (JVMC)**

William T. Holmes, Chair  
Rutherford and Chekene  
427 Thirteenth Street  
Oakland, CA 94612

Christopher Rojahn  
Applied Technology Council  
555 Twin Dolphin Dr., Suite 550  
Redwood City, CA 94065

Edwin T. Huston  
Smith & Huston, Inc.  
8618 Roosevelt Way NE  
Seattle, WA 98115

Arthur E. Ross  
Cole/Yee/Shubert & Associates  
2500 Venture Oaks Way, Suite 100  
Sacramento, CA 95833

Robert Reitherman  
California Universities for Research in  
Earthquake Engineering  
1301 South 46th St.  
Richmond, CA 94804

Robin Shepherd  
Earthquake Damage Analysis Corporation  
40585 Lakeview Drive, Suite 1B  
P.O. Box 1967  
Big Bear Lake, CA 92315

**Project Management Committee (PMC)**

Stephen A. Mahin, Project Manager  
Pacific Earthquake Engr. Research Center  
University of California  
Berkeley, CA 94720

William T. Holmes, JVMC  
Rutherford and Chekene  
427 Thirteenth Street  
Oakland, CA 94612

Ronald O. Hamburger, Project Director for  
Project Development  
EQE International  
1111 Broadway, 10th Floor  
Oakland, CA 94607-5500

Christopher Rojahn, JVMC  
Applied Technology Council  
555 Twin Dolphin Dr., Suite 550  
Redwood City, CA 94065

James O. Malley, Project Director for  
Topical Investigations  
Degenkolb Engineers  
225 Bush St., Suite 1000  
San Francisco, CA 94104-1737

Robin Shepherd, JVMC  
Earthquake Damage Analysis Corporation  
40585 Lakeview Drive, Suite 1B  
P.O. Box 1967  
Big Bear Lake, CA 92315

Peter W. Clark, Technical Assistant to PMC  
SAC Steel Project Technical Office  
1301 South 46th St.  
Richmond, CA 94804

### **Project Administration**

Allen Paul Goldstein, Project Administrator  
Allen Paul Goldstein and Associates  
1621B 13th Street  
Sacramento, CA 95814

Lori Campbell, Assistant to the Project  
Administrator  
4804 Polo Court  
Fair Oaks, CA 95628

### **Project Oversight Committee (POC)**

William J. Hall, Chair  
3105 Valley Brook Dr.  
Champaign, IL 61821

James R. Harris  
J.R. Harris and Co.  
1580 Lincoln St., Suite 550  
Denver, CO 80203-1509

Shirin Ader  
International Conference of Building  
Officials  
5360 Workman Mill Rd.  
Whittier, CA 90601-2298

Richard Holguin  
520 Kathryn Ct.  
Nipomo, CA 93444

John M. Barsom  
Barsom Consulting, Ltd.  
1316 Murray Ave, Suite 300  
Pittsburgh, PA 15217

Nestor Iwankiw  
American Institute of Steel Construction  
One East Wacker Dr., Suite 3100  
Chicago, IL 60601-2001

Roger Ferch  
Herrick Corporation  
7021 Koll Center Parkway  
P.O Box 9125  
Pleasanton, CA 94566-9125

Roy Johnston  
Brandow & Johnston Associates  
1600 West 3rd St.  
Los Angeles, CA 90017

Theodore V. Galambos  
University of Minnesota  
122 CE Building, 500 Pillsbury Dr. SE  
Minneapolis, MN 55455

Leonard Joseph  
Thornton-Tomassetti Engineers  
641 6th Ave., 7th Floor  
New York, NY 10011

John L. Gross  
National Institute of Stds. & Technology  
Building and Fire Research Lab,  
Building 226, Room B158  
Gaithersburg, MD 20899

Duane K. Miller  
The Lincoln Electric Company  
22801 St. Clair Ave.  
Cleveland, OH 44117-1194

John Theiss  
EQE/Theiss Engineers  
1848 Lackland Hills Parkway  
St. Louis, MO 63146-3572

John H. Wiggins  
J.H. Wiggins Company  
1650 South Pacific Coast Hwy, Suite 311  
Redondo Beach, CA 90277

### Team Leaders for Topical Investigations

Douglas A. Foutch  
University of Illinois  
MC-250, 205 N. Mathews Ave.  
3129 Newmark Civil Engineering Lab  
Urbana, IL 61801

Karl H. Frank  
University of Texas at Austin  
10100 Burnet Rd.  
Ferguson Lab, P.R.C. #177  
Austin, TX 78758

Matthew Johnson  
Edison Welding Institute  
1250 Arthur E. Adams Drive  
Columbus, OH 43221

Helmut Krawinkler  
Department of Civil Engineering  
Stanford University  
Stanford, CA 94305

Charles W. Roeder  
University of Washington  
233-B More Hall FX-10  
Dept. of Building and Safety  
Seattle, WA 98195-2700

L. Thomas Tobin  
Tobin and Associates  
134 California Ave.  
Mill Valley, CA 94941

### Lead Guideline Writers

John D. Hooper  
Skilling Ward Magnusson Barkshire, Inc.  
1301 Fifth Avenue, Suite 3200  
Seattle, WA 98101-2699

Lawrence D. Reaveley  
University of Utah  
Civil Engineering Dept.  
3220 Merrill Engineering Building  
Salt Lake City, UT 84112

Thomas A. Sabol  
Englekirk & Sabol Consulting Engineers  
P.O. Box 77-D  
Los Angeles, CA 90007

C. Mark Saunders  
Rutherford & Chekene  
303 Second St., Suite 800 North  
San Francisco, CA 94107

Robert E. Shaw  
Steel Structures Technology Center, Inc.  
42400 W Nine Mile Road  
Novi, MI 48375-4132

Raymond H. R. Tide  
Wiss, Janney, Elstner Associates, Inc.  
330 Pflingsten Road  
Northbrook, IL 60062-2095

C. Allin Cornell, Associate Guideline Writer  
Stanford University  
Terman Engineering Center  
Stanford, CA 94305-4020

### **Technical Advisory Panel (TAP) for Materials and Fracture**

John M. Barsom, POC  
Barsom Consulting, Ltd.  
1316 Murray Ave, Suite 300  
Pittsburgh, PA 15217

Serge Bouchard\*  
TradeARBED  
825 Third Avenue, 35th Floor  
New York, NY 10022

Michael F. Engestrom\*  
Nucor-Yamato Steel  
P.O. Box 678  
Frederick, MD 21705-0678

Karl H. Frank, Team Leader  
University of Texas at Austin  
10100 Burnet Rd.  
Ferguson Lab, P.R.C. #177  
Austin, TX 78758

Nestor Iwankiw, POC\*  
American Institute of Steel Construction  
One East Wacker Dr., Suite 3100  
Chicago, IL 60601-2001

Dean C. Krouse\*  
705 Pine Top Drive  
Bethlehem, PA 18017

Frederick V. Lawrence  
University of Illinois at Urbana-Champaign  
205 N. Mathews Ave.  
Room 2129 Newmark Lab  
Urbana, IL 61801

Robert F. Preece  
Preece, Goudie & Associates  
100 Bush St., Suite 410  
San Francisco, CA 94104

Raymond H. R. Tide, Guideline Writer  
Wiss, Janney, Elstner Associates, Inc.  
330 Pflingsten Road  
Northbrook, IL 60062-2095

### **TAP for Welding and Inspection**

John M. Barsom, POC  
Barsom Consulting, Ltd.  
1316 Murray Ave, Suite 300  
Pittsburgh, PA 15217

John W. Fisher  
Lehigh University  
117 ATLSS Drive  
Bethlehem, PA 18015-4729

J. Ernesto Indacochea  
University of Illinois at Chicago  
Civil and Materials Engineering (mc 246)  
842 West Taylor Street  
Chicago, IL 60607

Matthew Johnson, Team Leader  
Edison Welding Institute  
1250 Arthur E. Adams Drive  
Columbus, OH 43221

David Long  
PDM Strocal, Inc.  
2324 Navy Drive  
Stockton, CA 95206

Duane K. Miller, POC  
The Lincoln Electric Company  
22801 St. Clair Ave.  
Cleveland, OH 44117-1194

Robert Pyle\*  
AISC Marketing  
10101 South State Street  
Sandy, Utah 84070

Douglas Rees-Evans\*  
Steel Dynamics, Inc.  
Structural Mill Division  
2601 County Road 700 East  
Columbia City, IN 46725

Richard I. Seals  
P.O. Box 11327  
Berkeley, CA 94712-2327

Robert E. Shaw, Guideline Writer  
Steel Structures Technology Center, Inc.  
42400 W Nine Mile Road  
Novi, MI 48375-4132

### **TAP for Connection Performance**

Charlie Carter\*  
American Institute of Steel Construction  
One East Wacker Drive, Suite 3100  
Chicago, IL 60601-2001

Robert H. Dodds  
University of Illinois at Urbana-Champaign  
205 N. Mathews Ave.  
2129 Newmark Lab  
Urbana, IL 61801

Roger Ferch, POC  
Herrick Corporation  
7021 Koll Center Parkway  
P.O. Box 9125  
Pleasanton, CA 94566-9125

John D. Hooper, Guideline Writer  
Skilling Ward Magnusson Barkshire, Inc.  
1301 Fifth Avenue, Suite 3200  
Seattle, WA 98101-2699

Egor Popov  
University of California at Berkeley  
Department of Civil and Environmental  
Engineering, Davis Hall  
Berkeley, CA 94720

Steve Powell\*  
SME Steel Contractors  
5955 W. Wells Park Rd.  
West Jordan, UT 84088

Charles W. Roeder, Team Leader  
University of Washington  
233-B More Hall FX-10  
Dept. of Building and Safety  
Seattle, WA 98195-2700

Stanley T. Rolfe  
University of Kansas  
Civil Engineering Department  
2006 Learned Hall  
Lawrence, KS 66045-2225

Rick Wilkinson\*  
Gayle Manufacturing Company  
1455 East Kentucky  
Woodland, CA 95695

### **TAP for System Performance**

Jacques Cattan\*  
American Institute of Steel Construction  
One East Wacker Drive, Suite 3100  
Chicago, IL 60601-2001

Gary C. Hart  
Hart Consultant Group  
The Water Garden, Ste. 670E  
2425 Olympic Blvd.  
Santa Monica, CA 90404-4030

Y. Henry Huang\*  
Los Angeles County Dept. of Public Works  
900 S. Fremont Avenue, 8th Floor  
Alhambra, CA 91803

Helmut Krawinkler, Team Leader  
Department of Civil Engineering  
Stanford University  
Stanford, CA 94305

Dennis Randall\*  
SME Steel Contractors  
5955 West Wells Park Road  
West Jordan, UT 84088

Andrei M. Reinhorn  
State University of New York at Buffalo  
Civil Engineering Department  
231 Ketter Hall  
Buffalo, NY 14260

Arthur E. Ross, JVMC  
Cole/Yee/Shubert & Associates  
2500 Venture Oaks Way, Suite 100  
Sacramento, CA 95833

C. Mark Saunders, Guideline Writer  
Rutherford & Chekene  
303 Second St., Suite 800 North  
San Francisco, CA 94107

W. Lee Shoemaker\*  
Metal Building Manufacturers Association  
1300 Summer Avenue  
Cleveland, OH 44115

John Theiss, POC  
EQE/Theiss Engineers  
1848 Lackland Hills Parkway  
St. Louis, MO 63146-3572

### **TAP for Performance Prediction and Evaluation**

Vitelmo V. Bertero  
University of California at Berkeley  
Pacific Earthquake Engr. Research Center  
1301 S. 46th St.  
Richmond, CA 94804

Bruce R. Ellingwood  
Johns Hopkins University  
Department of Civil Engineering  
3400 N. Charles St.  
Baltimore, MD 21218

Douglas A. Foutch, Team Leader  
University of Illinois  
MC-250, 205 N. Mathews Ave.  
3129 Newmark Civil Engineering Lab  
Urbana, IL 61801

Theodore V. Galambos, POC  
University of Minnesota  
122 CE Building, 500 Pillsbury Dr. SE  
Minneapolis, MN 55455

Lawrence G. Griffis  
Walter P. Moore & Associates  
3131 Eastside, Second Floor  
Houston, TX 77098

Edwin T. Huston, JVMC  
Smith & Huston, Inc.  
8618 Roosevelt Way NE  
Seattle, WA 98115

Thomas A. Sabol, Guideline Writer  
Englekirk & Sabol Consulting Engineers  
P.O. Box 77-D  
Los Angeles, CA 90007

Harry Martin\*  
American Iron and Steel Institute  
11899 Edgewood Road, Suite G  
Auburn, CA 95603

Tom Schlafly\*  
American Institute of Steel Construction  
One East Wacker Drive, Suite 3100  
Chicago, IL 60601-2001

### Technical Advisors

Norm Abrahamson  
Pacific Gas & Electric  
P.O. Box 770000, MC N4C  
San Francisco, CA 94177

Robert Kennedy  
RPK Structural Mechanics Consultants  
18971 Villa Terr  
Yorba Linda, CA 92886

C.B. Crouse  
URS – Dames and Moore  
2025 First Avenue, Suite 500  
Seattle, WA 98121

### Social Economic and Policy Panel

Martha Cox-Nitikman  
Building and Owners and Managers  
Association, Los Angeles  
700 South Flower, Suite 2325  
Los Angeles, CA 90017

Alan Merson  
Morley Builders  
2901 28th Street, Suite 100  
Santa Monica, CA 90405

Karl Deppe  
27502 Fawnskin Dr.  
Rancho Palos Verdes, CA 90275

Joanne Nigg  
University of Delaware  
Disaster Research Center  
Newark, DE 19716

Eugene Lecomte  
Institute for Business and Home Safety  
6 Sheffield Drive  
Billerica, MA 01821

William Petak  
University of Southern California  
Lewis Hall, Room 201  
650 Childs Way  
Los Angeles, CA 90089

James Madison  
Attorney at Law, Mediator and Arbitrator  
750 Menlo Avenue, Suite 250  
Menlo Park, CA 94025

Francine Rabinovitz  
Hamilton, Rabinovitz and Alschuler  
1990 South Bundy Drive, Suite 777  
Los Angeles, CA 90025

Dennis Randall  
SME Steel Contractors  
5955 West Wells Park Road  
West Jordan, UT 84088

Stephen Toth  
TIAA-CREF  
730 Third Avenue  
New York, NY 10017-3206

David Ratterman  
Stites and Harbison  
400 West Market St., Suite 1800  
Louisville, KY 40202-3352

John H. Wiggins, POC  
J.H. Wiggins Company  
1650 South Pacific Coast Hwy, Suite 311  
Redondo Beach, CA 90277

L. Thomas Tobin, Panel Coordinator  
134 California Ave.  
Mill Valley, CA 94941

### **Performance of Steel Buildings in Past Earthquakes Subcontractors**

David Bonowitz  
887 Bush, No. 610  
San Francisco, CA 94108

Peter Maranian  
Brandow & Johnston Associates  
1660 West Third Street  
Los Angeles, CA 90017

Peter Clark  
SAC Steel Project Technical Office  
1301 South 46th St.  
Richmond, CA 94804

Terrence Paret  
Wiss Janney Elstner Associates, Inc.  
2200 Powell St. Suite 925  
Emeryville, CA 94602

Michael Durkin  
Michael Durkin & Associates  
22955 Leanora Dr.  
Woodland Hills, CA 91367

Maryann Phipps  
Degenkolb Engineers  
225 Bush Street, Suite 1000  
San Francisco, CA 94104

James Goltz  
California Institute of Technology  
Office of Earthquake Programs  
Mail Code 252-21  
Pasadena, CA 91125

Allan Porush  
Dames & Moore  
911 Wilshire Blvd., Suite 700  
Los Angeles, CA 90017

Bruce Maison  
7309 Lynn Ave  
Elcerrito, CA 94530

### **Access Current Knowledge Subcontractors**

David Bonowitz  
887 Bush , No. 610  
San Francisco, CA 94108

Stephen Liu  
Colorado School of Mines  
Mathematics and Computer Science  
Department  
Golden, CO 80401

**Materials and Fracture Subcontractors**

Robert Dexter  
University of Minnesota  
122 Civil Engineering Building  
500 Pillsbury Drive SE  
Minneapolis, MN 55455-0116

Karl H. Frank  
University of Texas at Austin  
10100 Burnet Rd.  
Ferguson Lab, P.R.C. #177  
Austin, TX 78758

**Welding and Inspection Subcontractors**

Pingsha Dong / Tom Kilinski  
Center for Welded Structures Research  
Battelle Memorial Institute  
501 King Avenue  
Columbus, OH 43201-2693

Glenn M. Light / George Gruber  
Southwest Research Institute  
6220 Culebra Road, P. O. Drawer 28510  
San Antonio, TX 78228-0510

Matthew Johnson  
Edison Welding Institute  
1250 Arthur E. Adams Drive  
Columbus, OH 43221

William C. Mohr  
Edison Welding Institute  
1250 Arthur E. Adams Drive  
Columbus, OH 43221

**Connection Performance Subcontractors**

Gregory Deierlein  
Stanford University  
Terman Engineering Center  
Department of Civil and Environmental Engr.  
Stanford, CA 94305-4020

Sherif El-Tawil / Sashi Kunnath  
University of Central Florida  
Civil and Environmental Engr. Department  
Orlando, FL. 32816-2450

Charles W. Roeder  
University of Washington  
233-B More Hall FX-10  
Seattle, WA 98195-2700

Anthony Ingraffea  
Cornell University  
School of Civil Engineering  
363 Hollister Hall  
Ithaca, NY 14853

**System Performance Subcontractors**

Paul Somerville  
Woodward-Clyde Federal Services  
566 El Dorado St., Suite 100  
Pasadena, CA 91101-2560

Andrei M. Reinhorn  
State University of New York at Buffalo  
Civil Engineering Department  
231 Ketter Hall  
Buffalo, NY 14260

Farzad Naeim  
John A. Martin & Associates  
1212 S. Flower Ave.  
Los Angeles, CA 90015

C. Allin Cornell  
Stanford University  
Terman Engineering Center  
Stanford, CA 94305-4020

Helmut Krawinkler  
Dept. of Civil Engineering  
Stanford University  
Stanford, CA 94305

Kazuhiko Kasai  
Tokyo Institute of Technology  
Structural Engineering Research Center  
Nagatsuta, Midori-Ku  
Yokohama 226-8503, JAPAN

Gregory MacRae  
University of Washington  
Civil Engineering Department  
Seattle, WA 98195-2700

Bruce F. Maison  
7309 Lynn Avenue  
El Cerrito, CA 94530

### **Performance Prediction and Evaluation Subcontractors**

James Anderson  
University of Southern California  
Civil Engineering Department  
Los Angeles, CA 90089-2531

Gary C. Hart  
Department of Civil and Environmental  
Engineering  
University of California  
Los Angeles, CA 90095

Douglas A. Foutch  
University of Illinois  
MC-250, 205 N. Mathews Ave.  
3129 Newmark Civil Engineering Lab  
Urbana, IL 61801

Y.K. Wen  
University of Illinois  
3129 Newmark Civil Engineering Lab  
205 N. Mathews Ave.  
Urbana, IL 61801

### **Testing Subcontractors**

Subhash Goel / Bozidar Stojadinovic  
University of Michigan  
Civil Engineering Department  
Ann Arbor, MI 48109

Thomas Murray  
Virginia Tech, Dept. of Civil Engineering  
200 Patton Hall  
Blacksburg, VA 24061

Roberto Leon  
Georgia Institute of Technology  
School of Civil & Environmental Engr.  
790 Atlantic Ave.  
Atlanta, GA 30332-0355

James M. Ricles / Le-Wu Lu  
Lehigh University  
c/o ATLSS Center  
117 ATLSS Drive, H Building  
Bethlehem, PA 18015-4729

Vitelmo V. Bertero / Andrew Whittaker  
UC Berkeley  
Pacific Earthquake Engr. Research Center  
1301 S. 46th St.  
Richmond, CA 94804

John M. Barsom  
Barsom Consulting, Ltd.  
1316 Murray Ave, Suite 300  
Pittsburgh, PA 15217

Hassan Astaneh  
University of California at Berkeley  
Dept. of Civil and Environmental Engr.  
781 Davis Hall  
Berkeley, CA 94720

Michael Engelhardt  
University of Texas at Austin  
Ferguson Laboratory  
10100 Burnet Road, Building 177  
Austin, TX 78712-1076

Gary T. Fry  
Texas A&M University  
Department of Civil Engineering  
Constructed Facilities Division, CE/TTI  
Building, Room 710D  
College Station, TX 77843-3136

Chia-Ming Uang  
University of California at San Diego  
Dept. of AMES, Division of Structural Engr.  
409 University Center  
La Jolla, California 92093-0085

Stephen Schneider  
University of Illinois at Urbana-Champaign  
3106 Newmark Civil Engr. Lab, MC-250  
205 N. Mathews Avenue  
Urbana, IL 61801

Matthew Johnson  
Edison Welding Institute  
1250 Arthur E. Adams Drive  
Columbus, OH 43221

James Anderson  
University of Southern California  
Civil Engineering Department  
Los Angeles, CA 90089-2531

Bozidar Stojadinovic  
Dept. of Civil & Environmental Engr.  
University of California  
Berkeley, CA 94720

### Inspection Procedure Consultants

Thomas Albert  
Digiray Corporation  
2235 Omega Road, No. 3  
San Ramon, CA 94583

Randal Fong  
Automated Inspection Systems, Inc.  
4861 Sunrise Drive, Suite 101  
Martinez, CA 94553

Andre Lamarre  
R.D Tech, Inc.  
1200 St. Jean Baptiste, Suite 120  
Quebec City, Quebec, Canada G2ZE 5E8

Glenn Light  
Southwest Research Institute  
6220 Culebra Road  
San Antonio, TX 78228

Andrey Mishin  
AS & E High Energy Systems  
330 Keller Street, Building 101  
Santa Clara, CA 95054

Robert Shaw  
Steel Structures Technology Center, Inc.  
42400 W. Nine Mile Road  
Novi, MI 48375-4132

Carlos Ventura  
Dept of Civil Engineering  
University of British Columbia  
2324 Main Hall  
Vancouver, BC, Canada V6T 1Z4

### **Guideline Trial Applications Subcontractors**

John Hopper  
Skilling Ward Magnusson Barkshire, Inc.  
1301 Fifth Avenue, Suite 320  
Seattle WA 98101-2699

Lawrence Novak  
Skidmore, Owings, and Merrill  
224 S. Michigan Ave, Suite 1000  
Chicago, IL 60604

Leonard Joseph  
Thornton-Tomassetti Engineers  
641 6th Avenue, 7th Floor  
New York, NY 10011

Maryann Phipps  
Degenkolb Engineers  
225 Bush Street, Suite 1000  
San Francisco, CA 94104

### **Economic and Social Impact Study Subcontractors**

Ronald Eguchi  
EQE Engineering and Design  
300 Commerce Dr., Ste. 200  
Irvine, CA 92602

Charles Kircher  
Charles Kircher & Associates  
1121 San Antonio Road, Suite D-202  
Palo Alto, CA 94303

Martin Gordon / Peter Morris  
Adamson Associates  
170 Columbus Avenue  
San Francisco, CA 94133

Lizandro Mercado  
Brandow & Johnston Associates  
1600 West 3rd St.  
Los Angeles, CA 90017

Richard Henige  
Lemessurier Consultants Inc.  
675 Massachusetts Ave.  
Cambridge, MA 02139-3309

Greg Schindler  
KPF Consulting Engineers  
1201 3rd Ave.  
Seattle, WA 98101-3000

### **Report Production and Administrative Services**

A. Gerald Brady, Technical Editor  
Patricia A. Mork, Administrative Asst.  
Peter N. Mork, Computer Specialist  
Bernadette A. Mosby, Operations Admin.  
Michelle S. Schwartzbach, Pub. Specialist  
Applied Technology Council  
555 Twin Dolphin Drive, Suite 550  
Redwood City, CA 94065

Carol Cameron, Publications Coordinator  
Ericka Holmon, Admin. Assistant  
California Universities for Research in  
Earthquake Engineering  
1301 S. 46<sup>th</sup> Street  
Richmond, CA 94804

\*indicates industrial or organizational contact representative